Enabling near real-time monitoring of phosphate in catchment areas

Joyce O'Grady, B.Sc. (Hons)

Thesis submitted in partial fulfilment of the requirements for the degree of

Doctor of Philosophy

to

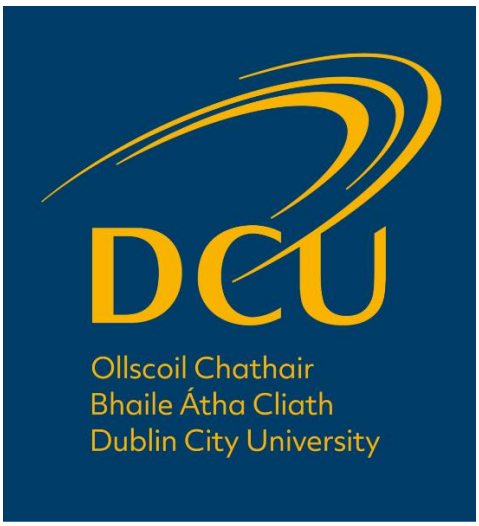

Dublin City University

October 2021

Supervisor: Professor Fiona Regan

School of Chemical Sciences

Declaration

I hereby certify that this material, which I now submit for assessment on the program of study leading to the award of Doctor of Philosophy is entirely my own work, and that I have exercised reasonable care to ensure that the work is original, and does not to the best of my knowledge breach any law of copyright, and has not been taken from the work of others save and to the extent that such work has been cited and acknowledged within the text of my work.

Signed: _____

Joyce O'Grady

ID No: 17213329

Date: 22/06/2022

Thesis abstract

As the need for more temporal and spatial monitoring grows due to the pressures from legislation and regulatory bodies, there is an increasing demand for low-cost nutrient sensors for water quality monitoring. The development of novel sensors emerging from new technologies is critical to protect and conserve our planets most valuable resource – water. The power of these new sensing devices can add value and supplement traditional methods of water sampling, collection, storage, and lab analysis, enabling more frequent and real-time monitoring with an increase data collection. Mitigating increased costs, excess personnel, and intensive labour. These devices have the potential to be integrated into a tiered monitoring framework to satisfy the demand to obtain more information about a catchment and its monitoring needs. The future of monitoring will involve satellite, *in-situ* and air borne devices with data analytics playing a key role in providing decision support tools.

The aim of this thesis was to design and fabricated a fully integrated lab on a disc low-cost sensor for rapid on-site detection of phosphate. The sensor consisted of a microfluidic disc for reagent integration and method automation, a motor, an absorbance-based detection system and electronics board. The system is fully portable enclosed in a robust case, to achieve the main objective of translating this device from lab to field. The novel system was validated during three case studies measuring concentrations of phosphate in surface water samples from various catchments across Ireland. A selection of high and low phosphate level catchments was chosen.

Table of Contents

Table of Figures

List of Abbreviations

Environmental Protection Agency (EPA)

Water Framework Directive (WFD)

Environmental Quality Standards (EQS)

Total phosphorus (TP)

Dissolved reactive phosphorus (DRP)

Double reactive phosphorous (SRP)

Molecular imprinted polymers (MIPs)

Limit of detection (LOD)

Phosphomolybdenum blue (PMB)

Information and communications technology (ICT)

Airborne Imaging Spectrometer for Applications (AISA)

Airborne Scanning Low Frequency Microwave Radiometers (SLFMRs)

Geographic Information System (GIS)

Chlorophyll a (Chl-a)

Harmful algal blooms (HAB)

Cyanobacteria harmful algal bloom (cyanoHABs)

Cyanobacteria index (CI)

Aerial unmanned systems (AUS)

Red, green, blue (RGB)

Colour-infrared (CIR)

Multispectral (MS)

Suspended sediment (SS)

Autonomous Underwater Vehicles (AUV)

Unmanned underwater vehicles (UUV)

Remotely operated vehicles (ROV)

Artificial intelligence (AI)

Internet of Things (IoT)

Wireless sensor networks (WSN)

Dissolved oxygen (DO)

Microfluidic paper-based analytical device (mPAD)

Pots per inch (dpi)

Lab-on-chip (LOC)

Manganese (Mn)

Polydimethylsiloxane (PDMS)

Lab-on-a-disc devices (LOAD)

Light-emitting diode (LED)

Photodiode (PD)

Polymethyl methacrylate (PMMA)

Pressure sensitive adhesive (PSA)

Total internal reflection (TIR)

Refractive index (RI)

Complementary metal–oxide–semiconductors (CMOS)

Scanning electron microscope (SEM)

Teflon (PTFE)

Point of care (POC)

Polyethylene terephthalate (PET)

Standard deviation (SD)

Deionised (DI)

Polycarbonate (PC)

Cyclic olefin copolymers (COC)

Analog to digital (A/D)

Millivolts (mV)

Absorbance units (A.U)

High Density Polyethylene (HDPE)

Dissolved reactive P (DRP)

Total phosphate (TP)

Particulate P (PP)

Dissolved unreactive P (DuP)

Total reactive phosphorus (TRP)

Total organic nitrogen (TON)

Revised universal soil loss equation (RUSLE)

Total soluble phosphorus (TSP)

Dissemination history

Conference poster presentations

1. Title: A novel effective, fast and frequent monitoring system for phosphate within a catchment

Authors: J. O'Grady, and F. Regan

Conference: Catchment Science 2019, Wexford, Ireland, 5-7 November 2019

2. Title: Optical enhancement strategies on centrifugal microfluidic water sensors for detection of phosphate

Authors: J. O'Grady, N. Kent, I. Maguire and F. Regan

Conference: OCEANS19, Marseille, France, 17-20 June 2019

3. Title: Enhancement in channel design for improved optical detection

Authors: J. O'Grady, I. Maguire, G. Duffy, N. Kent and F. Regan

Conference: Europtrode 2018, Naples, Italy, 25-28 March 2018

4. Title: Optical enhancement strategies on centrifugal microfluidic water sensors for detection of phosphate

Authors: J. O'Grady, I. Maguire, G. Duffy, N. Kent and F. Regan

Conference: CASi, Maynooth, Ireland, 21 May 2018

Conference presentations

1. Title: Improvements in detection in lab-on-a-disc for phosphate sensing

Authors: J. O'Grady, I. Maguire, G. Duffy, N. Kent and F. Regan

Conference: PGAC Chemistry Day, DCU, Dublin, Ireland, 3 May 2018

2. Title: Application of a centrifugal microfluidic sensing device to enable near real- time monitoring of phosphate in catchments

Authors: Joyce O'Grady, Nigel Kent and Fiona Regan

Conference: Environ 2021 - 31st Annual Irish Environmental Researchers Colloquium, Virtual, 16 – 18 June 2021

Papers published

1. Authors: J. O'Grady, N. Kent, I. Maguire and F. Regan

Paper title: In-channel modifications for improved optical detection of phosphate in a microfluidic chip design

Journal name: IEEE (OCEANS 19 Conference)

Date of Conference: 17-20 June 2019

Submitted: 10 May 2019

Accepted: 8 July 2019

DOI: https://doi.org/10.1109/OCEANSE.2019.8867516

2. Authors: Molly-Ann Williams, Joyce O'Grady, Bernard Ball, Jens Carlsson, Elvora de Eyto, Philop McGinnity, Eleanor Jennings, Fiona Regan and Anne Parle McDermott

Paper title: The application of CRISPR-Cas for single species identification from environmental DNA

Journal name: Molecular Ecology Resources

Submitted: 23 February 2019

Accepted: 8 June 2019

DOI: https://doi.org/10.1111/1755-0998.13045

3. Authors: Joyce O'Grady, Dian Zhang, Noel O'Connor, and Fiona Regan

Paper title: A comprehensive review of catchment water quality monitoring strategies using a tiered framework of integrated technologies

Journal name: Science of the Total Environment

Submitted: 1 July 2020

Accepted: 5 October 2020

DO1: https://doi.org/10.1016/j.scitotenv.2020.142766

4. Authors: Joyce O'Grady, Nigel Kent, and Fiona Regan

Paper title: Design, build and demonstration of a fast, reliable portable phosphate field analyser

Journal name: Chemical and Environmental Engineering (CSCEE)

Submitted: 15 October 2020

Accepted: Awaiting response

Book Chapters

1. Authors: Joyce O'Grady, Ciprian Briciu Burghina and Fiona Regan

Chapter title: Catchment based water monitoring using a hierarchy of sensor types

Book: Springer

Submitted: 29 July 2020

Reviewed: 28 September 2020

Accepted: Awaiting acceptance

Workshops and Communications

1. Science Futures – Agilent

Communication with Agilent where 3-4 'influential' rising star academics discuss the challenges and opportunities for their specific field of science/research, their career ambitions and views with regards to the impact and contributions of their research in the real world.

2. ASCOS

Advanced Study Course on Optical Sensors is an ECTS accredited European initiative to establish an education, discussion and contact platform for young researchers working in the rapidly growing field of optochemical sensors and biosensors

Workshop: Bertinoro, Bologna, Italy 21 – 28 July 2019

3. Maxon - Predicting future changes in water quality

Marketing communication with Maxon. Collaboration between academia and industry. How Maxon product was used in the development of a novel nutrient sensor for phosphate monitoring in catchment areas.

https://www.technologynetworks.com/analysis/blog/agilent-science-futures-the-impact-of-academia-industry-relationships-on-the-next-generation-of-354734

Acknowledgements

Firstly, I would like to extend my gratitude to my supervisor Professor Fiona Regan for affording me the opportunity to carry out this research. Thank you for your continuous support throughout this project. I would also like to extend a big thank you to Assistant Professor Nigel Kent, for sharing his knowledge and expertise with me and for always encouraging me. I enjoyed my time working with you both.

Many thanks to the Marine Institute for funding this research and giving me the opportunity to explore my interests. I would also like to extend my gratitude to the Marine Institute Research facility in Burrishoole, I enjoyed my trips back home sampling and I am extremely grateful for all the help I received.

A big thank you to all the technical staff in the School of Chemical Sciences and the NRF, I am very appreciative of all the help and assistance I received.

A massive thank you to all the members of the Regan research group, it was a joy to work with you all. Your help and encouragement will never be forgotten. I have decided not to write a list of friends and colleagues, as I believe that every person I met throughout my four years has had a positive impact on my time in DCU.

Mike, thank you for always being there for me through the good times and the bad. Particular mention to our memorable sampling trip. I consider myself extremely lucky to have you in my life. You truly are my best friend.

Finally, I am especially indebted to my incredible parents, Pat and Ann. Without you all of this would not have been possible. Thank you for the endless amount of belief, support, encouragement, and demonstration of incredible patience you have shown me throughout my life. Thank you for being the best parents. This thesis is dedicated to you.

“No amount of experimentation can ever prove me right; a single experiment can prove me wrong.”

Albert Einstein

Author Contribution

This thesis includes work from one original manuscript published in a peer reviewed journal, one conference paper and one chapter that is submitted to a peer reviewed journal. The focus of this thesis is the development of a novel fully integrated lab-on-a-disc analyser for phosphate level monitoring in catchments. The ideas, development and writing of all manuscripts in the thesis were done by me, the candidate, working within the School of Chemical Sciences under the supervision of Prof. Fiona Regan, with significant assistance with regards to the electronics and coding viewed in Chapter 4 provided by Assistant Prof. Nigel Kent. The inclusion of co-authors reflects the fact that part of the work came from active collaborations between researchers and industry and acknowledges the strong team-based research ethos. In the case of chapters 1, 2 and 4 my contribution to the work involved the following.

Thesis Chapter	Publication Title	Publication Status	Nature and extent of candidate's contribution
1	A comprehensive review of catchment water quality monitoring strategies using a tiered framework of integrated technologies	Published: Science of the Total Environment Accepted: 5 October 2020	First author, initiation, key ideas, data collection and analysis, manuscript development and writing up
2	In-channel modifications for improved optical detection of phosphate in a microfluidic chip design	Published: IEEE (OCEANS 19 Conference) Accepted: 8 July 2019	First author, initiation, key ideas, data collection and analysis, manuscript development and writing up
4	Design, build and demonstration of a fast, reliable portable phosphate field analyser	Published: Chemical and Environmental Engineering (CSCEE) Submitted: 15 October 2021	First author, initiation, key ideas, data collection and analysis, manuscript development and writing up

Signed:  Date: 22/06/2022

Signed: _____ Date: 22/06/2022

Chapter 1: Introduction

1.1 Aims and objectives

The aim of this chapter is to discuss the different processes, methods and techniques that have been applied to measure water quality parameters, observation of land use/land change involved with climate change events, and its environmental impacts on catchments. There are many differences in regulatory specifications for water quality measurements including geographical and geological variation been countries, land-use differences, and other site specificities, that can make integration of these monitoring techniques difficult to implement. This chapter aims to determine how these limitations can be overcome. Having a tiered approach to water quality monitoring enables the collection of a vast variety of data, to enhance the development of effective decision support tools for water quality management for catchments. The objectives of this chapter are to determine where the gaps are in the collection of water quality data and how they can be minimised using new and emerging technologies to add value to structured monitoring frameworks.

1.2 Catchment definition

Catchments are complex systems where the quality and quantity of the water is influenced by biological, chemical and physical factors [1]. A catchment area for water is usually defined as the area of land around a lake, river or some form of water body [2]. Catchment monitoring is important as it provides a strong approach to sustainable management of the area, it can also highlight problems or threats concerned with the area. Monitoring systems are put in place to better understand the key drivers influencing the quality of the water bodies and land surrounding the catchment. Due to the challenges in monitoring catchments, it can be difficult to link land use or land practices with water quality [3]. *In-situ,* remote sensing and hyperspectral imagery are used as an approach to water quality monitoring. These methods are rarely seen in operation together but often one method is used to ground truth another. Since catchments have presented themselves as demanding areas of land to monitor, it is interesting to see if this group of methods could be used in conjunction with one another to develop a fully integrated tiered approach to catchment monitoring (see Figure 1.2). The River Basin Management Plan was directed by the Environmental Protection Agency (EPA) as an incentive to protect the water bodies in different catchments across Ireland. Focusing on improving 726 water bodies with significant improvements in Water Framework Directive (EFD) water quality status in 152 water bodies by increasing the monitoring and observation of areas such as agriculture, source protection, management of resources and wastewater treatment, therefore demand for more monitoring techniques is continuously increasing. This plan aims to target the challenge of increasing phosphate levels in a quarter of rivers in Ireland by focusing on local water catchment level [4]. The key objectives of the River Basin Management plan is to:

- Improve wastewater treatment by investing €1.7 billion to improve the water quality and prevent further deterioration.
- Irish water to implement measures on water use to conserve and reduce leakage.
- Carry out water body assessments and implement local measures.
- Drive a Sustainability and Advisory Support Programme.
- Create sustainability initiatives for dairy farmers
- Assist local authorities with water and planning guidance.
- Manage the Blue Dot Catchment Programme to increase communication of a number of agencies to restore the quality of the water bodies.

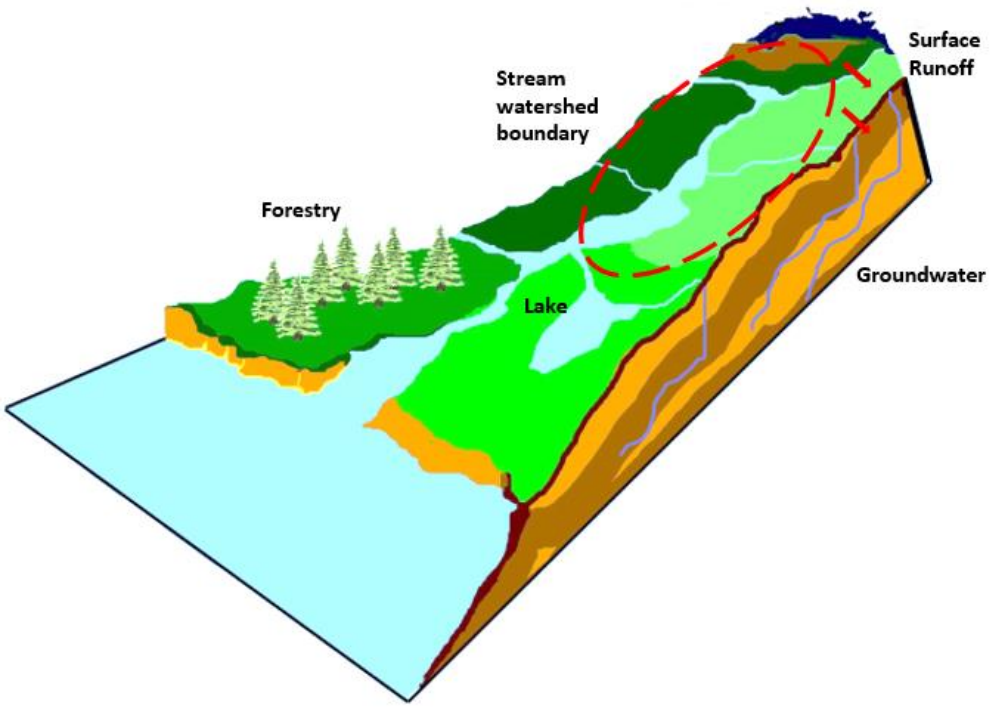

Figure 1.1 Schematic representation of typical catchment.

1.3 Current needs for water quality monitoring in catchments

Catchment monitoring with an emphasis on water quality is a growing area of importance within recent years [5]. Monitoring water quality is a local and global interest and is driven by legislation such as the WFD in Europe, the Water Act in Canada, the Australian Water Act and the US Clean Water Act. In order to obtain more information about a catchment, water monitoring and sampling must be as carried out as frequently as possible. Continuous monitoring overcomes the problem of frequency by providing long-term intensive observation, sampling and collection of data. It allows for the continuous measurement of specific parameters for the motivation of effective catchment management. To effectively monitor a

catchment, it involves an integrative framework. To develop an integrative modelling plan a layered approach to monitoring is desirable – this will enable the use of mapping, *in-situ* sensing, satellite, airborne and underwater devices and systems to achieve the collection of high level of information and data (see Figure 1.2).

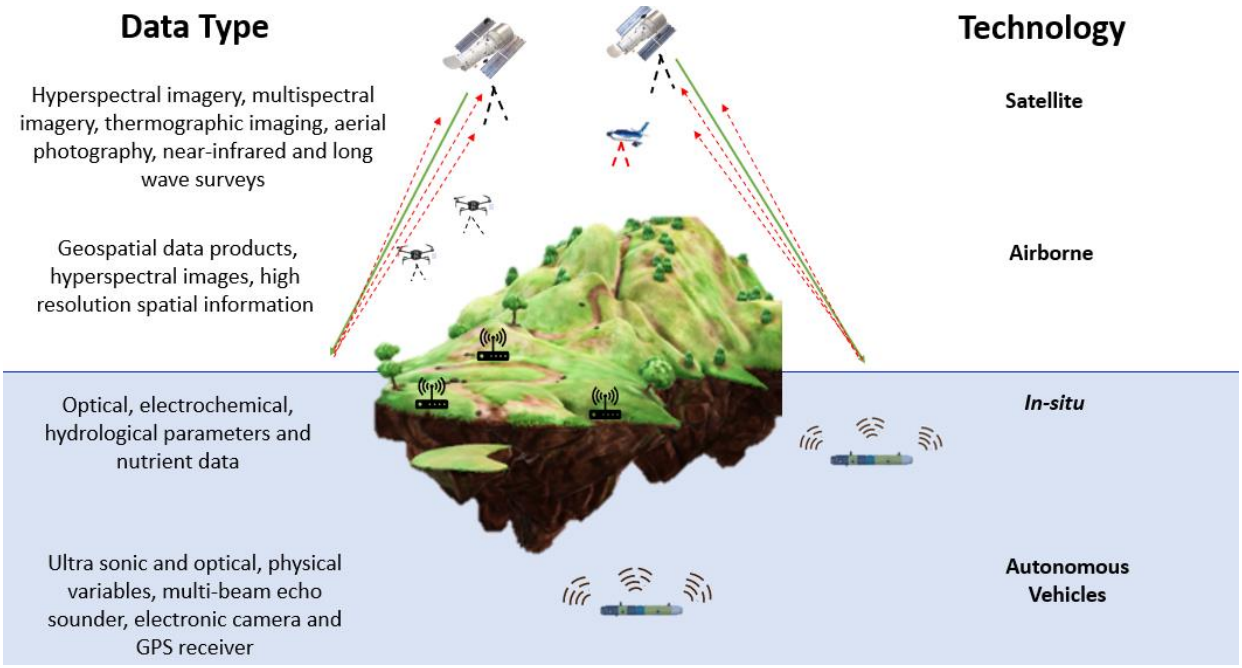

Figure 1.2 Illustration of a tiered framework approach to monitoring using integrative technologies. Linking different approaches of monitoring from high frequency (wireless sensor networks and *in-situ* probes) to relative frequency monitoring (spaceborne satellites and airborne sensors - drones).

It requires extensive information on environmental, chemical, biological and physical parameters so that effective decision-making processes can be put in place to protect and manage the catchment. The effective monitoring of water quality parameters has a profound impact on the overall quality of a catchment area [6]. With a number of aquatic systems and planktonic organisms dependent on the quality of the water for survival [7][8].

Problems such as nutrient enrichment, sediment influx and dissolved oxygen depletion are characteristics of stressed water bodies [9]. Excessive riverine nutrient concentrations can have harmful effects on the aquatic ecosystem structure and functioning of a catchment [10]. Different monitoring approaches are used to address these challenges, however gaps in data collection remain – these gaps have the potential to be filled by adopting a more integrative approach to monitoring. Water quality monitoring within catchments is essential to maintain the structure and functioning of the land, water bodies and aquatic ecosystem that inhabit the catchment. Figure 1.3 highlights the hierarchy of a tiered approach to catchment monitoring and the different layers of monitoring and technologies that are required to develop an

integrative approach so that the quality and quantity of monitoring data can be significantly improved.

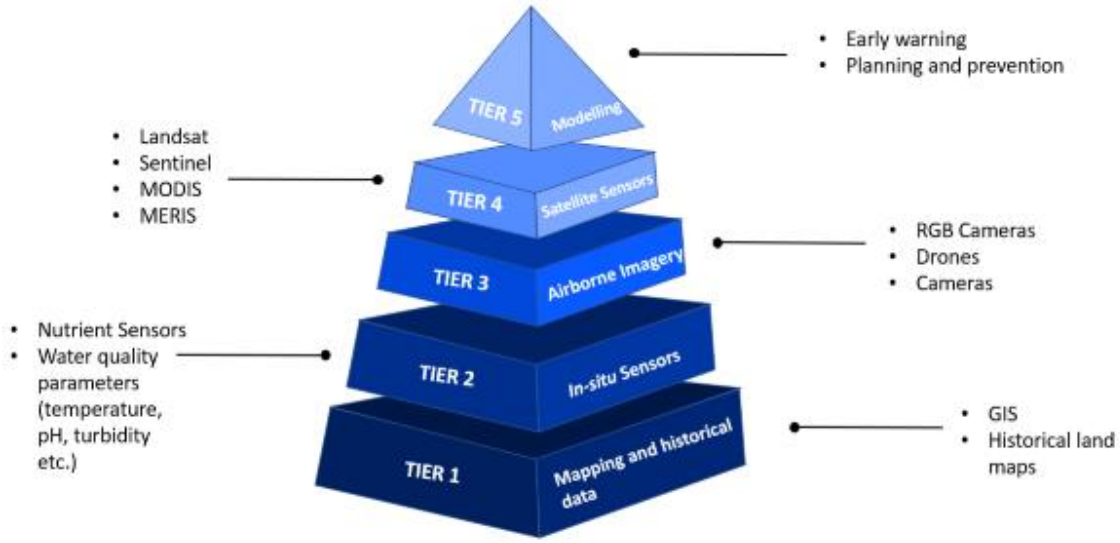

Figure 1.3 A tiered approach to monitoring a catchment. Incorporating all aspects over monitoring to obtain an integrated monitoring framework.

1.4 Phosphate monitoring in catchments

The monitoring of phosphorous (P) in catchment areas is a of significant importance, the transport of P from land to water systems has been the focal point of models and frameworks to highlight the different processes that are involved such as chemical, biological and hydrological [11]. Information on P levels are important requirements for any catchment based study or monitoring being performed on that area, in order to develop methods of control and prevention as well as providing detailed information on that area [12]. Table 1.1 represents the levels of phosphorous in rivers and what is deemed to be acceptable and unacceptable.

Table 1.1 Water quality phosphate levels for freshwater river environments according to the EPA.

Minimum (mg/L)	Maximum (mg/L)	Comment
0.01	0.025	Considered to be uncontaminated
0.025	0.035	Levels that facilitate plant growth
0.05	0.1	Maximum limit to avoid accelerated eutrophication
0.1	0.25	Excess growth

Phosphate concentrations in rivers are generally less 0.025 mg/L and concentrations above 0.035 mg/L are considered to cause nutrient pollution. These are legally binding environmental quality standards (EQS) that have been accepted by Ireland [13].

Although the P cycle does not contain an atmospheric component it is still complex due to the number of physical, chemical and biological processes it is influenced by. P is added into the soil through residues and manures and is then removed through erosion and plant uptake [14]. Figure 1.4 demonstrates the P cycle and the following further explains the different forms of P in the P cycle and how P is made available to plants.

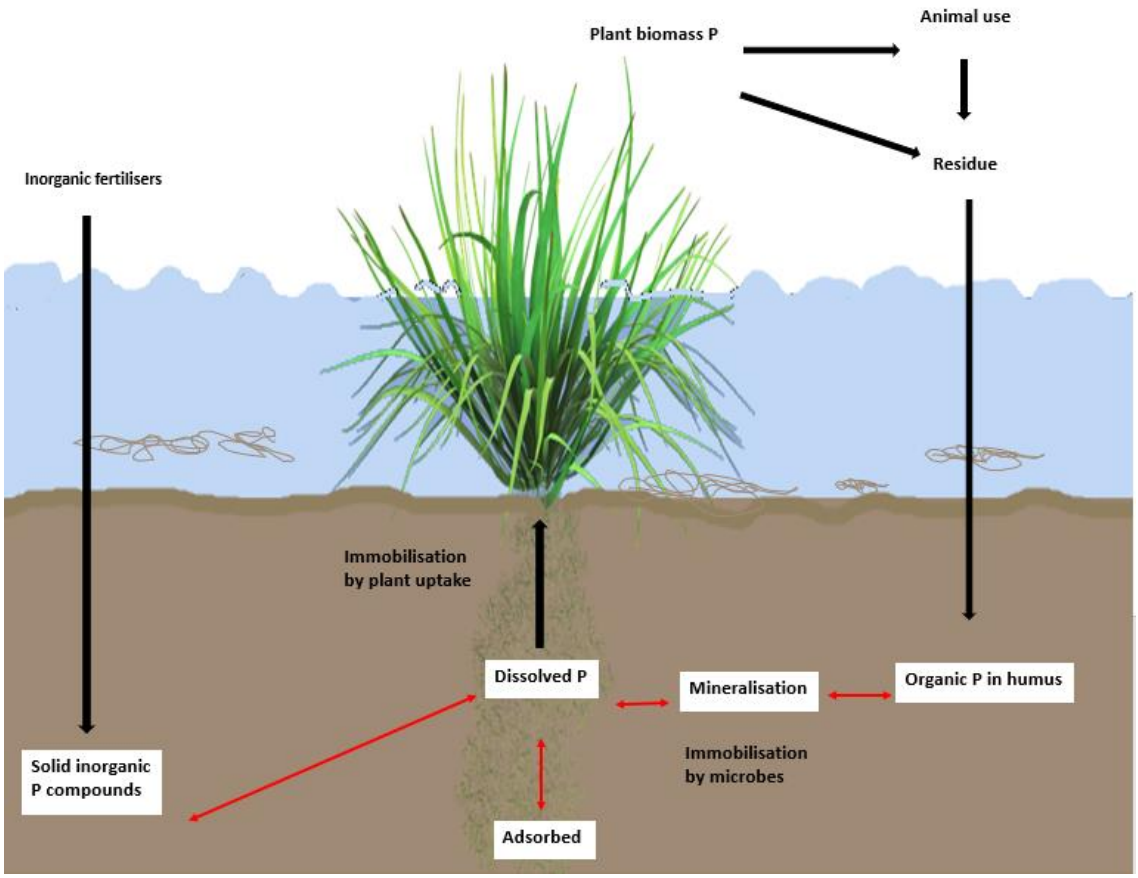

Figure 1.4 Phosphorus cycle in shallow vegetated fresh waters, (modified from Chaubey et al., 2006*)*

The mineralisation and immobilisation processes occur in the soil in organic forms. Organic P is generally unavailable to plant uptake due to the strong binding forces it has to other organic compounds [16]. The decomposition of organic compounds caused by microorganisms in the soil leads to the mineralisation of P, this results in increased levels of dissolved P available. When the organic P concentration levels are low in the soil immobilisation will occur, this is a process by which the inorganic P is absorbed into the living cells of soil microbes [17], this

immobilisation process is effected by soil matter, climate, soil pH (high – less organic P), temperature (high – more organic P) and land use (cultivation processes such as tillage – less organic P). The introduction of manures and residues into the soil releases plant available P due to the rate of decomposition. The rising levels of dissolved P concentration causes an influx in the immobilisation of P by increased microbial activity from microbes in the soil.

Adsorption and desorption of dissolved P exists as either $H_2PO_4^-$ or HPO_4^{2-} [18]. These compounds are adsorbed by soil minerals due to the charged positive sites which make the P unavailable for plant uptake [19]. Factors affecting the adsorption process are soil clay content, pH, concentrations of iron, aluminium and calcium carbonate and particulate organic matter. Desorption is affected by soil pH and moisture content [20].

The dissolution process involves the ability of inorganic P to dissolve into a solution. This process is associated with inorganic fertilizers and natural minerals. The introduction of inorganic P fertilizers increase the concentrations of inorganic P and can dissolve into a solution depending on soil conditions, making runoff and the leaching of P into waterbodies possible [21], creating huge concern for the quality of that water body.

Eutrophication of freshwater remains one of the most challenging environmental issues, causing problems for government and legislative bodies despite their efforts to control, manage and eliminate the nutrient inputs and transfers from land to water [22][23]. Eutrophication is the excessive enrichment of an ecosystem by chemical nutrients, often containing chemical compounds such as phosphorous, ammonia, nitrites and nitrates [24]. Excessive loading of nutrients such as phosphorus is commonly associated with agricultural land practices. Rural areas have been linked to point sources for nutrients loading from agricultural catchments and weather events. More urban areas are associated more with industrial pollution and human activity [25]. In the last 20 years the variation in magnitude and source of point and diffuse phosphorus pollution in rivers has improved due to the legislation, regulation and guidelines for works carried out on wastewater treatment plants and land use management practices [26]. However, the threat to water quality on many Irish rivers and lakes is still an ongoing challenge. In response to the negative impacts associated with nutrient pollution from nutrients such as P, a number of legislative and regulatory paperwork and bills exists in Europe and worldwide which demands the monitoring of chemical nutrients in water bodies such as the (EU Water Framework Directive 2000/60/EC; Council Directive 91/271/EC; Blueprint to Safeguard Europe's Water Resources, Clean Water Act 1972) [27].

1.4.1 Phosphate speciation

The speciation of P fractions has been widely studied and categorised. The occurrence of P in natural waters and in sediment is primarily found as orthophosphate. It can also be found as organic and condensed P that differs in molecular weight [28]. The easy method of analysing phosphorus is through total phosphorus (TP) and dissolved reactive phosphorus (DRP) [29]. TP includes both suspended and dissolved fragments. The dissolved species is the fraction that is still present after the sample has been put through a filtration process using a filter membrane. The DRP is the fraction which comprises the dissolved inorganic phosphorus which is made up of condensed phosphate fractions, orthophosphates and dissolved organic phosphates [30]. Orthophosphates are the most common form of soluble reactive phosphorous (SRP), the SRP method is widely used to determine the bioavailability of phosphorous in water [31][32]. Phosphate PO_4^{-3} ions are naturally formed when P goes through a natural process of weathering [33]. Three different forms of phosphate are available; orthophosphate, metaphosphate and organically bound phosphate [34]. The reason that phosphates are monitored is because they are the most common chemical form of P. The term given to the measured concentration of orthophosphate in environmental water is dissolved reactive phosphorus [35]. Figure 1.5 highlights the progressive deprotonation due to reactions with OH^- to produce PO_4^{-3} at high a pH [36].

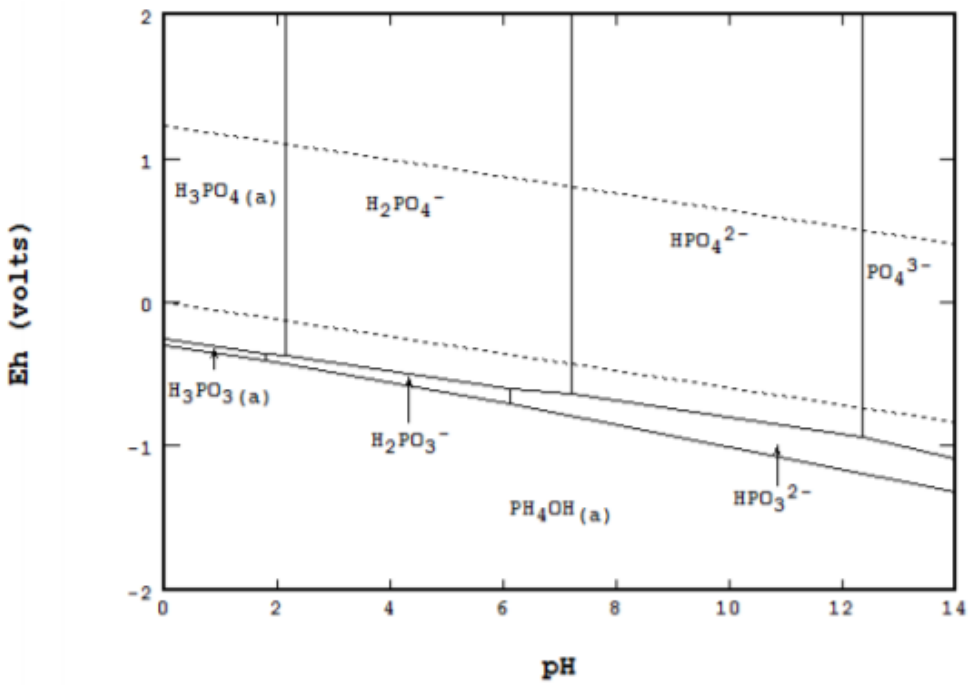

Figure 1.5 Eh pH diagram of a phosphorus water system of a dissolved phosphorus species [P] = 0.001 M. Oxidized species reside in high Eh areas and reduced species are found in low Eh areas.

The pH of a waterbody can affect the different forms of orthophosphate ions present [37]. The pH of a solution is determined by the Henderson-Hasselbach equation which defined the pH of a conjugate acid-base in terms of the dissociation constant associated with the weak acid and the equilibrium concentration of the undissociated acid. pH and pKa values are related using the following equation:

Equation 1.1 Henderson-Hasselbach for determination of pH

$$pH = pKa + \log_{10}\left(\frac{[A-]}{[HA]}\right)$$

Where $[A^-]$ is the dissociated species molar concentration and [HA] is the undissociated acid concentration [38]. When the concentration of $[A^-]$ and [HA] are the same, the pH is equal to the pKa of the acid. In dissociation for o-phosphoric acid is given in the following equations:

Equation 1.2

$$H_3PO_4 \leftrightarrow H_2PO_4^- + H^+$$

Equation 1.3

$$H_2PO_4^- \leftrightarrow HPO_4^{2-} + H^+$$

Equation 1.4

$$HPO_4^{2-} \leftrightarrow PO_4^{3-} + H^+$$

A tabulation of the pKa values are shown in Table 1.2:

Table 1.2 Dissociation constants for o-phosphoric acid

Phosphoric acid	**pKa 1**	**pKa 2**	**pKa 3**
H_3PO_4	$H_2PO_4^-$	HPO_4^{2-}	PO_4^{3-}
2.13	7.2	12.36	

The PO_4^{3-} ion does not occur naturally in waterbodies. The ions commonly found are a mixture of $H_2PO_4^-$ or HPO_4^{2-} [28][39].

1.4.2 Phosphate sensor criteria

The demand for rapid detection methods that provide real-time or near real-time quantification of phosphate levels in freshwater is recognised by both government and legislative bodies [40][41]. Different methods and technologies for monitoring and detecting phosphate levels in freshwater has been reviewed by *Warwick et al.,* these technologies include: biometric receptors (synthetic receptors and molecular imprinted polymers (MIPs)), electrochemical detection (potentiometric, amperometric, voltametric and conductometric analysis) and optical detection methodologies (colorimetric absorbance and luminescence/fluorescence) [42]. The first category is not routinely used in phosphate detection as the receptors do not function in aqueous solution deeming them unsuitable for environmental applications. The second category have been used for phosphate detection in environmental samples however, the instrumentation used in the quantification is expensive, time consuming and labour intensive. The last group using optical detection methods are the most employed methods for phosphate detection [43], as they are relatively cheap and most importantly can be translated from lab to field, facilitating the detection of phosphate in real-time or near real-time, helping to achieve the directives and frameworks set in place by legislation to provide temporal and spatial collection of water quality parameters such as phosphate levels. These detection methods using optical based sensing offer quick results (8-20 min) depending on the assay used [44][45]. They are simple to perform and compared to other instrumentation the cost is significantly cheaper. Absorbance based optical detection being the most used for phosphate determination. The ability to incorporate colorimetric reagents into absorbance based optical

detection methods satisfies the demand for rapid, robust, and reliable measurements on water quality parameter. Commonly used assays for optical based detection of phosphate include the molybdenum blue [46][47], vanadomolybdophosphoric acid [48] and stannous chloride [49]. These assays have some limitation related to their working complexity, chemical requirements (lifetime and stability) and monitoring duration.

Table 1.3 Summary of the colorimetric methods for the determination of phosphate [15]

Method	**Linear Range ($\mu g\ L^{-1}$)**	**LOD ($\mu g\ L^{-1}$)**	**Reagent Stability and lifetime**	**Complex develop-ment (min)**	**Interfering ions**	**Comments**
Molybdenum blue	10 - 200	10	Combined Reagent = 4 hours	8 – 20	AsO_4^{3-}, Cr^{6+} and SiO_2	Low level of detection, poor reagent stability. Commonly used with sensing devices.
Vanadomolybdo-phosphoric acid	100 - 1800	200	> 1 year	10	AsO_4^{3-} , F^-, Th, Bi, S_2^-, $S_2O_3^{2-}$ and SCN^-	Poor level of detection, not suitable for most freshwater applications, good reagent lifetime, commonly used in autonomous systems.
Stannous chloride	7 - 200	7	> 6 months	10 - 12	AsO_4^{3-} , F^-, Th, Bi, S_2^-, $S_2O_3^{2-}$ and SCN^-	Viscous reagent not suitable for micro/nano system integration. Good stability and sensitivity.

1.4.3 Molybdenum blue method background

The molybdenum blue method relies on the reaction between the ortho-phosphorus ion and molybdenum under highly acid conditions to form phosphomoyybdic acid. In literature a low pH (0-1) is routinely used in the analysis as it gives the best colour intensity and increased stability of the formed product [50][51][52]. The heteropoly acid is reduced by the addition of ascorbic acid to give an intense molybdenum blue colour which is measurable at a wavelength of 880 nm [53]. Antimonyl tartrate is used as a catalyst in the reaction and to prevent the formation of silicomolybdic acid, which is a known interference of the molybdenum blue assay [54]. This method is a highly sensitive method with a limit of detection (LOD) of 10 µg P/L. A drawback to using this method is that is it relatively unstable and when all components of the reagent are combined it has a lifetime of 4 h. Hence the need to prolong the lifetime and increase the stability of the reagent is extremely important. The unstable component of this reaction is the ascorbic acid which once isolated has a lifetime of 1 week [55]. The disposal of small, affordable, commonly used components, low limit of detection and simplicity of the method make it suitable for the integration into field deployable sensors [54] if the lifetime of the reagent can be prolonged.

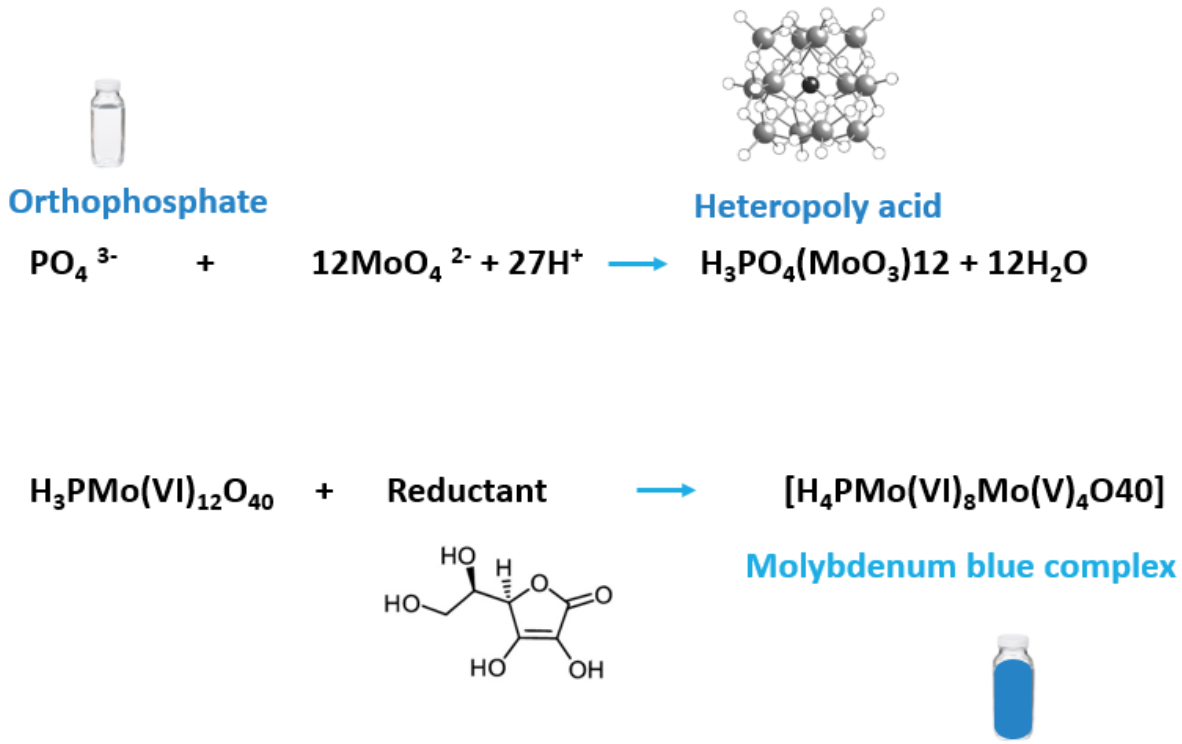

Figure 1.6 Schematic of the molybdenum blue reaction taking place in the presence of a water sample containing an ortho-phosphate ion forming a brightly coloured phosphomolybdenum blue (PMB) species.

The molybdenum blue method includes a number of components that are used to reduce the effects of potential inferences on the reaction. Ascorbic acid is used to counteract the effects of Arsenates on the reaction. When the reductant is increased the formation of arsenomolybdenum inhibited. The inclusion of a strong acid is used to counteract the effects that silcate can have on the reaction by lowering the pH and preventing the formation of SiO_4^{4-} ions, these ions are also inhibited when the reaction is carried out without heating [52].

1.5 Monitoring techniques currently being used at a global scale

Long term *in-situ* sensing platforms have been used for environmental monitoring for the past number of years. They include the measurement of a number of water quality parameters. Most of the instruments used to monitor these variables are multiparameter probes. These sensors are commercial devices and are widely available on the market, therefore are used frequently in long-term monitoring of different parameters. They provide real-time, periodic and for the most part reliable data. Through *in-situ* sensor monitoring, out-of-specification parameters can be instantly identified and managed [56][57]. The information being transported through the systems can identify the nature of the problem and what has caused it, therefore it can give further information regarding the level of water quality and in addition the level of nutrients at different stages using autonomous and *in-situ* monitoring [58].

In recent years there has been a surge towards remote sensing systems. Remote sensing can be defined as the “science of observation from a distance” [59], in order to achieve this class of monitoring, autonomous sensor sampling must be employed. Remote sensing plays a pivotal role in the development of an observation framework for a remote catchment area. Remote sensing as an application that allows for an area to be monitored in real-time without encountering the observed area. Satellite and airborne imagery are commonly used in the area of remote sensing due to their ability to provide information from 10 to 100 square meters [60], especially in the case of satellite imagery. There have been considerable developments in this area in the last number of years, the increase in spatial resolution has coincided with spectral resolution producing high quality images suitable for a number of applications and studies. In areas such as land-cover classification, water quality monitoring of nutrient speciation, hydrological parameters and species assemblages, which allow for effective conservation and planning management. Gaps in data collect can appear due to the upkeep and maintenance requirements. It has become more apparent than ever that to fully monitor a catchment area different monitoring techniques need to be employed to get a full representation of what is going on within the catchment area. The proposal of a tiered framework for water quality monitoring has been briefly discussed in literature but is usually used as a method for ground truthing remote sensing applications for water quality monitoring

[61]. This idea of a tiered approach enables the effective development of a continuous and remote based monitoring structure for water quality monitoring [62]. This structure meets the unmet needs of effective, reliable, frequent and real-time monitoring. To date there has been minimal research carried out on a complete tiered framework.

Globally there are many examples of *in-situ* long-term sensing data collection and remote sensing techniques. However, it is rare to see these approaches implemented together. Usually, one method is used to validate another. There has been minimal research to evaluate both methods in conjunction with mapping and modelling to further enhance assessment of water quality parameters.

In terms of *in-situ* sensing a lot of work has been done using high resolution monitoring for common water quality variables along with flow and water levels. Most of the instruments used to carry out the data collection include multi parameters, gauging stations, water level loggers, meteorological stations, wet chemistry analysers, field measurements and laboratory analysis. The literature presented on the use of long-term real-time monitoring aims to report the importance of high-resolution observation, frequent sampling to increase the level of knowledge and also to vary response and actions needed.

Many papers have reported on the usefulness of remote sensing and how this method of monitoring allows for more accurate, less labour intensive and free data collection. In terms of catchment monitoring, remote sensing is frequently used for capturing land use and land change over time, changes in water quality and colour, monitoring of certain species such as *chlorophyll a* [63][64][65] and poor water quality indicators. Table 1.7 below outlines different monitoring techniques to look at issues concerning water quality used in catchments around the globe and where more than one monitoring technique has been applied. Climate change has been shown to have a severe impact in nutrient levels, agriculture, flooding and sediment fluxes within catchments and the studies reviewed reflect the need for higher temporal and spatial frequency monitoring through the aid of satellite, airborne, *in-situ* and underwater vehicles and new technologies that can be used to fill gaps in data collection. From reviewing the literature, it is evident that the UK has carried out a number of studies concerning catchment monitoring, many of these published papers address long-term *in-situ* devices to do this. Rarely has remote sensing been applied to these studies (see Table 1.4). Catchment monitoring with an emphasis on remote sensing has generally been applied to countries in the eastern and southern hemisphere (see Table 1.5).

Table 1.4 Summary of in-situ water quality monitoring in catchments

Site	Sensor	Type of Monitoring	Duration (months)	Funding
5 sites across River Ray Catchment UK [66]	Starflow™ Ultrasonic Doppler YSI 6600 multiparameter sonde	Monitoring DO, ammonium, turbidity, conductivity (Field measurements)	11	Natural Environmental Research Council UK
Baldarado Catchment North East Scotland [67]	Autosampler	Suspended solids, Particulate phosphate, TDP, DOC, DOP Fortnightly sampling campaign (Field and lab measurements)	24 months	Scottish Government Rural Environmental sciences and analytical services division 2016-2021
Wylye and SEM catchments Hampshire Avon UK [68]	YSI 6-series Sonde Nitratax Plus SC Phosphax Sigma	Real time (15min data intervals)	9 months	Defra Project WQ0211
Wood Brook Birmingham UK [69]	OPUS UV Spectral Manta 2 multiprobe	High frequency *in-situ* monitoring NO3-N and DOC	9 months	Natural Environmental Research Council UK
Saarland Germany [70]	Commercial and wet chem analysers (Ion selective electrodes)	Real time sensing	108	Ministry of Environmental and consumer protection
Alicante province, SE Spain [71]	Tipping-bucket rain gauge, with a temporal resolution of 5 min	*In-situ*, field measurements	Long-term data (1976–2006 (Not real time)	Spanish Ministry of Innovation and Science
A set of 108 stream monitoring stations Across different regions in Sweden [72]	Hach-Lange SOLITAX sc and a SC-1000 controller	Turbidity, SS (*in-situ* field measurements and in lab tests)	24	Open access funding provided by Swedish University of Agricultural Sciences
5 meso-scale agricultural catchment in Ireland [73]	Hach Lange equipment. Phosphax. Sigmatax. Nitratax SC-Plus UV instrument	TP, TRP, TON, SS, turb. Transfer of nutrients Real time and not real time sampling	48	Dept. of Agriculture, Food and the Marine

Savijoki catchment Southwestern Finland [74]	S::can Nitrolyser probe. OBS3+ probe	Turb, nitrate and field monitoring. Automatic sampler (8h interval) TSS and PP	5	Finnish Ministry of Agriculture and Forestry
Blackwater River Ireland – 3 small catchments Northwestern Ireland [75]	Sigmatax Phosphax bankside analyser	TP and grab sampling	12	EU funding grant
3 catchment streams. Eastern part of Otago South Island New Zealand [76]	YSI Model 85 Model: Marsh McBiring Flowmate Model 2000 Hach 2100A Model Lab Instruments	DO, COND, TEMP, Flow, TURB, TSS Real time and near real time analysis	1	Foundation for Research Science and Technology New Zealand

Table 1.5 Summary of remote sensing and modelling of water quality for catchments

Site	Sensor	Type of Monitoring	Duration (month)	Funding
4 Catchments Zimbabwe [77]	Landsat 8	NDVI calculations and TSS in lab	➢ 2	Multi Donor Trust Fund
Australian Estuaries [61]	ArcGIS Landsat	Mapping on Arc, NDVI Landsat	Long-term data set (87 – 14) Not real time	Australian Research Council Linkage grant
Likangala River Catchment Malawi [78]	Landsat 5 + 8	Image processing 84, 94, 05, 13	Long-term data set (84-13) Not real time	Northwest University
Tollense river basin. Germany [79]	GW data loggers iArcGIS	Model simulation, open access data	Not real time	s HEC Pakistan /DAAD Germany scholarship during the PhD study period
The Shigenobu River basin [80]	DEM and DNI stream network map.	Long-term data sets and models	185-day discharge Long-term data set (1976 – 1997)	New Energy andIndustrial Technology Development Organization The Global Environment Research Fund
Southern New Zealand – intensively farmed catchment (Bog Burn Catchment) [81]	Model – OVERSEER™ Nutrient Budget Model	Nitrogen and Phosphorous	48	Dairy Insight Ministry of Agriculture and Forestry Sustainable Farming Association
Kielstau and Moorau catchment Northern Germany [82]	SWAT model	Nitrate, ammonium, TP, phosphate Daily sampling	Kielstau (31) Moorau (16)	N/A

1.6 Technologies used in catchment monitoring

Different monitoring technologies can be combined with information and communications technology (ICT) and advanced data analysis techniques to provide extensive long-term

datasets that can be effectively transmitted and managed with little cost involved to help support the decision-making processes involved in catchment monitoring [83]. Catchment monitoring of water quality can benefit from real-time, high-resolution data to maintain the quality of the water and provide alerts to threats that the catchment might be exposed to. *In-situ* sensors provide rapid, robust and reliable environmental monitoring. They provide near real or real-time analysis of environmental water pollution parameters. These devices are available for spot measurements or deployment, providing instantaneous readings and allowing many data points to be gathered within an hour every hour. Remote sensing facilitates the measuring of the reflected and emitted radiation of the area using cameras that can collect the remotely sensed images [84]. These monitoring platforms can be combined with ICT and advanced data analysis techniques to provide extensive long-term datasets that can be effectively transmitted and managed with little cost involved to help support the decision-making processes involved in catchment monitoring [83]. There are a range of technologies that address different water quality parameters (see Table 1.6). The analytical range, robustness and operational parameters affect how they are used in monitoring.

Table 1.6 List of common water quality parameters and their remotely sensed method of monitoring

Water Quality Parameter	Abbreviation	Units	Sensor	Reference
Secchi disk depth	SDD	m	Landsat MERIS	[85]
Temperature	T	◦C	Airborne TIR	[86]
Dissolved Oxygen	DO	mg/L	MODIS	[87]
Total suspended matter	TSM	mg/L	Landsat SPOT	[88]
Turbidity	TUR	NTU	Landsat MERIS	[89]
Conductivity	COND	µs/cm	CHRIS Proba satellite	[90]
Colour dissolved organic matter	CDOM	mg/L	Landsat	[91]
Chlorophyll-a	Chl-a	mg/L	Airborne Imaging Spectrometer for Applications (AISA)	[92]
Sea surface salinity	SSS	PSU	Airborne Scanning Low Frequency Microwave Radiometers (SLFMRs)	[93]

Table 1.7 Summary of remote and in-situ sensing for water quality monitoring in catchments

Site	Sensors	Monitoring	Duration (months)	Funding
Humber Catchment UK (10 Rivers) [7]	Partech turbidity sensor CASI	Field turbidity measurements, SS and aerial images	96	Institute of Hydrology York
Lake Chivero Zimbabwe [94]	Modis	Spatial and temporal patterns in chlorophyll_a RS and *in-situ*	(85 – 10) Long-term dataset (not real time)	University of Zimbabwe
Lake Chivero and Manyema Zimbabwe [95]	Landsat	Turbidity, TP, Chl-a, Near real-time sensing	(86 – 15) Long-term dataset (not real time)	N/A

1.6.1 Short-term monitoring

The short-term monitoring practices refer to the daily spot checks, single point sampling and lab analysis of the single sample. These monitoring methods are still used today to provide simple data on straight forward analysis that is important to the daily running and overall management of the catchment area. Depending on the type of catchment these sport checks can differ. Most of the short-term daily monitoring practices include manual sampling of water and soil. Tests and experiments are then carried out in the laboratory on the grab samples.

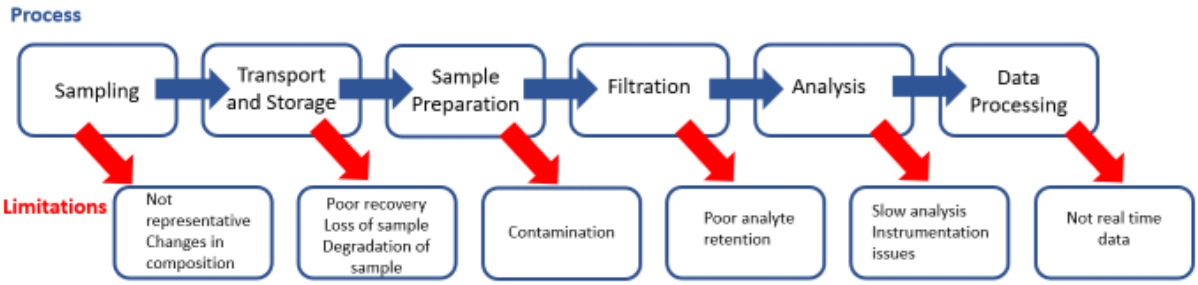

Figure 1.7 Systematic flow diagram of the different processes involved in obtaining grab samples and the relevant limitations associated with them.

1.6.2 Long-term monitoring

The need for long-term monitoring practices have been used to bridge the gaps between data collection and analysis has been widely recognised by the scientific community. Due to the complexity of effectively monitoring a catchment it is vital that long-term near/real-time practices are in place. To successfully monitor a catchment the collection of data must highlight sources and processes that are contributing to pollution [96]. Data collection and analysis is a major aspect of implementing long-term monitoring practices within catchment areas. For example, a long-term *in-situ* sensing device can collect data at a 15-min interval can collect 4 data points in an hour, 96 in a day and 35,000 in a week. The need to integrate data control flags are critical for successful data management. Common water quality parameters that are usually observed in long-term monitoring include; O_2, DO, pH, temperature, salinity, turbidity, conductivity, nutrients, alkalinity, BOD, TDS, TSS, TOC and heavy metals. The continuous monitoring of these water qualities provides valuable information on the status of the water, trends present and possible threats to the catchment. There is an abundance of studies carried out on the long-term monitoring of each of these parameters globally, see Table 1.4.

1.6.2.1 In-situ sensors

Water quality monitoring in remote and isolated locations can be an expensive task to undertake [97][98]. Even at its most basic level it still demands an engineer to visit the site and manually sample the water, this is also known as grab sampling. Manually taking samples from the site and bringing them back to the lab for analysis is both costly and time consuming. It is not possible to monitor a wide range of locations. Therefore, the area cannot be monitored in real-time or accurately as the sensor have only provide a spot analysis [99][100]. One of the drawbacks to using in-situ sensing is the level of maintenance required. *In-situ* sensing is commonly used for the measurement of common water quality parameters that contribute to and effect the environment. They have been employed for years to measure and obtain data on quality variables such as temperature, pH, oxygen, conductivity, turbidity and depth. *In*-situ sensors allow for high resolution monitoring, they can be used alone or deployed as part of an observation system [101].

The study carried out on the Ray catchment located in the upper Thames basin, UK, highlighted the importance of high-resolution monitoring of flow and water quality parameters, the study evaluated how the quality of surface water can be varied and the impact of flood hydrographs on water quality. This study used high resolution monitoring by means of *in-situ* commercial sensors to assess flow, rainfall, turbidity, specific conductivity, ammonium and DO. They also incorporated land use data into the study by using digital elevation model to investigate land cover. The study focused mainly on *in-situ* data to derive their conclusions. This resulted in the collection of a dataset that disclosed a wide range of water quality response to series of extreme storm events during the winter of 2013/2014 [66].

Lloyd et al., also utilizes *in-situ* sensors for water quality monitoring. This paper discussed the use of Hysteresis analysis as a valuable tool for assessing storm events and patterns to assess the comparisons and differences within and between catchments. In this study the authors assessed 2 years of high temporal water quality and discharge. It showed that catchment character and function play a major role in responses. This study examined up to 76 different storm events using only *in-situ* sensors which monitored three water quality parameters; turbidity, Nitrate (N) and phosphorus (TP) [68].

1.6.2.2 Current commercial sensors

The current market includes a number of robust and reliable water quality and chemical sensors that can be deployed in a catchment for lengthy period of time. These sensors are widely available with number of trading businesses that supply them. However, these chemical sensors are expensive with costs that range between €10,000 to €100,000. These costs are increased depending on the instrument and what it is measuring. For example, the chemical reagents, waste disposable, data processing controllers, and other electronic and functioning components can cause fluctuations in cost point [102].

Table 1.8 List of commercial sensors for water quality monitoring currently on the market that have been employed in catchment monitoring studies. *FTU =, NTU =*

Sensor	**Parameter**	**LOD / Resolution**	**Dynamic/ Linear Range**	**Analysis Time**	**Manufacturer**	**Reference**
Sea-Bird Scientific SUNA Optical Nitrate Sensor	Nitrate	0.004 mg/L	14 – 56 mg N/L	Real-time measurements	Sea-Bird Scientific	[103]
Sea-Bird Scientific HydroCycle-PO4 Phosphate Sensor	Phosphate	0.0023 mg/L	0-0.3 mg/L	Real-time measurements	Sea-Bird Scientific	[96]
UniLux Turbidty	Turbidity	<0.02 FTU	0 – 100 FTU	Real-time measurements	Chelsea Technologies	[83]
Starflow™ Ultrasonic Doppler	Depth-velocity	1mm/s	21mm/s to 4500mm/s bi-directional	Real-time measurements	Unidata Pty Ltd	[66]
YSI 6600 multiparameter sonde	Turbidity	0 .1 NTU	0 to 1,000 NTU	Real-Time	YSI xylem a brand	[66]
	Conductivity	0 to 100 mS/cm	0.001 to 0.1 mS/cm			
	Ammonium	0.31–1.28 mg/l				
	DO	0.01 mg/L	0 to 50 mg/L			

YSI 6 series sonde	Turbidity	0.1 NTU	0 to 1,000 NTU	Real-time	YSI xylem a brand	[73]
Hach Lange Nitratax Plus SC	Nitrate	0.1 mg/L	0.1 to 100 mg/L NO3-N	Real-time	Hach	[73]
Hach Lange Phosphax Sigma	Phosphate	0.01mg/l	0.01 … 5.0 mg/l total – P	Real-time	Hach	[73]
OPUS UV spectral	Nitrate	0.3 mg/l	0…100 mg/l	Real-time	TriOS Optical Sensors	[69]
Manta 2 multiprobe	Conductivity	4 digits	0 – 100 mS/cm	Real-time	Eureka Water Probes	[69]
	Temperature	0.01 °C	-5 °C – 50 °C			
	Turbidity	0.1 NTU	0 – 3000 NTU			
Decagon 5TM VWC	Soil moisture	N/A	VWC: 0-100%	150 ms	Decagon	[69]
OTT ADC	Discharge	N/A	-0.2 m/s - +2.5 m/s	Realtime	OTT Hydromet	[73]
C31 Flowmeter	Flow	N/A	0.025 – 10 m/s	Realtime	OTT Hydromet	[73]
S::can Nitrolyser probe	Nitrate	0.005 mg/L	0-100 mg/l	Realtime	S::can	[74]
TT Thalimedes	level	0.001 m / 0.01 m / 0.01ft	N/A	Realtime	OTT	[104]
Stream pro ADCP	Flow (high)	1 mm/s	+/- 10 m/s	Realtime	OTT Hydromet	[104]
YSI model 85 model	Conductivity	0.1 µS/cm	0 to 499.9 µS/cm	Real-time	YSI xylem a brand	[80]
	Temperature	0.1°C	-5 to +65°C			
	Salinity	0.1 ppt	0 to 80 ppt			
	DO	0.01 mg/L	0 to 20mg/L			

1.6.2.3 Handheld sensors

Handheld sensors are platforms that are developed for rapid, robust and reliable environmental monitoring. They can provide near real or real-time analysis of environmental water pollution parameters. There is an increase in the demand for cheap, reliable and robust sensing devices that can be used out in the field daily to collect real-time or near real-time data on water quality parameters. These sensors will facility the high sampling and monitoring that is needed for a dynamic environment such as a catchment. The price point of these sensors is required to be cost efficient so that more can be deployed around the catchment area for continuous and frequent monitoring of a specific water quality parameter such as nutrient detection. A major advantage of these sensing technologies is the variety in manufacturing techniques and material chemistries, which drive down the costs significantly when compared to sensors that are currently on the market to date. Commercially available sensors cost a considerable amount to make, maintain and deploy. A typical commercial sensor can cost up to €25,000 per unit [105], due to their size, high power consumption and reagent storage chambers, see Table 1.4 and Table 1.8 for nutrient sensors and water quality parameter sensors available on the market.

The demand for these low-cost handheld analysers is still unfulfilled. There is a gap in the market for a handheld portable, cost efficient, self-contained nutrient sensor that can bridge the gaps in data that current *in-situ* sensors cannot facilitate due to their size and cost point. This type of device would be extremely useful for catchment studies, there are a number of different waterbodies and water networks that make up a catchment area, therefore one *in-situ* sensor at a single location in a catchment will not provide enough data to monitor an entire catchment. A portable sensor that can be transported around the catchment and detect the levels of specific nutrients in real-time will give more information about the quality of water in the overall catchment, not just one waterbody, improving the temporal and spatial resolution of the data being obtained. These types of sensors can add value to integrative observation frameworks by overcoming the limitations presented by *in-situ* autonomous devices and remote sensing. These devices are easily transported around a catchment, therefore can increase the temporal and spatial data collection, filling in data gaps from the use of *in-situ* and remote sensing.

1.6.2.4 Satellite Imagery

Remote sensing data is generally used to monitor water qualitative parameters such as secchi disk depth, temperature, total organic carbon, total suspended matter, turbidity, conductivity, colour dissolved organic matter, chlorophyll-a, suspended solids and sea surface salinity [106].

Satellite imagery is a remote sensing and geospatial space-based technique that allows the user to monitor land and water changes, it also allows the user to observe isolated and rural areas of interest. Geographic Information System (GIS) is commonly used alongside remote sensing techniques, it is a tool that is used to process and analyse the changes observed in satellite imagery. Satellite imagery provides useful and detailed data for environmental monitoring, management and mapping, in order to explore all the details that can be used through satellite imagery other tools must be employed in conjunction with it. Tools such as GIS allow the appropriate information to be obtained and presented in a format that can then be analysed by the user.

The spatial resolution of the instrument chosen is the at-ground representation of an individual detector in a satellite sensor array and again differs from sensor to sensor. Table 1.9 presents the satellite sensing platforms used in remote sensing.

Table 1.9 Summary of the different remote sensing platforms used in catchment monitoring.

Sensor	Image Type	Application	Comments
Landsat and Sentinel	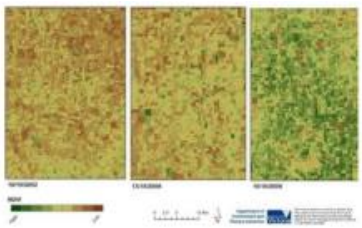 Image adapted from: https://www.usgs.gov/centers/fort/science/agriculture-landsat-imagery-a-unique-resource?qt-science_center_objects=0#qt-science_center_objects 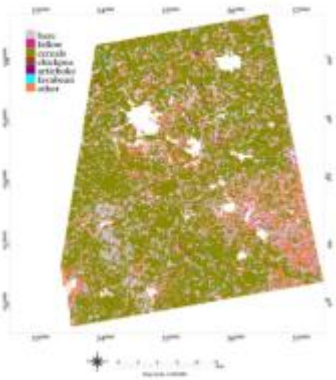 [107]	Agriculture	Record leaf area indices, monitor crop productivity (rich vs poor crop growth), also provide high-tech analysis on farming practices "precision agriculture" [108].

Landsat and SPOT satellite manager	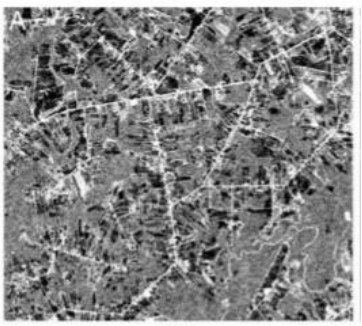 Image adapted from: [109]	Forestry	Monitor forest growth/deforestation identify tree species and observe and forest or burnt areas.
SeaWiFS – MODIS and MERIS	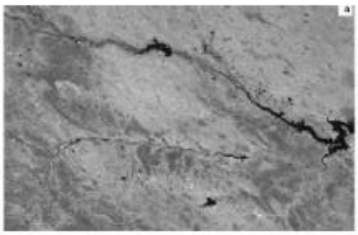 MODIS image adapted from: [110] 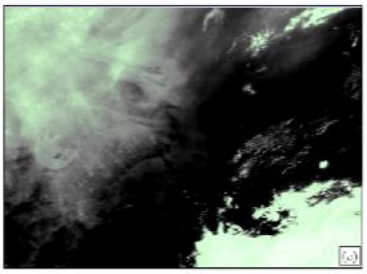 MERIS image: [111]	Fisheries, water sources and emergency response	Ocean and water body parameter monitoring such as: sediment transfer, turbidity, pH, chlorophyll concentration, dissolved oxygen, algal blooms and marine phytoplankton. SeaWiFS can also monitor oil spills, water pollution and characterization of fish habitats.
Total Ozone Mapping Spectrometer	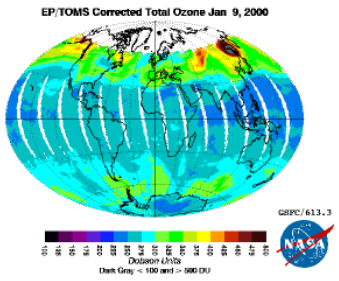 Image adapted from: https://disc.gsfc.nasa.gov/datasets/TOMSEPL3_008/summary	Climate activity	Used to monitor the ozone as well as monitoring and observing cloud cover, pollution and aerosols within the atmosphere.

A common application of remote sensing for water quality monitoring in catchment is the detection of chlorophyll a (Chl-a) in water bodies, an indicator for harmful algal blooms (HAB) associated with an overabundance of nutrients such as phosphate in the water body. *Jian et al.,* investigated the use of MERIS derived data to characterise the short term variance and temporal scale of Chl-a [112]. The author and co-workers used *in-situ* measurements and remote sensing Chl-a products using MERIS satellite images from 2003 to 2012. The study was carried out on the Poyang River, the largest freshwater lake in China. The study found that the optimisation of sampling and monitoring strategies are of vital importance for the investigation of short-term dynamics of Chl-a concentrations, the study took advantage of high frequency *in-situ* measurements as well as remote sensing platforms to characterise the variation in Chl-a levels*. Liu et al.,* also discusses the use of MERIS data to investigate secchi disk depth in immensely turbid waters [85]. The MERIS data was used to measure water colour so that the concentration of secchi disk depth could be estimated. MERIS data only be acquired once illumination conditions are suitable [113], by incorporating Landsat data into the study may have added value in the different images that could have been collected when illumination conditions were poor.

Although remote sensing techniques contribute to very promising outputs and offers a replacement method for field sampling, enabling fast, temporal, spatial and frequent observations [114], it still deals with some limitations concerning the accuracy of the products obtained, data continuity, excess tools and software for atmospheric correction (scattering and absorption effects, cloud cover etc) and the precision of the results [115][114]. Hence the added valve of combining remote sensing with another monitoring tool such as *in-situ* sensing devices. *In-situ* sensor technologies are often used in operation with remote sensing techniques to fill in gaps in the data as demonstrated in the above case study. Incorporating both monitoring technologies together leads to an increase in knowledge of the water quality within a catchment area. Adding different layers or monitoring technologies can significantly improve the impact of a study. *Vander Woude et al.,* perfectly demonstrates the use of a multi-tiered approach to monitoring HABs. This study was also carried out on Lake Erie and involved using a hyperspectral sensor to detect cyanobacteria harmful algal bloom (cyanoHABs) by carrying out frequent flyovers of the area. This study reported on the advantages of using satellite, airborne, and *in-situ* sensors as an integrative approach to investigate the variability of cyanoHAB events in Lake Erie and how these variances change over time and seasonally. It also demonstrated the use of airborne imagery and the cyanobacteria index (CI) as an indicator of the early detection of cyanoHABs.

1.6.2.5 Airborne Imagery

The term airborne imagery is given to the images that are taken of an area from an aircraft or a flying object such as a drone. They are also known as aerial unmanned systems (AUS). These systems are composed of red, green, blue (RGB), colour-infrared (CIR) and multispectral (MS) cameras attached to these AUS' [117]. They allow for near real-time monitoring of an area and comparably low operational costs, with the RGB cameras being the most economical [118]. Images from airborne sensors provide a unique method of monitoring seasonal changes in crop and soil conditions that can be time critical for catchment monitoring [119]. However, for more complex analysis RGB cameras are not sufficient, an MS camera would be required. MS cameras have more spectral bands and therefore allow for more detailed studies to be carried out on the area [117]. Drones are more efficient and cost effective, they are generally the more common method for carrying out analysis. These systems are used to get a better visual representation of the area being studied. These images are generally taken from a height between 500 and 1,000 meters. The drawback to this method of monitoring is that the payload for most of these systems is relatively low, therefore what instruments are chosen are important.

Airborne imagery is used in water quality catchment monitoring by utilising high resolution spatial information it can gather. In a study carried out in 1997 the authors used airborne imagery to develop a semi empirical relationship between the images processed and suspended solid (SS) concentrations in a river in the Humber catchment, York, UK. They used the irradiation reflectance to determine the SS concentration calculations. They used an imaging spectrometer mounted to an aircraft to map the distribution of SS [120]. This method represents a less intensive and less invasive way to carry out water quality measurements, however similar to the previous remote sensing techniques, this is not a stand-alone method and is often used in parallel to *in-situ* monitoring to validate the data being obtained. These techniques generally only use *in-situ* methods to calibrate or validate their method, there has not been many published results to show the effectiveness and importance of incorporating both aspects of monitoring to better observe and protect a catchment.

1.6.2.6 Autonomous Underwater Vehicles (AUV)

The most recent developments in the area of remote sensing is the growth of autonomous underwater vehicles which are also known as unmanned underwater vehicles (UUV) or remotely operated vehicles (ROV) [121]. AUV's are commonly used in oceanographic monitoring and are becoming more popular for industrial applications and environmental monitoring. These new machines have demonstrated to be cost-effective, efficient and safe alternatives [122] for water quality assessment and monitoring. They employ the same "deploy and forget" ethos as autonomous sensors. They facilitate the ability to mount multiple water quality key parameters on board the vehicle which can then be deployed in remote areas. AUV's require tether connections in order for them to be powered and controlled, this is done via fiber microwave transmissions, fiber optics, remote controllers, communication media and satellites so that they can receive and send data [122]. The hulls of these devices are becoming smaller as the need to minimize manufacturing resources increases, cutting down on power, fabrication costs and time [56] are all important aspects for the new wave of AUV's.

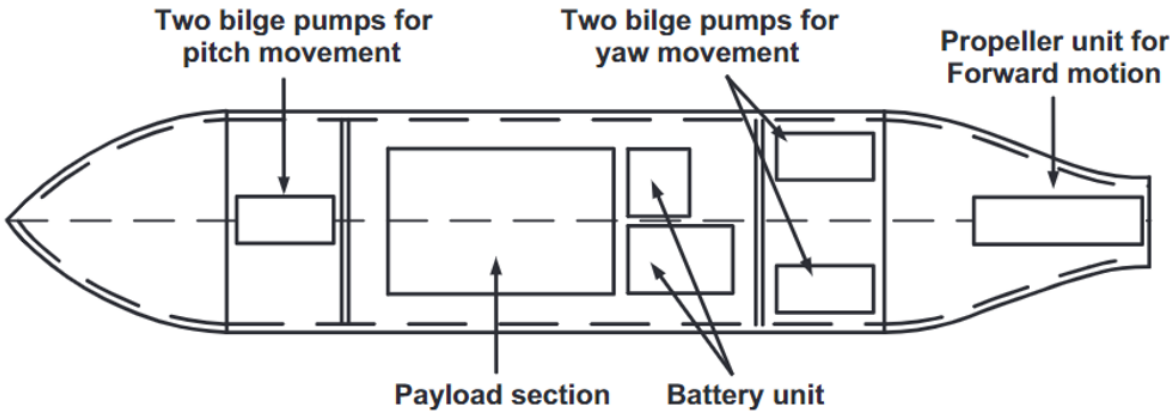

Figure 1.8 Schematic of a typical AUV system.

Figure 1.8 displays a simple schematic of a typical AUV, this is an early prototype and new models have been fitted with more sophisticated gear but still rely on the same components mentioned above for controlling an operation [123]. The simple building blocks of an AUV have been enhanced with more current technologies such as cameras, image transmission antennas, GPS navigation system, water sample collection compartment, ultrasonic sensors and a communication antenna on board the device. The more that can be added to the vehicle is dependent on the payload the design can hold, therefore the bigger the payload the more sensors and applications that can be added to the vehicle [124]. The designs are generally based on a prototype that is easy to deploy and recover without the need for specialised equipment. Most of these devices are built from readily available off-shelf components so that costs are kept to a minimum. The specific design requirements are based on the potential

applications for these machines such as environmental monitoring, the possible requirements to be considered for this application are as follows:

1 The operating speed of the AUV commonly used for surveying [125].
2 Length of the hull must be easily transported but have a high enough payload to support all potential environmental sensors.
3 Efficient room on board to facilitate a controller unit, batteries, as mentioned sensor for environmental use and a potential water sampling component.

Capable of maintaining a modular configuration for ease of access to the components within the system [126].

1.7 Data Management and integration challenges

With a tiered approach comes the challenge of data management. Data management involves data collection, storage, analysis, interpretation and provision of information for the user. The main purpose of data management is to extract high level information from the raw data collected from the physical world, to assist environmental scientists in better understanding, better modelling, better planning and better protecting of our natural environments.

The integrated and coordinated sectors of sensing, communication and computation has led to a rise in connected devices (new reaching at Internet level) that are low-powered, relatively high accurate and cost effective. The increase in sensor data has facilitated the utilisation of web-based data services such as cloud storage and processing [127]. New data management technologies have been accelerated with artificial intelligence (AI), data management automation has been enabled through AI capabilities. By integrating AI into data management strategies, it may potentially solve the problem of “Data rich but Information poor” [128].

The development of novel AI methods, especially the introduction of deep learning in recent years, and the increase of computing power, the time is right for internet scale water monitoring. The concept of Internet of Things (IoT) has previously been described as an integrative system that incorporates computing devices, digital and mechanical machines so that data can be transferred and analysed without the need for human interaction [129][130]. Data driven environmental monitoring includes the collection of dynamic, complicated, extensive, temporal and spatial data that needs to be efficiently stored and processed. The type of data collected is dependent on the type of sensing technology used, this can range from; 1D electrical signals, 2D images to 3D videos. The use of data management platforms allows for the “big data” to be collected, stored and processed. Wireless sensor networks (WSN) are commonly used for catchment monitoring [131]. WSNs enable real-time collection of spatial and temporal data, providing catchments with trends on water quality pollutants and contaminants. Allowing for integrated water quality monitoring, control and management

decisions to be made [132]. However, obtaining WSN data can be challenging for environmental applications. The networks require a large set of sensors, they must be affordable, relatively reliable, low maintenance, long battery life and robust (withstand varied climatic conditions) [133], adding to the challenges of incorporating WSN into catchment monitoring programmes.

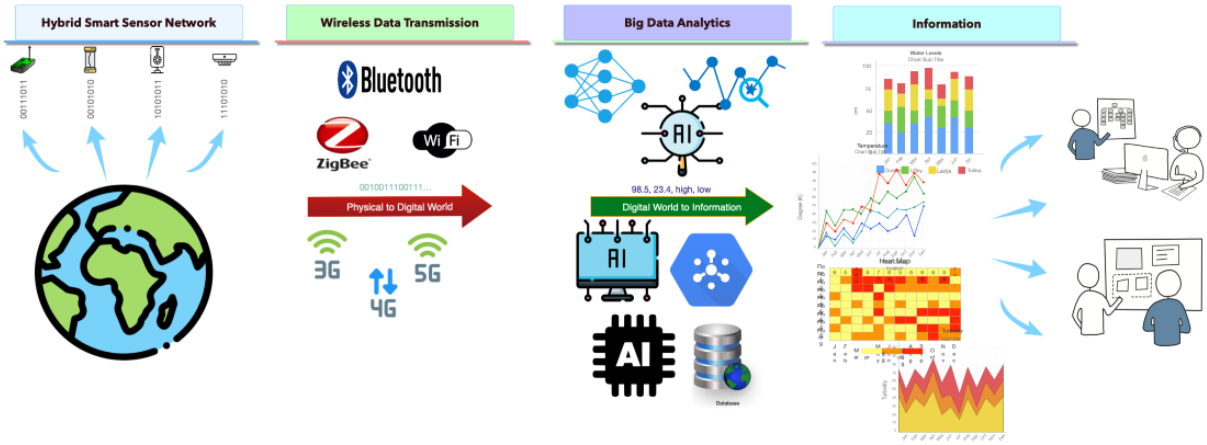

Figure 1.9 Flowchart of data management and analytics used in catchment monitoring.(Freepik, Eucalyp and Payungkead from www.flaticon.com)

Recent developments in the area of portable *in-situ* sensing technologies have grown in the last 10 years, sensors are now capable of long-term deployment with real-time data analysis [83][134][135][136]. The main drawback to these sensors is the cost point, which restricts the adoption of this technology at the scale needed for useful catchment management, provided a gap in the market for low-cost handheld sensors. The development of these long-term monitoring technologies has shown strong correlations between the surrounding climate and catchment properties enabling the temporal and spatial detection of environmental change [137]. The advances made in smart devices linking sensors and other platforms to the IoT which can be programmed and monitored remotely has led to the increase in demand for technology driven monitoring. It has enabled the ability to monitor significant water quality parameters in real-time.

1.7.1 Needs and opportunities

Having a tiered approach to water quality monitoring enables the collection of a vast variety of data. Satellite images can detect, land cover/land use changes and water quality indicators using colour indices. Airborne imaging using RGB cameras are commonly deployed to carry out less intensive field surveys. *In-situ* monitoring is regularly used in catchments to observe

and changes and trends in the catchment including common water quality parameters such as nutrients, sediment transfer, turbidity, pH, chlorophyll concentration, dissolved oxygen, algal blooms, flows, water levels and conductivity to name a few. Mapping of the area gives a detailed account for the type of land and soil in the area and how it has changed in recent years. Lastly using predictive models allows catchment managers to forecast or prevent threats to the catchment, the predictive models act as early warning signs and alarms to help maintain the quality of the catchment. This tiered approach has proven extremely important in recent years due to the overwhelming threat of climate change. It highlights the value of using a combined approach to monitoring as it enhances the level quality (satellite and airborne imagery) and the quantity (*in-situ* and handheld devices) of data being collected.

1.8 Conclusion

The application of a tiered framework of integrated technologies for catchment monitoring will enable us to extend our perspective and apprehend the dynamic processes and behaviours of individual catchments with specific focus on nutrient levels. Few studies have demonstrated the full use of a tiered approach to water quality monitoring in a catchment. The main barrier of implementing each layer involves the availability and cost of technologies. Although efforts have been made to drive down the cost of these *in-situ* and autonomous sensing technologies, maintenance of the sensing equipment and vandalism can also incur repair costs or replacements. The main remote sensing limitations involve the knowledge needed to capture and analysis data, such as the excess tools and software needed for processing and the non-availability of continuous monitoring. There shows great potential for new technologies such as handheld devices to be used in conjunction with more sophisticated technologies such as remote sensing and autonomous devices. Handheld sensors can be used to compliment or provide a method of ground truthing. These types of sensors can be used to bridge the gaps in data collection and add value to an existing observation framework.

Chapter 2: Design and fabrication of a multi-test analyte microfluidic disc for the determination of phosphate

2.1 Introduction

Microfluidic systems are miniaturised reaction devices that are produced by using microscale technologies [138]. Within the last 20 years the motive for using microfluidics platforms for environmental applications has increased. The concept of microfluidics provides a wide array of opportunistic merits that benefit many environmental applications. Environmental monitoring is presented with a number of challenges such as the samples and reagents required for analysis, operation period, robustness, size and integrative systems. This has led to a demand for growth and research within this area. More emphasis has been put on analytical techniques that can be used to monitor the growing number of environmental pollutants [139]–[141]. The instruments and technologies such as UV/vis spectrometry and ion chromatography, previously used for analysis generally consisted of large, high powered, labour intensive, time consuming and costly equipment [142]. The evolution of fast, efficient, reliable, microscale technology and engineering to appoint a three-dimensional structure with diameters typically within the ranges of 10-500µm [138] robust microscale systems which offer solutions to the issues and challenges raised by current sensor systems available, will have a massive impact on existing commercial market.

2.1.1 Microfluidic sensors used in environmental monitoring

The expansion in the biochemical, pharmaceutical, and medical industries has led to an ever-growing list of contaminants and with that has come additional environmental legislation and regulations. The growth in the number of pollutants being regulated has increased the demand for more environmental monitoring. The use of microfluidics used in the monitoring analysis provides an alternative to the time-consuming and the large costs involved with standard laboratory instrumentation. The involvement of microfluidics has enabled the complete assessment of pollutant distribution through on-site, real-time and continuous monitoring [142]. The use of microfluidics in environmental monitoring has been demonstrated through the development of a microfluidic paper-based analytical device (mPAD) for the colorimetric detection and determination of nitrate in environmental samples. *Cardoso et al.,* describes the importance of disposable microfluidic paper-based devices for environmental monitoring. The device is based on a modified Griess method, has an LOD of 5.6 µM, low sample volume of 400 µL and a stability profile of 12 h. Two environmental water samples were tested on the device. The colorimetric detection was carried out using a scanner with 600 pots per inch (dpi) resolution. The images were captured 15 min after the reaction period [143] (see Figure 2.1).

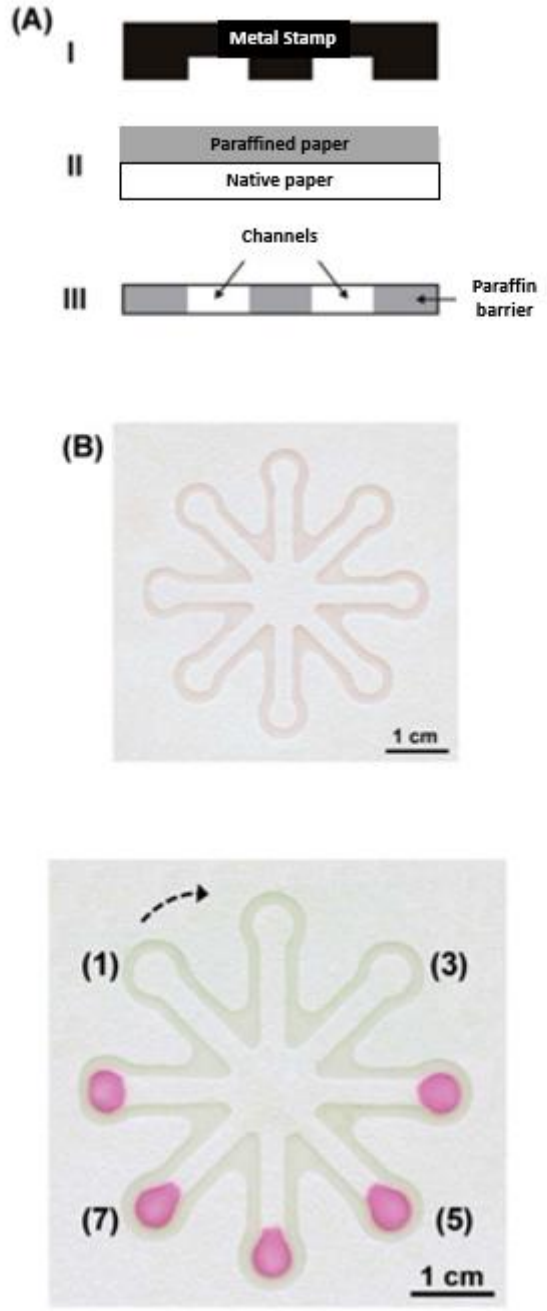

Figure 2.1 (A) steps involved in the stamping-based fabrication technique, including (I) metal stamp with microfluidic microchannels, (II) parafilm place on paper, (III) hydrophilic channels formed from paraffin barriers and (B) a final stamped mPAD, the magenta spots in spots (5-7) correspond to the presence of nitrate in the sample being analysed.

The device described in this paper presents an extremely sensitive method for the detection of nitrate. However due to the nature of the materials involved in the fabrication of the device may cause problems concerning robustness of the sensor for field applications.

A Lab-on-chip (LOC) analyser for the *in-situ* determination of dissolved manganese (Mn) in seawater samples was developed by *Geißler et al.,* and co-workers. This LOC device was developed based on the principle of spectroscopy, with low power and high sensitivity, ~1.5 W and 27 nM respectively. It also has an extremely low sample volume of 63 µL. The sensor was deployed in coastal waters in Germany, where Mn concentrations were high due to sediment levels, runoff from freshwater and other anthropogenic inputs. This paper demonstrates the importance of fabricating a robust device that can be used continuously in the field [144].

Another area taking advantage of microfluidic analysis is the detection of microorganisms, this study describes the development of a device for the detection and measurement of algal toxins using a microfluidic immunoassay carried out by *Zhang et al.,* The immuno-enzyme assay was integrated into a Polydimethylsiloxane (PDMS) microfluidic chip for rapid and automated analysis of algal toxins. The system has a linear range of 0 – 5 ng mL^{-1} and an LOD of 0.02 ng mL^{-1} with a detection time of 25 min, this device illustrated the successful detection of microcystin, saxitoxin and cylindrospermopsin. The microfluidic chip was manufactured using multilayer soft lithography, using moulds to create the microchannels. The chip itself is 30 mm x 30 mm in dimension, consisting of two layers the top layer used to incorporate the fluidic pattern and the bottom layer used as the pneumatic control layer [145], see Figure 2.2.

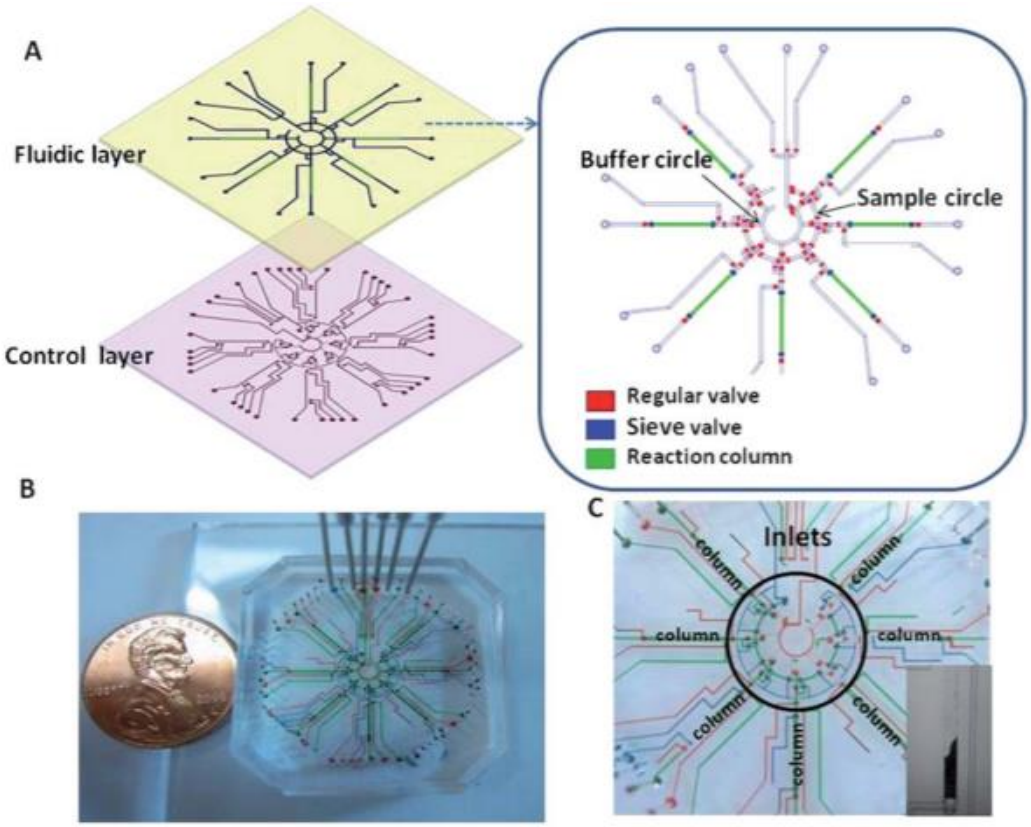

Figure 2.2 Schematic of the microfluidic lab-on-a-chip devices used for the detection of algal toxins. (A) The valves (red and blue) are used for the isolation and capture of protein A beads. (B) Channels filled with food dyes for visualisation of the components of the chip, an 18.9 mm diameter coin shown for reference. (C) Showing the area containing the immune-reaction columns.

2.1.2 Criteria for the development of a microfluidic device for nutrient detection

The desirable criteria for a field nutrient sensor typically include real-time or near real-time measurements, on-site detection, robust, reliable, low limit of detection, dynamic linear range and cost effective. The attributes of microfluidics and its ability to manipulate fluidics, provide high precision metering, storage and creation of sequence pauses, transport of materials through microchannels, storage of reagents in chambers or reservoirs and the incorporation of detection systems enables the development of fully integrated and successful platforms suitable for use out in the field. One of the first major advantages of using microfluidics was the volume of liquid required within a microfluidic system to carry out an analysis [146][142]. The volume of fluid typically found in these devices range from micro-litre (10^{-6}) to nano-litre (10^{-9}) with other devices reporting volumes as low as atto-litres (10^{-18}) [147]. The small fluid volumes that microfluidic devices require to function facilitate a reduction in the consumption of sample and reagent, this can lead to a decrease in reaction and detection time [148]. For microfluidic systems to progress from lab to field they need to become a fully integrate d device.

Essentially what the end user would like is to simply load the sample into the device and obtain the result. The need for reduced steps to simplify the process is crucial for these devices to be used out of laboratory settings eliminating possible risk of contamination, hence why reagent storage is now a requirement for many systems. Reagent storage addresses two main limitations of microfluidics devices gaining commercial and field-testing abilities as it provides answers to long term reagent storage and increased lifetime. In addition, it can provide valves that act like micro dispensers. Integrating these into microfluidic devices allows for storing, valving and metering to take place on a single unit [149]. This will be further discussed in Chapter 3.

2.2 Theory behind centrifugal microfluidics

The hydrodynamics of a microfluidic system is extremely important for the successful development of pressure-driven systems [150]. This section gives a brief insight into the theory of microfluidics with emphasis on centrifugally based systems. It will discuss how different theoretical fluid flow and fluid attributes are utilised in the development of microfluidic devices. Focusing on the use of centrifugal systems and how these theories can be applied to the system, and the additional forces that centrifugal systems are susceptible to.

2.2.1 Laminar Flow

Laminar flow is the name given to the non-turbulent flow of fluid that occurs in microfluidic systems. The flow of the fluid is said to be sheet-like adjacent layers that slide over one another [150][151][152]. There are three main flow conditions for laminar flow to occur: (a) low fluid velocity, (b) adjacent layers do not mix and (c) field of velocity vectors constant in time. A schematic representation of a laminar flow inside of a microfluidic channel is demonstration in Figure 2.3.

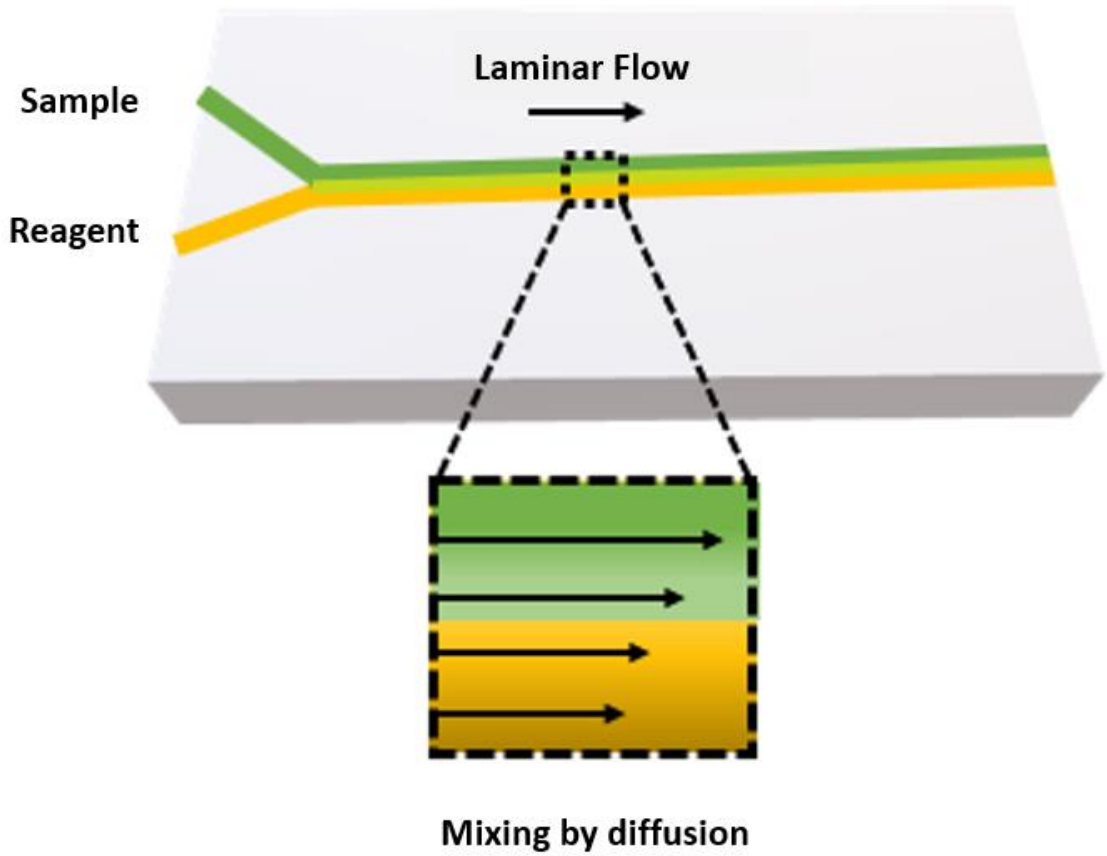

Figure 2.3 Graphical representation of laminar flow inside of a microfluidic channel.

2.2.2 Surface tension and cohesion

Fluids at a microscale level behave differently to fluids at a macroscopic level [153]. Fluids in macro systems are hugely affected by atmospheric and gravitational pressures. Whereas surface tension, cohesion and capillary action are reliable for the fluid dynamics generally seen in micro systems [154]. As the volumes decrease in these microsystems the surface-to-volume ratios increase, this leads surface tension becoming the dominate force of the fluid it is acting on [155].

2.2.3 Acting forces

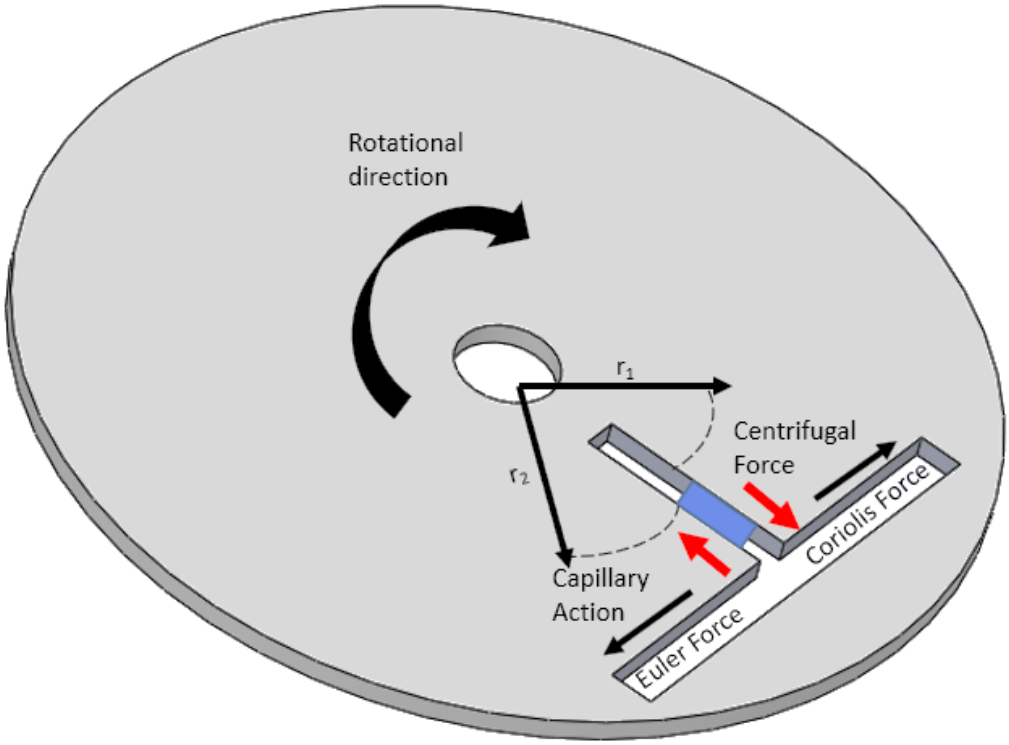

Figure 2.4 Illustration of the different physical forces encountered on a centrifugal disc.

Figure 2.4 illustrates the difference in intrinsic and extrinsic forces and what roles they play in centrifugal microfluidics. Intrinsic forces are inertial body forces that manipulate fluids on a rotating body [156]. These forces are generated for centripetal force supplied by some sort of motor/power source. Extrinsic forces are forces that generate motion in fluids, this can be done magnetically, electrically, or by using pneumatic forces [153].

Euler force is the term given to the pseudo diverging force that when a non-uniform moving frame is used for motion analysis [157]. The forces that are produced by these rotating devices are used to drive and manipulate microfluidic fluids and carry out functions such as mixing, fluid storage, metering and diluting. Another force that influences how fluids move on rotating bodies is the Coriolis effect, this is important for microfluidic discs as it controls how the fluid

mixes and also switches [158]. The centrifugal force relates to the force that is seen on a moving body and appears to be moving away from the centre of the rotating platform [159]. The last force that impacts the movement of fluid in microfluidic discs is capillary action, this is the movement of fluid within space and the different forces that occur during that movement such as adhesion, cohesion, and surface tension. It depends on the type of material, whether the fluid is polar or non-polar. For example, if the water was travelling through a glass tunnel it would have a concave shape due to the capillary attraction between the water and the glass.

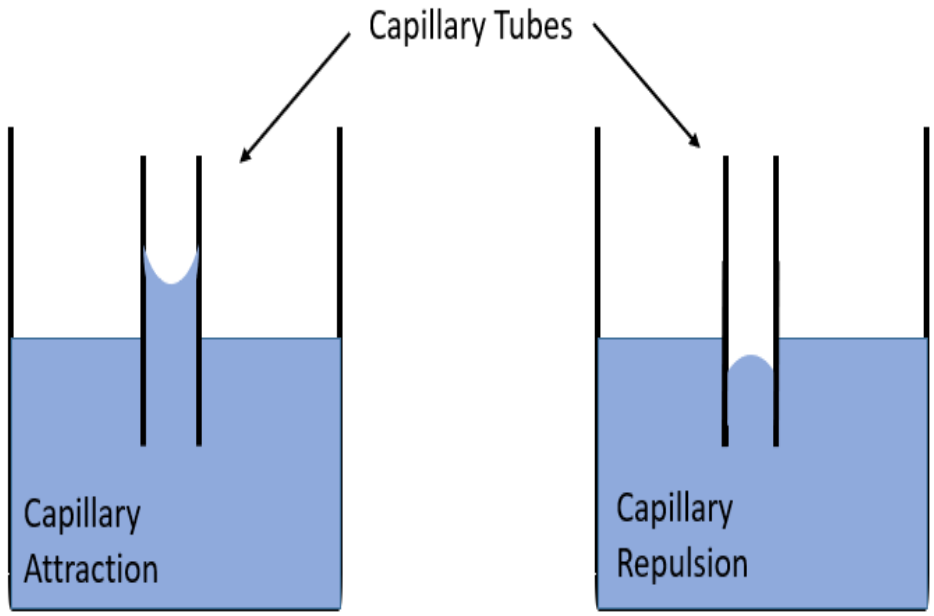

Figure 2.5 Schematic diagram of capillary action in microfluidic channels.

Capillary forces are a common phenomenon in pressure-driven centrifugal microfluidics [160]. Siphon valve techniques usually utilise capillary forces to enable fluid transport [161]. Most materials used in lab-on-a-disc (LOAD) devices are hydrophobic and therefore to employ siphon valves successfully some surface alterations are needed for capillary action to occur [162]. The use of capillary driven flow for the bases of a microfluidic device is described by *Hassan et al.,* this study describes the use of capillary valves to manufacture a "chip and dip" device for the determination of β-lactamase activity and cortisol. Capillary action is used to load the sample into the microchannels, where it reacts with the reagents to produce a colorimetric signal [163].

The design for the centrifugal microfluidic disc described in this chapter takes advantage of capillary action using it to facilitate fluid flow from the mixing chamber to the detection zone, this has to do with the liquid and the surrounding surface. The air vent is also wider than the microchannels to ensure that the water does not travel up the air vent when measurements

are being carried out in the pathlength. Depending on the surrounding surface material it can cause capillary attraction or repulsion. Capillary action was also introduced into the design of the disc by controlling the sizes of the microchannels and increasing the diameter of the air vent channels. In addition, centrifugally spinning the discs allows for capillary action to take place causing pressure driven flow.

2.3 Design, fabrication, and manufacturing techniques used in microfluidic devices

There are a wide span of approaches that can be taken when manufacturing microfluidic systems, these include reaction ion etching [164], wet etching [165], machining [166], soft lithography [167], photolithography [168], hot embossing [169], laser ablation [170] and injection moulding [171][172]. The two most common approaches used in microfluidic device manufacture include: photolithography and non-photolithography, which will be emphasised in this section and will provide a brief description (materials specificities, equipment required, cost and feature size), characterisation and list of advantages and disadvantages associated with each method.

1. Photolithography: this method is used in microfabrication is used to produce a pattern on a film substrate by using light. This light is used to transfer a pattern from a photomask to a light-sensitive photoresist [173]. Because this method generally only allows for two layers it would be more consider for LOC technologies rather LOAD devices. This method allows for sub-micron resolution (usually 1 µm); however, it requires expensive lab equipment (for example a spin coater, deep reactive ion etcher, convection incubator and a laminar tissue culture flow hood [174]), clean room requirements and can increase manufacturing time.

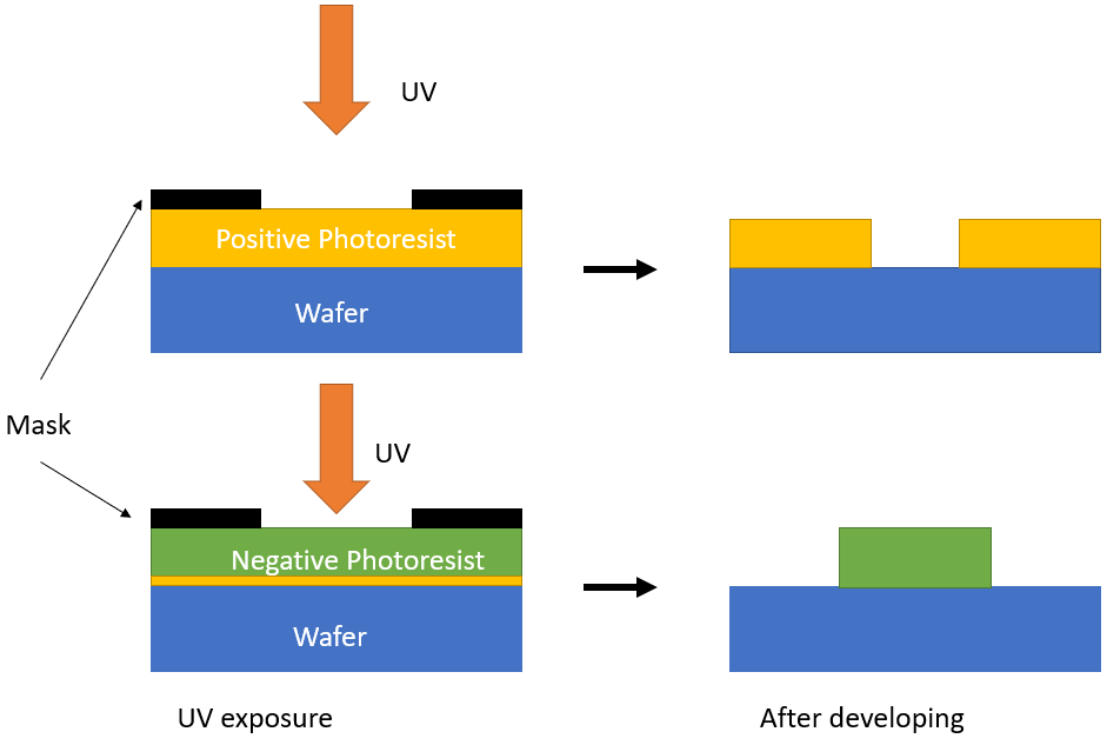

Figure 2.6 Two different fabrication methods that are used in the manufacture of microfluidic discs.

2. Non-photolithography: Most common method for developing centrifugal microfluidic discs. This method is used to develop a pattern on a surface [175][176]. This approach is better fitted to the idea of a multilayer microfluidic disc over the typical photolithographic method as it allowed for more layers to be incorporated into the design. In comparison to the previous method, non-photolithography has lower costs associated as the equipment is less expensive and therefore the cost per disc is reduced, however it has a lower resolution of about 500 µm.

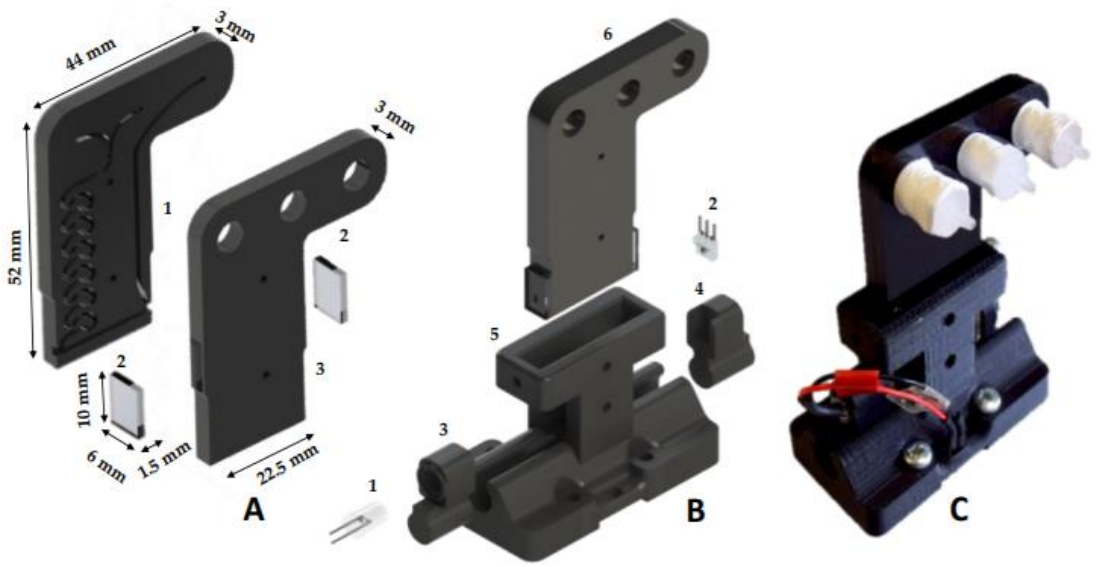

Figure 2.7 A) Rendered image of the two layered microfluidic chip, the top PMMA layer contains the milled reagent/sample inlet and waste outlet. (B) 3D printed alignment mount and detector components (LED and PD) and (C) Image integrated components [177].

Microfluidic chips consists mainly of two layers [178][179][180] (but can be multi-layered depending on functionality [172]), one-layer housing the channel design which contains all the pumps and vessels and the other layer which housed the optical components such as the Light-emitting diode (LED) and Photodiode (PD). The two dominant layers are bonded together by chemical, adhesive or thermal bonding [181], shown in Figure 2.7. In comparison the work carried out by Cogan *et al.*, also discusses the development of a microfluidic chip for the detection of nitrate in natural waters using a multi-layered chip design. The design is included 7 layers incorporating a cap layer, inlet features, waste line, serpentine mixing channel and base layer. The chip is sealed using a thermally bonded method and applying pressure to the layers using a callipers [99].

For a microfluidic disc, generally more than two layers are required. In the design presented in Figure 2.8, three layers of poly(methyl methacrylate) (PMMA) and two layers pressure sensitive adhesive (PSA) were used to manufacture the disc for the detection of nitrite. These different layers house the inlets (Top PMMA), reservoirs (Middle PMMA), valves (Bottom

PMMA) and microchannels (Bottom PSA) which are desired to manipulate and direct the fluid around the disc in a highly ordered manner.

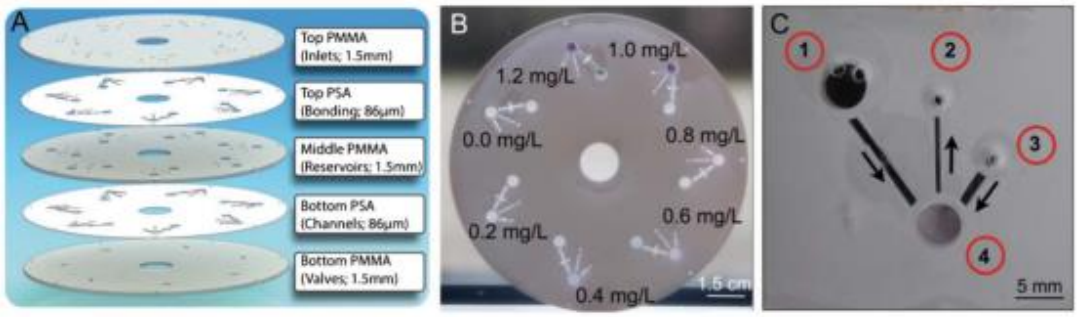

Figure 2.8 (A) Multi-layered microfluidic disc, assembled using three layers of PMMA and two layers of bonding PSA used for the detection of nitrite, (B) Assembled disc with seven microfluidic features filled with varying concentrations of nitrite and (C) Microfluidic feature functions: 1–inlet, 2–air vent, 3–inlet reagent, 4–mixing/detection chamber [182].

2.4 Enhancement of optical components for high sensitivity detection

Enhancement techniques are generally applied to amplify or strengthen the optics within a system. They are used to create phenomena such as total internal reflection (TIR), change the refractive index (RI), increase, or decrease light scattering or alter the reflectance properties.

Light travels in three distinct ways; through material/medium, directly, or indirectly. The definition of a ray is derived from a mathematical term that is used to describe a straight line that is created from a certain point [183]. A ray of light will continue to travel in a straight line, whether it is passing through or reflecting off a certain medium. The way in which a ray moves is conveyed through trigonometry and is commonly referred to as geometric optics [184].

Reflectance is an important aspect of manipulating light within a detection pathlength. It refers to the light that is returned when bounced back of a certain type of reflective material such as a mirror. Reflectance occurs when a light ray is reflected at a specific angle (angle of reflection) [184]. This is illustrated Figure 2.9 in where the angle of incidence is greater than the critical. An extension of this phenomenon is TIR which refers to when a propagating light wave hits a medium at an angle that is larger than the critical angle. This critical angle θc is the angle above which TIR can occur [185][186]. The equation to describes this is given as:

Equation 2.1 Critical angle θc calculation is derived from Snell's Law

$$\theta c \; arcsin \frac{n2}{n1}$$

If a light wave is incident upon an optical fibre with an angle of incidence greater than the critical angle, then the light will remain "trapped" inside the medium – this light can travel a

long distance in this medium without a significant loss of light occurring. For TIR to occur there are two conditions that must be met:

1. The light travelling through a medium with a higher index of refraction and must be approaching a medium with a lower index of refraction.
2. The angle of incidence must be greater than the critical angle.

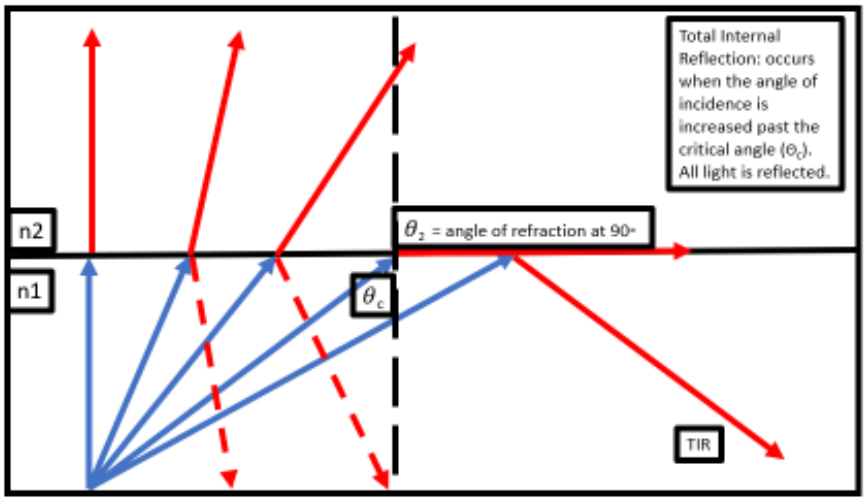

Figure 2.9 Schematic illustrating TIR, the critical is the angle of incidence that produces an angle of refraction of 90◦. Increasing the angle of incidence past 90◦ no light will be reflected across the medium boundary.

The critical angle is the angle of incidence above which TIR can occur, θc is given by Snell's Law:

Equation 2.2 Snell's Law

$$n1sin\theta1 = n2sin\theta2$$

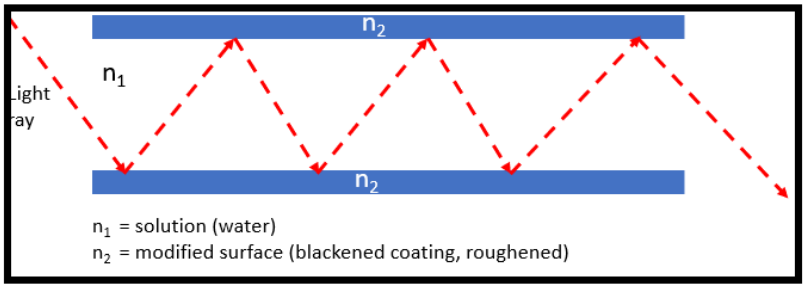

Figure 2.10 Schematic representation of TIR. The light does not refract into the second medium due to the index of refraction of the first medium being higher than the second and the angle of incidence being greater than the critical angle.

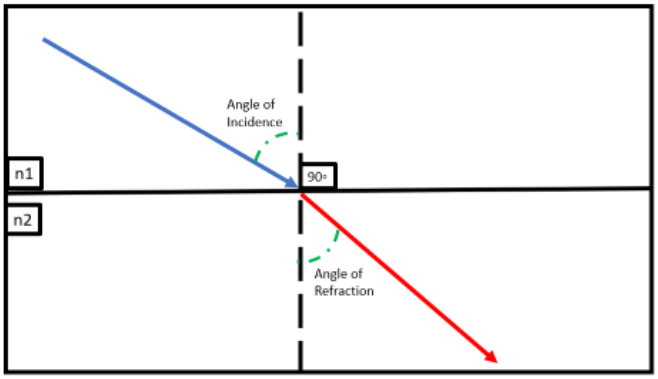

Figure 2.11 The principle of refraction of light passing from one medium through another with varying density.

Refraction refers to the bending of light, this usually occurs when a light ray passed from one medium through another. How much or little the light bends depends on: (1) speed difference between the two mediums, if the medium causes the ray to slow down or speed up it will be refracted more and (2) the angle of the incident ray – if the angle is greater than the incident ray it will cause more refraction [187]. RI alterations have been investigated to increase the sensitivity of a sensor. *Dmitriev et al.,* presents a RI sensitivity enhancement strategy by lifting the metal nanoparticles above the substrate by a dielectric nanopillar to double the sensitivity of the refractive index. This was achieved by enhancing the bulk refractive index sensitivity of the particle localised surface plasmon resonance, the pillar reduced the spatial overlap between the substrate and enhanced fields generated at plasmon resonance [188].

2.4.1 Optical enhancements used in sensing devices

Current components integrated into optical detectors include laser diodes, LEDs, optical fibers, optic lenses (convex, concave, confocal), diffraction or gradient elements, and camera imaging modules. These different elements are constructed together to manufacture a microfluidic device that can carry out analysis outside of a laboratory. They are integrated into devices to transfer light between the microscopic and the macroscopic world [63]. Waveguides such as fiber optics are the most commonly used in microfluidic device integration [189][186]. Waveguides are used to control or guide light propagation in a certain structure, the waveguide is usually utilized to increase the RI compared to the surrounding material known as cladding. A study published in 2018, described the use of graphene as a wave guide for an optical tactile sensor see Figure 2.12 for reference. The study showed that by placing an elastomeric superstrate such as PDMS on the graphene waveguide a prism structure will be formed, which resulted in a broader superstrate interface which was in contact with the graphene film. Hence this showed a reduction in strength of the interface and the intensity. This study was fundamental for exploring different materials for other coupler-based optical tactile sensors. [190]

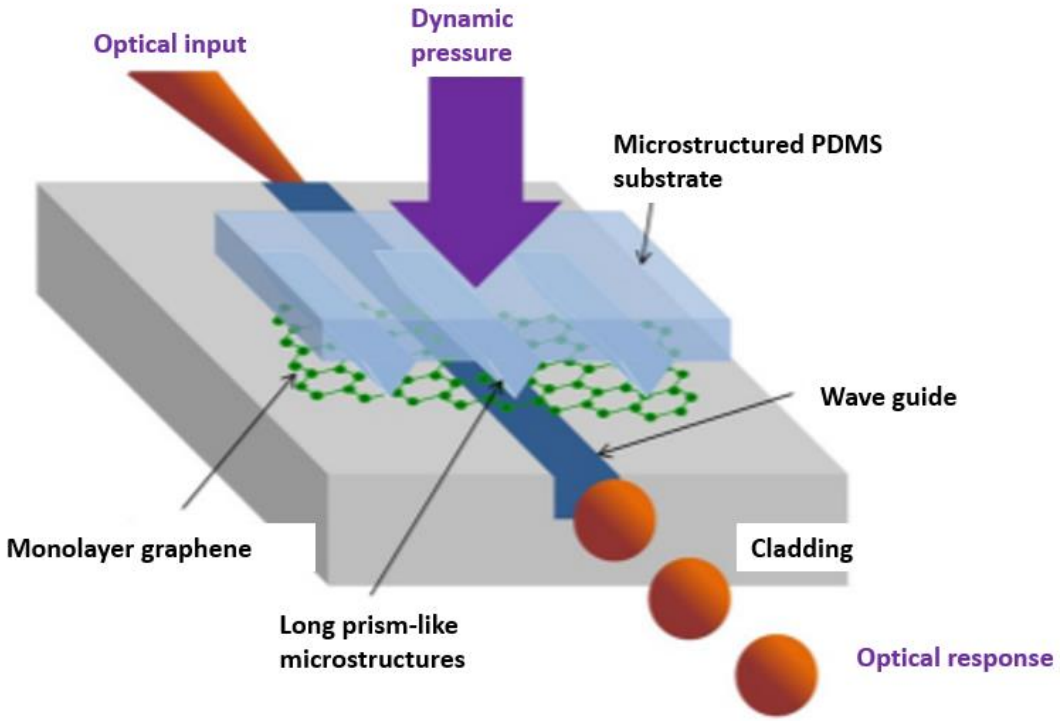

Figure 2.12 A graphene-based optical waveguide tactile sensor. Fabricated using graphene material and elastomeric superstrate. The graphene-elastomer interface became wider and guided light in the which was subjected to high attenuation due to the graphene.

Another method of enhancing optical performance in sensing devices is the use of mirrored or optical coatings. These types of optical enhancement techniques are usually employed to alter the RI within the detection channel of an optical device. The simplest method for developing a mirrored coating for integration is to use a metal mirror coating, usually aluminium or silver is used for this purpose, with a thickness of 100 nm. The reason these two elements are commonly used is due to their reflective properties [191][192]. *Reid and Martin et al.*, demsonstrate the relevance of developing mirrored coatings for gravitational waveguide detection sensors. The mirrors were used as highly reflective components to detect differential fluctuating quadrupolar tidal strains along perpendicular paths in space. This paper also discusses the thermal noise effect that mirror coatings can have in a sensor creating problems with sensitivity and detection [193]. *Krogmeier et al.,* illustrates how the development of these mirrored coatings can be applied to microfluidic devices. This study highlights the integration of microfluidic device for DNA stretching and the combination of a plano-aspheric refractive lens as an illuminator for fluorescence excitation and a parabolic reflective mirror for fluorescence collection [194], see Figure 2.13.

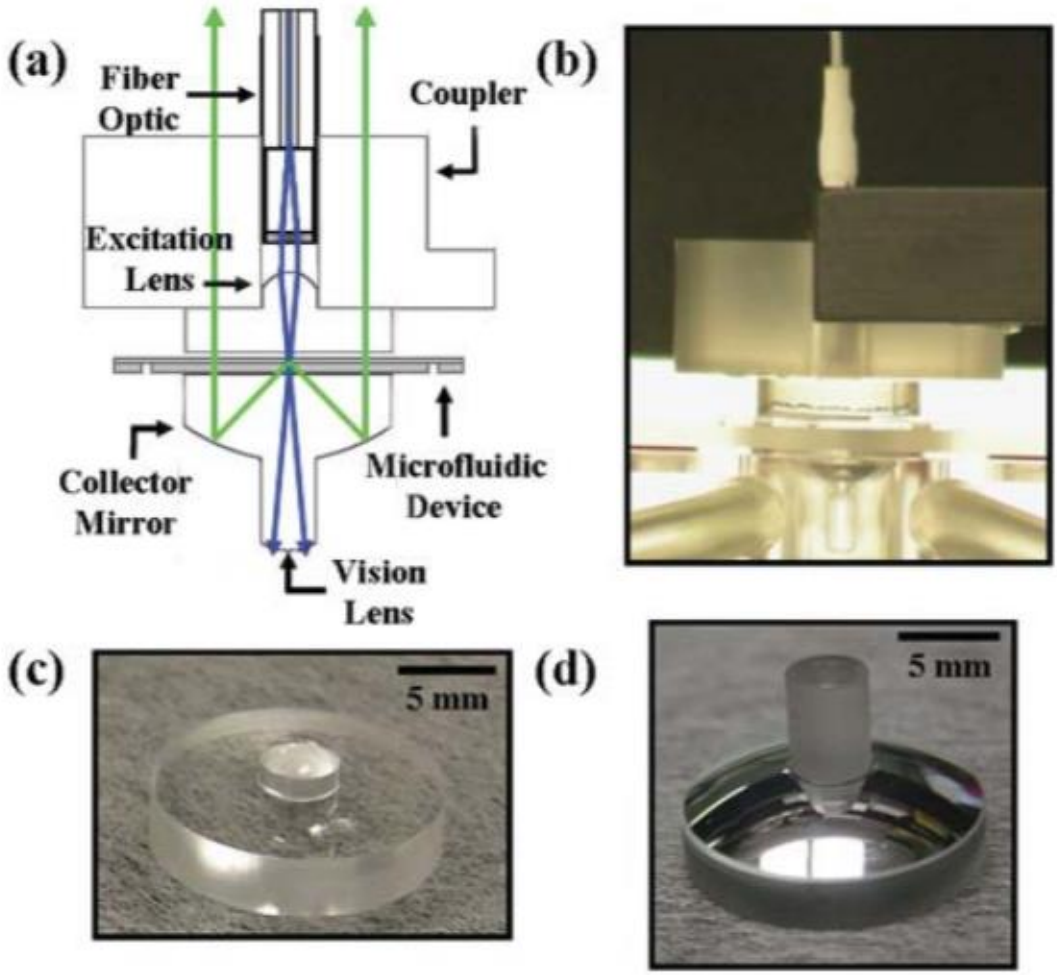

Figure 2.13 (A) Optics device with all components including refractive excitation lens, microfluidic device, reflective mirror and vision lens. (Excitation laser in blue and fluorescence in green), (B) assembled device, (C) collector mirror and (D) the illuminator lens is constructed on a 15 mm planar disc for ease of manufacturing.

Other types of coatings include sol gels. These types of coatings are usually doped with nanoparticles (for example ZnO_2 [195] or SnO_2 [196]) to enhance specific optical properties. *Pènard et al.,* and co-workers discuss three main areas where sol gel coatings are used in optical applications: [197]

1. Development of luminescent and transparent films.
2. Low refractive index films such as mesoporous silica films.
3. Using silica films as binders for nanoparticles in photocatalytic devices.

The increase in demand for development of new technologies in the area of digital and mobile imaging, internet-based videoing capabilities and biometrics has led the in the growth of interest in using cameras as an optical enhancement technique [198].

The last 10 years has seen a rise in the interest in camera imaging being integrated into optical devices to enhance detection properties. More recently complementary metal–oxide–semiconductors (CMOS) have been researched and developed to fabricate low cost optical sensors [199][200]. The technical progression and cost efficiency saw an increase in the demand for CMOS cameras. They are incorporated into these devices as optical detectors and provide fast and sensitive detection due to their dynamic range and high signal to noise [201]. *Yan et al.,* demonstrated the integration of a CMOS imager and microfluidics to develop a point-of-care diagnostic tool. This integration of the CMOS camera facilitates a high throughput of 6000 frames/second and achieves excellent low-light sensitivity by the large pixel size (10 µm x 10 µm), increasing the resolution by four fold compared to conventional microfluidic imaging systems [202].

One of the most importance components in a device for optical enhancement is the light source and its intended use. The two most common light sources used in optical sensors are LEDs and lasers. LEDs are widely used in electronic platforms due to their low cost, robust, low power, small size and energy efficient nature [203]. They cover a broad spectral range from UV to near infrared and are widely integrated into optical sensors and reflectometer devices. Figure 2.14 conveys a schematic illustration of a common microfluidic device with an integrated optical detector. The incorporation of optical components into this microfluidic manifold enables it to carry out all chemical functions and detection in a single device, this requires the integration of all electrical and fluidic elements to be incorporated, creating an “on-chip” or “on-disc” approach. The device described here incorporates electrical components (power supply and microprocessor), fluidic components (pump and chip module) and a detection system (optical). For a typical microfluidic and optical integrated device, LEDs are the most cost-efficient light source as they require low-power driving currents. They are compact in size making them suitable for, integration into microfluidic device [204]. The power supply produces the energy required for unit controls the processes data collection and transmission [130]. The power supply need to operate an LED based microfluidic sensor usually ranges from 2 - 5 V [205][206]. However, to interpret the data and analysis it, additional wireless technology such as Bluetooth, WIFI and mobile phone pairing devices increase the power needed to operate and transform the device into a smart system increasing the power supply to ~ 12 V [207], such as the battery employed in the system described in this thesis, see Table 4.2. Compared to commercial sensors on the market to date which require 10.5 – 18 V [208], this is a significantly low power supply requirement.

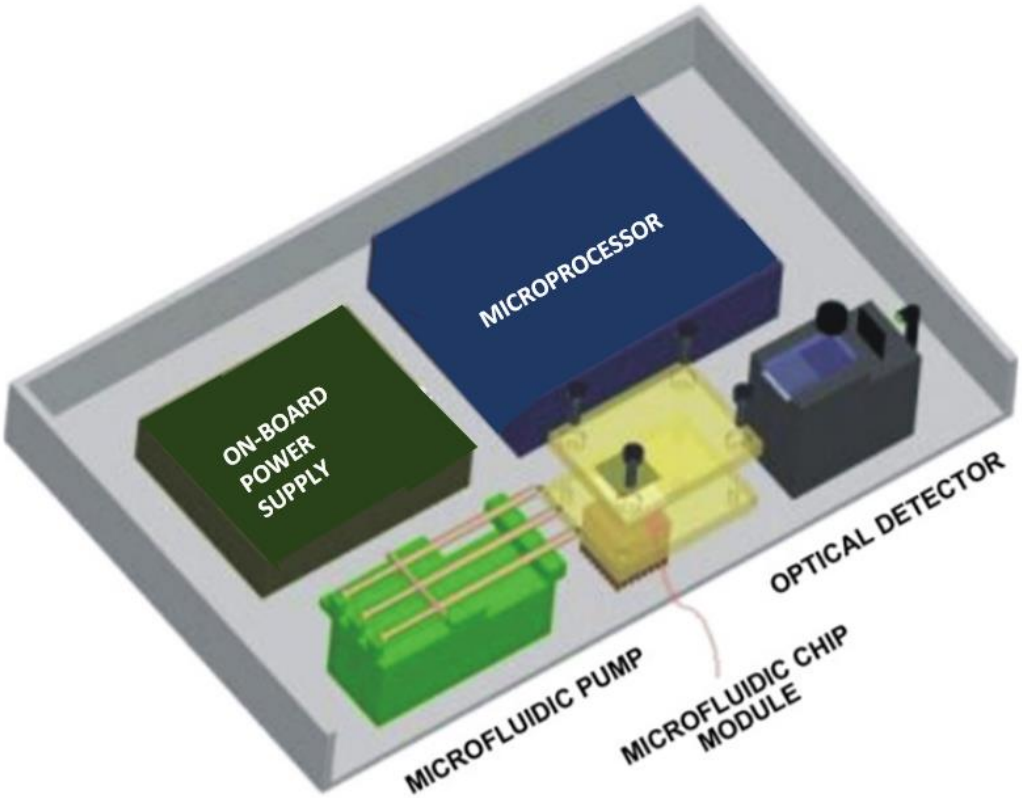

Figure 2.14 Schematic illustration of a portable microfluidic chip device with on board optical detection.

2.5 Aims and Objectives

The aim of this work is to showcase the use of microfluidics in the fabrication of a phosphate LOAD device for environmental analysis in freshwater catchments. The objectives are: (1) present to the reader a background in microfluidic theory and how these devices are manufactured, (2) demonstrate the design process of a LOAD device that can be used for multisampling detection of phosphate (3) investigate optical enhancement techniques to increase the sensitivity of the device to comply with the detection range and limit of detection set out by EU legislative (4) compare different microfluidic disc manufacturing methods to determine the impact on performance and (5) ensure that cost of manufacturing was low so that this disc could potentially be commercialised.

2.6 Materials and Methods

2.6.1 Chemicals

Chemicals and reagents used include potassium dihydrogen phosphate monobasic, ammonium molybdate tetrahydrate, potassium antimonyl tartrate, sodium hydrogen bisulfate and L-ascorbic acid (all purchased from Sigma Aldrich, Arklow, Ireland). Solutions and standards were made up using ultra-pure water (Elga Maxima®, 18.2 MΩ.cm. A 0.032 M solution of ammonium molybdate tetrahydrate, a 0.004 M solution of potassium antimonyl tartrate and a 0.1 M solution of L-ascorbic acid were prepared. 5 N sulphuric acid was prepared by adding 7 mL concentrated sulphuric acid (96%) to 50 mL of deionised water. The combined ascorbic acid reagent was made freshly each day by mixing 5 mL sulphuric acid solution, 0.5 mL potassium antimonyl solution, 1.5 mL ammonium molybdate solution and 3 mL ascorbic acid solution. The volume ratio of water sample to combined reagent used for all experiments was 1:0.16. A range from 0–600 mg/L P–PO_4^{3-} of standard solutions were prepared from dilutions of a 50 g PO_4-P mL^{-1} stock solution. The stock solution was prepared from potassium dihydrogen phosphate monobasic.

2.6.2 Materials

Sandpaper of different grades was purchased from Radionics Ltd, Ireland. The grades of sandpaper included: P800, P120 and P80. P80 was the roughest grade and P800 was finest grain.

Matt black Ambersil acrylic paint was purchased from Radionics Ltd, Ireland. It was used to spray paint the inside of the top and bottom layers of the chip and the walls of the detection channel. The matt painted was chosen so that it would not affect light transmittance.

2.6.3 Instrumentation

Spectrometric reference measurements were obtained using a Shimadzu mini 1240 spectrometer (Shimadzu Corporation, Japan). Brandtech cuvettes (Sigma Aldrich, Ireland) were used for optical pathlengths of 10 mm.

Stratasys Objet260 Connex 1 3D printer (7665 Commerce Way Eden Prairie, MN 55344, United States) was used in the fabrication of the test bench and optical head for the LED and PD used in the device.

A scanning electron microscope (SEM) Hitachi S-3400N instrument (10 North Martingale Road, Suite 500, Schaumburg, Illinois 60173-2295, U.S.A) was used to characterise the altered PMMA structure from a roughened (modified) surface compared to that of an unroughened (unmodified) surface.

A Bruker Contour GT Optical Profiler instrument (Billerica, Massachusetts, United States) was used to characterise the average surface roughness of each of the different grades of sandpaper and the surface roughness of the outsourced and manually prepared optical windows.

Bruker HYSITRON TI Premier Nano indenter instrument (Billerica, Massachusetts, United States) was used to measure the hardness, elastic modulus and fracture toughness of a material.

2.6.4 Microfluidic disc manufacturing

The multi-layered microfluidic discs were designed used SolidWorks™ (https://www.solidworks.com/domain/design-engineering**)** and AutoCAD software **(**https://www.autodesk.eu/products/autocad/overview). The manufacturing process for the layered discs were manually assembled by hand in a cleanroom environment. The discs were fabricated using sheets of PMMA ranging from 3 mm to 0.5 mm in thickness and layers of PSA which were used for the dual purpose of creating microchannels and also sealing the disc layers preventing leaks, 46 µm thick. Both the PMMA and PSA were sourced from Radionics™ and Adhesives Research™ respectively. A laser (Epilog, Golden, Colorado, United States.) and a Graphtec cutter potter (Armstrong Avenue, Irvine, CA, 92614, United States) were used in the manufacturing process to cut the layers of the different plastic material and to create the gaskets in the microchannel layers.

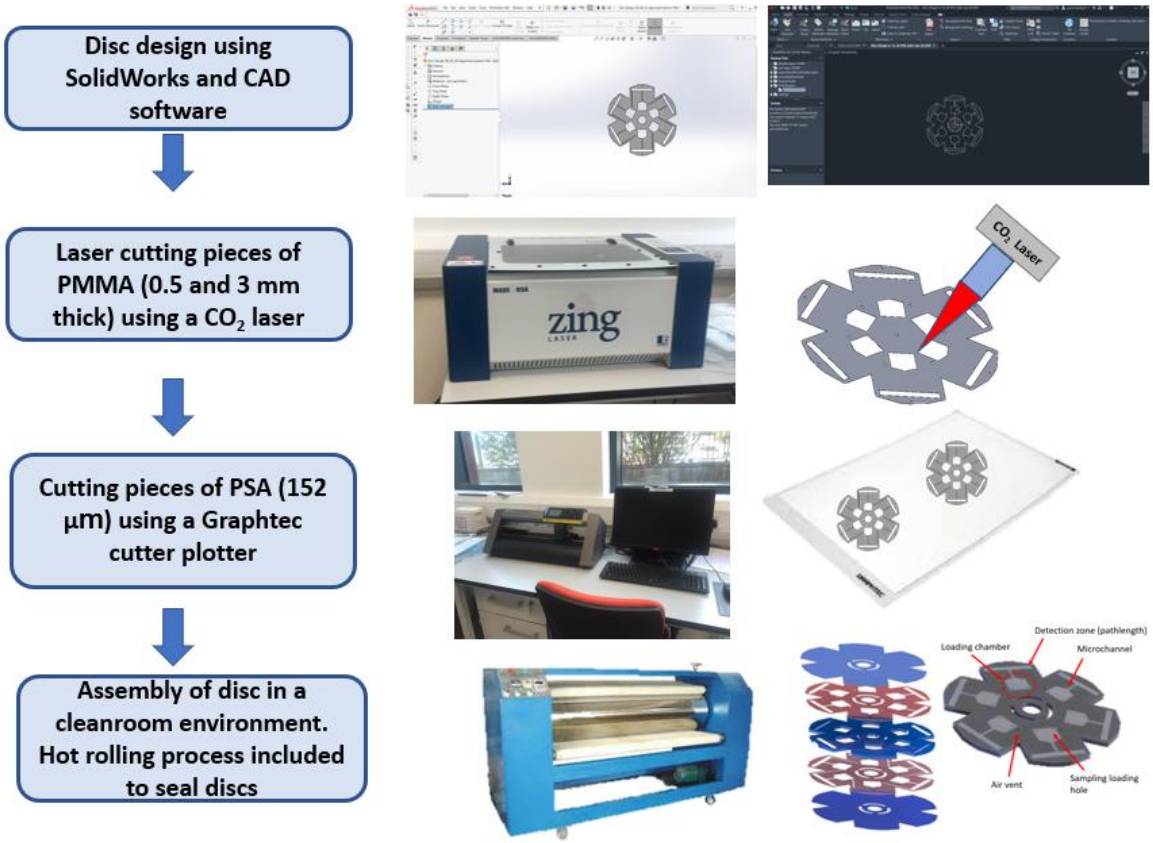

Figure 2.15 Flow chart highlighting the steps involved in putting the discs together, from design to final assembly.

2.6.5 Altering refractive index

Varying grades of sandpaper was used alter the refractive index of the pathlength channel. Each grade of sandpaper was applied using the same method. The sanding of the microfluidic test chip was done manually by hand. The top and bottom layers of the chip were sanded in a two-directional method, from left to right and right to left a total of 30 times, the walls of the detection channel were also roughened using this technique.

The black paint was spray painted by hand until the whole surface of the chip/disc was covered evenly with the paint to block ambient light from entering the detection channel. The PMMA layer was held 10 cm away from the nozzle of spray can and the was sprayed over and back for 10 s to achieve a black opaque paint layer over the chip. Adhesive tape was wrapped around the optical windows of the chips before spraying to make sure that these were kept free from paint.

2.6.7 Test bench for optical enhancement investigations

Optical enhancement techniques were investigated within the detection channel of microfluidic manifold to determine if the sensitivity could be increased, and system noise decreased. For the purpose of this investigation a bench top system was fabricated to carry out the optical detection of the pathlength variations.

The test bench system consisted of a 3D printed holder manufactured using Stratasys Objet 260 Connex 1 polyjet printing 3D printer (United Kingdom). The detector device used within the system contained an LED and PD, one acting as the light source and the other acting as a detector. The detector device was powered using a controller board and Arduino. A voltage source was used to power the LED. An LED was used with a λ_{max} of 880 nm which overlaps with the absorbance spectrum of the molybdenum blue complex formed in the reaction. A resistor was used to adjust the light intensity of the LED, this was paired with a transistor which was used to turn the LED on. The PD was connected to the microcontroller which had an input/output (I/O) pin and was supplied with 5 V. LED and PD were situated at either end of the 3D printed holder. Image of bench top system is shown below in Figure 2.16.

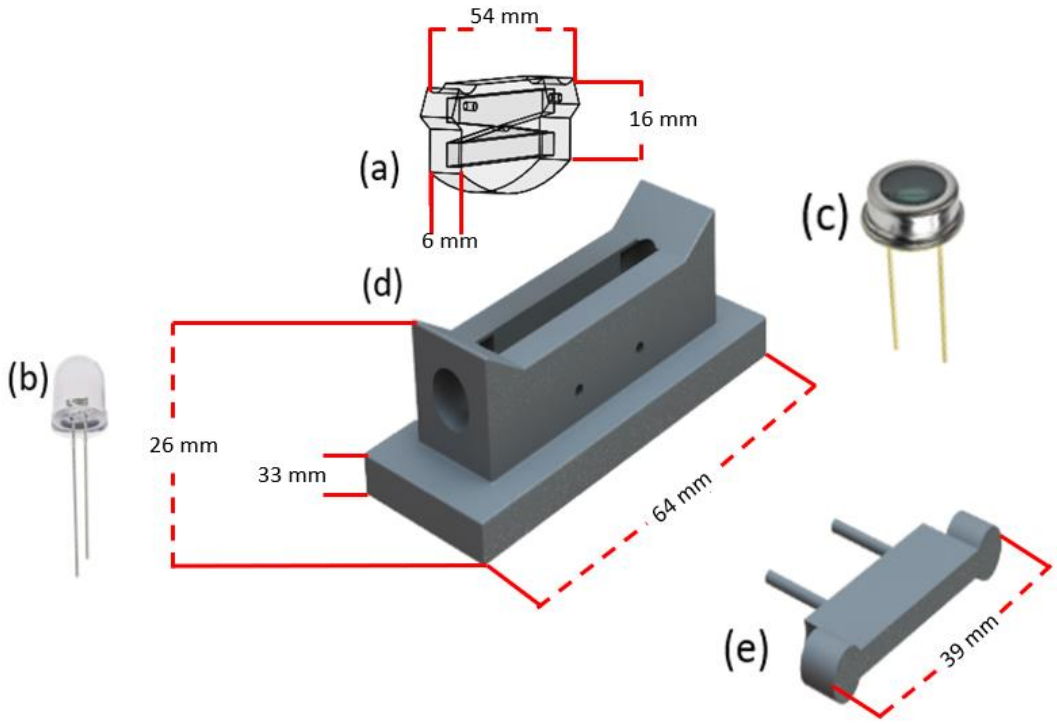

Figure 2.16 This image displays the test bench set up that was used to carry out all experiments on the modified detection channels within the microfluidic chips. (a) microfluidic test chip, (b) LED, (c) PD, (d) 3D printed test bench and (e) alignment pins.

The proposed disc was manufactured as a microfluidic test chip as shown see in Figure 2.17 (c), to minimise costs in the early stages of fabrication. This allowed for a sufficient number of chips to be manufactured and tested using less material. Before the disc was manufactured it was important to determine if the enhancement techniques would improve the sensitivity by altering the refractive index in the detection channel or by inhibiting external light getting into the detection channel and falling incident on the detector. The fabrication process involved designing the microfluidic test chip on SolidWorks™ and AutoCAD. The manufacturing process involved two components: PMMA and PSA, processed using two different instruments. PMMA is melted and vaporised when it encounters the CO_2 laser. The PSA was used to create microstructures and seal the chips. The Graphtec cutter plotter can achieve a feature resolution of 500 µm. The PSA was cut using cut force '19' at a machine speed of '10' with 3 passes (cuts) per feature.

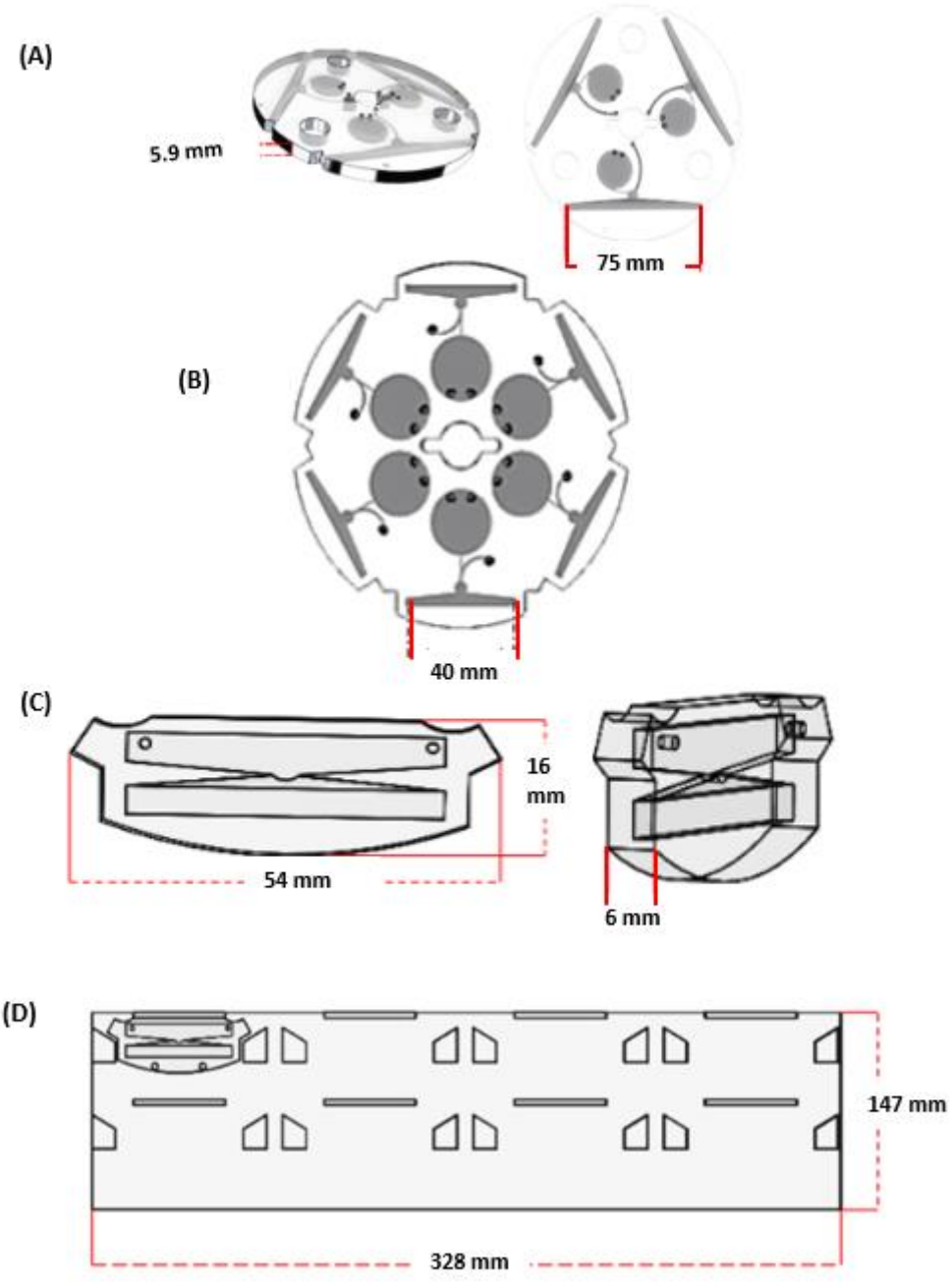

Figure 2.17 (a) the old microfluidic disc, (b) the new proposed design for the six-analyte disc, (c) 2D and 3D rendered image of the microfluidic test chip and (d) the alignment stage used in fabrication of the test chips.

2.6.8 Onboard reagent storage

Each component of the molybdenum blue reagent was incorporated into the device using small pieces of PSA cut using a Graphtec cutter plotter. The bottom protective layer of the PSA was stuck to the base of the disc (PMMA) and the top layer (protective layer removed) was used to create a hydrophobic surface to prevent spread of the reagent droplet and mixing with the other chemical components in the introduction chamber. The four reagents were pipetted down in the desired dosage using a micropipette. The liquid chemistries were then dried down using heat to evaporate off the water in an oven with a low constant temperature of 37 °C for 2 h, the developmental process of this method is described in more detail in Chapter 3.

2.7 Results and Discussion

2.7.1 Microfluidic disc development

Several design iterations were used throughout the fabrication process, these iterations included changes and improvements to the disc. The modifications were done to facilitate a good performance microfluidic disc capable of loading fluid, holding fluid, reagent storage, reagent and sample mixing and analyte detection with good sensitivity and good optical performance. A total of 12 disc iterations were manufactured and tested leading to the final design.

Table 2.1 Disc design iterations log summary.

Iteration		Disc Design	Problem	Solution
Version 1 (v.1)		Using 2 mm PMMA	Correct alignment with LED and PD	3 mm PMMA was chosen for correct alignment with the optical head.
Version 2 (v.2)	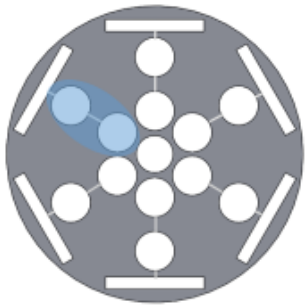	Two circular reservoirs for reagent storage, sample loading and mixing	No vent – liquid did not move from first chamber	Inclusion of air vent at highest possible point.
Version 3 (v.3)	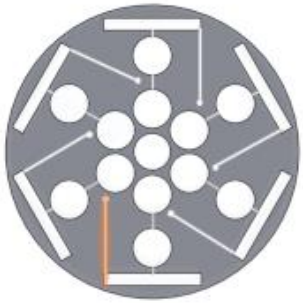	Two circular reservoirs for reagent storage, sample loading and mixing with vents (straight)	Pathlength not long enough to hold fluid	Increase the dimensions of the pathlength (40 mm x 5mm x 3 mm).

Version 4 (v.4)	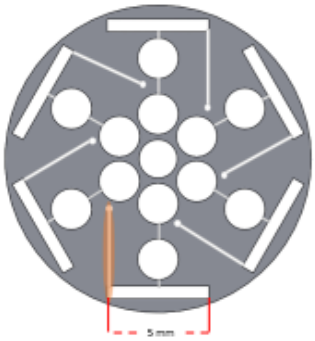	Two reservoirs designed	No need to have two reservoirs	Remove the second reservoir from the design
Version 5 (v.5)		One reservoir with wider detection channel	4 mm width detection channel (vol. 480 µL) 5 mm detection channel (vol. 600 µL)	Circular design reservoir filled too quickly.
Version 6 (v.6)	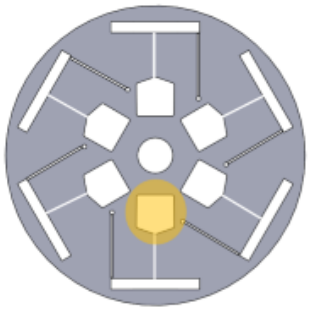	One reservoir with shield shape	Notches needed in disc design for LED and PD light path	Include optical pathway notches into design
Version 7 (v.7)	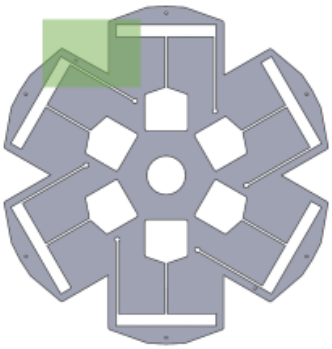	One reservoir with shield shape and notches	Alignment holes needed to aid fabrication	Include alignment holes into design for assembly.

Version 8 (v.8)	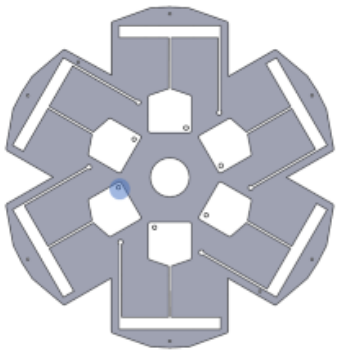	One reservoir with shield shape and notches and one loading hole	Liquid travelled too quickly into microchannel.	Included second air hole in the introduction reservoir.
Version 9 (v.9)	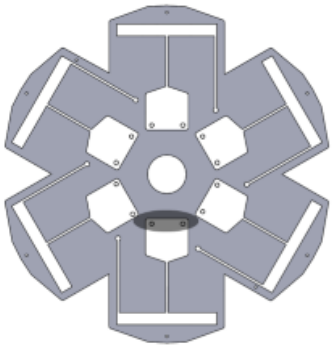	One reservoir with shield shape, notches and one loading one air hole - in clear PMMA	Minimise light scatter and ambient light	Black disc to minimise light getting into the detection pathlength.
Version 10 (v.10)		Disc design using clear PMMA sprayed in black acrylic paint – optical window left clear	Issues with transfer of black spray paint on optical windows	Removing the bulk material to reduce light scatter.
Version 11 (v.11)		Clear disc with cut outs in bulk material. Shorter microchannel, longer air vent (higher than intro reservoir)	Investigate if this reduces noise and light scatter. Prevent fluid from traveling out of the pathlength and into the air vent whilst centrifugally	No indication that any of the cut-outs made an improvement to enhance the optics, therefore omitted from the design.

	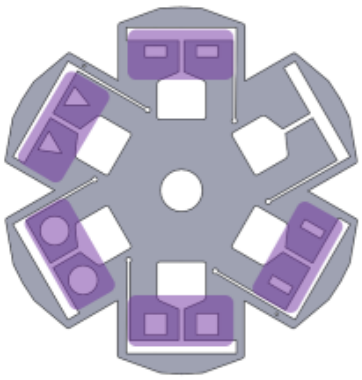		spinning the discs.	
Version 12 (v.12)	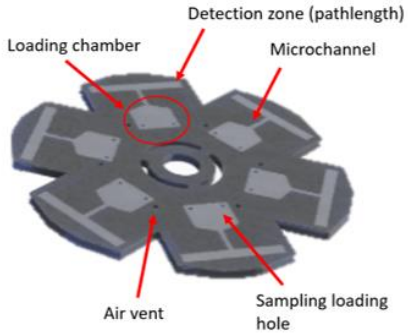	Finalised disc design – clear disc, 3 mm and 0.5 mm PMMA. Introduction chamber, pathlength (40 mm), 2 microchannels and one air vent (highest position). Loading holes and reagents separated out. in single introduction chamber.	No additional changes.	

2.7.2 Enhancement of optics by altering pathlength properties

Due to the restrictions in space on a disc, the pathlength was decreased to enable an adequate number of test reservoirs to be located on a single disc. Therefore, the optimisation of channel length with optical enhancement techniques was carried out to achieve a low limit of detection.

The Beer-Lambert law states that the amount of light absorbed (A) is directly proportional to the absorption co-efficient (ϵ), concentration (c) and the length of the detection pathway (l) [209]:

Equation 2.3 Beer-Lambert Law

$$A = \epsilon c l$$

Equation 2.3 shows a directly proportional relationship between the two parameters of interest (a) and (l), thus large pathways are shown to detect low concentrations [209]. To overcome this problem, enhancement techniques are required to enable the shorter pathlengths to detect low concentrations of the analyte.

This study involved the investigation of surface modifications within the detection channel of the microfluidic discs to enhance their optical performance, these included matt black paint coating and roughening of the microfluidic test chips manually with different grades of sandpaper. The black paint coating on the test chips acted as a barrier, by absorbing the light and inhibiting the external light from getting into the detection channel. External light is also referred to as stray light, this is the action of light being detected that is not from the intended source. The black paint was tested to investigate the reduction of this stray light therefore, decreasing the amount of noise in the system [210]. The roughened test chips were roughened manually with different grades of sandpaper ranging from P80 to P800. The aim was to roughen the pathlength to increase light scatter within the detection channel, increasing the pathlength of the light within the channel. This was done to investigate an increase in sensitivity of the roughened and blacken pathlength when compared to the unmodified pathlength. The increase in light scatter allowed an increase in the amount of light entering the detection channel (pathlength) and reduce the amount of light escaping into the bulk material (PMMA) and getting “lost”. Roughening of the pathlength allowed for less light to escape into the bulk material, in the hope that more light would travel straight to the detector. It also made it difficult for stray light to become incident on the photodiode – thus ideally reducing the noise, see schematic representation in Figure 2.18.

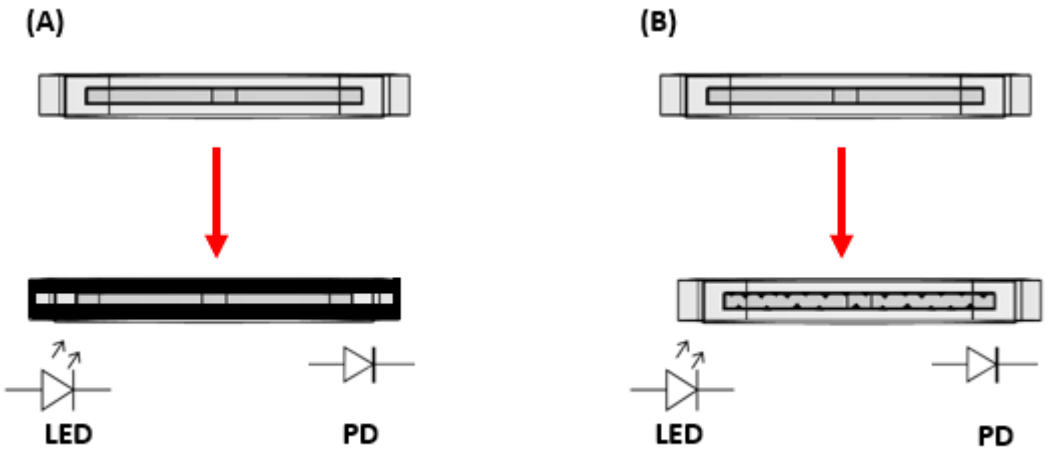

Figure 2.18 Schematic illustration of the optical enhancement techniques investigated. (A) black absorbing coating to minimize stray light and (B) roughening of the detection channel to create light scatter, the degree of roughness is dependent on the grade of sandpaper used.

The results in Figure 2.19 show the performance of the unmodified chips compared with the modified. This was carried out using a standard calibration curve and a range of phosphate standards ranging from 5-50 µg/L^{-1} (n=3) for each chip and each concentration tested. From this, the LOD of each chip could be determined. From analysing the data, the black painted chip achieved the highest increase in sensitivity compared to the other test chips. The blackened chip achieved an LOD 6 µg L^{-1} PO_4-P, compared to the unmodified chip which achieved an LOD of 15 µg L^{-1} PO_4-P. The roughened chip which achieved the best result was grade P80. The LOD obtained from using this grade was 13 µg L^{-1}. PO_4-P. This shows an appreciable increase in sensitivity compared to the untreated (unmodified) test chip.

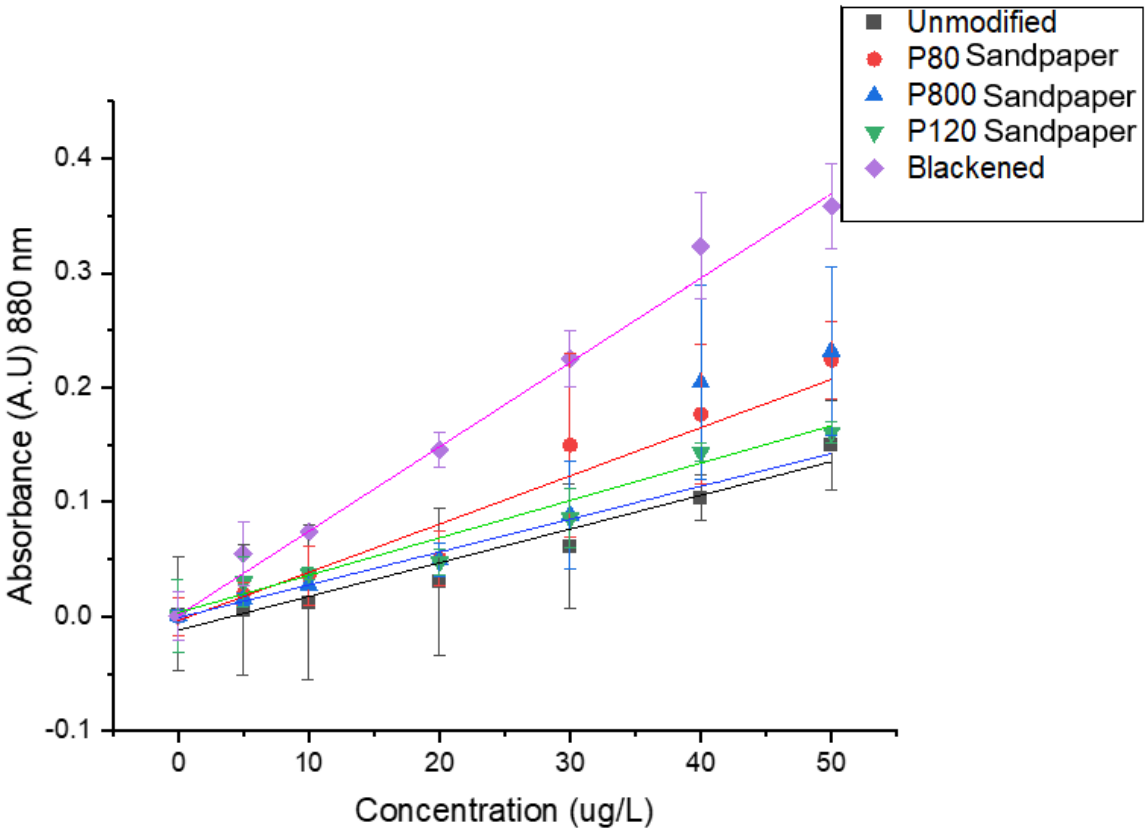

Figure 2.19 Calibration curve obtained comparing the unmodified microfluidic chip (slope 0.003) against each of the modifications tested (roughened P80 (slope 0.005), P120 (slope 0.004), P800 (slope 0.0036) and the blackened chip (slope 0.007).

The LOD and LOQ were calculated using the standard error (σ). σ is calculated using the STDEV function in excel. This value is then used with its corresponding slope value to calculate the LOD and LOQ of each modification. The equations used to calculate LOD and LOQ are as follows:

Equation 2.4 Limit of Detection

$$LOD = \frac{\sigma}{S} x\ 3.3$$

Equation 2.5 Limit of Quantification

$$LOQ = \frac{\sigma}{S} x\ 10$$

where σ = to the standard error of the response and S = to the slope of the calibration curve. Table 2.2 shows the linear correlation between roughness and sensitivity, as the roughness is increased so is the sensitivity.

Table 2.2 Relationship between roughness and sensitivity.

Treated Chip	Values for LOD and LOQ	
	LOD (µg/L)	**LOQ (µg/L)**
Unmodified	15.3	45.9
P80	12.8	38.4
P120	13.4	40.1
P800	18.5	55.5
Black	6.4	19.4

2.7.2.1 Characterisation of surface roughness using Scanning Electron Microscopy

Scanning Electron Microscopy (SEM) was used to characterise the surface topography [211] of the roughened PMMA, which varied in roughness. As depicted in Figure 2.20 below, the degree of roughness varies from each grade of sandpaper that was used. All SEM images were taken using 20.0kV at a distance of 500 µm.

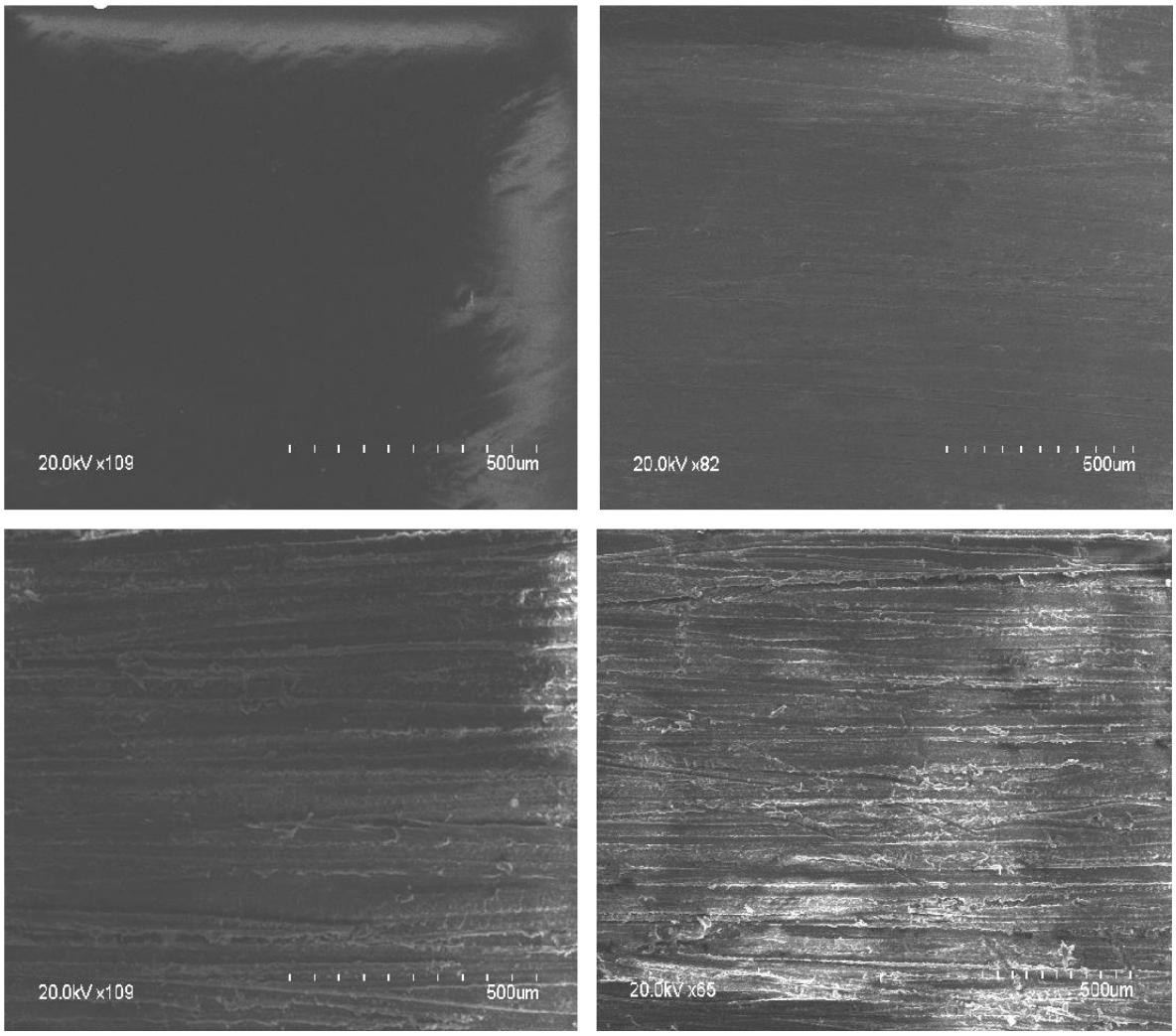

Figure 2.20 Images obtained using SEM to illustrate the unmodified chip as being a clear unroughened surface and displaying an in-depth analysis of the degrees of roughness of each different grade investigated. Unmodified (top left), P800 (top right), P120 (bottom)

2.7.2.2 Characterisation of surface roughness using Profilometry

The roughened surfaces were also investigated using profilometry. The reason why this method was explored was to characterise the surface morphology, surface roughness and step heights of each of the different grades of sandpaper on PMMA to determine why P80 obtained the best results in terms of increasing sensitivity compared to the other grades that were used in the experiments, P80 had the roughest grain and therefore increased light scattered within the channel.

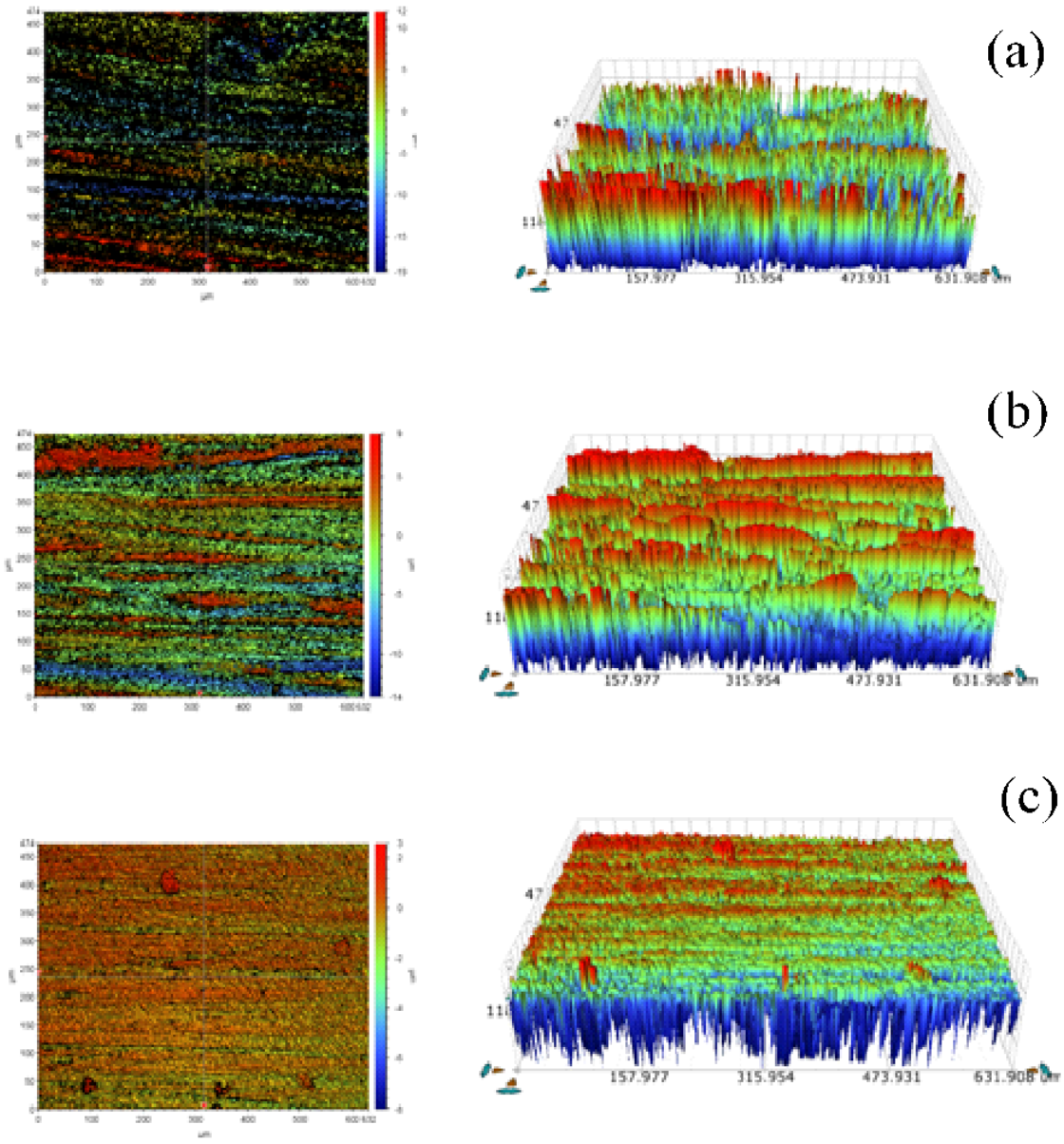

Figure 2.21 Images taken on the Contour Profiler Instrument to investigate the effects of the different grades of sandpaper. (a) P80 (top), (b) P120 (middle) and P800 (bottom).

Table 2.3 Average roughness of the different grades of sandpaper on the microfluidic chips.

Grade	Roughness of each grade of sandpaper		
	Average	St. Dev	Units
P80	3329	751	nm
P120	3102	764	nm
P800	485	149	nm

A method of decreasing detection channel length without a significant reduction in sensitivity has been developed by using optical enhancement techniques. The techniques used in this experiment included roughening of the detection channel and blackening of the test chip. These modifications have allowed for an increased test number on a single sensing disc whilst maintaining the required low sensitivity essential for the sensor and its area of monitoring. This chapter reports the optimisation of the detection channel on a microfluidic disc to facilitate an increase in test number on a confined space. The work presented displays the excellent analytical standard of the new decreased path length and increased sensitivity when the optical enhancements are applied to the detection channel. The use of roughening and blackening the test chips shows a significant increase in sensitivity compared to the untreated chips. Achieving an LOD OF 6 µg L^{-1} compared to that of the unmodified which obtained 15 µg L^{-1} PO_4-P.

The modification that achieved the best result was the blackened chips, these showed the highest increase in sensitivity compared to all the other chips tested. Roughening of the detection channel showed an increase in sensitivity as the grade of roughness increased, hence conveying a correlation between roughness and sensitivity. By adapting this optical enhancement technique onto a microfluidic device, using a simple design to facilitate mixing, an optimized optical path length, to facilitate the measurement of six analytes/sites. Hence making the system suitable for measurement of water bodies within a catchment area with low levels of phosphate. However, the method of roughening the detection channel was very unreproducible and therefore cause significant deviation from chip to chip and therefore only the blackened enhancement techniques was selected for further development.

2.7.3 Comparison of blackened discs versus clear discs

The following tests were carried out to determine if the blackened discs performed better than the clear finalised disc design and developed detection platform. The blackened modification was predetermined from the previous optical enhancement study carried out. Each detection channel (well) was filled with a reagent blank (deionised water and reagent (1:0.16)) and the voltage system readout (mV) was read on the system. As shown in Figure 2.22, there is no conclusive answer proving that the blackened disc performed significantly better than the clear

disc. There is still a significant variation from well to well on both discs. The system mV reading obtained is proportional to the absorbance. The blackened disc experiences more deviation, evident in the error bars. The method of coating the discs was also unreproducible and was difficult to stop the paint from coming into contact with the optical windows on the discs.

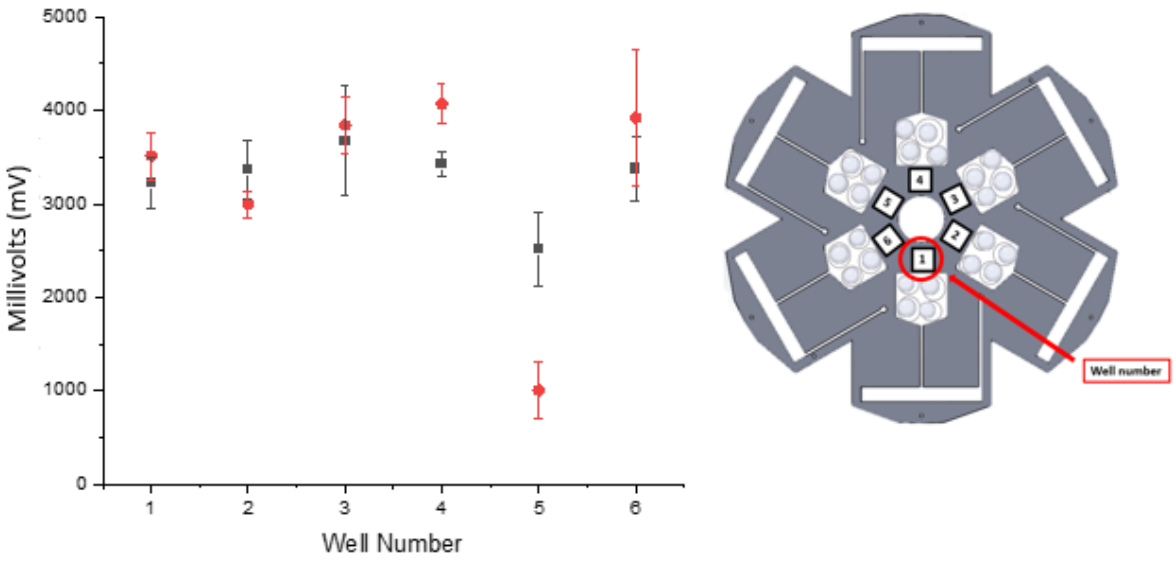

Figure 2.22 Investigating the performance of the clear (black) discs compared to the blackened (red) discs to determine if the blackened discs improved the optics by blocking any external light getting into the pathlength of the discs.

From the preliminary study with the discs and analysing the results obtained from Figure 2.22 the blackened discs do not make a significant difference in blocking external ambient light getting in into the detection channel or help guide the light coming from the LED to the PD.

2.7.4 Enhancement of optics by altering bulk material

As the modifications to the opaqueness of the discs did not seem to enhance the optics, a method of altering the bulk material was investigated. This involved laser cutting different shapes into the bulk material of the disc to inhibit the light from getting trapped. As there are six pathlengths on a single disc, five different shape cut-outs were tested; circle, square, vertical rectangle, horizontal rectangle, and a triangle, they were all compared to the control on the disc which had no cut-out.

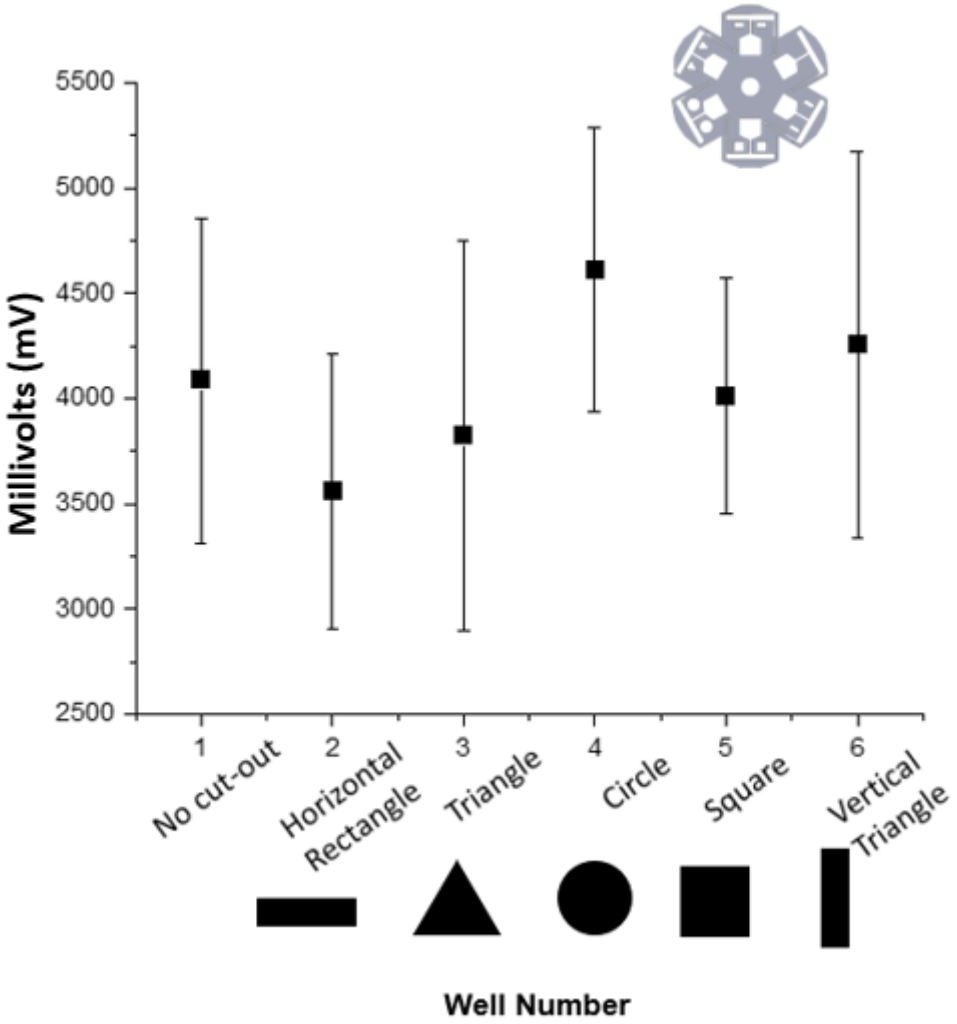

Figure 2.23 Investigation into altering the bulk material on the discs to see how it effects the optics on outsourced disc manufacture (n=3).

From the results present in Figure 2.23, show no clear indication that any of the shapes cut-out in the bulk material had a positive impact enhancing the sensitivity of the disc design, the error bars and standard deviations for all cut-out shapes is too high to determine if one performed better than another.

2.7.5 Disc manufacturing – manually prepared vs outsourced fabrication

During the previous optical enhancement investigations, the variation between the different wells (pathlengths) on a single disc and between discs was observed, therefore different disc manufacturing methods were analysed, comparing manually prepared and outsourced manufacturing techniques.

To investigate the variation from well to well for both the manually prepared and outsourced manufacture (EFJ Engineering, Clonskeagh Industrial Park, Dublin, Ireland). Both methods were used to assemble three discs each. The wells were filled with DI water and read on the system. The results displayed in Figure 2.24, convey that the outsourced discs show a decrease in variation from well to well (data points) and from disc-to-disc (error bars). The results determined that outsourcing the lasering of the discs was the best method for mass production as they were significantly more reproducible than the manually prepared discs.

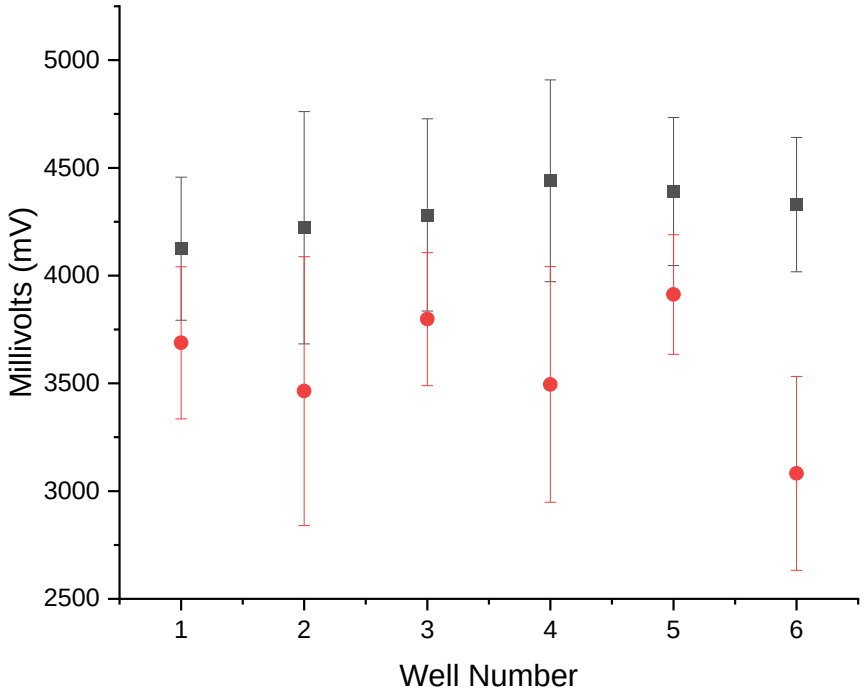

Figure 2.24 Comparison of well to well variation on each of the manually prepared (red) and outsourced (black) disc manufacture (n=3) for both methoods.

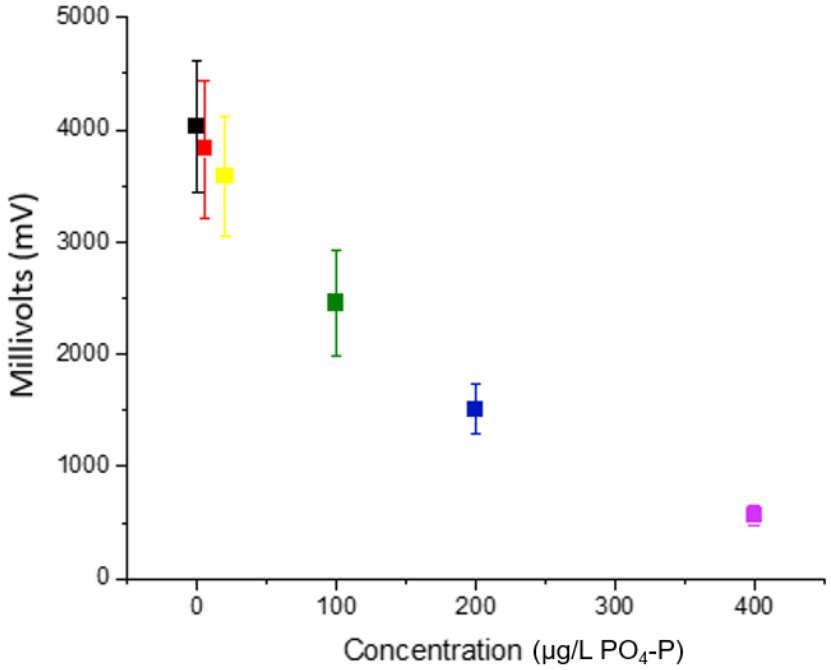

Figure 2.25 Graph illustrating the variation from well to well on a single disc over a range of phosphate standards, highlighting the variation in system readings from well to well.

Figure 2.25 demonstrates the variation from well-to-well on a single disc using a range of phosphate standards (0-400 ug/L). This experiment involved measuring each phosphate standards in each of the six wells on a disc, to determine the variation from well-to-well and how this effects the correct determination of the concentration of phosphate in the standard. For example, the 5 µg/L phosphate standard system reading ranges from approximately 3400 to 4600 mV, this is a significant difference in readings and impacts the low concentrations more, the 600 µg/L standard has significantly less variation in system readings as it ranges from 500 – 650 mV. The variation is discussed further in Section 2.7.6. Where the cause of the variation is investigated by analysing the optical windows on the discs.

2.7.6 Characterisation of disc performance

This section investigated the performance of the discs by measuring their reproducibility and determining the causes of variation between discs and manufacturing methods. To maximise the reproducibility of the discs and optimise their performance.

2.7.6.1 Investigation of clarity of the optical window

Optimal transparency of the optical window is required to ensure that no light scatter occurred or that none of the incident light was "lost" into the bulk PMMA material which contributes to the overall performance of the device.

2.7.6.2 Characterisation of surface roughness

The surface roughness of the optical window was investigated using profilometry. The variation in surface roughness (see Table 2.4) is the cause of the variation in the optical windows. There are six optical windows per disc and each laser cut on the windows is not uniform therefore causing different degrees of light scatter. The results highlight that the outsourced discs contain less surface roughness than the manually prepared discs and therefore the optical windows are more uniform, with less variation between each window on a single disc. However, there is still variation relating to the 0.504 µm surface roughness recorded in the outsourced discs.

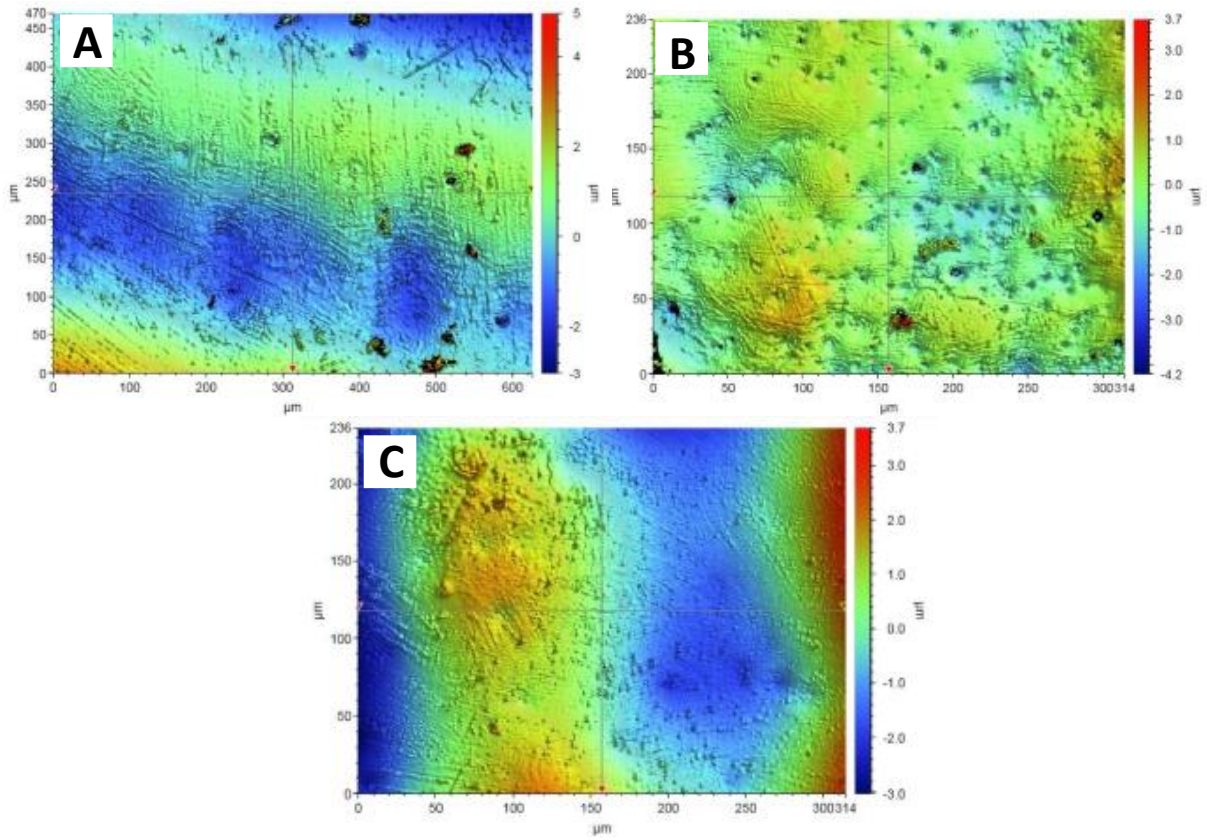

Figure 2.26 Images taken using the Contour Profiler Instrument to investigate the variances in surface roughness of the optical window with different methods of manufacture and to determine if the differences in PMMA supplier effects the clarity of the optical window. (A) Outsourced manufacture with good optical clarify; (B) outsourced manufacture with poor optical clarity; and (C) manually prepared discs.

Table 2.4 Average roughness of the different methods of manufacturing the microfluidic discs.

	Surface Roughness of the optical window	
	Average (µm)	**St. Deviation**
Manually prepared	1.525	1.307
Outsource manufacture (good optical clarity)	0.504	0.259
Outsource manufacture (poor optical clarity)	0.897	0.555

2.7.6.3 Characterisation of variation of PMMA material

To determine the variation in PMMA material from manually prepared and outsourced manufacture, nanoindentation analysis was carried out on the material to measure the hardness, elastic modulus, fracture toughness and other mechanical properties using controlled nanoindentation of materials to determine if the clarity of the optical window is affected by the properties in the material itself.

The analysis showed variances in the hardness (H) and reduced Modulus (Er), for the three different PMMA materials used: 1. Manually prepared, 2. Outsourced manufacture with good optical clarity and 3. Outsourced manufacture with poor optical clarity. All the tests were identical, using a diamond berkovich tip to 5000 uN. The "reduced modulus" was measured as the Poisson Ratio is unknown. Modulus is a measure of how much elastic recovery there is, as the material springs back as the load is removed. Hardness is a measurement of how much the material will permanently deform under stress.

Table 2.5 Average variance in hardness and reduced modulus of the different methods of manufacturing the microfluidic discs.

Manufacturing method	**Average Hardness (GPa)**	**St. Dev Hardness**	**Average reduced Modulus (GPa)**	**St. Dev reduced Modulus**
Manually prepared	5.147	0.035	0.280	0.002618
Outsourced manufacture (good optical clarity)	5.291	0.255	0.304	0.019
Outsourced manufacture (poor optical clarity)	5.277	0.274	0.303	0.0202

The repeatability of the materials for the manually prepared and outsourced manufacture with good optical clarity had a low standard deviation suggesting a homogenous material. In the outsourced manufacture with poor optical clarity, there was significant scattering suggesting localised variations (such as bubble inclusions which can be seen optically), shown in Figure 2.26, image C.

2.7.6.4 Scaling factor

Although the performance of the microfluidic discs is improved by outsourcing the lasering and manufacture (see Figure 2.24) there is still some variation between well-to-well and disc-to-disc. To minimise this issue a scaling method for each disc was developed. The scaling method was introduced to put measures on continuation of gradual changes in the pre-assigned values of each well. This pre-calibration step enabled the determination of the well-to-well optical window variability on a single disc. The pre-calibration of the disc is carried out to ensure all wells on that disc can be referenced to a single well. Water is used to obtained readings in this pre calibration step, mimicking the medium of an actual sample.

An experiment was carried out to investigate the influence of using a scale factor to normalise the wells on a single disc. The well readings for an unassembled disc with water in the pathlengths was recorded. The disc was then fully assembled and the readings with water in the pathlengths were recorded. The unassembled and assembled readings were then compared (n=5). A calibration curve was then performed on all the wells and a scaling factor was then applied to the wells using well 1 for reference and the raw data and scaled data was compared. The reason why the unassembled data is important is due the dried reagents on the disc. Using the unassembled data provides a pre-calibration of the disc before the dried reagent are integrated onto the disc.

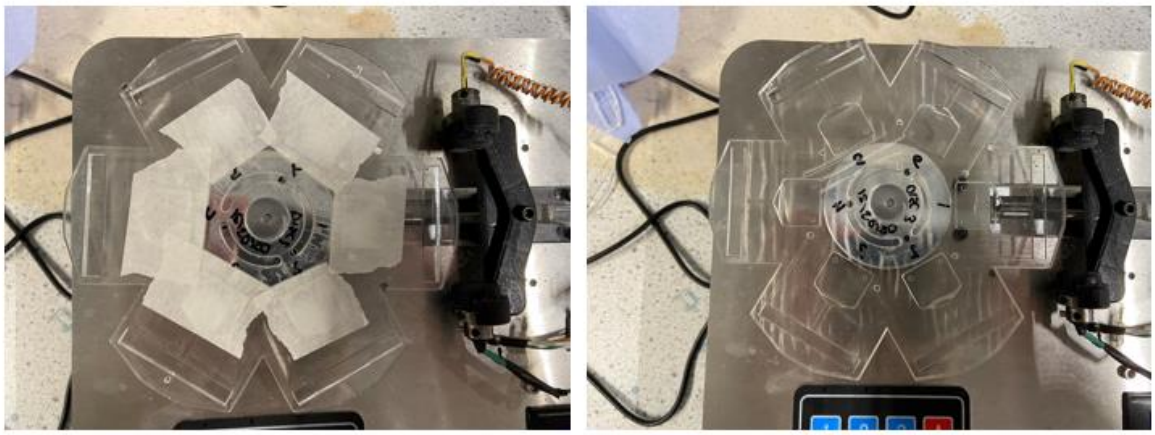

Figure 2.27 Image showing the procedure for pre calibrating the microfluidic discs using an unassembled and assembled disc. The introduction chamber and microchannel opening are covered on the unassembled disc to prevent liquid traveling up the microchannel by capillary action, to ensure correct liquid volume (600 µL) is present in the pathlength for each reading.

The data shown in Figure 2.28 and Figure 2.29 determine that the data from scaled values are much closer together than that of the unscaled, therefore different wells from the same disc can be used to measure the same concentrations of phosphate more accurately. This then leads to a better performance in detecting and distinguishing between lower concentrations of phosphate. As the variance in the optical window clarity of the pathlength channel is shown to have more of an effect on low concentration ranges.

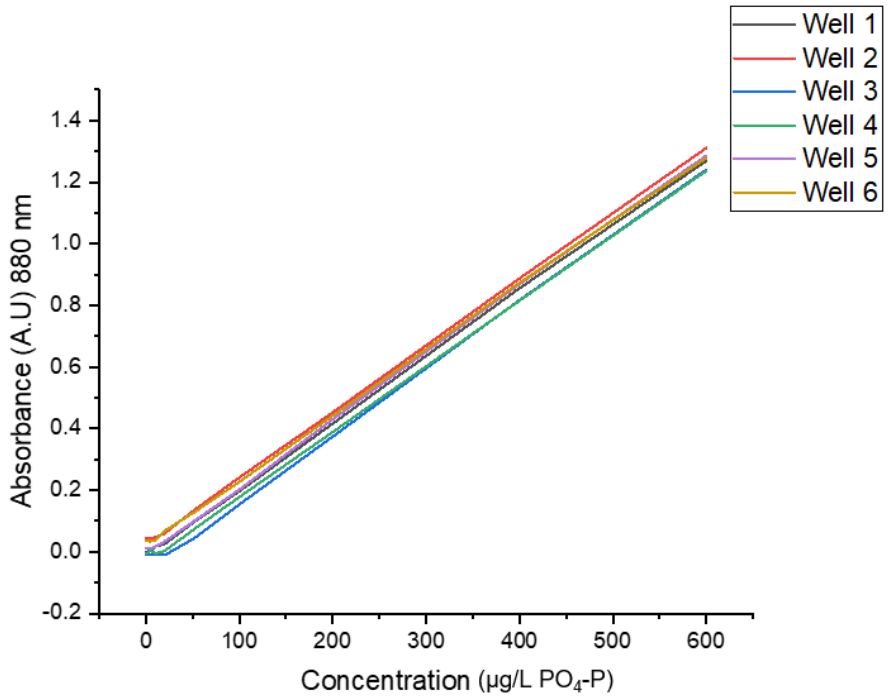

Figure 2.28 Unscaled raw data, range of phosphate standards (5-600 ug/L) were run through each path length (n=6) of the disc to investigate the variance in the optical window clarity of each pathlength on a single disc.

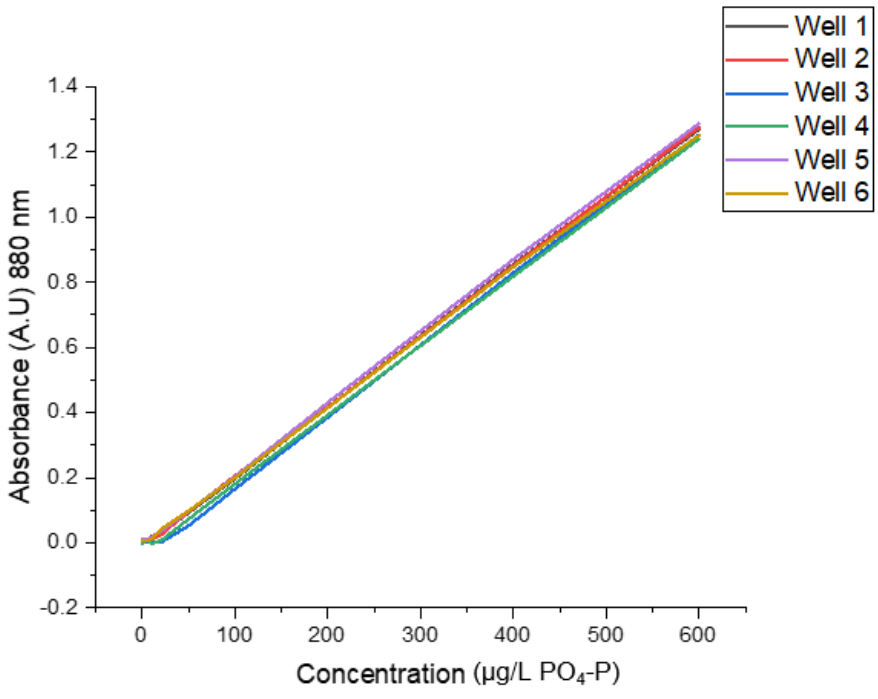

Figure 2.29 Scaled data of a set of phosphate standards (5-600 ug/L) run through each pathlength on a disc (n=6) to determine if scaling the data achieved a more representative picture of the actual concentrations of the standards compared to the raw data.

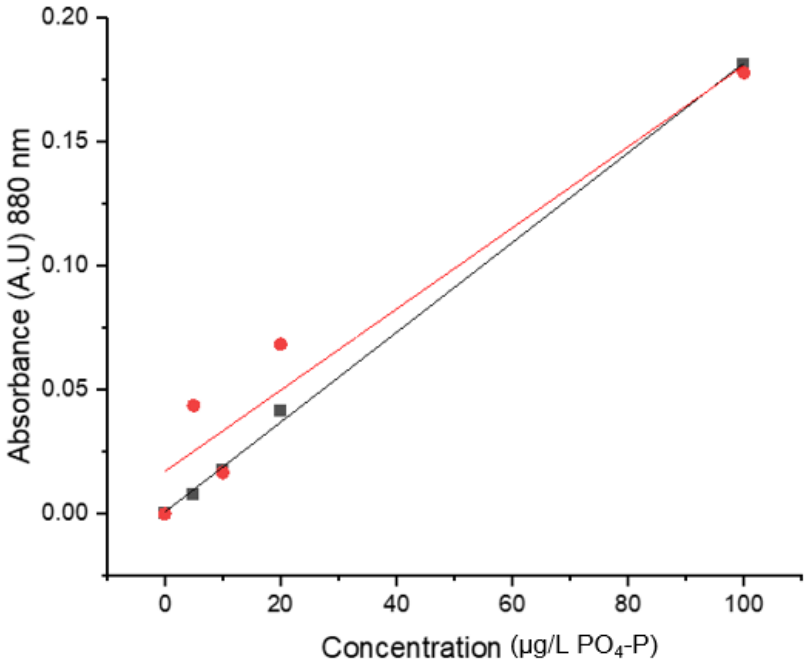

Figure 2.30 Comparison of the scaled and raw data sets. R2 values obtained for the scaled (black) and raw (red) data were 0.999 and 0.9673 respectively

Figure 2.30 shows a direct comparison of the raw and scaled data applied to a data set containing a calibration from (0-100 µg/L). Each data point is taken from a different well on the same disc.

2.7.7 Validation and characterisation of the disc and platform combined

Figure 2.31 demonstrates the performance of the fully integrated system and highlights its ability to detect low levels of phosphate in freshwater. The system achieved an LOD of 16 µg/L which is lower than a number of sensors currently on the market to date [212][213]. The experiment was run in triplicate with a range of phosphate standards ranging from (0-200 µg/L). Three different discs were used in the experiment to get a true representation of the results including the variation from well-to-well and disc to disc-to-get a true LOD for the integrated system. If the variation of the discs was minimised the LOD could be further enhanced, as an LOD of 5 µg/L was achieved by running a number of standards through the same well on a single disc, this was done to eliminate the effects of the clarity of the optical window.

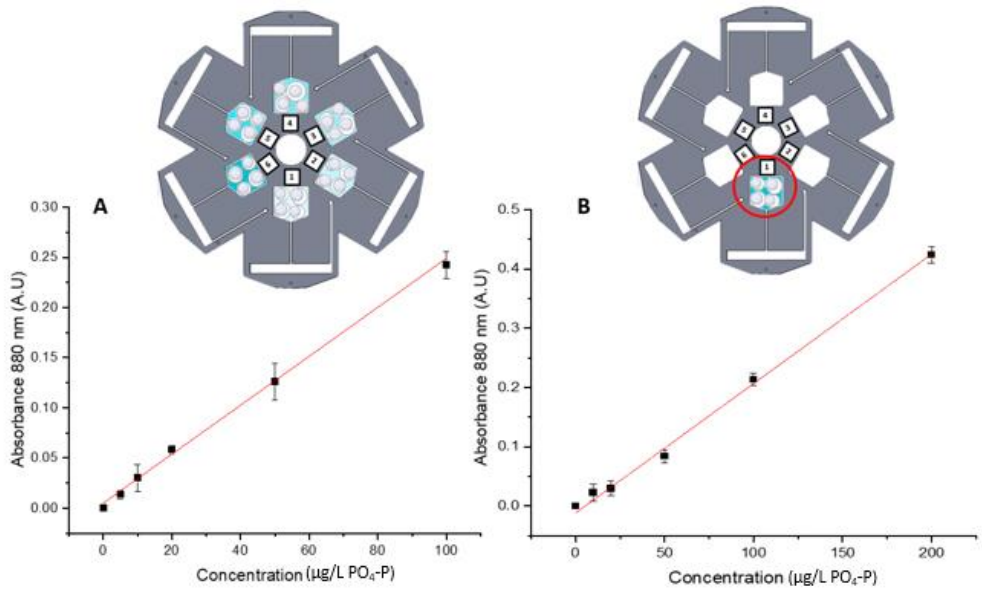

Figure 2.31 Representation of a (A) range of phosphate standards run on the phosphate system through all 6 pathlengths generating an LOD of 16 ug/L considering optical window variation, (0-100 µg/L range), compared to (B) all readings obtained from a single pathlength on one disc to achieve an LOD of 5 ug/L (0-200 µg/L range). The calibration curve (A) obtained an R^2 value of 0.9963 and a slope of 0.0021, (B) achieved an R^2 value of 0.9983 and a high sensitivity slope of 0.0024.

2.8 Conclusion

A centrifugal microfluidic disc for multi-sample phosphate detection has been developed. The disc itself has been designed and fabricated using material chemistries and manufactured to ensure optimum optical clarity to enhance sensitivity. The success of this disc was achieved through developments and optical enhancement improvements to the initial design of the disc. The design of the disc focused on key requirements for disc LOAD developments such as fabrication of a low-cost, robust, repeatable, and easy to use platform.

The results presented in this chapter highlight the many different tests and iterations involved in successfully developing a microfluidic disc for specific nutrient detection. This disc forms the basis for a simple, low cost and easy to use sensing device which could be used in place of other more expensive. The use of microfluidics used in the integrated platform scales down the size of the sensor and also the volumes of sample and reagent needed, therefore making it suitable for field applications.

This chapter discussed the different optical enhancement techniques that were investigated to improve the sensitivity of the disc to achieve an accepted LOD for phosphate detection in freshwater environments. The results presented here are the first for a microfluidic disc analyser with the onboard storage of the molybdenum blue assay. This chapter demonstrates the complexities and rewards of developing a microfluidic disc capable of detecting phosphate which includes a low limit of detection of 16 µg/L. This LOD is determined by the variation in optical clarity of the discs. From the studies carried out in this chapter, the variances between each optical window on a single disc and the variance that occurs from disc-to-disc is determined by the surface roughness caused by laser cutting process of each optical window and the variation in the material used. As shown in the chapter if this variation can be minimised the LOD of the sensing device can be improved to facilitate measurements of 5 µg/L of phosphate in a water sample.

Chapter 3: Development of a novel method for chemical on-board storage of the molybdenum blue assay in a microfluidic manifold

3.1 Introduction

As discussed in Chapter 2 microfluidics has presented itself as a useful technique for a wide variety of applications. Its rapid development in the past number of years has had a profound effect in fields such as biochemical analysis, chemical analysis, biochemical engineering, medical diagnostics and more recently environmental analysis [214]. Many detection systems that were previously used in these fields are laboratory-based instruments and require large pieces of equipment (spectrometers and ion chromatograph instruments), with a various number of steps and highly trained personnel to operate the equipment. Making them difficult if not impossible to operate outside of a laboratory environment. Microfluidics takes advantage of these limitations by manufacturing simple, accurate and reliable devices that can be used in different areas of detection and analysis. Development in microfluidics has led to the integration of many processes such as sample loading, mixing, heating/cooling and reagent storage, this chapter will focus on reagent storage and how this is achieved in microfluidic platforms. For microfluidics systems to progress from lab to field they need to become a fully integrated device. Essentially what they end user would like to be able to do is to load the sample into the device and obtain the result. The need for reduced steps is crucial for these devices to be used out of laboratory settings, hence why reagent storage is now a requirement for many systems. Reagent storage addresses two main limitations of microfluidics devices gaining commercial and field testing as it provides (1) long-term reagent storage and (2) increases the lifetime of a reagent. Integrating reagent storage onto microfluidic devices allows for storing, valving, metering and detection to take place on a single unit [149].

In microfluidics fluid handling can be carried out using passive or active methods [215]. Passive techniques use physical properties to induce a force (capillary valves [216]). This method is receptive to vibrations and instantaneous movements, generally used for wetting liquids. Active liquid handling generally involves an external force such as a laser ablation [217] or finger pressure [218][219]. The use of active methods of fluid handling in microfluidic devices generally increases the cost of fabricating, adds additional steps and decrease the simplicity of the device. Therefore, the method of reagent integration and storage is extremely important in developing a system that can be commercialised.

The advancements that have been made in the area of microfabrication techniques has led to the idea of developing fully integrated self-contained microfluidic devices. This idea of reagent storage on microfluidic platforms has increased the lifetime of the reagents by employing robust integration techniques. *Tupik et al.,* discusses the use of a dehydration technique by integrating primers into a glass microchip for loop mediated isothermal amplification of nucleic acids obtaining a shelf life of approximately 3 months [220]. *Wentland et al.,* also discusses

the development of a method for dry storage of reagents to monitor phenylalanine in the field. In this study the dry storage of three different reagents were dried down using nitrogen gas and observed over a period of one month. The results indicate that using this drying method prevented degradation of reagents and provided a shelf life of 15 days, method illustrated in Figure 3.1 [221].

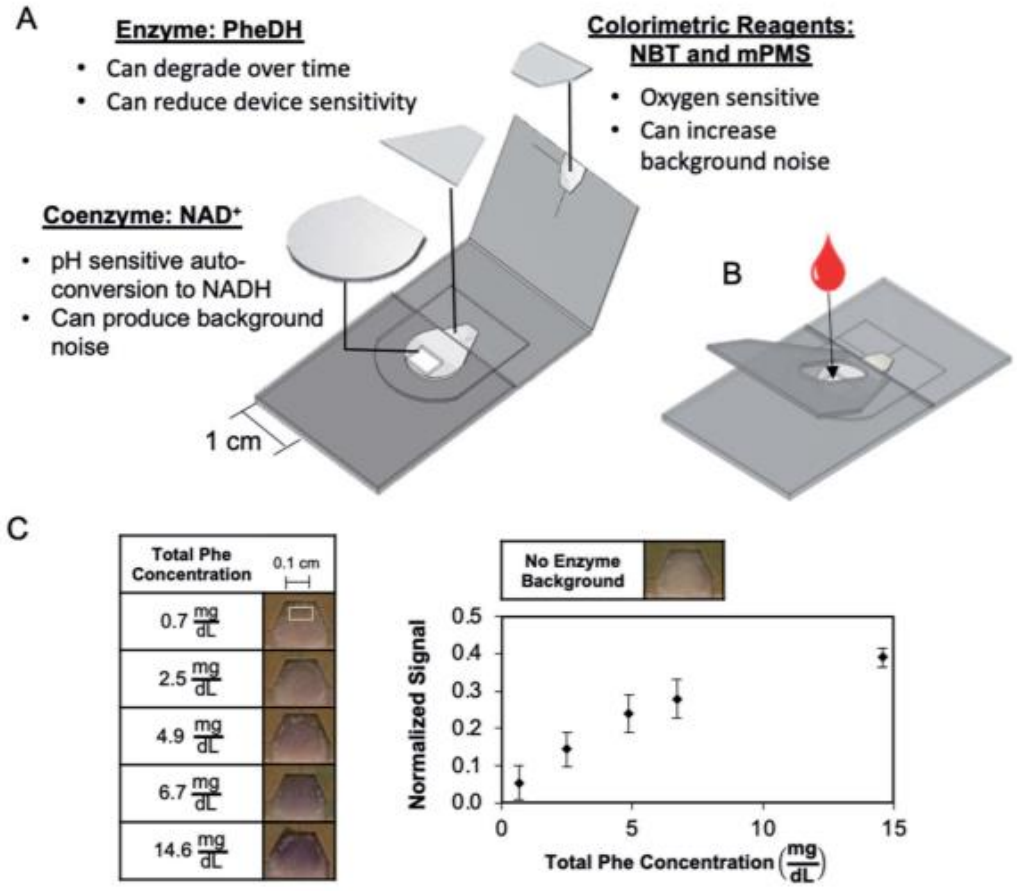

Figure 3.1 Assembled phenylalanine monitoring device with integrated dried reagents. (A) Schematic of the three modules with different reagents dried on, (B) Schematic of pull-tab which creates a layer between the colorimetric and enzymatic glass fiber pads and (C) Left: Images of colorimetric reaction on pull-tabs, with different concentrations of phenylalanine in blood samples. Right: Comparative analysis using a LC-MS for reference.

3.1.1 Microfluidics and onboard reagent storage for environmental applications

The reagents involved in many environmental measurements can be complex, they may involve the use of harmful chemicals and different reagents require different storage conditions depending on the compounds used in that test. Therefore, the need to develop robust, precise, accurate and repeatable methods of integration is extremely important and of huge advantage to not only environmental applications but also in other disciplines in the scientific field. There have been many successful cases of reagent integration in microfluidic devices in these fields [222][223][224][219].

The application of combining microfluidics with reagent storage for environmental analysis has been presented by *Jayawardane et al.,* This paper demonstrates the implementation of a paper-based microfluidic device for on-site detection of reactive phosphorus in water (see Figure 3.2). The reagents are integrated onto the paper device by using a liquid storage technique on a 3D paper design. The reagents were separated out in different zones and a thin layer of Teflon (PTFE) or cellulose acetate. The reaction was detected using a flatbed scanner (Canoscan™ Lide 700 f) and the image was then processed by Image J software. This device achieved a shelf life of 15 days at room temperature and an excellent LOD of 0.05 mg L^{-1}, however the reaction time is approximately 40 min, which is not desirable for onsite detection of nutrients [225].

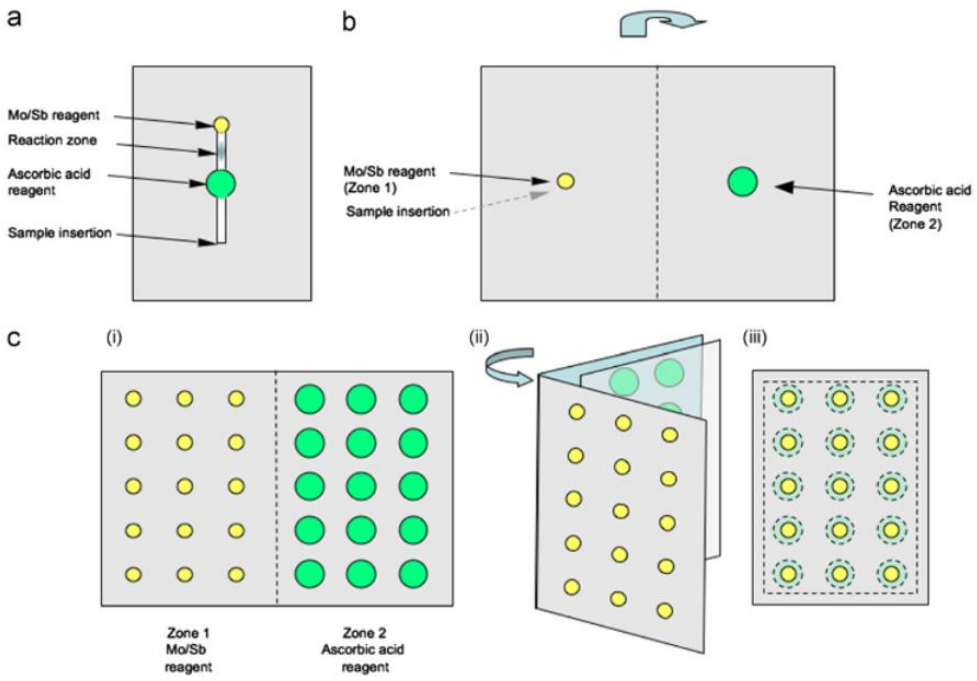

Figure 3.2 Illustration of the development of the paper-based device for reactive phosphorus measurements in water samples. (A) Channel design and sample fluid path; (B) Folded design, migration of sample from molybdate zone to ascorbic acid zone; (C) Final 3D folded paper design. Device sealed by lamination in plastic pouch.

A study carried out by *Grand et al.,* also discusses the used of the molybdenum blue method for integration onto a microfluidic device for field applications. The design is centred on an LOC device. This sensing platform was development for deployments with an LOD of 30 nM and a reagent lifetime of 60 days if the sensor is operated hourly and connected to shore power. Unlike the previous microfluidic devices, the reagents are not stored in the microfluidic chip but are stored in the housing platform, increasing the size of the sensor [47]. This device has a much longer lifetime but because of this requires much more power is needed and therefore there are more costs involved. Highlighting the advantage smaller self-contained microfluidic devices have over larger autonomous sensing platforms.

Jayawardane et al., also investigated the determination of nitrate and nitrite, using a single and disposable lab-on-paper device. The detection was based on the Griess method and results achieved a high sensitivity (1.0 and 19 µM for nitrite and nitrate respectively), good repeatability (less than 2.9 and 5.6 % for nitrite and nitrate respectively) and inexpensive to manufacture [226]. However, the robustness and performance in the field may be jeopardised due to the materials used in the fabrication.

3.1.2 Methods of storage

The advances in microfabrication techniques have enabled the integration of reagents onto microfluidic devices to produce self-contained devices. However, the requirements for the storage of chemicals and reagents can be diverse and complex, making integration difficult. These challenges can be overcome by the great research and developments carried out in storage techniques [214].

3.1.2.1 Valves used for reagent storage

Valving is critical for integrating time delays or sample holds in microfluidic systems therefore, it is no surprise that they have been adapted for liquid storage. The valves are typically used to pre-store a fluid in a reservoir until required, it is usually separated from the rest of the system by a weakly bonded interface [227]. This allows the reagent to be held for a period of time until a certain pressure or force is applied to release the stored liquid. There are two types of valving categories generally used in microfluidics – those being active and passive valves [228]. Active microvalves are microfluidic valves which require a physical parameter changed by an external interaction to induce actuation for example mechanical (magnetic, electrical, thermal), non-mechanical (electrochemical) and external (pneumatic or modular) processes [229][230][231]. Passive valves are microvalves that don't require any external process for actuation to occur, it takes advantage of natural physical parameters, such as sample interaction; mechanical (check valve) and non-mechanical (capillary action) [232][233]. Many valves incorporated into microfluidics must match the following criteria; (1) fabrication feasibility (will not fail due to interfacial adhesion), (2) provide reduced residual stress (especially for thin membrane valves) [234], (3) account for the amount of fluid being held and (4) the pressure/energy needed to release liquid must be known. A common type of valve used in microfluidic devices is an electrostatic microvalve [234] [235]. Electrostatic valves are most commonly designed using hard materials such as silicon and glass, but recent developments have led to the design and fabrication of valves using soft lithography by applying low potentials so that the valves don't collapse during that manufacturing process.

Electrostatic microvalves are produced in a bilayer membrane formation where the first layer is composed of a thin layer of PDMS for insulation and the second layer is comprised of thick backing layer of PDMS [234]. As mentioned in Chapter 2 soft lithography is used in the fabrication of these valves by use of a multilayering technique [236] whereby a micro design already engraved onto a wafer can be cast onto the mould and a membrane valve can be produce. *Desai et al.,* describes how a electrostatic membrane was fabricated for implementation into a microfluidic device [234]. This membrane consisted of a smooth, thin, elastomeric membrane that was placed above a microfluidic channel. This membrane was

subsequently treated with a layer of conducting nanoparticles to form the top electrode. The bottom of the channel formed the bottom of the electrode. An electric field is formed when a certain potential is applied, this creates electrostatic forces which causes the membrane to collapse and therefore closing the microvalve within the channel. A schematic of the design is shown in Figure 3.3.

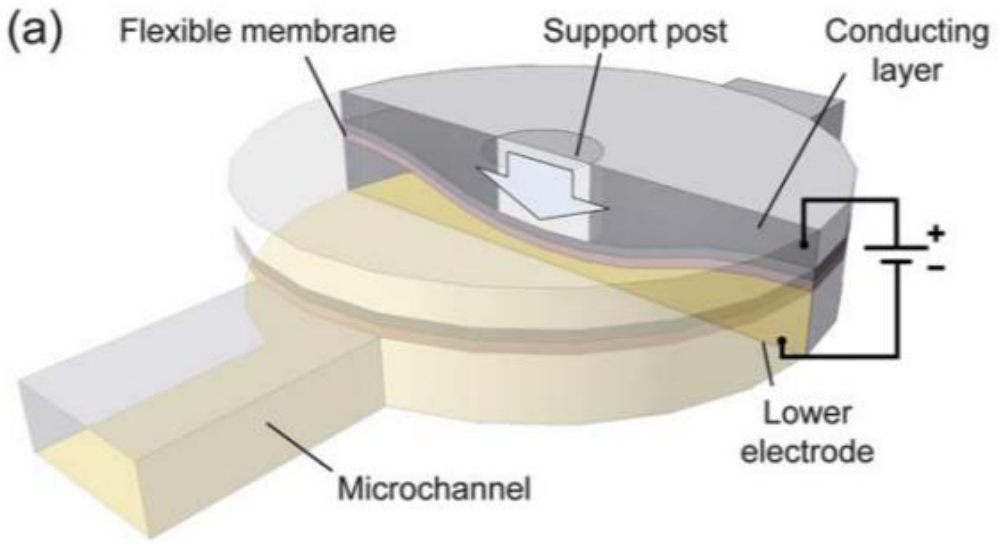

Figure 3.3 Presents a schematic of the electrostatic microvalve.

The advantage of this technique is that it can be applied across a wide variety of microfluidic applications as electrostatic valves can be used in continuous flow and droplet fluidics. These types of valves allow for ease of operation once an electric field has been applied and minimising variables that are needed for consideration compared to other techniques such as pneumatic valves [237]. The valves can be opened and closed therefore they can be reused if that application allows for this. Another advantage to using valving for reagent storage is that no other chemicals are involved, therefore the only lifetime or stability study needed to be carried out is on the reagent itself. Studies and tests must be carried out on leaks and the fluidic holds but having no other chemical parameters makes the microfluidic device simple and relatively easy to manufacture.

However, using this method of reagent storage would need an external potential to initiate the opening closing of the valve to trap the fluid. Many devices being manufactured for field applications may see this as complicated step with potential cost increases.

3.1.2.2 Hydrogels and ionogels

Hydrogels and ionogels are successfully used in reagent storage due to their crosslinked polymeric structures which make them capable of holding different chemical substances [238]. Hydrogels are commonly used in point of care (POC) detection systems and over the past number of years have been increasingly integrated into microfluidic chips for reagent storage. Similarly ionogels which are ionic liquids which are incorporated into polymeric molecules are commonly used in the same way as hydrogels [239]. They are generally composed by deposition of the polymeric composition (thermo sensitive monomer and photo initiator) onto a surface. Deposition of the polymeric mix can be done by ink-jet printing [239] or another immobilisation technique.

To design a hydrogel that can store reagents, they must first be polymerised. This can be done in a number of ways; (1) by using a chemical reaction to link polymer chains (2) use an ionising radiation to produce free radicals that recombine cross-link junctions or (3) taking advantage of physical interactions [240]. The use of hydrogels was reported by *Haefner et al.,* this study investigates the swelling and shrinking capabilities and how this facilitates reagent storage.

The study details the use of a mask and temperature. PDMS was poured onto the mask before being integrated into the device. The polymerisation solution was placed into a chamber and sealed with black polyethylene terephthalate (PET). This was then exposed to UV light for the polymerisation process. The hydrogel could then be integrated and sealed by plasma activation, shown in Figure 3.4.

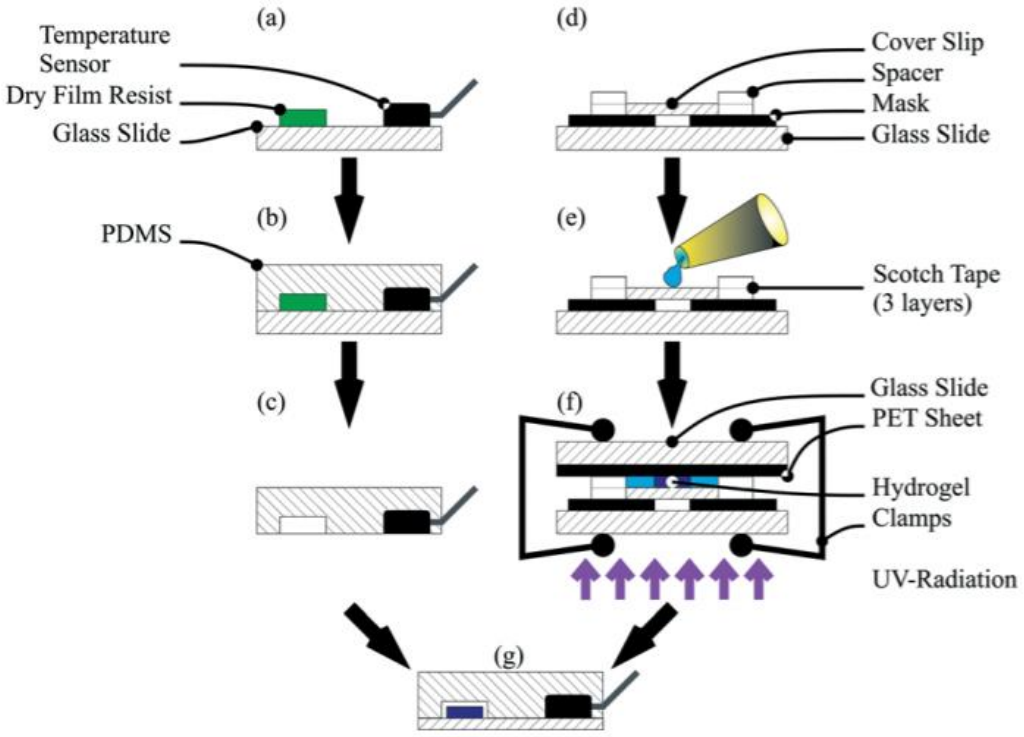

Figure 3.4 Schematic illustration of the fabrication process in manufacturing the device.

This method of reagent integration is particularly interesting as it incorporates both chemical and physical aspects into the microfluidic platform design. The fabrication of the hydrogels involves a great deal of chemical knowledge in how these monomers will react once polymerised and how they will react in the system. The chip design involves both physical and engineering comprehension in how these hydrogels will be integrated into the system. The swelling and shrinking of the hydrogels were carried out by submerging the hydrogels in water and fluorescein dye to initiate the swelling effect, once this was done the hydrogels were placed in mineral oil and the shrinking process was carried out under 3 heating steps (1. 35 °C, 2. 20 °C and 3. the heat was ramped back up to 35 °C). The stability of the hydrogel showed a storage time of 1 h. Due to the limitation in storage time it would be ideal for this this method to be still used in a laboratory set up, as an 1h storage time would not be ideal for many field studies.

3.1.2.3 Liquid storage of reagents

The storage of liquid reagents can be more difficult than their dried counterparts, there are more considerations that need to be taken into account when it comes to storing liquids in microfluidic devices, including; stability (humidity), sensitive to temperature, presence of organic solvents and if the liquid is photoactivated. To overcome some of these challenges' researchers have developed methods of integrating liquid reagents into devices without altering their chemical composition. One method that will be discussed in this chapter is the use of blisters to enable liquid storage in a microfluidic chip design used for POC diagnostics [224].

Blister packs differ to films due to their shape; they maintain a constant shape with or without the presence of a liquid inside. They enable the long term storage of liquids for fabrication of micro dispensers [219]. Blisters consist of the two main components, the first being the blister dome which is used to define the volume of liquid that the blister is capable of holding and secondly a film which is used to enclose the liquid [224]. The films used in fabrication generally consist of different polymers such as polyethylene terephthalate, polyamide, polypropylene and aluminium. The aluminium is used to as a blockade. The dome shape of the blister is formed using a process known as thermoforming [241]. Thermoforming allows the films to be heated to a high temperature and then moulded into the dome shape by using a certain pressure, this can be done using a mechanical stamp, vacuum or a pressure stamp. After the pressure is applied it is allowed to cool to room temperature [224] (see Figure 3.5).

The blister is incorporated into the microfluidic chip by first inclosing the liquid into the blister and then incorporating it into the device. The microfluidic chip is designed to securely hold the blister is place and then the device is assembled. The blisters are usually burst using actuation or they can be manually burst.

Smith et al., reports the use of a needle structure to pierce the blister for reagent release. The use of an actuation force to lower the blister onto the needles to rupture the bottom film. Actuation time used during this process was t = 45 s. Figure 3.5 illustrates how the blister was burst. As shown in the schematic two needles were used to burst the blister to aid in controlling the burst flow. The foil layer is stabilised by the adhesive layer and the actuation force acts downwards on the system.

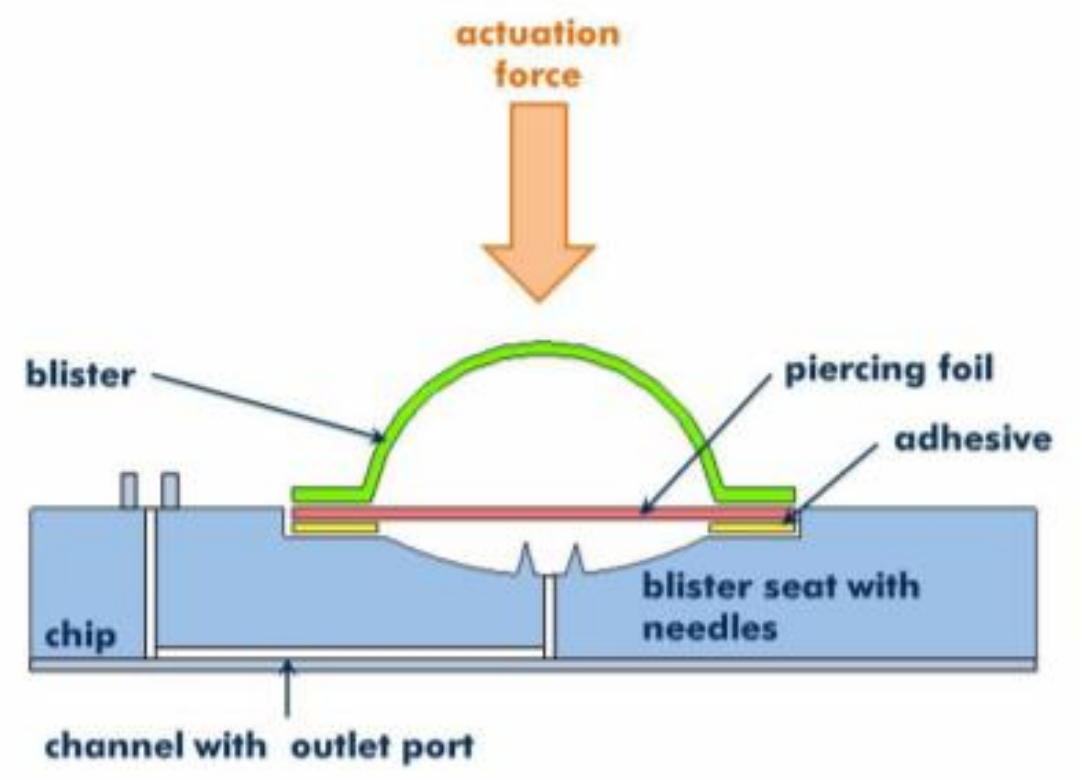

Figure 3.5 Schematic illustration of the needle structure and method used in reagent release from the blister.

The use of blisters for reagent storage has helped overcome many issues regards to the stability of liquid reagents in microfluidic platforms. If the liquid is sealed correctly no leaks will occur, in addition to this it also deals with lifetime and complexity issues regarding the reagents themselves as many cannot be dried down and must stay in liquid form. It also overcomes problems associated with photosensitive liquids as they are sealed away from the light, therefore making them an attractive method for liquid storage. The challenges with this method are concerned with the manufacturing and fabrication processes. This method can be a lengthy process design wise as controlling the bursting flow can be difficult as it is not uniform. Problems may also arise with leaks if the blisters are not sealed correctly, or they are not compatible with the reagent being stored in them.

3.1.3 Aims and objectives

The aim of this chapter is to investigate different methods for onboard chemical storage for implementation onto a microfluidic device for the successful detection of phosphate in environmental waters. For commercialisation purposes it is important that all chemistries are stored on the device to facilitate automation of obtaining results and simplify the device for the end user. This also reduces the risk of contamination on site and reduces the time required to obtain a measurement. The objectives of this chapter are: (1) test and validate three potential methods of onboard chemical integration of the molybdenum blue method. Which includes the analysis of dried chemicals, liquid chemicals and reagent integration using material impregnation (2) identify methods or adaptations to the assay that can be used to prolong the lifetime of these reagents to increase long-term storage on these platforms and (3) validate the successful onboard chemical storage method with real world environmental samples.

3.2 Materials and methods

3.2.1 Chemicals

All chemicals and reagents used in this chapter are discussed in detail in Chapter 2.

In this chapter a modification was made to the molybdenum blue method for phosphate detection. This involved the substitute of 5N sulfuric acid with the equivalent sodium bisulfate to facilitate the drying down of the reagents onto the microfluidic manifold for field applications. This substitute involved dissolving 9 g of sodium bisulfate in 20 mL of DI water. For the purpose of clarification the method containing sodium bisulfate will be referred to as the "adapted method" and the original molybdenum blue method [242] will be referred to as the "control method".

3.2.2 Instrumentation

All phosphate samples were read on a UV/vis shimadzu mini 1240 spectrometer (Shimadzu Corporation, Japan) and BrandTech® cuvettes (Sigma Aldrich, Ireland) were used for optical path lengths of 10 mm. The use of a spectrometer is common method for the determination of molybdenum blue reaction. The spectrometer was used to obtain photometric and spectrum scans of the formation of the phosphomolybdenum blue complex.

The measurement procedure involved adding the colorimetric reagent in a 1:0.16 v/v sample to reagent ratio and allowing the solution to develop for at least 8 min. The absorbance of the sample and reagent solution was measurement on the spectrometer at a λ_{max} of 880 nm for all photometric measurements which were used to generate the calibration curved used in the validation and optimisation of the method.

3.3 Results and discussion

This section details the different investigates that were carried out on the adapted method to examine its suitability for the successful detection of phosphate, by comparing it to the control method. Different reagent storage techniques were also explored to determine the most suitable method for onboard storage of the molybdenum blue assay.

3.3.1 Optimisation of method parameters

The investigation and optimisation of the adapted method was explored in the following experiments which analysed its similarities to the control method and its ability to form a stable phosphomolybdenum complex for phosphate determination. The adapted molybdenum blue method refers to the replacement of sulfuric acid with sodium bisulfate. From these experiments LOD, linear range, stability and lifetime of the adapted method were determined.

3.3.1.1 Calibration

The optimum wavelength was investigated by obtaining the absorbance spectrum of the molybdenum blue assay using a 400 µg/L phosphate complex sample. The absorbance of the complex formed was quite broad with the λmax around 880 nm. This is consistent with literature values which can typically range from 825 – 880 nm [243]. A calibration plot was performed using a set of prepared low concentration phosphate standards ranging from 5 – 50 µg/L in a 1:0.16 v/v sample to reagent ratio [55] (see Figure 3.8).

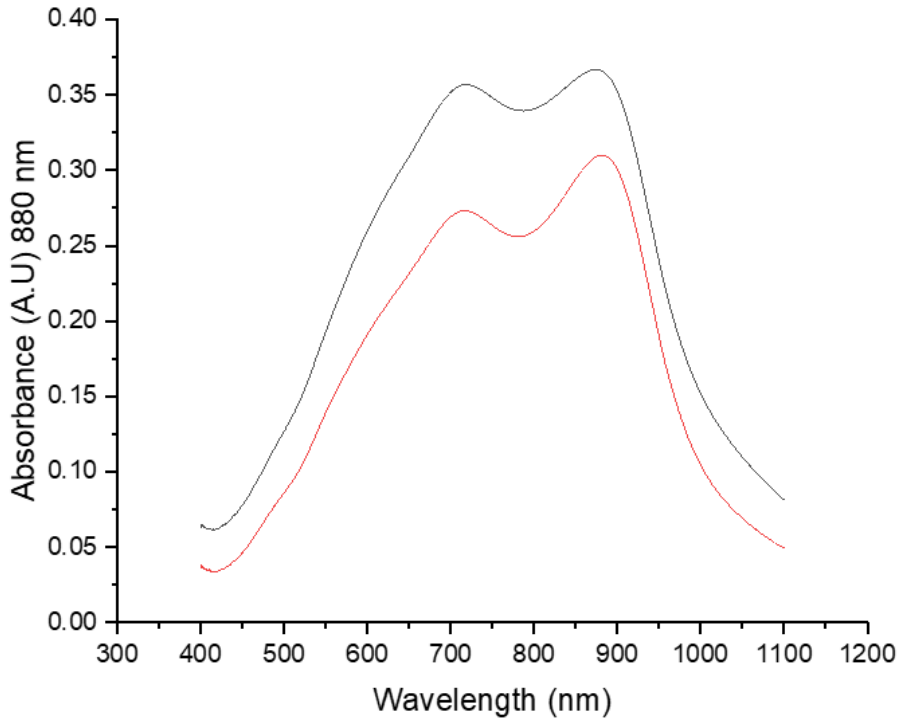

Figure 3.6 Spectrum scan for both molybdenum blue methods (control (red) and adapted (black)) using a phosphate standard of 400 ug/L.

3.3.1.2 Limit of detection

The LOD for the optimised adapted method was determined by generating a calibration curve of low phosphate standard concentrations ranging from 5 µg/L to 50 µg/L. The LOD was calculated as the concentration equivalent of 3 standard deviation (SD) of the blank solution, resulting a value of 2 µg/L for phosphate, this is a significant improvement on the sensitivity of the method previously reported as 10 µg/L [55]. With a linear range of 6.4 – 400 µg/L (see Figure 3.8).

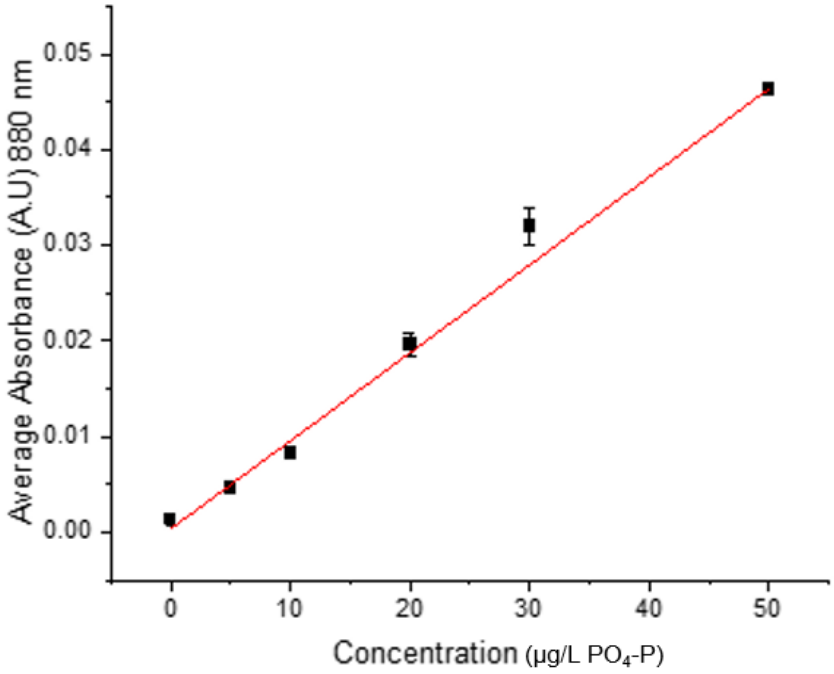

Figure 3.7 Calibration curve obtained to determine LOD of adapted molybdenum blue method for phosphate detection (n=3), using a low range of phosphate standards (0-50 ug/L) measured on a UV/vis spectrometer.

3.3.1.3 Validation of method

The validation process of the method involved applying the optimised adapted method to environmental samples from a freshwater river, the samples were obtained from the River Tolka in Dublin. The samples were collected in separate HPDD bottles so that, controlled and adapted molybdenum blue method could be run in parallel on the water samples. The water samples were filtered prior to analysis using a glass fibre filter paper with a pore size of 0.45 µm, the filtration method used was vacuum filtration. The environmental samples were divided into six aliquots which enabled each method to be tested in triplicate. The concentrations of the unknown environmental samples were extrapolated from the calibration curves that were generated from each method, see Figure 3.8. Table 3.1 contains the phosphate concentrations obtained for the controlled and adapted method run on a UV/vis spectrometer.

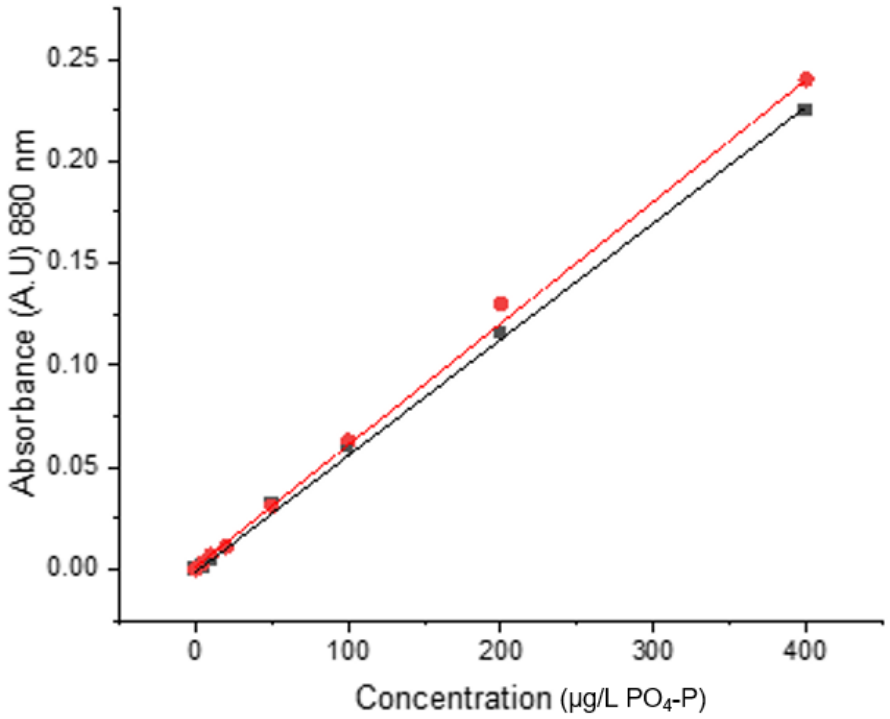

Figure 3.8 Calibration curve of the adapted method (red) compared to the control method (black) measured on a UV/vis spectrometer for standard reference using a range of phosphate standards (0-400 ug/L), (n=3) for both methods, the adapted method obtained a slope.

Table 3.1 Control and adapted molybdenum blue method applied to a river sample

Sample	Concentration of phosphate (µg/L) Control method	Concentration of phosphate (µg/L) Adapted method
1	60	50
2	67	51
3	64	50
Average	64	50
St. Dev	3	1

3.3.1.4 Limitation of method

The limitations of this method arise from the reagent stability and lifetime cited by [244][52][55]. As mentioned in Chapter 1 the combined reagent lifetime for the control molybdenum blue method is up to 4 h. The instability of ascorbic acid used as a reductant in the reagent causes problems for increasing the lifetime of the reagent. Ascorbic acid in solution has the lifetime of 1 week before degradation occurs, this is visible in the production of an orange colour change. Difficulties in implementing this assay onto the microfluidic disc are due to its instability and the combination of chemical components. Methods and techniques have been developed to mitigate these challenges, increasing the stability and adaptability of the assay.

3.3.2 Performance of the optimised ascorbic acid method for phosphate detection

Figure 3.9 shows the spectrum scan for 3 different phosphate standard concentrations for both the adapted and control method, the scan was run from 1100 – 400 nm as the expected peak should be seen at approximately 880 nm (determined in Figure 3.6). The spectrum scan was obtained to investigate the absorbance of both methods at different wavelengths and at varying phosphate concentrations. This graph shows that both the adapted and the control method have the same absorbance peak and the λmax for both is 880 nm. A low, medium, and high phosphate standard were chosen to analyse the adapted method across a wide range of phosphate concentrations. The control method was used as reference data and the strong correlation between the two methods is shown in Figure 3.9. The adapted method shows an increase in sensitivity, this is evident in the slope obtained in Figure 3.8, and obtained slightly higher absorbance compared to the control; this will be an advantage for detection on the disc. This experiment was carried out at varying concentrations to investigate that both low and high phosphate solutions performed the same with the adapted method as they would using the controlled method.

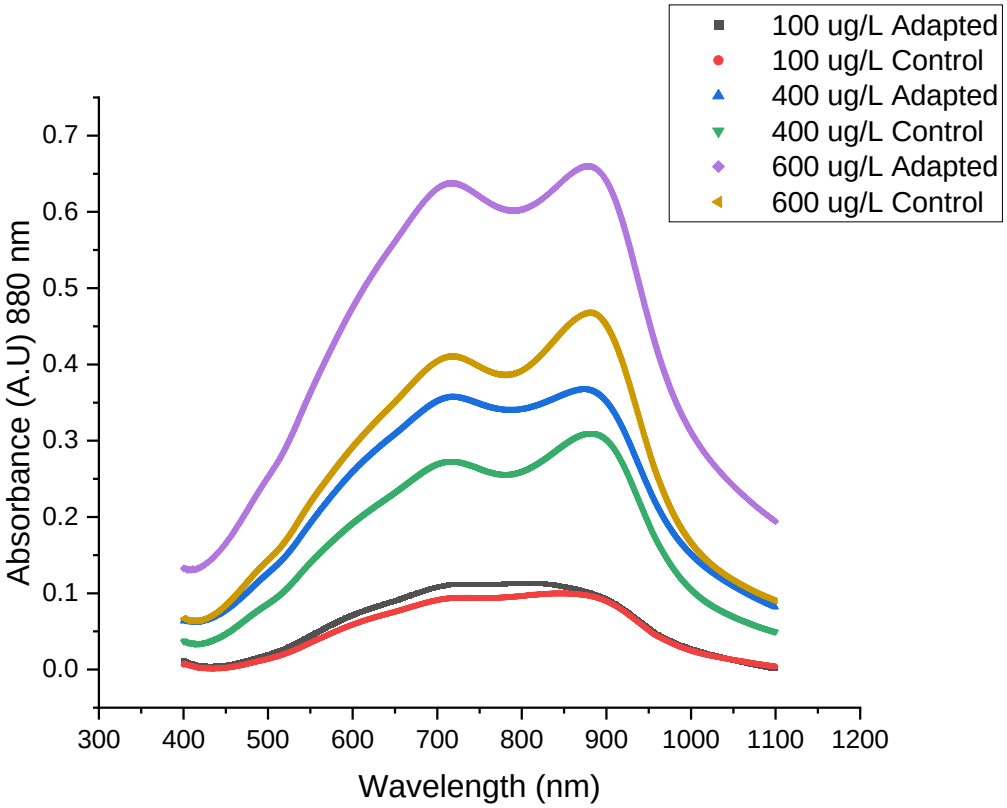

Figure 3.9 UV-visible Spectrum scan of a range of phosphate standards applied to both the adapted and control methods for comparison using a range of phospahte concentrations ranging from (100 µg/L to 600 µg/L).

3.3.3 pH optimisation

It was necessary to investigate on the influence of pH on colour formation, absorption of the phosphomolybdate complex and to determine the optimum pH value for the adapted method. The determination of the optimum pH for reaction is important for the characterisation reaction conditions. It is important that the solution is strongly acidic to ensure that molybdenum speciation occurs, and direct molybdenum reduction is inhibited. The pH of the solution contributes to the overall colour intensity that is produced from the phosphomolybdenum complex. Figure 3.10 highlights this effect on the absorbance valves obtained for the same phosphate standard and reagent mix at four different pH's.

The relative acidity of a solution is important in terms of analyte speciation – in this case phosphate. As mentioned previously phosphorus can present itself in different forms in a solution depending on the pH of that solution, described in Chapter 1. The pH of a solution also determines the rate of the reaction and can influence the physical and chemical composition of the heteropoly complex being formed. To measure the optimum pH for formation of the blue heteropoly acid a phosphate standard with a concentration of 100 µg/L was reacted with the molybdenum blue reagent which varied in acid strength to alter the pH.

The pH of the sulfuric and sodium bisulfate solutions ranged from 0 - 3 on the pH scale. The standard and combined reagent each made with the different acid solutions were allowed to react for 8 min and then an absorbance measurement of each was obtained on the spectrometer.

From the graph it is clearly observed that pH 0 - 1 was the optimum pH for the acid solution as it obtained the highest absorbance valves for both the adapted and control method. There is a significant decline in absorbance at the high pH values. The adapted method also shows a slightly decreased absorbance value to that of the control method.

Table 3.2 pH and molar concentrations of sodium hydrogen bisulfate and sulfuric acid.

pH	-log[H_3O^+]	Na_2SO_4 Molar (M)	-log[H^+]	H_2SO_4 Molar (M)
0	- log (1.0)	1	- log (1.0)	0.5
1	- log (0.1)	0.1	- log (0.05)	0.025
2	- log (0.01)	0.01	- log (0.005)	0.0025
3	- log (0.001)	0.001	- log (0.0005)	0.00025

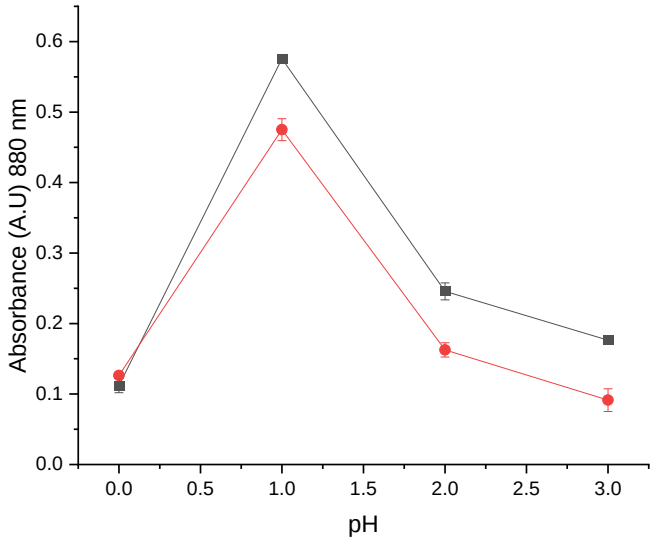

Figure 3.10 pH optimisation study, comparing the control and adapted methods. Ensuring full optimisation of the adapted method for successful and stable determination of phosphate, (n=3) for both methods. The black line represents the control method, and the red line represents the adapted method

3.3.4 Novel method for storage of reagents in a microfluidic disc design

To satisfy the criteria for the integration of the molybdenum blue method onto a microfluidic disc it involved investigating the ability to dehydrate the reagent, to reduce risk of evaporation and leaking from one reservoir to another. The reagents had to be all compatible with disc material, enabling them to be stored for a suitable period. The recovery of the reagents was also an important factor. Three different methods were investigated in this chapter (1) impregnation of filter paper, (2) dried solid compounds and (3) dried down liquid reagent solutions. The optimum and most suitable method for reagent integration was determined by the ease of integration, recovery of reagents, stability and lifetime of the method.

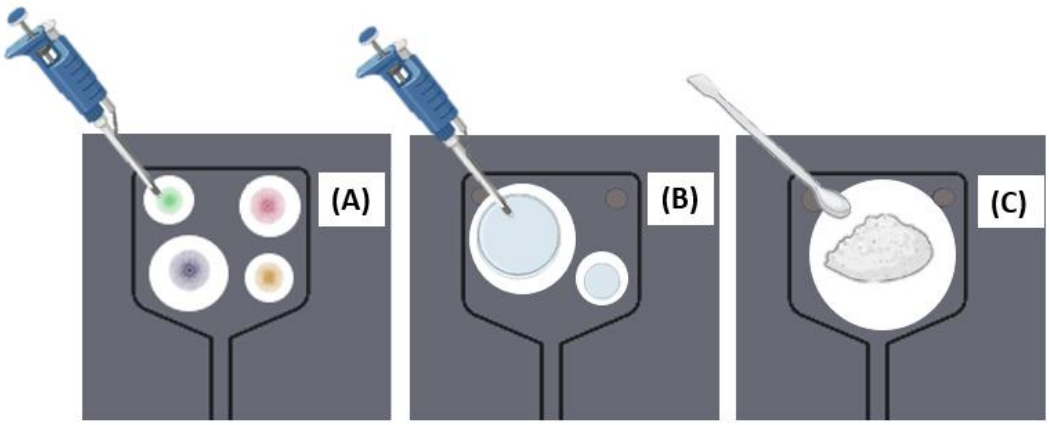

Figure 3.11 (A) Liquid dried reagents all separated out on individual pieces of PSA; (B) Impregnated filter paper with liquid reagents solutions, ascorbic acid separated out; and (C) Salt compounds weighted out in specific ratios and stuck down onto PSA.

3.3.4.1 Impregnated filter paper

The reagents were dried onto 0.45 µm ashless filter paper. The 5N sulfuric acid, ammonium molybdate and potassium antimonyl tartrate were all dried in the same piece of filter paper and the L-ascorbic acid was dried on a separate piece. This was done to isolate the most unstable compound in the combined reagent the L-ascorbic acid. To ensure full resuspension of the reagents, the ratio of reagent to sample was increased by a factor of 2. The two pieces of filter paper were dried in a glass petri dish under a constant low-pressure stream of N_2 gas for approximately 1 h. Once dried the filter paper was transferred into the partially assembled microfluidic disc, and full assembly was completed by sealing the top PMMA layer onto the top PSA layer in a clean room environment. The dried reagents were resuspended by adding in a water sample (see Figure 3.12). This was added into the introduction chamber using a micropipette. The sample and dried reagents were allowed to mix for 5 min and the liquid was drawn back out of the introduction chamber and pipetted into a cuvette where it could be transferred to a UV/vis spectrometer for analysis. A calibration curve was generated using a range of phosphate standards (0-400 ug/L).

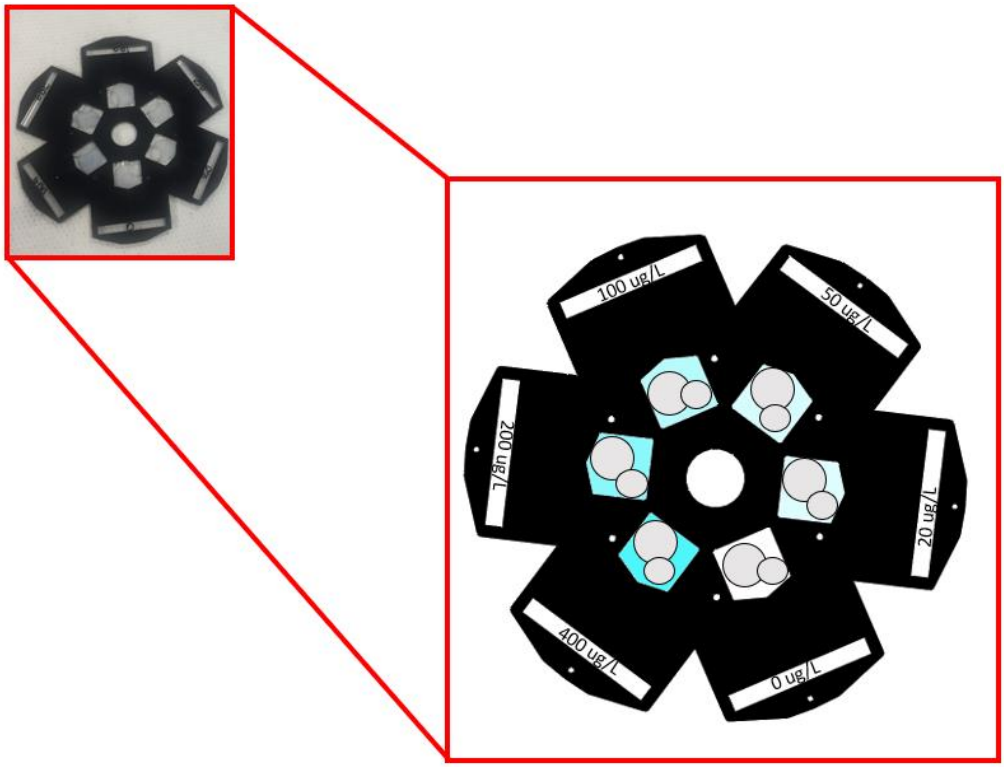

Figure 3.12 Impregnated filter paper incorporated into microfluidic disc. Calibration curve generated from a range of phosphate standards (0-400 µg/L) n=3 on 3 individual discs.

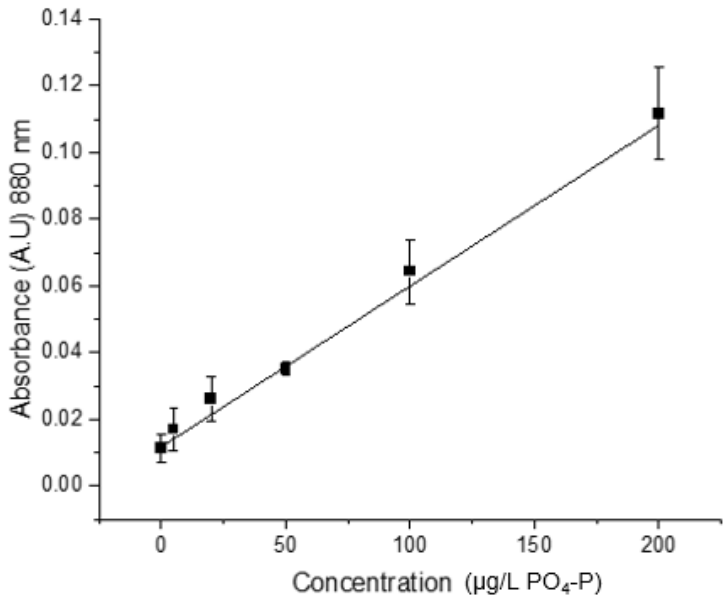

Figure 3.13 Calibration curve of the impregnated filter paper with reagents for the molybdenum blue method, (n=3) which obtained an R2 value of 0.993 and a slope of 0.005.

Figure 3.13 highlights the success of this method in producing a linear graph with a good slope and R^2 value of 0.993. However, when the method was investigated to determine the lifetime, it was observed that the filter paper began to degrade after 2 days, there was also a slight colour development on the paper. Therefore, it was confirmed that this method was not stable or reproducible enough to be considered for long-term reagent storage of the molybdenum blue method. The difficulty of storing a strong acid such as sulfuric acid also proved to be a problem as that is what caused to degradation of the filter material. To examine this, all components of the combined reagent were stored on separate filter pieces and the piece that was used to store the sulfuric acid demonstrated the degradation of the fibres. The next two methods of reagent storage incorporated an adapted version of the molybdenum blue method to facilitate the storage of the reagent with an increased lifetime.

3.3.4.2 Dried compounds

This method of reagent integration involves incorporating the dried compounds out of solution onto the disc. The sulfuric acid was replaced with sodium hydrogen bisulfate to create the acid medium needed for the reaction to take place. As the compound measurements were extremely small for the 600 µL reservoir volume, the original design was altered to facilitate an increased volume so that the reagent compound measurements could be scaled up for ease of the experiment. The new sample volume was 6 mL, therefore, all reagents were increased to facilitate the 1:0.16 sample reagent ratio. The compounds were all stuck down to the base of the disc using double sided PSA. This study was carried out to determine the linearity, stability and reproducibility of this method. Once the compounds were stuck down the top PMMA layer was assembled and sealed to prevent any air or moisture getting into the introduction chamber and having an undesirable effect on the dried compounds (see Figure 3.14). The samples were then pipetted into the chambers and the reaction was left to develop for 5 min (Figure 3.15). The solutions were then drawn back out the disc and pipetted into cuvettes for measurement on the spectrometer. The standards ranged from 10 – 600 µg/L. The graph generated in Figure 3.16, showed excellent linearity for this method which obtained an R^2 value of 0.998. However, upon further analysis this method was too difficult to incorporate onto a disc as the compound measurements required were too small to measure accurately therefore, effecting the reproducibility of the method.

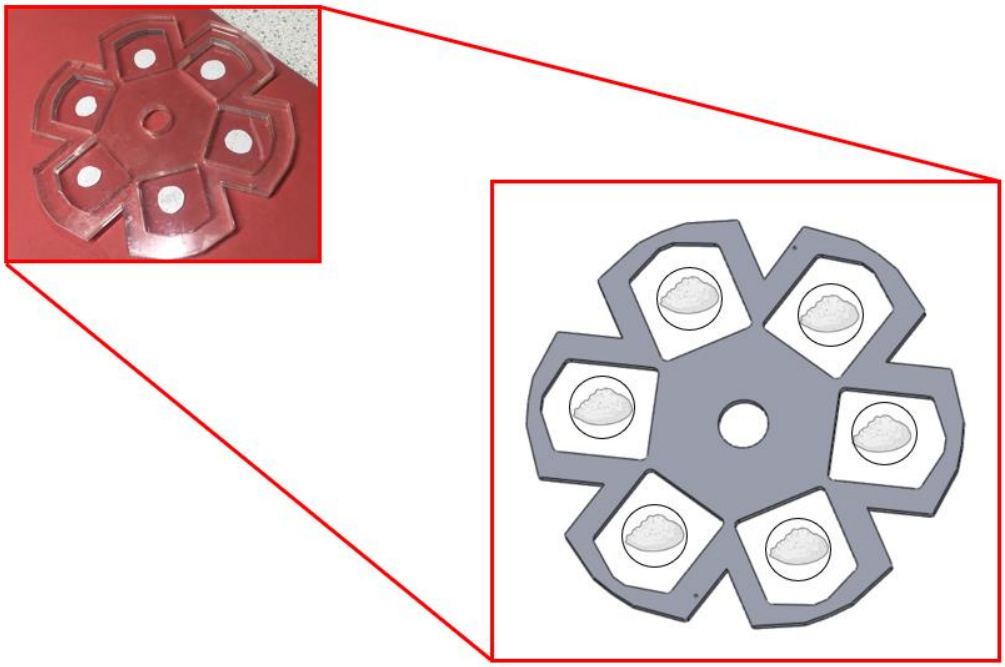

Figure 3.14 Dried compounds incorporated onto disc to determine storage stability and recovery ability, disc design altered to facilitate the increase in reagent and sample volume. All dried compounds stuck down onto a single piece of PSA.

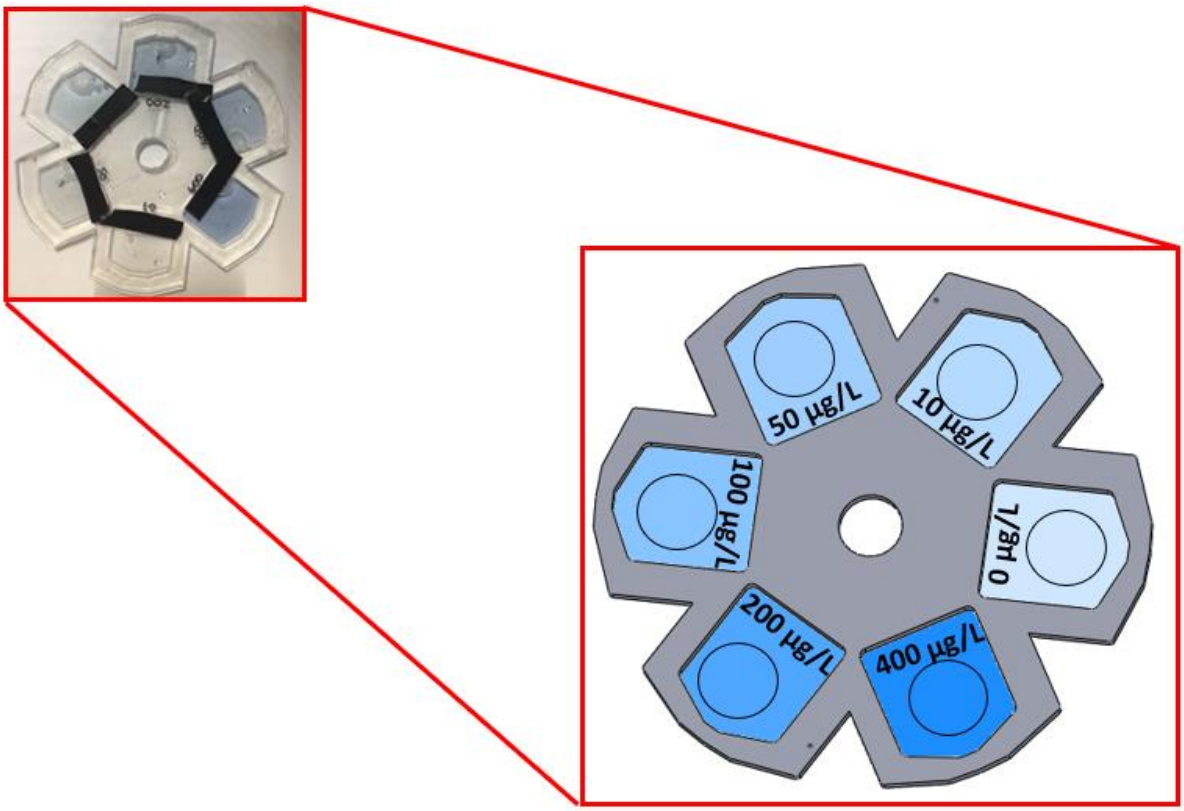

Figure 3.15 Dried compounds and phosphate standards on disc. A range of phosphate standards (10-600 ug/L) were used to investigating the recovery and linearity of the method. Reagents were scaled up to facilitate ease of weighing out the compounds on an analytical.

Figure 3.14 shows the storage of the dried compounds on the discs and Figure 3.15 illustrates the reaction of the reagents with standards. to produce the blue coloured complex. These images also show the successful recovery of the reagents when mixed with the phosphate standards in the introduction chamber.

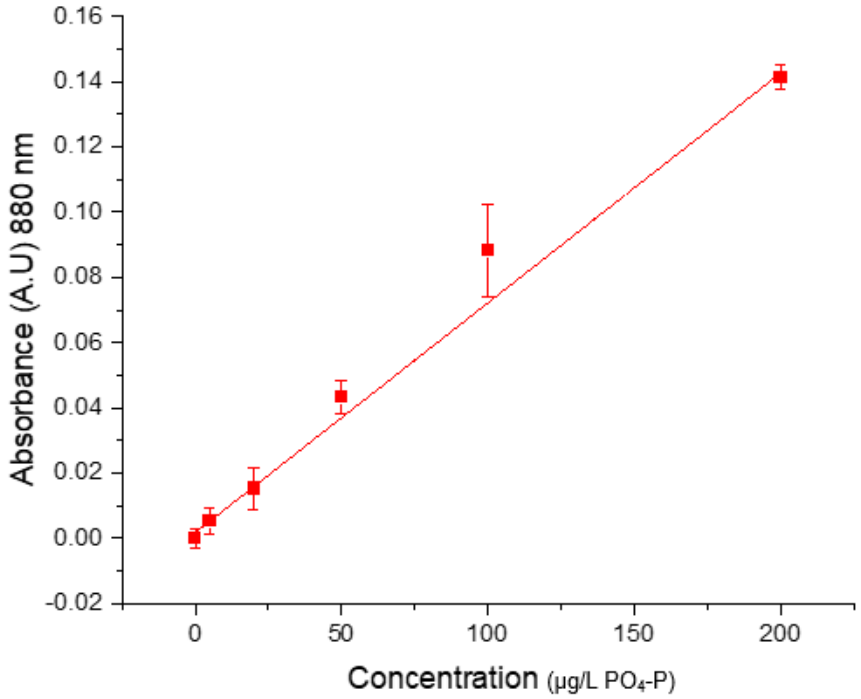

Figure 3.16 Calibration curve of the scaled up dried compounds for the molybdenum blue method, (n=3) which obtained an R^2 value of 0.998 and a slope of 0.006.

The results obtained from the dried compound integration produced a calibration curve slightly more linear than the impregnated filter paper with an R^2 value of 0.998. However due to the volumes of weighed compounds required for the combined reagent this method was difficult to measure out the exact quantities, resulting in a complex technique.

3.3.4.3 Dried down liquid reagents on PSA

The last method involved the drying down of the four components of the combined reagent in liquid form. This method was investigated to combat the limitations of the previous two methods. This technique involved drying down potassium antimoyl tartrate, ammonium moybdate tetrahydrate, L-ascorbic acid and sodium hydrogen bisulfate in the specific ratios to form the combined reagent. The reagents were pipetted down on a partially assembled disc and dried in an oven heated to 37 °C for 2 h. Once all reagent droplets had dried the partially assembled disc was fully assembled by placing the top PMMA layer on and sealing. The discs were all stored in tinfoil to prevent dried sunlight from interfering with the chemistries causing evaporation, condensation or colour development. The first drying technique that was trialled was the drying down of the reagents on two separate pieces of PSA. The larger Graphtec cut piece was used to integrate potassium antimoyl tartrate, ammonium moybdate tetrahydrate and sodium hydrogen bisulfate and the second was used to isolate L-ascorbic acid. This method produced linear results with good sensitivity however, after 1 day there was a noticeable colour development on the PSA that incorporated the combined compounds. Figure 3.17 highlights this slight colour development in well 2 of the disc. A control using the sulfuric acid was also used in this experiment shown in well 3 and 4. From this it was determined that the most successful drying method involved the separation of all the compounds on separate pieces of PSA (see Figure 3.18)

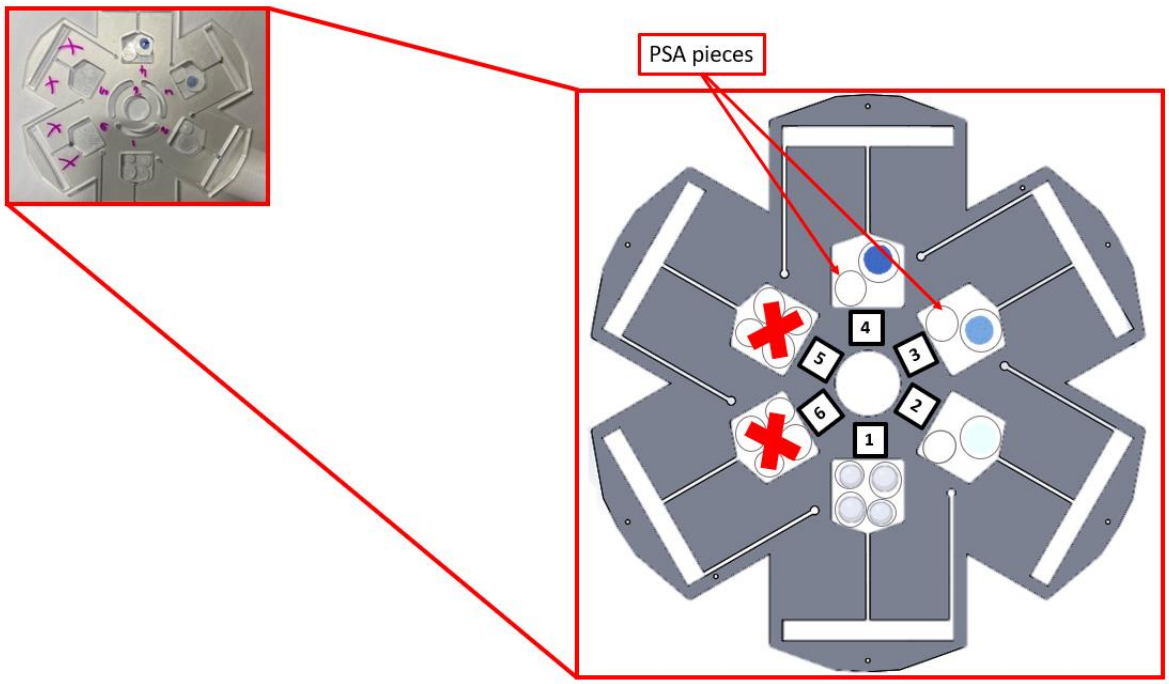

Figure 3.17 Schematic of a disc testing different methods for the oven dried technique. Well 1; liquid dried all separated out, well 2; adapted method with ascorbic acid isolated and well 3 and 4; control molybdenum blue method. Images conveying a strong colour development in wells 3 and 4 and a slight colour development in well 2 after 1 day storage.

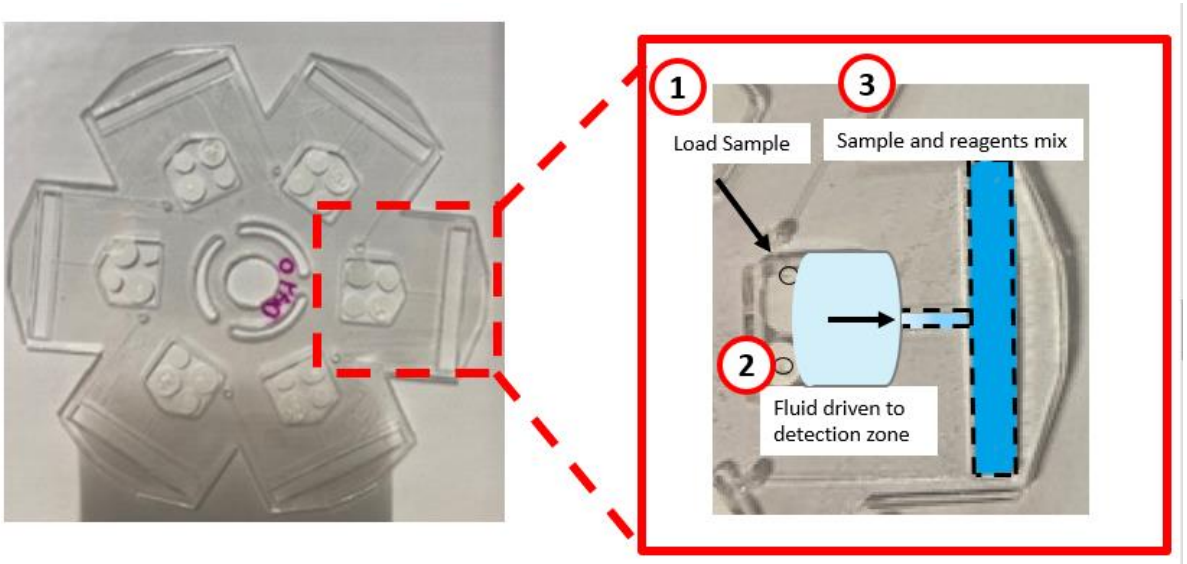

Figure 3.18 Left; Final design for reagent integration. Incorporated the liquid dried reagents on separate pieces of PSA into the introduction chambers on the disc. Right; fluid flow of samples entering the disc, centrifugally driven down into the pathlength well via the microchannel.

An IR spectrum of the liquid dried method was obtained and analysed. The spectrum includes the control liquid reagent for reference. The region around 3300 – 3600 is typically where the O-H bonds are represented, and the spectrum highlights the O-H bond has been significantly reduced compared to that of the control liquid sample. The control sample contains a broad O-H bond whereas the crystal sample shows the decrease in strength of the bond.

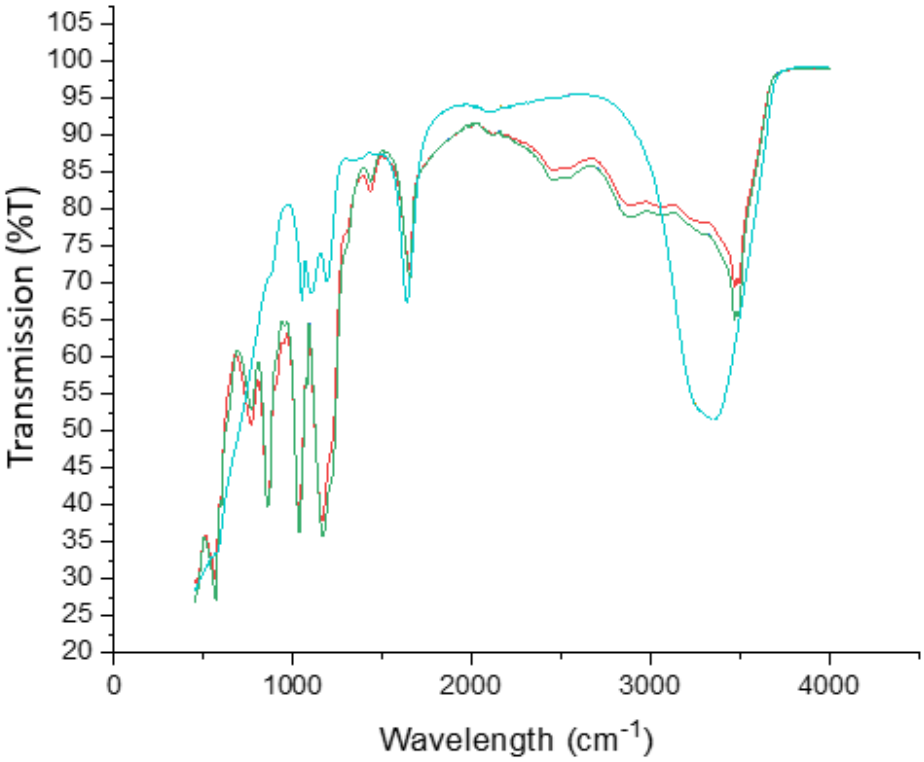

Figure 3.19 IR spectrum scan on the liquid dried reagents, observing O-H peak ~ 3000-3500, this peak has significantly decreased in the dried reagents (n=3) showing successful drying down of the method.

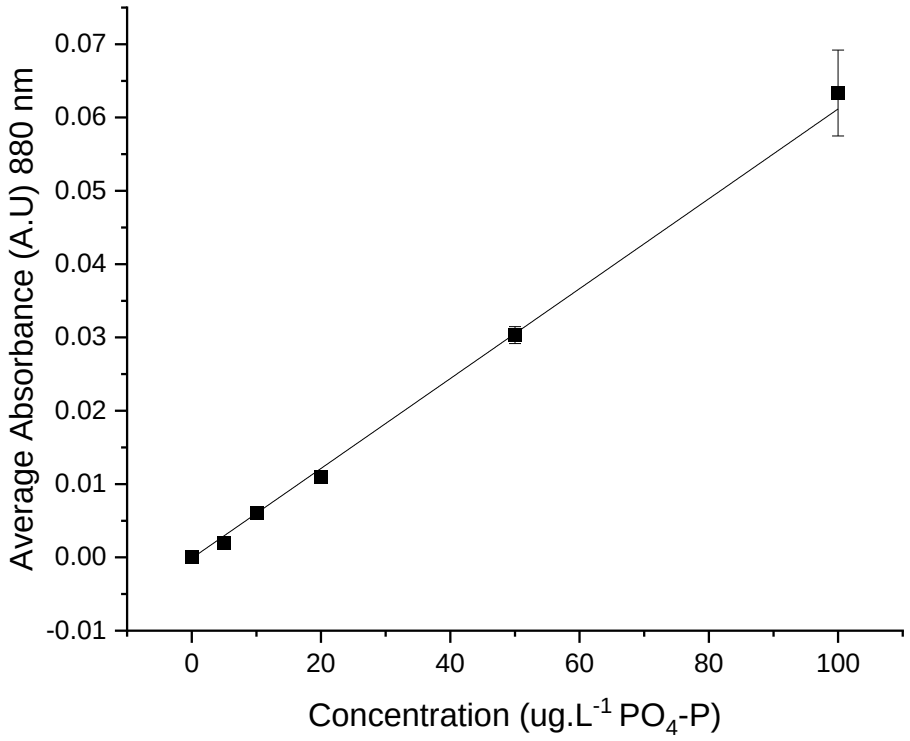

Figure 3.20 Calibration curve obtained from liquid dried reagents on PSA. Range of phosphate standards used to generate the graph (0-100 ug/L), n=3 for each measurement obtaining an R2 value of 0.999 and a slope of 0.0006.

A linear range was achieved with an R^2 value of 0.999 and with a slope of 0.0006, which directly compares to that of the slope generated for the control method. It also achieved an LOD of 2 µg/L making it suitable for phosphate detection in freshwater low phosphate catchments.

3.3.5 Kinetic analysis of the adapted method

A kinetics experiment was carried out on the adapted method to further investigate the effects of pH on stability of the reaction. This experiment involved observing the adapted method with normal amount of sodium bisulfate and an increased amount to determine its effect on the stability of the reaction. The concentration of sodium bisulfate was increased giving it a lower pH and therefore a more stable reaction over a longer period. Figure 3.21 and Figure 3.22 highlight the variation in stability by caused by the amount of sodium bisulfate present. Figure 3.21 shows the increase in absorbance over a 60 min time period, the slope is also increasing and in comparison, Figure 3.22 shows a stable reaction for 60 min, with the same absorbance and slope achieved for each reading over the controlled time period, this was then compared to the control method.

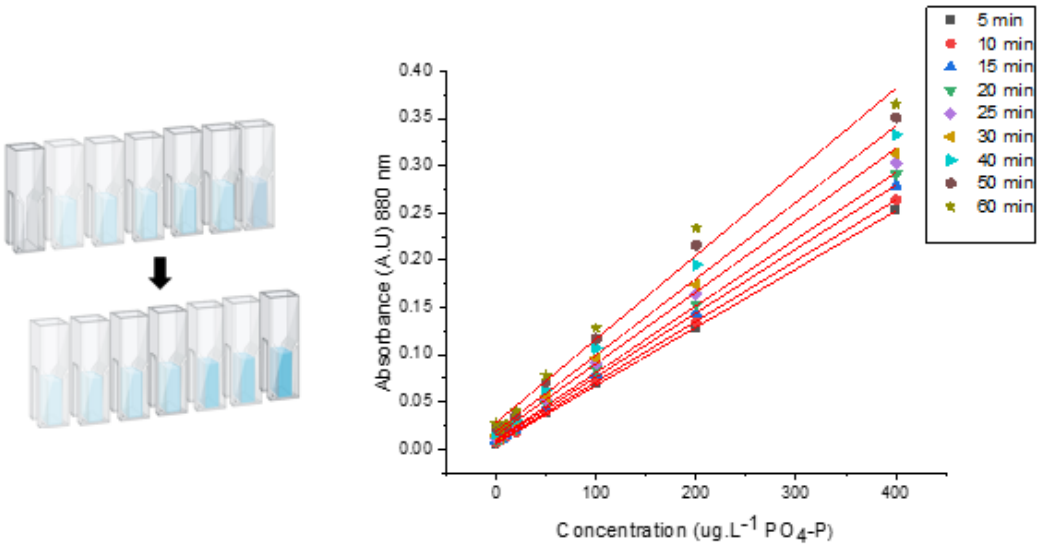

Figure 3.21 Left: Schematic of the unstable reagent, continual colour development. Right: Development study for the adapted method with decreased Na2SO4 concentration (higher pH) over a 60 min period.

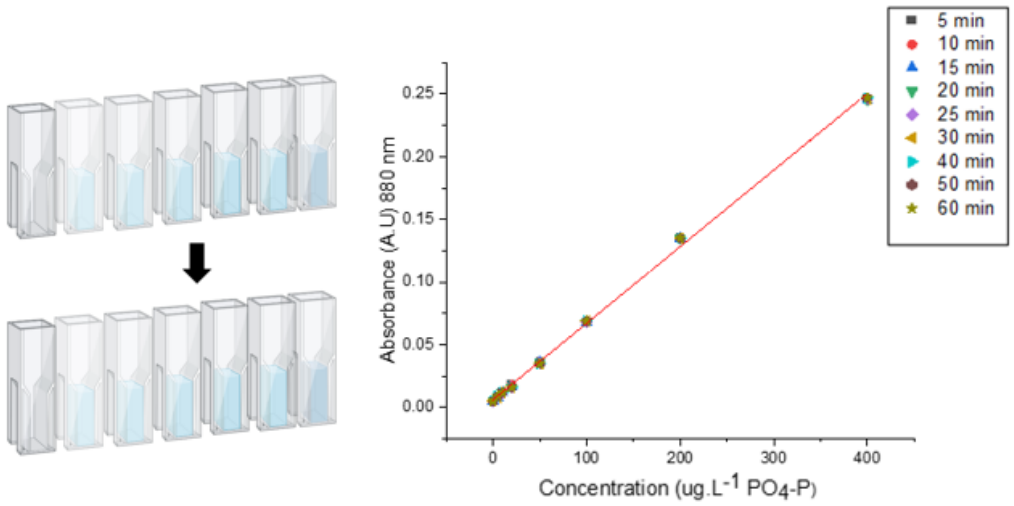

Figure 3.22 Left: Schematic of stable reagents with no further colour development. Right: Development study for the adapted method with increased Na2SO4 concentration (lower pH) over a 60 min period.

Figure 3.23 and Figure 3.24 shows the effects of stability on the development time of the reaction. The adapted method with a decrease amount of sodium bisulfate takes a longer time to come to completion as it is more unstable (see Figure 3.23)

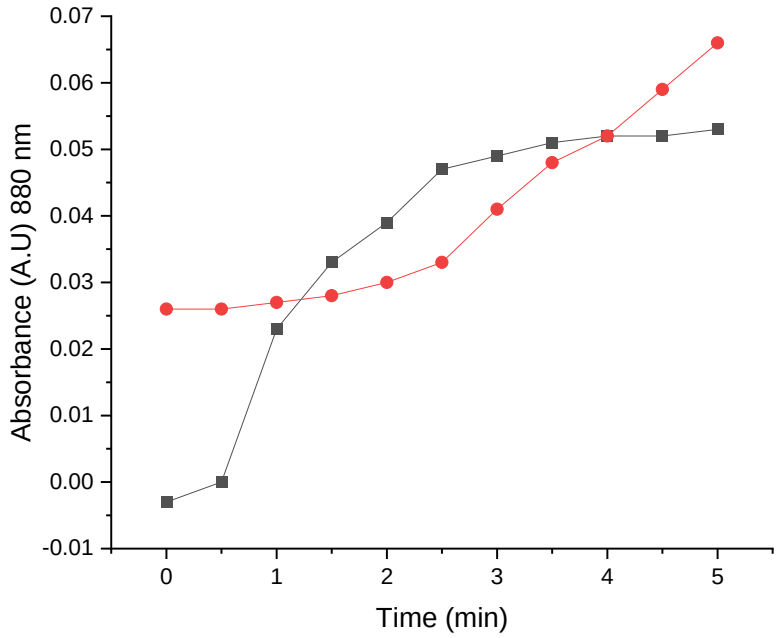

Figure 3.23 Use of the lower acidic medium concentration in the adapted (red) compared to the controlled method (black). Conveying a less stabilised reaction time to that of the control method.

Once the concentration of sodium bisulfate is increased it behaves similarly to the control method (Figure 3.24) and takes less time to come to completion, therefore making it more suitable for long-term storage on a microfluidic device. It also determines the reaction time for the sample and reagent solution which has been defined between 5-10 min, this is accepted within literature values which range between 8 – 20 min [50].

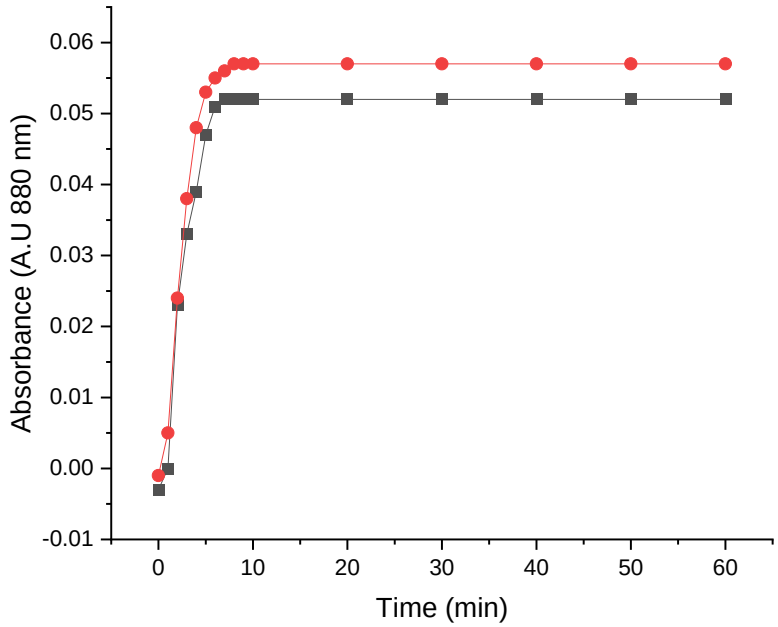

Figure 3.24 Increasing the acid medium (decreasing the pH) to stabilise the reaction time. The adapted method reaction time (red) is compared to the control method (black) for reference.

3.3.6 Investigation into the optimal development time for the dried reagents

Optimal development time for the adapted dried method was also investigated. This study involved assembling a microfluidic disc with on-board dried chemistry and adding a phosphate standard (400 µg/L). Three different development times were chosen, 0, 5 and 10 min, each well was left for a specific development time and then read on the system every 15 s from 0 – 10 min. The analysis from the results displayed in Figure 3.25 determined that the optimum development time for the dried reagents and sample is about >10 min. This was determined by the stability of the reaction when read after 10 min compared to the variance in readings when read after 0 and 5 min.

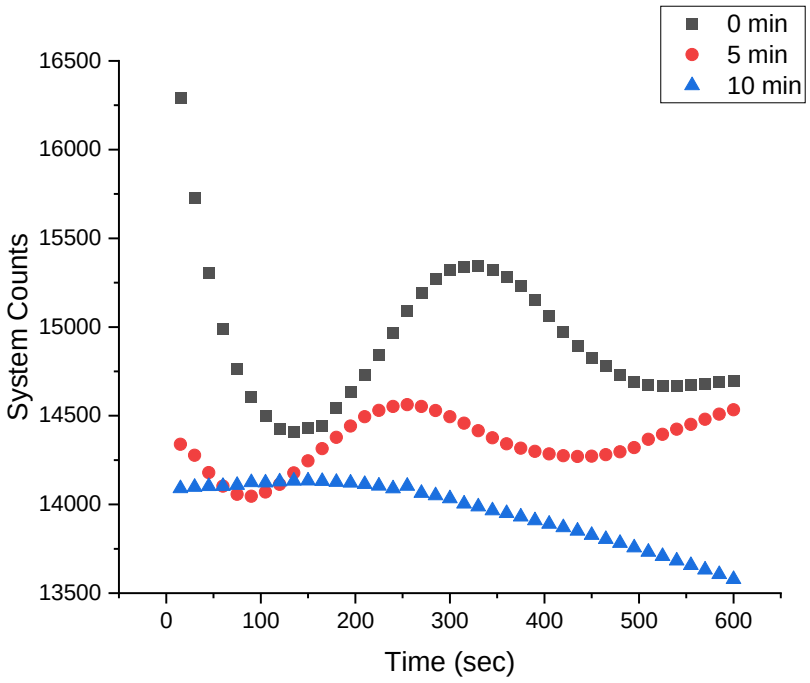

Figure 3.25 Study to determine optimum development time, three time periods were chosen (0, 5 and 10 min).

3.3.7 Investigation of lifetime of on-board storage of reagents

In this chapter, we pay particular attention to the long-term stability of molybdenum blue method, and its suitability for use in a microfluidic device paying focusing on the long-term reproducibility of the adapted method, the lifetime of the reagent, and the simplification of the assay integration.

The lifetime of the assay was determined to demonstrate the chemical stability derived from the calibration curves generated. A total of 42 discs were prepared on the same day, to allow for a 30-day lifetime study. The discs were planned to be tested on day 0, 1, 3, 5, 7, 10, 12, 15, 17, 20, 23, 25, 27 and 30. Each disc in triplicate was used to obtain a calibration curve. A range of low concentration phosphate standards (0 – 100 µg/L) were pipetted into the six introduction chambers of each disc and allowed to develop. The sample and reagent mixed solution were then drawn back out of the disc via a micro pipette and placed into a standard 1-cm cuvette to obtain an absorbance value of the blue complex formed in the UV/vis spectrometer and a λ of 880 nm.

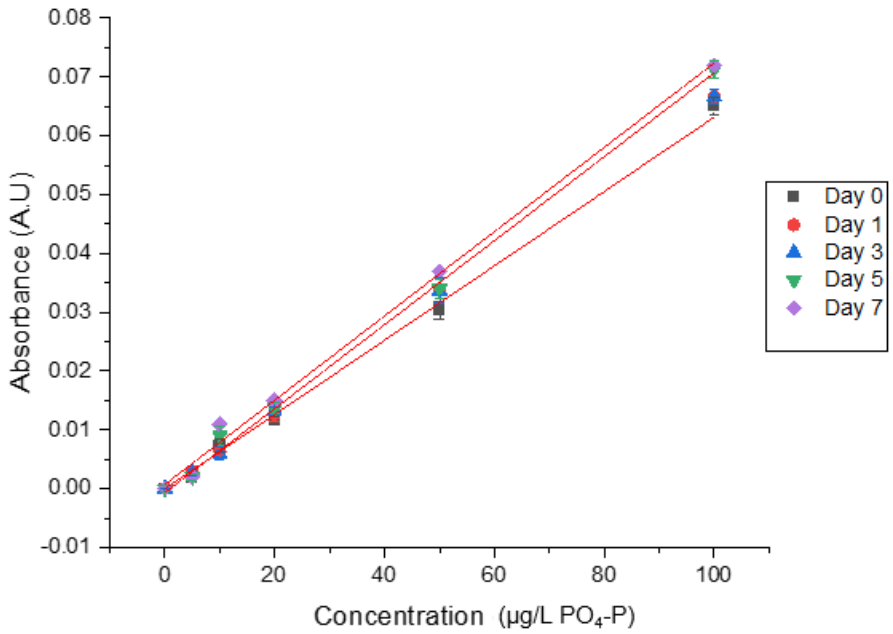

Figure 3.26 Lifetime study for the onboard stored reagent for a 7-day period.

On Day 10 an orange colour development on the spot where the ascorbic acid droplet was placed was observed, see Figure 3.27 for reference. This is a common colour change for the degradation of ascorbic acid. Therefore, this suggests that this method of drying down liquid reagents is stable for up to 7 days.

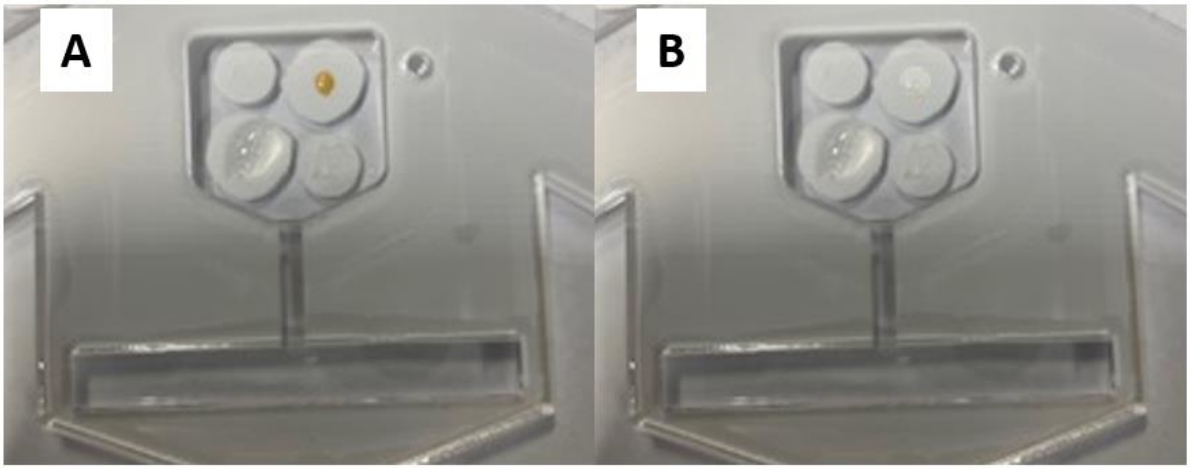

Figure 3.27 Degradation of the ascorbic acid solution after a 10-day period showing a strong colour formation compared to (B) dried reagents after 1 day, no colour development on the ascorbic acid.

3.4 Application to environmental samples

3.4.1 River samples

Water samples for method validation were sourced from two rivers, the River Rye in Co. Meath and the River Tolka in Co. Dublin. Grab samples were obtained from a single sampling location on both rivers and were measured using both the control and adapted method on a UV/vis spectrometer. This was a once off sampling campaign to validate the adapted method, therefore a single grab sample from each river sufficed.

3.4.2 Sampling and storage

The river samples were collected in 500 mL sterile rinsed, amber plastic sampling bottles. All bottles were soaked in a non-phosphorus containing detergent to sterilise them. Once sterilised the bottles were then rinsed under a stream of deionised water. On-site the samples were collected in a wide neck plastic bottle attached to a sampling rod where it was used to obtain water from the surface of the water body. From this 10 mL aliquots were extracted using a plastic syringe with a 0.45 µm filter attached. The filtered samples were stored in the sterile amber plastic bottles, this was repeated until the 500 mL bottle was full. The bottle was then sealed with the airtight cap, to mitigate degradation of the phosphate ions in solution. This was an important step as the samples had to be transported back to the laboratory for analysis, as orthophosphate becomes bio-available and leaches onto glass – therefore plastic bottles should be used to help preserve the sample [55].

3.4.3 Locations

The EPA publish a report entitled “State of the Environment” on a four-year cycle. This report presents detailed information on the quality of Irelands environment, a sub-section of this report disclosed information on water quality which includes nutrient pollution is a useful tool for implementing a sampling campaign. For the purpose of this study, samples were obtained from known DCU sampling sites carried out by members of DCU Water Institute. This facilitated ease of sample transportation back to DCU laboratories for analysis. The River Tolka was chosen due to its, densely populated urban landscape and the River Rye was chosen as a comparison site as it has a more suburban landscape.

3.4.4 Validation of the dried method on environmental samples

The measurements for the dried adapted molybdenum blue method were validated against a reference standard control spectrometric method. Figure 3.28 provides a comparison of the adapted method to that of the controlled molybdenum blue standard method using environmental samples. The error bars are masked by the plotted dues, conveying good reproducibility and linearity with an R^2 values for 0.999 and 0.998 for the control and dried adapted method respectively, yielding a low relative standard deviation of 1.33% and 1.34% for both calibrations. This graph provides the linear plot of the absorbances for each method over a concentration range of 0-400 ug/L at the reference wavelength of 880 nm.

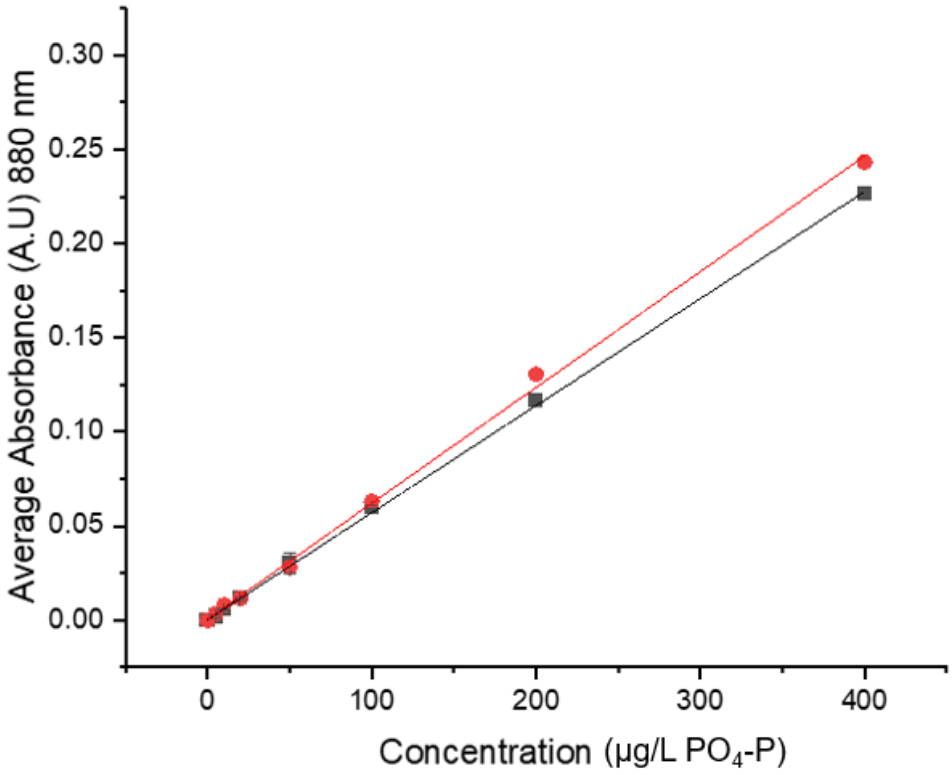

Figure 3.28 Comparison of the control (black line) and adapted method (red line) over a concentration range of 0-400 ug/L for validation of the adapted method applied to environmental river samples, n=3 for both curves.

To make a direct comparison of the absorbance values obtained the experimental concentrations of each of the measured environmental samples were determined using the equation the line generated from calibration curve.

The experimental concentrations for the unspiked and spiked River Tolka and River Rye samples are summarised in Table 3.3. Overall, the comparison for both methods was good, showing similar absorbance values to the control method. This indicates that the adapted method is a valid way of detection phosphate in environmental samples and can produce reproducible and repeatable measurements.

Table 3.3 Spectrometric measurements for environmental samples applied to the control and adapted molybdenum blue method.

Sample Concentration (ug/L) P	Absorbance (Control method)	Concentration (ug/L)	%RSD (n=3)	Absorbance (Adapted method)	Concentration (ug/L)	%RSD (n=3)
Rye Unspiked	0.02	33	2.28	0.03	43	3.70
Rye Spiked 100	0.08	126	1.23	0.08	138	1.19
Tolka Unspiked	0.03	50	2.63	0.07	59	3.15
Tolka Spiked 100	0.10	165	1.41	0.11	180	1.84

3.5 Conclusion

A novel method for the on-board storage of the molybdenum blue assay in a microfluidic manifold for on-site detection of phosphate has been developed. The molybdenum blue assay is proven to be an excellent choice for the determination of phosphate in terms of its, low LOD, wide linear range and now from this work its improved lifetime and stability. Adoption of this adapted method and novel storage technique has produced a self-contained device that eliminates reagent handling, reduced contamination and simplifies the steps to be carried out on-site.

In this study the development and examination of three methods for reagent integration were designed and tested. The results demonstrate that the most successful method of storing reagents on-board was by drying down the liquid reagents onto PSA. This method facilitated an LOD of 2 µg/L, a linear range of 6 – 400 µg/L and a reaction time of >10 min. This method satisfies the demand for the development of simple and stable reagent integration techniques.

The method has a lifetime of 7 days which has been improved from the 4 h lifetime of the original wet chemistry method. This lifetime could be further improved through optimisation of storage conditions. It was also proved in this study that the replacement of sulfuric acid with sodium bisulfate is possible and maintained satisfactory analytical results, making the reagent easier to dry down and facilitates the ability for other drying methods to be investigated.

The ability of this method to be dried down for reagent storage on a microfluidic device transforms how the manufacture of a low-cost, sensitive, self-contained, and robust sensor can be developed. Therefore, the vision of an instrument to monitor levels of phosphate in freshwater environments in an inexpensive, simple, and rapid manner can be realised.

Chapter 4: PhosphaLOAD: Characterisation and validation of an integrated phosphate analyser

4.1 Introduction

The traditional methods of monitoring nutrient contaminants generally involve the invasive collection of samples in the field and transporting them back to laboratories to be analysed [245]. Regrettably due to the speciation of many nutrient contaminants their forms may have altered as a result of a biological, physical or chemical reaction [246], the long delays involved with this type of monitoring method is currently unacceptable. Catchment managers are demanding the rapid onsite detection of contaminants for a more intensive environmental monitoring [247]. In recent years important progress has been made in the improvement of analysis and data quality obtained by *in-situ* sensing devices, which are rapidly becoming integrated into observation frameworks [101]. This chapter aims to discuss the current limitations of commercially available *in-situ* sensors on the market, providing evidence for new sensing technologies in the form of portable handheld devices for chemical analysis. The main body of this chapter involves the design, characterisation and validation of a LOAD integrated phosphate analyser for the detection of phosphate in freshwater catchments, known as PhosphaLOAD.

4.1.1 Limitations with current monitoring technologies

There are significant issues in terms of calibration and supporting infrastructure required with conventional *in-situ* chemical sensors on the market. They require a large amount of reagents and standards and also expensive pumps and flow systems [83], increasing the cost of manufacturing. One of the biggest problems associated with automated sensors is biofouling. There are over 4,000 organisms that can contribute to fouling on these *in-situ* platforms [105], increasing the costs by the level of maintenance required to keep them in operation. Major concern surrounding these problems have been highlighted by regulatory agencies concerned with evaluating water resources in attempts to ensure that all environmental levels of chemical, biological and physical variables are maintained within an acceptable criterion. Due to the cost, service requirements, power consumption and risk of the vandalism or theft to this devices, there is a demand for more low cost handheld sensing devices that can provide quality assurance and control of the sensor data being obtained [248].

The quality assurance and reliability for obtaining long-term sensing data in complex environments is scarce. Some current commercial sensors suffer from sensitivity to high background ion concentration [96], effecting the quality of the data being analysed.

The field of microfluidic based sensing systems has been widely developed in various fields from environmental to point of care in the last decade because of the many advantages it possesses such as low sample volume, high throughput, reduced contamination, fast detection times and elimination of reagent handling and integration capabilities (discussed in

more detail in Chapter 2). A number of chemical sensors have been commercialised that are capable of detecting phosphate in natural waters, see Table 4.1. Compared to some the commercial sensors available, the use of microfluidics scales down the size of the instruments needed for *in-situ* measurements without compromising the efficiency and reliability of the results.

Table 4.1 Comparison of handheld/portable phosphate detection devices

Sensor	LOD	Linear Range	Analysis Time	Comments	Approximate market cost
Sea-Bird Scientific HydroCycle-PO4 Phosphate Sensor Sea-Bird Scientific	0.002 mg/L	0.0 - 0.3 mg/L	Real-time measurements	Commercial device, low limit of detection but high cost. No sample preparation required.	~ €20,000
IQ SensorNet Alyza Analyzer PO4 YSI xylem a brand	0.05 mg/L	0.0 - 50.0 mg/L	Real-time measurements	Commercial device. Vanadomolybdate (yellow) method of detection, LOD not low enough for freshwater, high cost involved. No sample preparation required.	€16,000
Flow injection analysis microfluidic chip [213]	0.2 mg/L	0 –50 mg/L	3 min	High LOD, not suitable for detecting low limits of phosphate. Sample preparation required.	≥ €3,500
Smart-phone, paper-based fluorescent sensor for ultra-low inorganic phosphate [249]	0.001 mg/L	0.001 – 0.064 mg/L	Real-time (4 s)	Small, portable and can detect ultra-low levels of inorganic phosphate. Single use sensor – increased cost and waste	≥ €1,000

				associated. Sample preparation required.	

In-field sensor technology can add value to the traditional methods of water quality monitoring. These devices are used to record a number of chemical properties and water parameters such as pH, temperature, conductivity, turbidity salinity, dissolved oxygen, nitrate and phosphate which are used for groundwater profiling and improvements, wastewater treatment and monitoring agricultural production. The main advantage of these sensors is their portability and a limitation of them is their cost price. Sensors used to monitor pH, temperature, conductivity, turbidity, salinity and dissolved oxygen are widely established on the market to date, however sensors programmed to monitor nitrate and phosphate are less widely understood. The work currently involved in the development of phosphate sensor is generally centred on improving the level of sensitivity and selectivity, as common interferences such as silicate, chloride and manganese have been associated with them [250].

The advantage of developing *in-situ* sampling sensors based on the principle of microfluidics is to drive down the cost of fabrication and manufacture. The more cost effective these devices are means that more can be manufactured and therefore deployed. In turn generating more data and analysis. A major advantage of *in-situ* sensing is the material chemistries that can be used, which minimise costs significantly, offering a solution to the many limitations of current commercial sensors. Thermoplastics are composed of branched chain molecules and therefore makes them resistant against, pressure or temperature changes [251]. Thermoplastics are the most common and compatible substate material used in microfluidic devices, these materials have improved on more common materials that would have been used previously such as glass or silicon [252]. Microfluidic devices using thermoplastics can be easily manufactured by direct milling or machining methods. The mircochannels can be fabricated using inexpensive methods such as milling [253], hot embossing [254], laser ablation [255] or injection moulding [256]. Microfluidic components used for colorimetric nutrient sensors, require the material substrate to be optically transparent. PMMA, polycarbonate (PC), cyclic olefin copolymers (COC) and polydimethylsiloxane (PDMS) are commonly used in the fabrication of microfluidic chips and discs [257]. An important consideration when choosing a thermoplastic substate is the compatibility for the analyte, reagents, and environment it will be used in. For example PC is highly sensitive to photodegradation and with long periods of UV exposure can develop a yellowing on the material [258]. In recent years, materials such as PMMA and PDMS have become more

popular for colorimetric nutrient microfluidic applications. These materials demonstrate good compatibility, are inexpensive and have good transparent and optical properties [259].

4.1.2 State of the art microfluidic sensing devices for nutrient monitoring

The development and innovation of portable handheld devices are pivotal in the transitioning these instruments from lab to field [260]. The systems need to achieve good sample processing automation and measurement, portability, low sample and reagent consumption, near real-time to real-time measurements [261]. *Cleary et al.,* discusses the development of an autonomous microfluidic analyser for environmental monitoring. The device was manufactured to measure phosphate in the field. The sensor is based on the molybdenum yellow method for phosphate detection. This device utilised low sample and reagent volumes, portability and cost effectiveness [262]. However due to the wet chemistry method chosen the limit of detection is not sensitive enough for the effective monitoring of low phosphate levels in many waterbodies, as this method has an LOD of 100 µg/L. In comparison *Grand et al.,* demonstrates the performance of a LOC phosphate analyser for long-term *in-situ* monitoring with a low LOD of 30 nM. The two phosphate analysers provide a strong basis for successful new sensing technologies being deployed in the field but fail to demonstrate wide analysis of the site being monitored as they are only capturing a snapshot of the area. Long-term routine analysers for water quality sampling are commonly used in nutrient monitoring, this type of monitoring provides information on long-term trends [263], but fails to provide insight on higher resolution data into the hydrological processes going on within the water body [264]. The advances in environmental monitoring mentioned above provide evidence as to why these new areas of technology integration are required to provide and collect higher spatial data for a wide range of water quality parameters.

To obtain more information about the levels of phosphate present in surface waters – monitoring and sampling must be as frequent as possible. Monitoring systems are put in place to improve the quality of information being gathered about an area. Continuous monitoring overcomes the problem of frequency by providing long-term intensive observation and sampling.

While autonomous sensors have value, the nature of phosphate occurrence in surface waters is linked to land use practices, erosion etc. which can vary along a water course. A single sensor at a single location can provide good temporal information, but additional spatial information is desirable. This would be costly to achieve with numerous autonomous *in-situ* sensors. Hence providing a market of low-cost portable handheld sensors.

Wang et al., explores the use of a portable LOC device for on-site detection of nitrate. The sensor provides fast detection time (115 s per sample), low reagent consumptions (26.8 µL per sample) and in contrast to the work carried out by *Cleary et al.,* and *Grand et al.,* it is a portable device, that can gather information from a number of sites on a single field monitoring campaign [265].

4.1.3 Aims and objectives

The aim of this piece of work is to provide justification for the use of handheld sensing devices for the detection of nutrients such as phosphate in freshwater. By designing and fabricating a low cost, robust, reliable and highly sensitive monitoring device. The objectives of this chapter are (1) optimise sensor components to enhance the successful and low-cost development of a phosphate analyser "PhosphaLOAD" for freshwater environments, (2) combine the microfluidic disc described in Chapter 2 with the analysis platform to manufacture a self-contained device. The capillary active micro-channels used in the disc are integrated internally, enabling precise volumes of fluids to be moved from one area on the disc to another. Upon loading the water sample into the disc, the fluid is mixed with the dried reagents and subsequently moved through the disc using centrifugal force. This is created by rotation of the disc by the incorporated motor. Once mixing has occurred, this force will then drive the fluid into the optical detection pathlength. The low-cost optical detection system consists of an LED-photodiode transducing pair that measures the absorbance of light by the molybdenum blue complex formed at 880 nm. This is housed in a robust and secure pelicase, making the integrated system portable and convenient for field applications. (3) demonstrate the application of the PhosphaLOAD device on environmental samples.

4.2 Materials and Methods

4.2.1 Chemicals

List of chemical and reagents used are discussed in detail in Chapter 2.

4.2.2 Environmental samples

A raw unfiltered 250 mL water sample was collected from the River Tolka in Co. Dublin using a HDPP plastic bottle. This sampling site was selected as it has it is known for its high level's phosphate [41]. The sample was filtered through a 0.45 µm pore size filter paper in a vacuum filtration setup prior to analysis on the PhosphaLOAD system and UV/vis spectrometer.

4.2.3 Instrumentation

All measurements obtained on the PhosphaLOAD system were compared to the measurements taken using a Shimadzu mini 1240 spectrometer (Shimadzu Corporation, Japan) as a reference standard. Photometric absorbance values were recorded using a VWR UV-1600PC UV–vis spectrophotometer (VWR, Ireland). BrandTech® cuvettes (Sigma Aldrich, Ireland) were used for optical path lengths of 1 cm. A Stratasys Objet260 Connex polyjet 3D printer (7665 Commerce Way Eden Prairie, MN 55344, United States.) was used to 3D print components such as the optics holder for the housing platform using an opaque rigid polymer. The optics used in the system included a plastic infrared LED (part number: QED223) and a Vishay silicon PIN PD (part number: BPW24R) purchased from Farnell, Ireland. Optics holder with transducing pair shown in Figure 4.2.

An oven using a low heat of 37 °C for a duration of 2 h was used to dry down the reagents onto PSA in their specific ratios for integration onto the PMMA base layer of the microfluidic disc, method discussed in more detail in Chapter 3.

4.2.4 Disc design software and fabrication techniques

The design of the centrifugal microfluidic discs is discussed in detail in Chapter 2. The top PMMA layer consists of a loading hole and air vents to prevent the formation of air bubbles in the optical pathlength and allow for air displacement, the top and bottom PSA layers were used to create the microchannels, the middle PMMA layer created the chambers and reservoirs essential for fluid capture and reagent storage and the base PMMA layer was used to enclose the fluid and reagents within the disc. The manufacturing of the microfluidic disc layers was outsourced to a laser engineering company (EFJ engineering, Dublin, Ireland) and later assembled in DCU in a clean room using a hot roll laminator (ChemInstruments, OH, USA) to activate the PSA, see Figure 4.1 for reference.

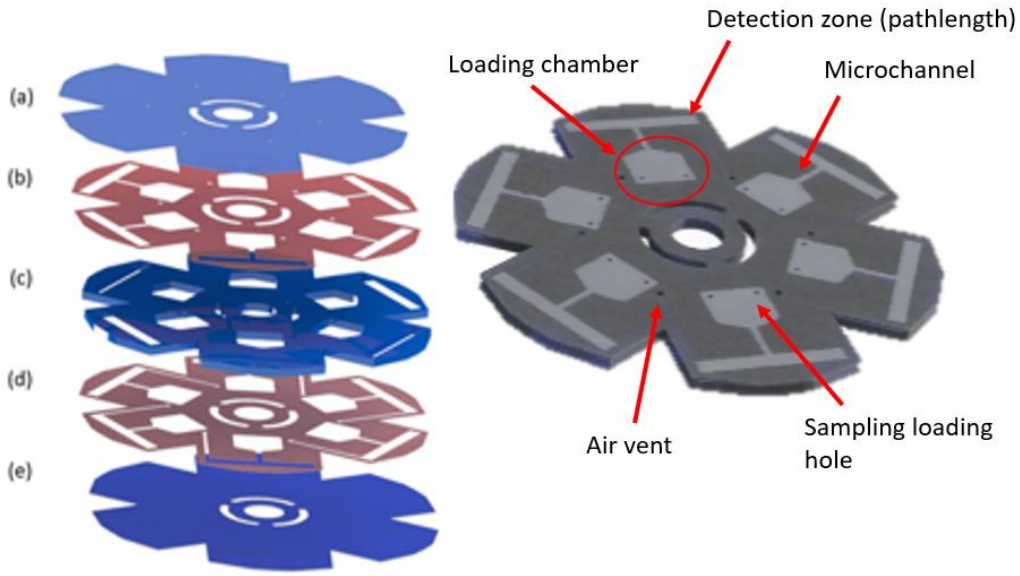

Figure 4.1 Left; Rendered image showing each layer of the microfluidic disc, where the blue layers represent PMMA and red represents PSA layers. (a) PMMA layer with sample loading and air vents (0.5 mm thickness); (b) PSA layer with top microfluidic channels (46 µm); (c) PMMA layer with reagent chamber and detection zone (3 mm); (d) PSA layer with air vent and bottom microchannels (46 µm); and (e) base layer to enclose fluid within the disc and prevent leaks (0.5 mm). Right; Rendered image of the assembled disc with features labelled; loading chamber: facilitates the storage of chemical reagents and sampling loading, allowing dried reagents and sample to mix. Detection zone, pathlength 40 mm: detection of phosphate present in sample. Microchannel: allows liquid to flow from introduction chamber to detection zone for measurement. Air vent: air displacement and allows fluid to fill detection zone. Sampling loading hole: enables sample to be micro pipetted into disc.

4.2.5 System design and operation

The complete integrated PhosphaLOAD sensing platform (see Figure 4.2) comprises of motor, actuator, transducing pair, LCD screen, keypad, switch, and an electronics board, stored within the peli case.

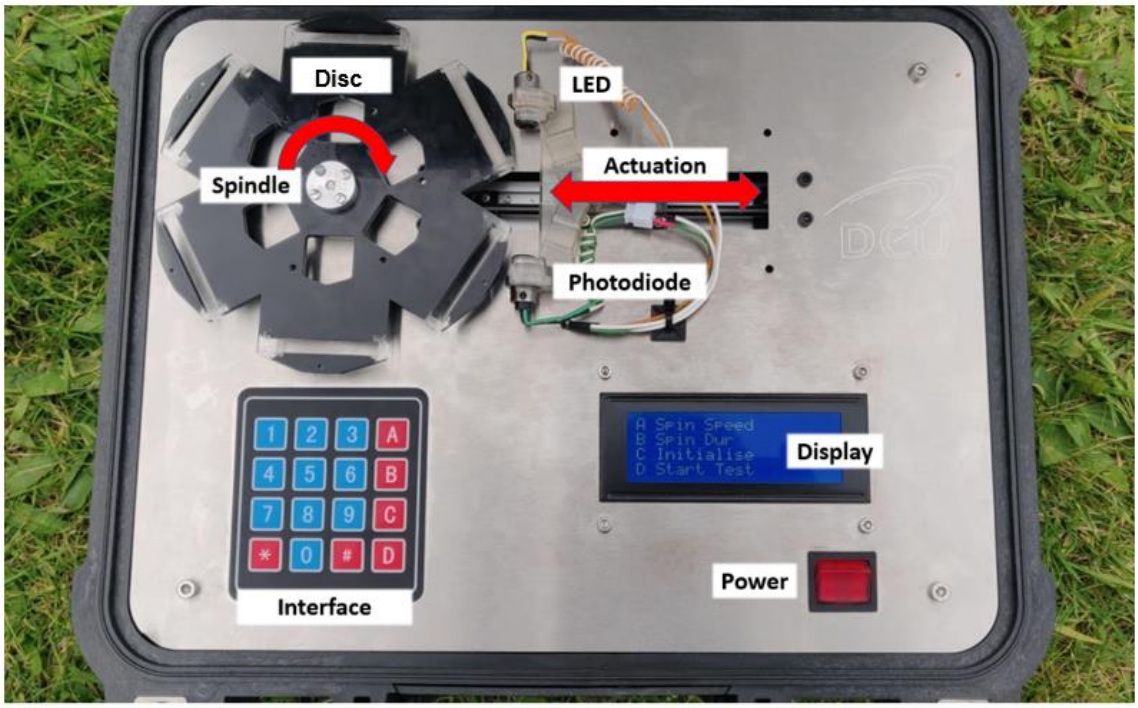

Figure 4.2 Portable handheld field sensor in the field. Pictured is the peli case (lid not pictured) as a housing platform. System incorporates a rotator for the discs that is powered by a motor, spindle to mount and secure discs, a keypad and LCD screen. The motor and electronics are stored underneath the metal sheet in the peli case.

4.2.5.1 Motor

The motor used in the system is a customised DC motor with a magnetic encoder (purchased from Maxon, Berkshire, United Kingdom) which facilitates a spin speed (0-110%) (0-6200 rpm - excluding load) a spin duration from 0-99 seconds. The motor also controls the indexing positions of the disc. Any combination of up to six detection zones on the disc can be selected in any order.

4.2.5.2 Actuator

The actuator bed (purchased from Igus, Cologne, Germany) enables a number of readout mechanisms within the platform, this system incorporates an LED/PD coupled end. The actuator bed carries out the function of moving the LED and PD in and out for read functions. When the actuator (Figure 4.3) is moved in readings can be performed and when the actuator is in the start position (moved out) the disc can be mounted on the spindle and spun.

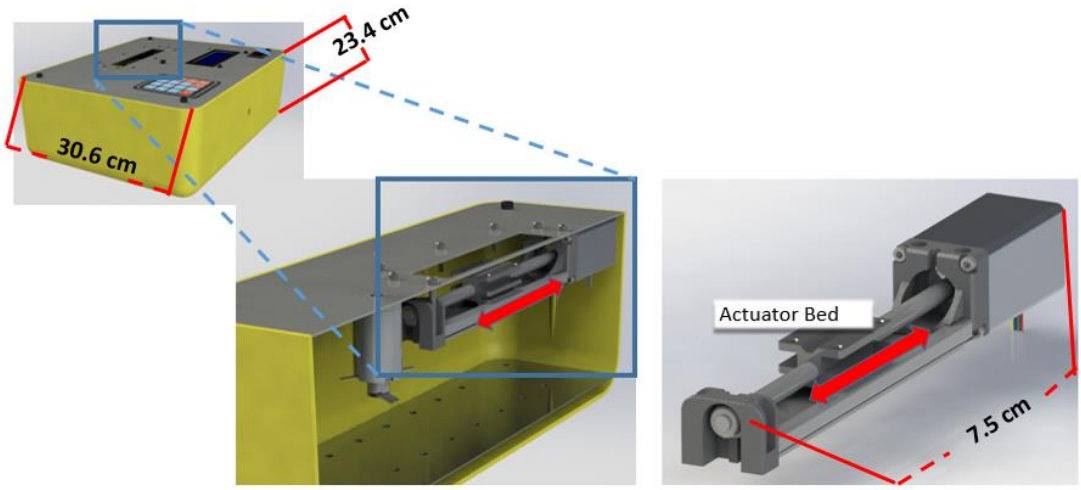

Figure 4.3 Render of the customised actuator bed, used to move the transducing pair (LED and PD) in and out for reading of samples.

An optics holder was 3D printed using a Stratasys Objet260 Connex (Tri-Tech 3D Ltd. Trent, UK). The part was designed using SolidWorks™ and fabricated using a rigid opaque COC material. The optic holder was designed to hold the LED and PD in place and to ensure correct alignment with the optical detection channel on the disc.

As the pathlength dimensions were designed to facilitate six measurements per disc the optics and optical alignment for the system and discs were critical. To minimise light scatter and to ensure that all incident light from the LED was directed straight through the pathlength channel to the detector (PD) an optics holder with a narrow aperture of 1.75 mm was chosen, as shown in Figure 4.4 and discussed in detail in Chapter 2.

4.2.5.3 Optical head

Different sized apertures were incorporated into the design for the optics head to investigate the optimal size for the aperture on the LED.

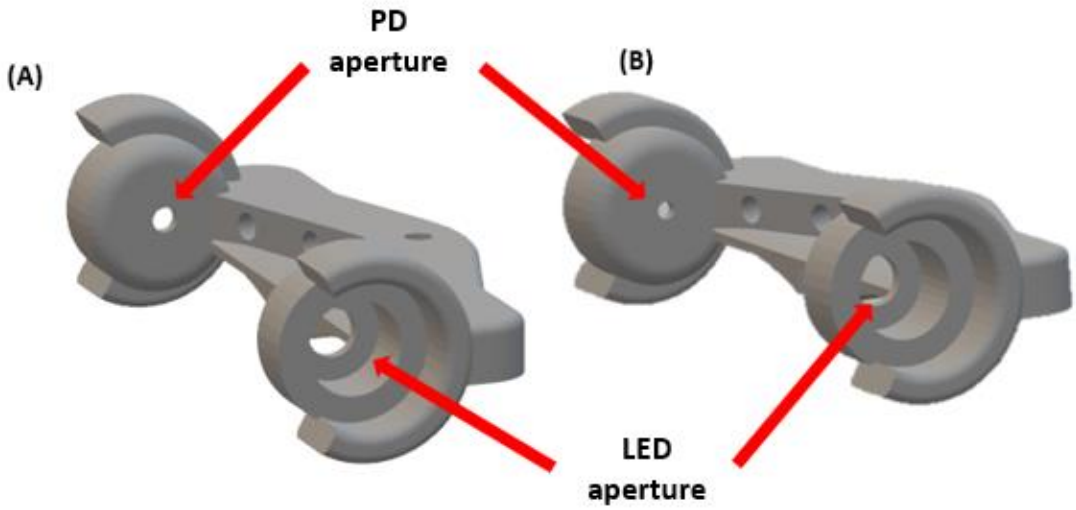

Figure 4.4 Optics head with (A) 2.5 mm LED aperture and (B) 1.75 mm narrower LED aperture for improved optical detection.

To minimise light scatter and to ensure that all incident light from the LED was directed straight through the pathlength channel to the detector (PD) an optics holder with a narrow aperture of 1.75 mm was chosen.

4.2.5.4 Spindle

The spindle was attached to the motor within the system to facilitate the mounting of the microfluidic discs for spinning. The spindle was also used to ensure correct alignment with the optical detection channel and the transducing pair. The spindle was designed using SolidWorks™ and manufactured by EFJ Engineering (Clonshaugh Industrial Estate, Dublin, Ireland). The manufacturing process involving using a milling machine to increase the tolerance and stability of the spindle, producing a more robust spindle for spinning and disc alignment. A 3D printed spindle was also fabricated, compared to the machined spindle and evaluated on performance to determine which had the lowest tolerance, therefore would align accurately with the LED and PD.

4.2.5.5 Transducing pair

The optics used within the detection system was comprised of an OSRAM Opto Semi-conductor LED (purchased from Radionics Ltd., Ireland) and an 880nm Silicon Photosensor has 40° wide reception angle PD. This PD has daylight filter coupling (purchased from Farnell, Ireland).

4.2.5.6 LCD Screen, keypad and switch

The LCD screen was purchased from Mouser, United Kingdom. The screen was used to view options and commands and was also used to view readouts from sample measurements. The keypad interface is used to key desired functions and commands such as, spin speed, spin duration and number of tests. The switch is used to turn on and off the operating motor, see Figure 4.2.

4.2.6 Electronics and coding

The electronics and written code to operate the system were developed by Assistant Prof. Nigel Kent. In terms of the electronics for the instrument the fundamental circuit for reading the amount of incident light on the PD is a trans-impedance amplifier. The 1MOhm feedback resistor was adjusted such that the system blank measured just below the saturation level of the MCP601 operational amplifier. The amplifier output voltage from the MCP601 is passed to a 16-bit analog to digital (A/D) converter (ADS1115, Adafruit) to enable conversion and storage of this reading on a digital microcontroller platform.

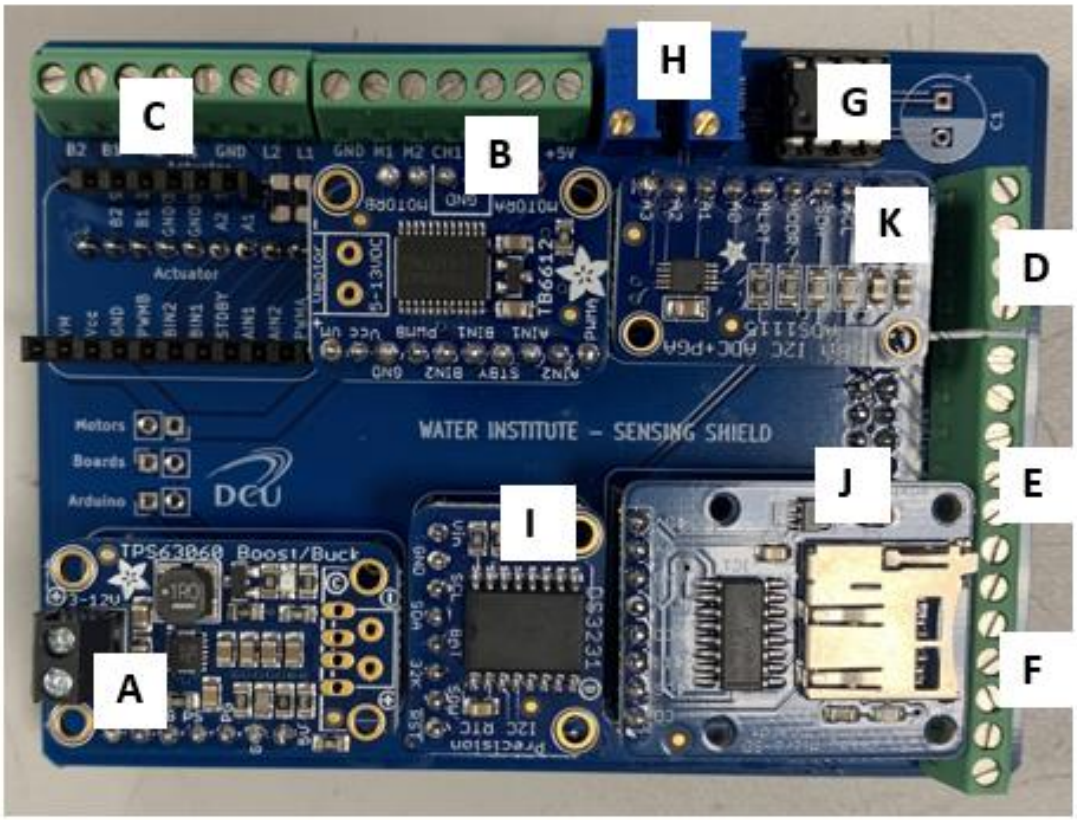

Figure 4.5 Controller board used to power the system. (A) Power input, (B) Spindle driver, (C) Actuator output, (D) LED/PD inputs, (E) Keypad, (F) LCD screen LED/PD inputs, (G) Transimpedance circuit (PD amplifier), (H) LED and Amplifier gain settings, (I) Real time clock, (J) SD card and (K) Analog to digital converter.

The chosen microcontroller was an ATMega 2560 embedded within an Arduino Mega development board. To interface with the Ardunio Mega a custom printed circuit board was designed and spun to allow both the transimpedance circuitry and additional functionality be incorporated onto a single board that mated directly with the Arduino Mega. The additional functionality was, in the main, enabled through the use of off the shelf breakout boards that enabled rapid debug and repair for on field testing. Should a subsystem component fail, it was easily replaced in the field. This additional functionality included:

Power management to step down and isolate the 5V logic supply for the Arduino Mega2560 from the 12V supply required for the motors. Separate motor drivers to provide drive instructions to both the linear and rotary actuators.

SD card for onboard storage of results both for subsequent use and to produce rudimentary statical data on site during field testing. Real Time clock to time stamp each experimental run. The custom printed circuit board also facilitated connections to the LCD screen and from both the keyboard and DC motor encoder.

To integrate both mechanical and electronic systems and to realise a functional instrument, firmware was written to allow the user to interact with and take data from the instrument. The firmware functionality allowed the user to determine test parameters such as rotational velocity, duration the velocity was applied for and what test areas of the disc should be interrogated. On start of the test the disc will accelerate to the determined rotational velocity. This required velocity is then maintained for user defined duration. Once the duration has been reached the disc decelerates until the rotational velocity is zero. At this stage the disc slowly rotates to the first defined test location. The linear actuator then moves the optical housing the required linear distance such that the LED, detection zone and PD are aligned (measurement method discussed in Section 4.2.7). With the LED illuminated, a total of 50 readings are recorded from the transimpedance amplifier circuit representing the amount of absorbance of the LED through the detection zone. The actuator then retracts and allows the disc to rotate to the next user defined detection zone where the read process is repeated. This process continues until all locations, as defined by the user, have been read. Once the experiment is complete, the user has access to both the average and standard deviation readings from each measured well. Should the need arise all captured data is stored, and time stamped on the SD card within the instrument.

4.2.7 System user protocol

The system was powered using the switch (see Figure 4.2), to initialise the system the motor moves to the load position. Once initialising period was complete the disc was mounted and secured onto the spindle, aligning disc pathlength between transducing pair. The # key was used to move the actuator back to starting position. The sample was then introduced into the loading chamber of the disc. Desired spin speed, spin duration and number/order of tests were selected via the keypad interface. The # key was then selected to run the tests. The results from each test were observed via the LCD screen and a printout of all tests can be viewed at the end by pressing the * key. All measurements were recorded in millivolts (mV), the data was processed by converting mV into absorbance units (A.U). This was done by converting mV into % transmittance using the following equation:

Equation 4.1 mV to % transmittance conversion

$$\left(\frac{Sample\ Absorbance\ Reading}{Blank\ Absorbance\ Reading}\right) * 100 = \%T$$

and then to absorbance:

Equation 4.2 percentage transmittance to absorbance units

$$2 - log * (\%T) = A.U$$

4.2.8 Bill of materials

The cost of manufacturing the handheld phosphate analyser totalled at €1,002.2 including VAT, a fraction of the cost of the commercial autonomous analysers listed in Table 4.2 [102].

Table 4.2 Summary of the bill of materials used in the fabrication of the phosphate analyser platform

Item Type	Item Description	Part number	Supplier	Total cost
Mechanical	Peli Case 1400	Peli-1400	Peli.ie	115.00
Electronic	Battery	2777017	Farnell	77.16
Mechanical	LCD Display	485-198	Mouser	16.16
Breakout Board	Analog - Digital	485-1085	Mouser	13.46
Breakout Board	Real Time Clock	485-3013	Mouser	12.56
Mechanical	Enclosure	1526656	Farnell	11.78
Mechanical	i2c Backback	485-292	Mouser	8.43
Breakout Board	Power Regulator	485-2190	Mouser	8.43
Breakout Board	SD Card Reader	485-254	Mouser	6.35
Electronic	Terminal block	651-1751345	Mouser	6.33
Mechanical	Keypad	619-27899	Mouser	6.29
Breakout Board	Actuator Driver	485-2448	Mouser	4.46
Breakout Board	Spindle Driver	485-2448	Mouser	4.46
Mechanical	Power Switch	152266	Farnell	4.03
Electronic	Terminal block	651-1751293	Mouser	7.92

Electronic	8 Core Cable (1metre)	3855170	Farnell	2.63
Electronic	PD Pot (2M)	9353607	Farnell	2.63
Electronic	Terminal block	651-1751264	Mouser	2.33
Electronic	LED Pot (10k)	9353526	Farnell	2.21
Electronic	D Sub Female	3482558	Farnell	7.00
Electronic	D Sub Male	1345230	Farnell	4.76
Electronic	2 Row Header	2356147	Farnell	1.14
Breakout Board	*Custom PCB*	*Custom Design*	*Seed Studios*	*0.49*
Electronic	OP Amp	579-MCP601-E/P	Mouser	0.43
Electronic	LED Transistor	1084507	Farnell	0.36
Electronic	Female Pin Sockets	1593464	Farnell	0.24
Electronic	Op Amp Socket	2668408	Farnell	0.15
Electronic	D Sub Pin Female	1776447	Farnell	0.14
Electronic	SMD Resistors	2307295	Farnell	1.21
Electronic	D Sub Pin male	1776435	Farnell	10.90
Electronic	Male Pin Headers	1593417	Farnell	2.92
Mechanical	Readout Actuator	Custom Design	igus	165.84
Mechanical	Stainless Sheets	Custom Design	Kent Stainless	89.00
Mechanical	Spindle Motor	Custom Design	Maxon	141.50
Electronic	LED	SFH 485	Radionics	0.50
Electronic	PD	QSD2030F	Farnell	2.60
Mechanical	Spindle	Custom Design	EFJ Engineering	73.00
			Total:	€814.80
			Total (VAT 23%)	€1002.20

4.2.9 Assay for phosphate detection

The assay and method of integration for onboard storage is discussed in detail in Chapter 3. This method was chosen due to its ability to detect levels of phosphate in the region of 10 µg/L [55]. Figure 4.6 illustrates the method of chemical storage within the microfluidic disc.

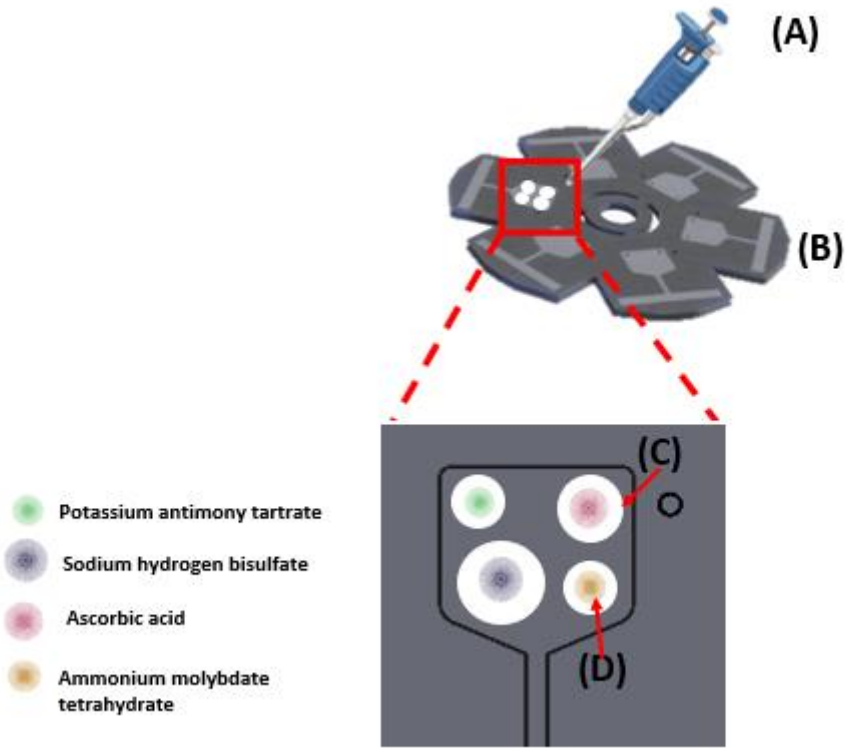

Figure 4.6 Rendered image of the assembled disc with on-board reagent storage in the introduction chamber. The combined reagent is stored on the disc by separating out each of the combine reagent compounds and dried down. (A) micropipette for reagent integration; (B) unassembled disc, top PMMA layer removed for reagent integration; (C) graphtec cut PSA pieces for reagent integration; and (D) compounds of the combined reagent for the molybdenum blue method separated out.

4.2.10 Sampling site

The River Tolka flows from County Meath to Fingal and through the north of Dublin city, Ireland. The samples were obtained from Griffith Park, located 53.37047, -6.26226 where there was a footbridge and easy sampling access. The samples were collected in High Density Polyethylene (HDPE) wide mouth plastic bottles unfiltered, in the lab the samples were then filtered through a 0.45 µm glass fibre filter paper and vacuum filtration apparatus set up and stored in the fridge until analysed.

Figure 4.7 Map of the sampling site for the River Tolka, Co. Dublin used for the matrix sample analysis. This image was obtained using Google maps to obtain GPS coordinates.

4.3 Results and Discussion

This section of the chapter investigates the performance of the LOAD combined with the analysis system to ensure that it is highly sensitive, robust, reliable and cost effective. This was done by carrying out optimisations on different components within the system. Examining the performance of the LOAD integration with the analysis platform by optimising the method for disc manufacture. It also involved the determination of LOD for the PhosphaLOAD device using a range of phosphate standards. The evaluation of the PhosphaLOAD device was determined by the performance using real world environmental samples.

4.3.1 Evaluation of disc performance with the system

A study was carried out to determine if outsourcing the disc manufacture to a laser company would achieve a better finish on the optical window. This was done to decrease the variation from well-to-well on a single disc and from disc-to-disc. Outsourcing the discs to a laser company means that the machinery used in production would be capable of creating different parameters that would allow for a clearer transparent optical window, reducing the variation from each optical window per disc. This study involved the assessment of six discs. Three discs were prepared manually and three of the discs were manufactured by a laser company (EFJ Engineering, Clonskeagh Industrial Park, Dublin, Ireland).

Table 4.3 Comparison of variation from disc-to-disc for both manufacturing processes (manually prepared and outsourced), n=3 for both methods

Outsourced disc manufacture average readings (n=3)				Manual disc preparation average readings (n=3)			
Disc Well Number	**Average System Counts (mV)**	**St. Dev**	**%RSD**	**Disc Well Number**	**Average System Counts (mV)**	**St. Dev**	**%RSD**
1	4125.0	331.9	8.0	1	3688.4	352.9	9.6
2	4222.3	538.9	12.8	2	3464.1	623.9	18.0
3	4281.8	446.0	10.4	3	3798.2	308.7	8.1
4	4439.9	468.0	10.5	4	3495.1	546.9	15.6
5	4390.3	343.7	7.8	5	3912.4	277.7	7.1
6	4329.9	311.7	7.2	6	3081.9	449.9	14.6

Although the performance of the microfluidic discs is improved by opting to outsource the lasering and manufacture reducing overall %RSD of variation per disc (see Table 4.3). There is still some variation between well-to-well. To minimise this issue a scaling method for each disc was developed. Pre-calibration of the disc is carried out to ensure all wells on that disc can be referenced to a single well. Water is used to obtained readings in this pre calibration step to mimic the medium of the intended samples, this method is described in Chapter 2.

4.3.2 Limit of detection

Taking the optimal disc design, ideal reagent storage method and complete analysis platform the LOD for the PhosphaLOAD system was determined. This study was carried out by generating a calibration curve using low concentration phosphate standards, ranging from 5 – 200 µg/L (see Figure 4.8). The blank consisted of the reagent and a 0 µg/L phosphate standard (DI water). The LOD was determined using the equation:

Equation 4.3 Limit of detection

$$\frac{3\,s}{m}$$

which resulted in an LOD value of 16 µg/L phosphate.

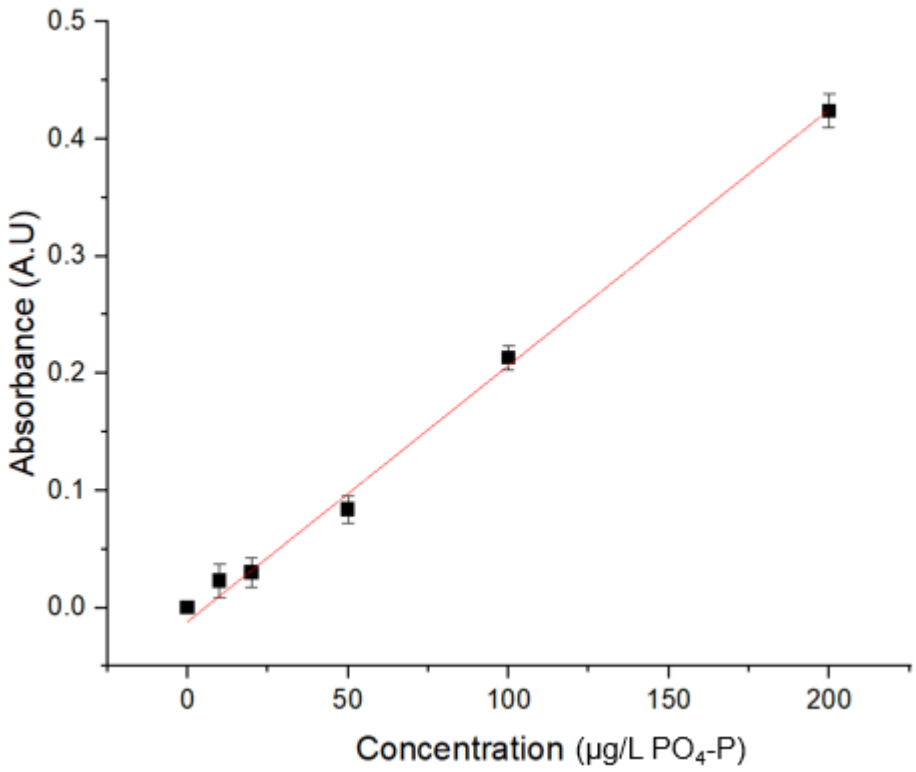

Figure 4.8 Calibration curve of low concentrations of phosphate standards (n=3) to determine the LOD of the system, R2 value of 0.995 and a slope of 0.0021

4.3.3 Optimisation of system component performance

The performance of the spindle, optical head and lenses were optimised to ensure the system could operate at a high standard. Different methods of spindle manufacture were investigated to determine the most robust method for fabrication. The optical head apertures sizes were also altered to determine if they could increase sensitivity by focusing light on the detector.

Lenses were trialled in the system to determine if they could enhance the optics. Increasing the sensitivity of the device, again by focusing the light coming from the LED onto the detector.

4.3.3.1 Spindle

Two methods of manufacturing the spindles for the system was analysed. The first method involved 3D printing the spindle using a polyjet 3D printer (Stratasys Objet260 Connex 1, United Kingdom) to provide the hard, rigid COC material required for spindle operation.

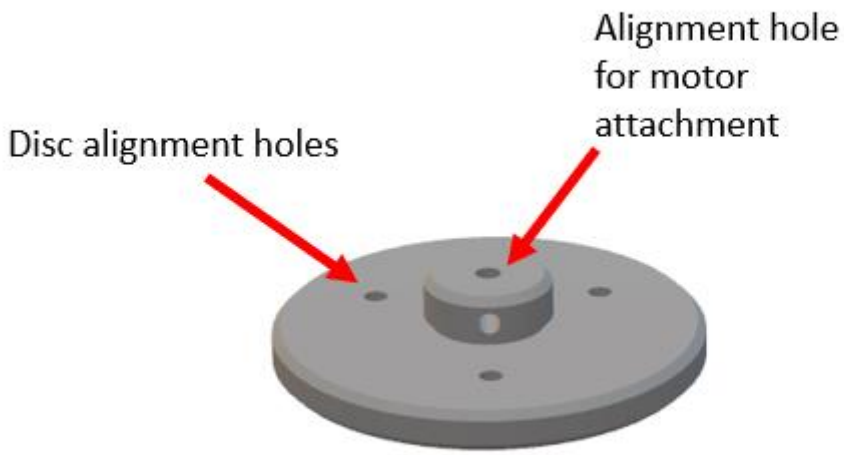

Figure 4.9 3D printed design for spindle, rigid COC opaque polymer used in the fabrication.

The second involved machining the spindle from metal by outsourcing the machining (EFJ Engineering, Clonskeagh Industrial Park, Dublin, Ireland.)

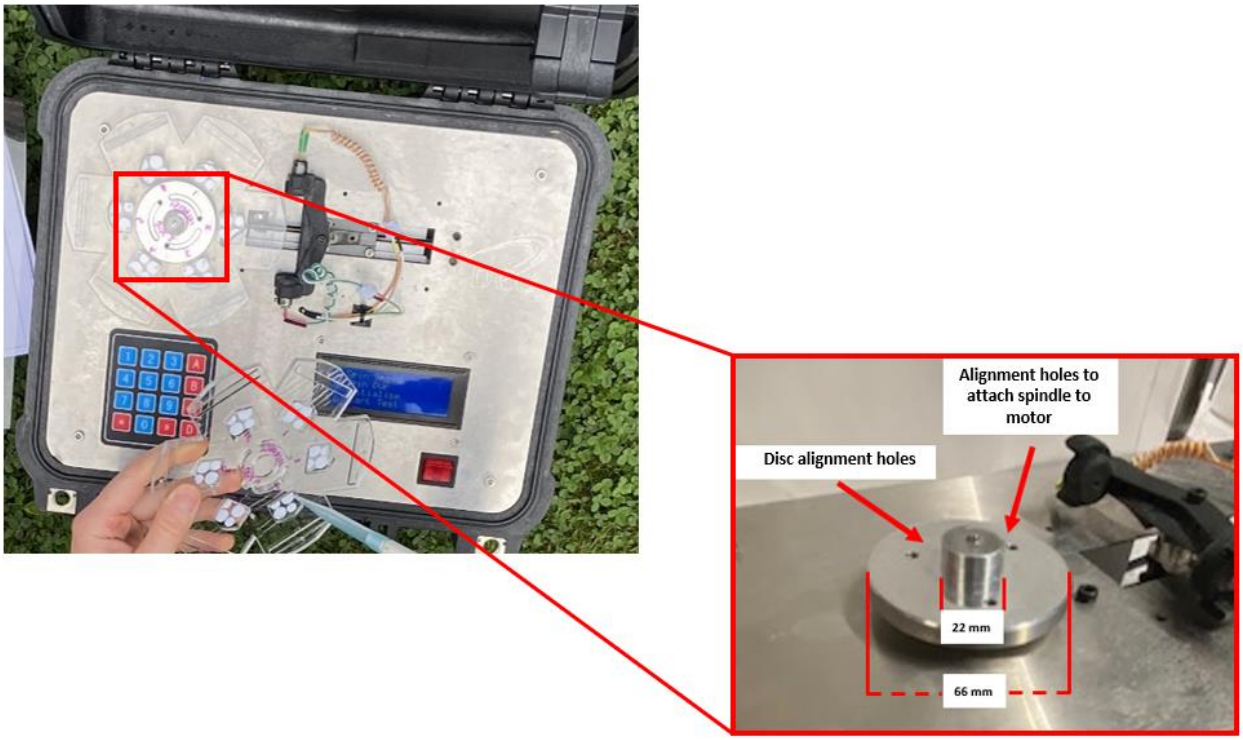

Figure 4.10 Image of the machined spindle used in the final PhosphaLOAD system.

The purpose of determining the most efficient technique of manufacturing the spindle used in the system was to investigate the tolerance of the machining and 3D printing techniques. An increased tolerance produces an undesirable variation in alignment between the optical head and each well (path length) on a disc.

For the purpose of this experiment all wells were filled with the sample volume of DI water to mimic the medium that the incident light would be traveling through if a sample were present. It was found that the machined spindle performs significantly better than the 3D printed spindle. There is a noticeable "wobble" in the 3D printed spindle caused by the tolerance. The increased tolerance is highlighted in Figure 4.11, the system readings obtained for each of the six wells on a single disc highlights this variation.

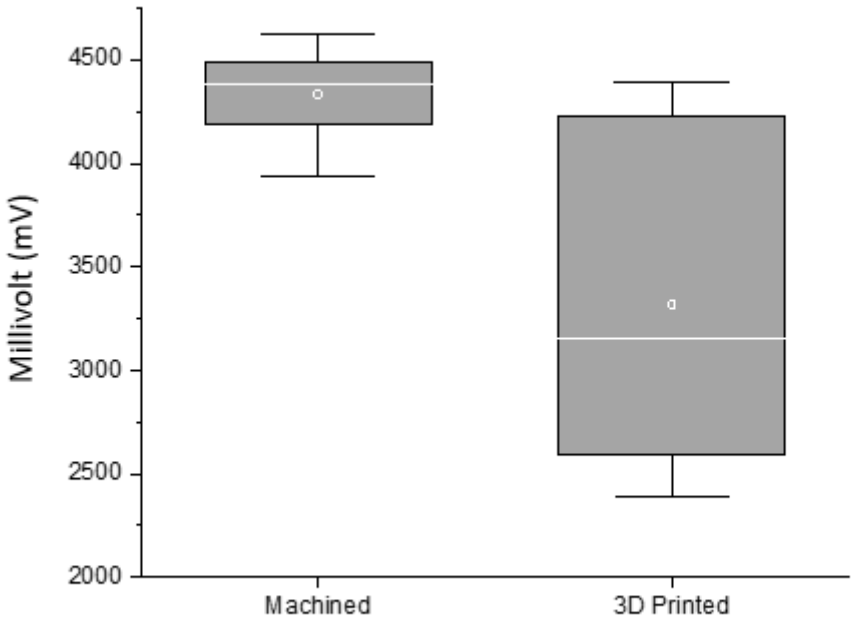

Figure 4.11 Box plot demonstrating the variation in readings in the six different detection zones on a disc due to increased tolerance in the 3D printed spindle, (n=3). The increased tolerance impacted the alignment of the disc with the transducing pair. Each pathlength of the disc aligned differently which was dependant on the slope of the spindle. Decreased variation in pathlength reading due to the machined spindle. The machined spindles had a tighter tolerance and therefore decreased the wobble of the spindle decreasing the impact it had on the alignment

The machined spindle is much more rigid and there is a significantly reduced wobble shown by the significant decrease in mV readings from well-to-well on the three discs. The results highlight the increased tolerance in the 3D printed spindles that cause a wobble of the discs which is amplified by the centrifugal spinning of the discs.

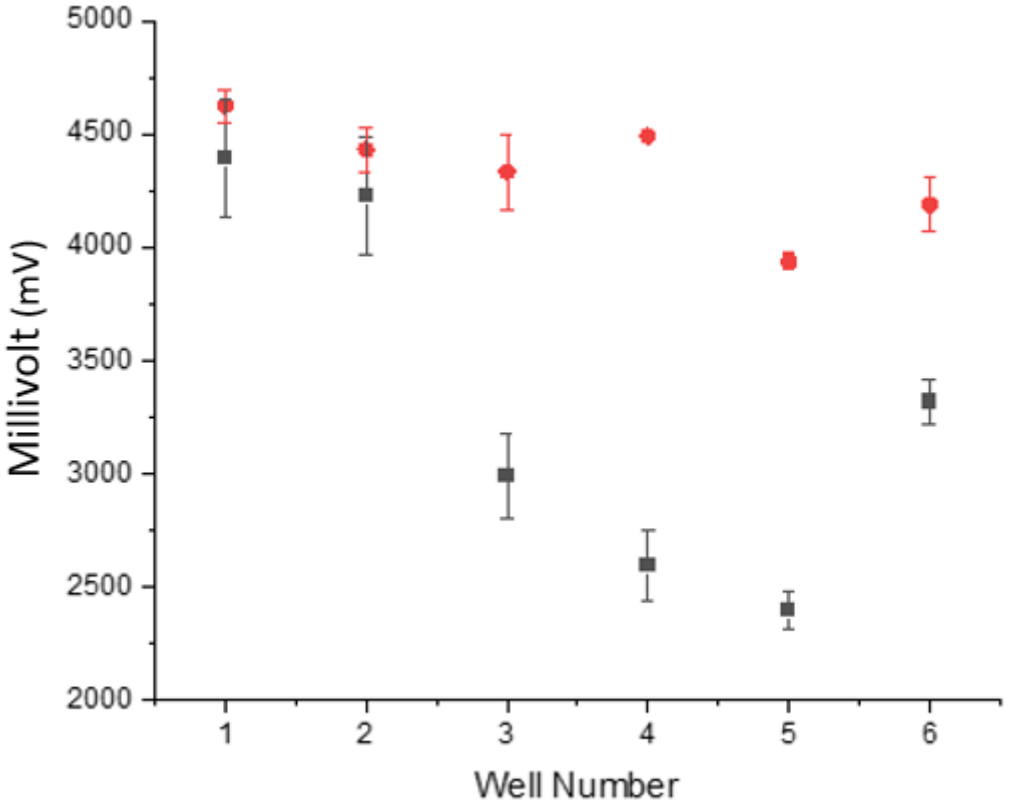

Figure 4.12 Comparison of the performance of the 3D printed (black data points) and machined (red data points) spindles (n=3) each well filled with DI water

A direct comparison in the performance of the 3D printed spindle compared to the machined spindle is shown in Figure 4.12. Due to the machined spindles having a reduced tolerance the data points for each well show a decrease in variation, the mV readings obtained for the machine spindle spans from 4000 – 4600 mV compared to that of the 3D printed spindle which show a significant variation in readings 4400 – 2400 mV from well-to-well on a single disc. All reading identical volumes of water filled wells. A total of three discs were used in this study, all discs were tested on both methods.

4.3.3.2 LED lenses

The optical head was fitted with two ocean optics lenses to collimate the light and focus it straight onto the pathlength to be detected by the PD. This was compared against an optics head that was not fitted with lenses and the results are observed in Figure 4.13, the slope of the graph obtained with the lenses was 0.0019 and the slope generated from the graph without lenses was 0.0018.

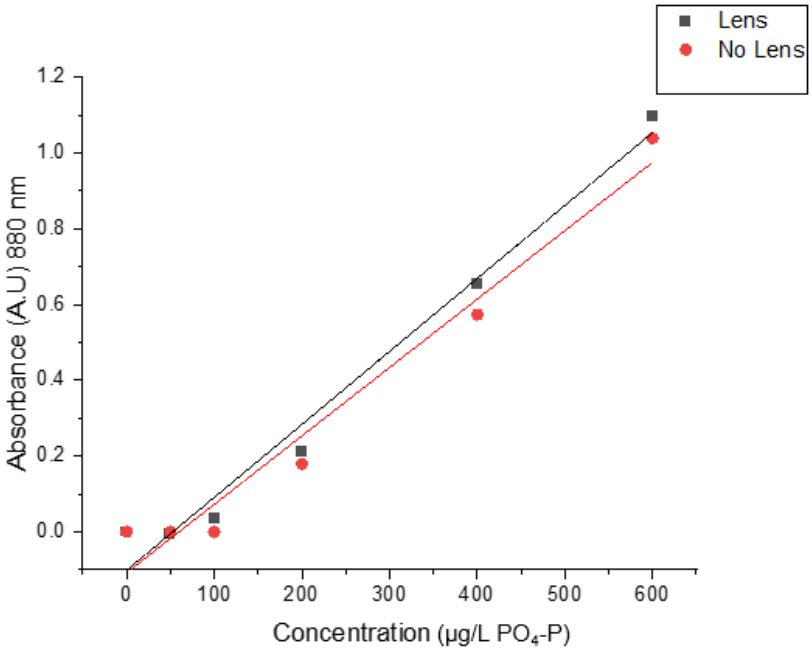

Figure 4.13 Lens experiment, the calibration curve investigates the performance of the optics with lenses and without lenses, with a slope of 0.0019 and 0.0018 for the lens and without the lens respectively.

The results from this experiment determine that the lenses in the optics head do not perform significantly better that the optics head without lenses, therefore it was not necessary to include the lenses in the system as it only achieved a slightly higher slope value as shown in Figure 4.13. This result means that the system BOM is reduced by €398.

4.3.4 Demonstration of the PhosphaLOAD device on environmental samples

The evaluation of the PhosphaLOAD device was investigated using environmental samples obtained from the River Tolka in Co. Dublin, these samples were used as a spiked matrix sample to test the performance of the sensor, demonstrating the accuracy and reliability of the system for phosphate detection in a matrix sample. The samples collected represented a relatively low phosphate level and was spiked with a higher concentration of 100 µg/L. A four-point calibration curve was carried out to determine the concentration of the spiked and unspiked sample. This experiment was carried out in triplicate, on three separate discs, with results obtained with 10 min. The samples were filtered prior to analysis. The sensor results were compared to a reference standard UV/vis spectrometer. The results obtained from the system showed close agreement to that demonstrated from the spectrometer, with a relatively low standard error displaying great accuracy for the PhosphaLOAD system (n=3).

Figure 4.14 presents the calibration curve obtained using the optimised PhosphaLOAD system with the adapted molybdenum blue method. The comparison of the two methods

displays the good analytical performance of the PhosphaLOAD system with an increase in slope and sensitivity compared to that of the reference method. The novel system shows good linearity with an R^2 value of 0.9963. The first trial of this sensor achieved a linear response signal to phosphate concentration from 54 to 600 µg L^{-1} PO_4-P and a system LOD of 16 µg L^{-1}.

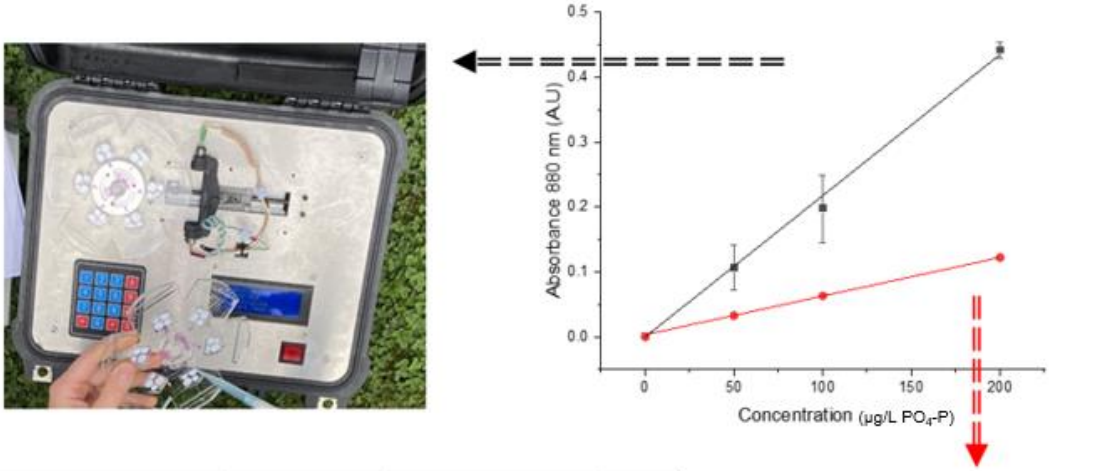

Sample	PhosphaLOAD (µg/L)	UV/vis Spectrometer (µg/L)	%RSD
Matrix Unspiked	46.9	40.3	11
Matrix Spiked 100 µg/L	163.9	153.6	4

Figure 4.14 Calibration curve obtained on the handheld system (black) using the adapted molybdenum blue method on phosphate standards, where error bars show standard deviation, with a slope of 0.0021 AU L g^{-1} showing high sensitivity and an R^2 of 0.9963. Compared to that of a UV-vis spectrometer (red) for reference, n=3 for both methods. Table of measurements for PhosphaLOAD and UV/vis spectrometer included

The error bars in Figure 4.14 are related to the disc-to-disc variation rather than sample measurements. The table in Figure 4.14 shows the closeness in agreement for the phosphate system compared to the standard reference method. The unspiked matrix sample and matrix spiked sample obtained RSD values of 11 and 4 %, demonstrating the excellent performance of the phosphate system.

4.4 Conclusion

This work demonstrates for the first time the application of a novel fully integrated LOAD field sensor capable of multi-sample phosphate detection in surface waters. The incorporation of a centrifugal microfluidic disc with integrated chemistry was crucial in the development of the PhosphaLOAD sensor as it facilitated on board reagent storage, mixing and detection of phosphate via a 40 mm pathlength. The incorporation of microfluidics also allowed for a low sample volume and a fast detection time.

The system can measure six samples per disc in 10 min. The measurements observed by the PhosphaLOAD system showed close agreement with the conventional method used in lab analysis. The sample and reagent volume (600 µL) and low power consumption of the microfluidic device is orders of magnitude lower than for conventional laboratory systems.

The drying down of the molybdenum blue method increased the stability of the reagent lifetime facilitating the prolonged monitoring of phosphate in freshwater systems. The advantage of having the reagent dried down and sealed within the disc decreases time spent obtaining data in the field and also reduces the size of the system compared to current commercially available system which do not include reagent storage therefore sub 1 L bottles are required for onsite analysis [47].

The portability of the PhosphaLOAD device makes it easily transported around multiple sites and water systems with catchments. The facilitation of six samples per disc means that less discs are needed for measuring an entire catchment. The housing for the system, functions as a light weight, robust, portable, and convenient holder for *in-situ* measurements. A number of sensors on the market are too big to be transported from site to site and therefore are deployed in a single water body, taking spot measurements in real-time but only for one site [244]. The housing securely encloses the motor, electronics, optical components, and actuator to ensure that no damage occurs to any component of the sensor so that it can be transported around a catchment.

While system optimisation can continue, this is the first demonstration of a multi sample phosphate analyser capable of measuring low levels of phosphate (16 μgL^{-1}). We aim to develop this device further to achieve the 5 μgL^{-1} detection level required under WFD legislation.

Chapter 5: Test and demonstration of a novel lab-on-a-disc sensor for catchment scale monitoring of phosphate

5.1 Introduction

There is a need to improve how monitoring is carried out. Monitoring can involve a hierarchy of technologies, such as remote sensing (satellite and airborne imagery), *in-situ* sensors (autonomous and handheld) to monitor specific parameters. There are significant developments in the area of satellite monitoring. However, there is a need for *in-situ* technologies that can support and ground truth remote monitoring applications. The vision of an ideal monitoring system is a tiered approach with multi modal data management to provide decision support at catchment level.

Across Ireland the water quality monitoring programmes typically measure total phosphorus (TP) at the outflow of a catchment. Frequent sampling data can then be used to make hypothesis about annual nutrient loads. While frequent sampling protocols prove successful in collecting data on the ecological health of a catchment waterbody it fails to determine the source of the contaminant. Generally, the P fractions that are analysed are dissolved reactive P (DRP) and total phosphate (TP). The analysis of particulate P (PP) and dissolved unreactive P (DuP) demand a more intensive monitoring protocol [266].

Natural concentrations of phosphate (most common form of phosphorus detected) can vary between catchments depending on factors such as geology, soil type and land use. The natural ranges at which orthophosphate is found is approximately between 0 to 10 µg/L [151]. Over half of the surface waters in European are at a less than good status according to assessments carried out by the WFD [267].

Concentration	Cateogories of phosphorus concentrations in rivers					
mg/l P	< 0.025	0.025 – 0.035	0.035 – 0.05	0.05 – 0.1	0.1 – 0.25	> 0.25

Figure 5.1 low, good, acceptable, high, very high, extremely high levels

A major contributor to diffuse pollution of P is agriculture but is not the only culprit [25]. An increase in human population has led to an increase in the volume of wastewater treatment discharge from wastewater treatment plants and domestic wastewater treatment solutions, which have the potential to act as point sources of P. Both of these contributors to phosphate loading can be influenced heavily depending on seasons, rainfall, intensive agricultural practices and drainage works [268].

Land use practices and other natural processes such as weathering and erosion can influence the P source loading within a catchment [264][265]. The loading and fraction of P observed

in-stream is controlled by a catchments hydrogeology and geomorphology [271]. Well drained catchments generally are found to have lower levels of P compared to poorly drained catchment [272]. P loss to streams is more abundant in agricultural farms with heavy soils, these types of farms are mostly associated with open drains. Hence why poorly drained catchments tend to have high levels of P export due to the intensive agricultural practices being carried out. The extent on P loads transported in surface and subsurface water pathways from grassland catchment types is usually controlled by the flow route. Surface runoff is a major contributor for P loss and weather conditions such as heavy rainfall events can have a severe impact on the magnitude of P losses [271]. *Heathwaite et al.,* discusses this impact over a year and a half long study (September 1994 to February 1996). This study investigated the transport of P in surface and subsurface flow during 10 storm events. The findings indicate that high P levels were found to be transported in the dissolved fraction, in addition the soil macropores and drains in field were major contributors to the general P loads, most of this P being transported in the particulate matter [272].

To eradicate or lessen the amount of P transfer from land to water an in depth and better understand of the hydrological and chemical pathways is required. In terms of *in-situ* sensing a lot of work has been done using high resolution monitoring for common water quality variables along with flow and water levels providing spatial and temporal resolution. Most of the instruments used to carry out the data collection included multi parameters, gauging stations, water level loggers, meteorological stations, wet chemistry analysers, field measurements and laboratory analysis.

The use of long-term real-time monitoring aims to report the importance of high-resolution observation, frequent sampling to increase the level of knowledge and to vary response and actions needed.

Excessive riverine nutrient concentrations can have harmful effects on the aquatic ecosystem structure and functioning of a catchment. Therefore, the need to provide adequate monitoring strategies and long-term data sets are essential to improve the quality of catchment water bodies and understand the processes that affect nutrient fluxes [69]. Five meso-scale agricultural catchments in Ireland were used as a case study for determining incidental nutrient influxes associated with liquid slurry applications. *Shore et al.,* demonstrated the importance of high-resolution data that can be obtained using *in-situ* measuring devices for the effective monitoring of nutrients within catchments. The study involved monitoring TP, total reactive phosphorus (TRP), total organic nitrogen (TON) and SS concentrations using bank side Hach instruments to determine the timing and extent of nutrient losses after periods of slurry spreading and how storm effects can impact this. One of the key findings from the four-year

monitoring period was that during the closed spreading period the average TP and TON loads were considerably higher and may have been caused by residual losses and incidental losses from slurry applied in autumn. However, validation of these findings required more monitoring tools, providing a basis for incorporating another monitoring technology such as satellite imaging.

The River Swale catchment in the UK was the area of interest chosen for a contrasting study to the work carried out by *Shore et al.,.* This study examined the effects of weather conditions on three 100 h intensive sampling campaigns for the nutrient stability monitoring of phosphorus (SRP, TDP and TP) and dissolved nitrogen (NO_3^-, NO_2^- and NH_4^+) concentrations [273]. The results found a hysteresis effect in concentrations of nutrients after a major storm event and the influences that diffuse sources have on nutrient fluxes. Automatic samplers, a Hydrolab Datalogger (Datasond 3), a water flow sensor (Ultra sonic-sensor SENSA RC2) and a field meter (Mettler Toledo) were used. The addition of autonomous *in-situ* sensors could provide complementary data to support the lab analysis reported. It would also reduce the amount of labour required to carry out the campaign. Remote sensing could also be used to identify key diffuse in-put sources. For example, *Japitana et al.,* investigated the effects of point source pollution within a catchment. The study focused on using remote sensing and GIS to monitor water quality in catchments. The use of remote sensing derived data sets was used to characterise contaminants and identify pollution sources by using spectral data to develop maps and water quality models. Combining more than one monitoring tool allowed the author to take advantage of the strengths that each integrative monitoring tool can provide for long-term monitoring applications.

The Oona water catchment in Ireland was used in a study to investigate the extent of phosphorus and sediment transfer from field, farm and landscape [75]. This investigation involved the use of autosamplers, water level recorders, rain gauges, weather stations and lab experiments. Sampling was carried out once or twice a week between storm events over a two-year period. The study found that the use of discrete sampling tended to measure only low flow P transfers from non-diffuse sources. These results suggest that discrete sampling for catchment scale monitoring does not provide enough data to develop strategies that can help reduce the amount of diffuse nutrient transfer and that more temporal and spatial monitoring is needed, supporting the hypothesis that an integrated approach to monitoring facilitates a greater level of data and knowledge to be obtained. The use of hyperspectral images from satellite or airborne imagery could have enhanced the data set obtained by adding value in areas such as land use and land type between the catchments and if the

surrounding land had an influence, like that shown in the study carried out by *Schmedtmann et al.,* [274].

Sediment delivery into waterways can heavily impact the quality of the water body and is one of the main contributors to excess phosphorus in waterways [275]. SS can adsorb pollutants in water systems and deposit them into the river or lake bed. This accumulation in the bed can have major effects on the water health and bio-community inhabiting that water system [276]. A reduction in evapotranspiration of rainfall due to the removal of forestry and increases in water runoff from storm events has had a crucial influence on erosion and sediment transfer of receiving waters. Agricultural land can contribute to a number of different ground and surface water entry points for pollutants such as SS [277]. Therefore, there is a need for implementing technologies that can monitor and help mitigate or reduce the effects of elevated SS concentrations. *Sun et al.,* carried out a study on the continuous long-term monitoring of turbidity, it showed that the relationship between turbidity and sediment could be used to estimate erosion in the Sauerbier Creek catchment, South Australia. This was done by estimating erosion on a storm basis using extensive collection of turbidity and sediment sampling data measurements. Field sampling and a sensing probe for turbidity measurement was used to gather the relevant data to estimate erosion loads in the catchment. *Boggs et al.,* reported on rapid erosion assessment for elevation datasets on erosion predictions using vector land data in GIS. It involved a method based on the revised universal soil loss equation (RUSLE). Application of a rapid erosion assessment method was performed within GIS on a grid cell basis by determining the effects of elevation data resolution on erosion predictions. However more established methods of erosion measurement and detection within catchments are required to validate the findings, hence the need to incorporate field measurements [279]. This study also provides an opportunity for remote sensing techniques to supply supplementary data needed to validate this model. *Panagos et al.,* demonstrated the use remote sensing platforms for validation of erosion models. This study explored the recent advances in remote sensing applications as applied to soil erosion models. It reviews the capabilities of remote sensing in evaluating erosion risk factors such as vegetation coverage. The results conveyed that MODIS-derived data products showed progress in spatial and temporal monitoring of vegetation biophysical characteristics across a large geographic to help validate this model [280].

Therefore, the need for more real-time technologies for monitoring the quality if water is essential to provide increased data availability. The main driver for new emerging technologies is legislation. The European Union's WFD [281][282], is supported by a range of directives such the Urban Wastewater Directive [283], the Drinking Water Directive [284] and the

Groundwater Directive [285], and forms a basis for the management and protection of water resources within the EU. The primary objectives of the WFD are to obviate further deterioration and to protect and strengthen the quality of water resources and to advocate for more sustainable water use based on long term monitoring of water resources [262].

5.1.1 Aims and objectives

The aim of this chapter is to: (1) Investigate the performance of a novel, fully integrated, low-cost, phosphate sensor, and how this type of handheld sensor can be integrated into a tiered monitoring framework for water quality monitoring at catchment scale. The system was tested using three case studies across Ireland. The case studies included the River Liffey, Co. Dublin, the Unshin catchment, Co. Sligo and the Burrishoole catchment in Newport, Co. Mayo with differing levels of phosphate present in each catchment. (2) Determine the effectiveness of using satellite and airborne imaging for catchment scale monitoring by processing and analysing satellite images of areas of interest. (3) Address a number of technical and practical issues from translating this device from lab to field.

5.2 Materials and methods

5.2.1 Disc Pre-calibration

The pre-calibration of the microfluidic discs involved characterisation of variances between all optical windows for the discs used for analysis. To pre-calibrate the discs, they must be partially assembled and filled with a blank (water). The optical windows are then aligned with the transducing pair in the system and readings for all the optical windows are recorded. A scaling factor is then applied to the discs (refer to Chapter 2). From the lab analysis is it shown that any error above 10% variance from each well on the disc is not suitable for the scaling factor and that disc is subsequently discarded. The air vents and microchannel are blocked off during the pre-calibration to avoid any fluid traveling up these channels and giving an inaccurate reading due to loss of fluid in the detection channel during measurements.

All reagents were prepared in advance of the case studies. Each component of the combined reagent was dried down separately to avoid any cross contamination or reaction occurring during the heat drying process. The reagents were dried down in their specific ratios (see Chapter 3 for more detail). This method has been adapted from the method described by Murphy and Riley [55].

5.2.2 Remote sensing and GIS

For the case study on the Burrishoole catchment, images were obtained using Sentinel 2 (https://scihub.copernicus.eu/) and Landsat 8 (https://earthexplorer.usgs.gov/). The images were then processed using a pre-processing tool in qGIS (https://www.qgis.org/en/site/). In order to process the images a Semi-Automatic Classification plugin must be installed in the qGIS application. This facilitates the successful download of satellite images and adjustments to the band settings can be made depending on the purpose by selecting download products tab.

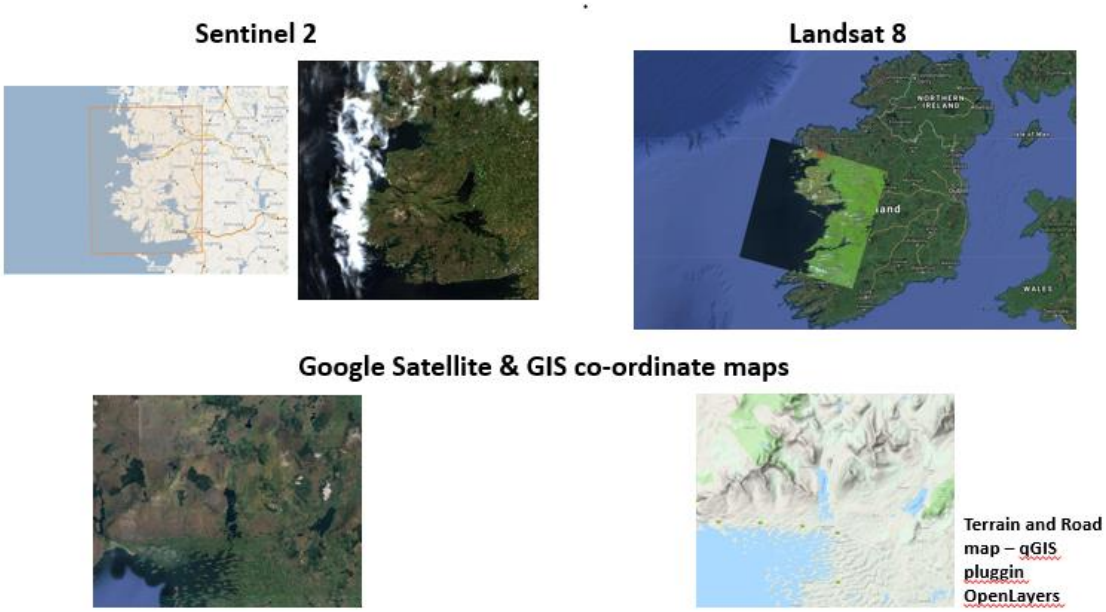

Figure 5.2 Types of satellite images available and examples of layering satellite images.

qGIS was also used to layer sampling points over maps, using excel sampling co-ordinate data and satellite images of the area of interest. The browser and layer panels must be displayed. Once the “browser” and “layers” are selected they will appear in the left hand side of the screen and the layers can be clicked and dragged to display.

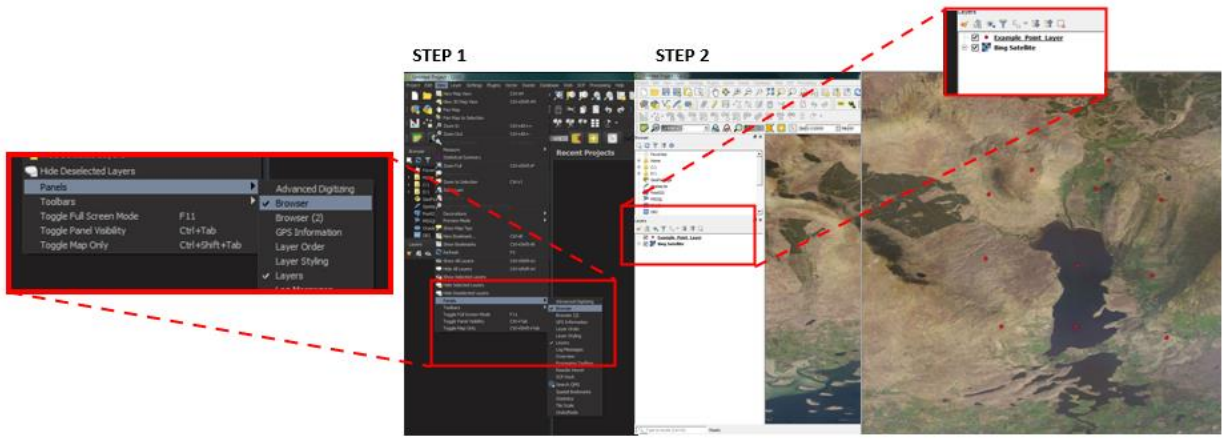

Figure 5.3 Step by step guide on how to merge layers using qGIS.

5.2.3 Sampling analysis and phosphate standards

5.2.3.1 Colorimetric reagents

Method and standard preparation are described in detail in Chapter 3.

5.3.2.2 Phosphate measurement procedure

The combined reagent was added in a 1:0.16 v/v sample to reagent ratio with a combined volume of 600 µL as per disc volume. The solution was allowed to stand for 8 min for the molybdenum blue colour to develop. The absorbance of the solution was measured at a λ_{max} of 880 nm using a VWR UV-1600PC spectrophotometer.

Kyoritsu PackTest kits [286] were used to measure phosphate-phosphorus for comparison measurements. These tests have an LOD of 0.02 mg L^{-1} for. The test takes 5 minutes to complete, it is a water chemistry colorimetric test, a card is also provided with the kits to help visually determine the concentration of phosphate-phosphorus within the water body.

5.3.2.3 Phosphorus analysis

Phosphorus analysis was carried out on the manual grab samples from the Burrishoole and Sligo case studies. The protocol for phosphorus analysis was adapted from the Standard Method 4500 P-E method [55]. River water samples were collected in 1000 mL HDPE plastic bottles for TP analysis and 250 mL HDPE plastic bottles for total soluble phosphorus (TSP) and SRP analysis. The samples were transported in a cooler box with cooler blocks where they were stored in a freezer (-18 ◦C) until analysed. Ideally the experiments should be carried out as soon as possible after sample collection but as the sampling sites are 196 km (Sligo) and 209 km (Burrishoole) away from the lab samples were preserved by freezing. The samples collected for TSP and SRP were filtered on site through a 0.45 µm cellulose nitrate filter membrane and were determined from the filtered samples. The samples collected for TP and TSS were determined from the raw unfiltered water samples. TP and TSP analysis involved a digestion step, where the samples were digested using acidified potassium persulfate and autoclaving for 30 min at 121 °C and 15 psi [287]. The LOD obtained was 4.3 µg/L and had a working range between 16.5 and 100 µg/L PO_4-P. Calibrations were carried out using a Shimadzu UV-1800 spectrophotometer.

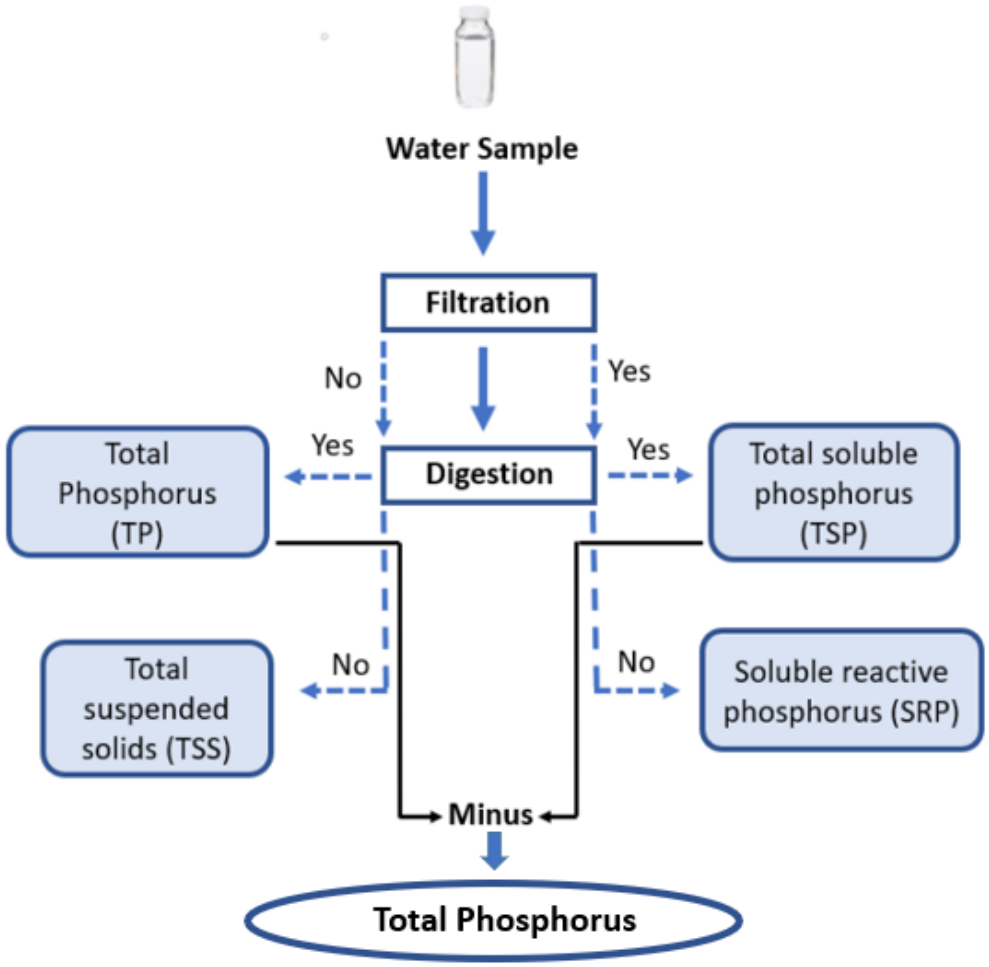

Figure 5.4 Method for phosphorus fractionation.

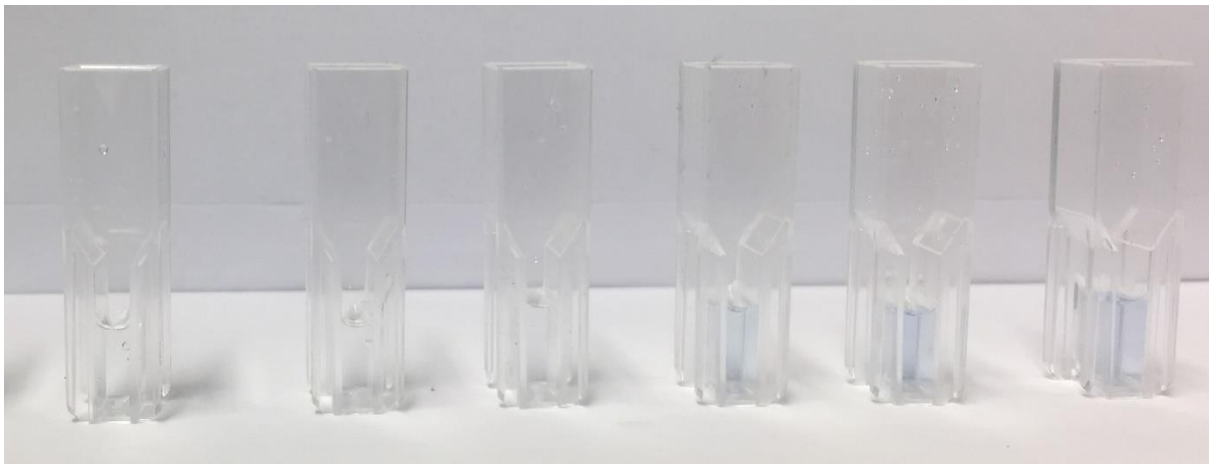

Figure 5.5 Range of low concentration of phosphate standards used in the total phosphorus analysis, in order to generate a calibration curve which the concentrations of the environmental samples could be determined.

5.2.3.4 Total suspended solids

Samples were collected in 1000 mL HDPP bottles, water was stored unfiltered in a freezer (-18 °C) until analysis was carried out. Samples were analysed as described in Standard Method 2540 D [55]. Microfiber glass filters with a pore size and diameter of 1.2 µm and 47 mm respectively. The filters were prewashed and placed in aluminium dishes and dried at 105 °C in an oven for 1 h. The filters were then weighed, labelled, and stored in a desiccator until analysis was carried out. 250 mL aliquots of the water samples were then vacuum filtered and then dried in the oven at 105 °C for 1 h and re-weighed.

5.2.4 Protocol for phosphate measurements using the PhosphaLOAD system

Three discs were used per site, with a total of six measurements per disc. An on-disc QC method of a high and low phosphate standard was employed. Sample and standards were loaded onto the disc using a micro pipette and the standard/sample and dried reagents were allowed to mix for 10 min. System protocol described in detail in Chapter 4. Full image of the phosphate analyser pictured in the field in Figure 5.40.

5.2.5 Meteorological rainfall data

Precipitation data for the case studies was obtained from the weather stations at Newport Furnace (Black 6.8 km, Rough 8.3 km, Green Bridge 9.1 km and Maumaratta 9.1 km north of weather station), Markree Castle (Lisconny Bridge 7 km, Ballysadare River 8.6 km north, Bridge u/s Ballysadare 3.2 km west and Ballygrania Bridge 1.8 km south of weather station) and Phoenix park (all sampling sites accessed by boat east of weather station) through Met Éireann (Figure 5.6).

Figure 5.6 Map of weather stations used for collection of rainfall data prior to all sampling campaigns. Map generated used qGIS.

5.3 Results and discussion

The results and analysis for the three case studies is discussed in this section. All field trial results for each of the catchment studies were compared to lab-based reference method using a UV/vis. The first case study on the R. Liffey was carried out as a preliminary field trial and to determine the impact of using the PhosphaLOAD system on a boat. The R. Liffey study was carried out in conjunction with the Water Blitz citizen science freshwater watch activity for the community, run by DCU Water Institute. The second catchment tested was the Burrishoole catchment, this catchment was the central area of interest for testing and provided a testbed for the evaluation of a tiered framework for catchment monitoring, described in Chapter 1. This catchment provided a low phosphate sampling site that was highly instrumented and documented, therefore all measurements obtained during the field trial could be verified. The third case study involved the Unshin catchment, this catchment was assessed to determine the capability of the novel PhosphaLOAD analyser for successful determination of phosphate in a high-risk catchment, that varied in flow, land type and land use. This catchment involved the monitoring of phosphate levels in both rural and urbanised areas.

5.4 Case Study: River Liffey

5.4.1 Site description

The River Liffey flows for approximately 125 km through Wicklow, Kildare and Dublin, it rises in the Wicklow mountains situated 32 km southwest of Dublin and is drained in Dublin Bay where it enters tidal water. The catchment is a diverse ecosystem that combines, marine birds, shellfish, fish, and some marine animals. The largest urban centre in the catchment is Dublin City, along which the sampling sites were chosen. One of the four sampling sites was selected in the tidal/brackish water section and the remaining three in the freshwater section of the river. The Liffey is categorised as a nutrient sensitive water body and is at risk of pollution impact from groundwater and urban runoff from point sources [166][288]. Anthropogenic activities impacting the quality of the water include, aquaculture, recreation, heavy port use and marine transportation. It accommodates the largest population of any catchment in Ireland and this section of the catchment is a densely populated low flat lying landscape, suitable for the potential measurement of high phosphates.

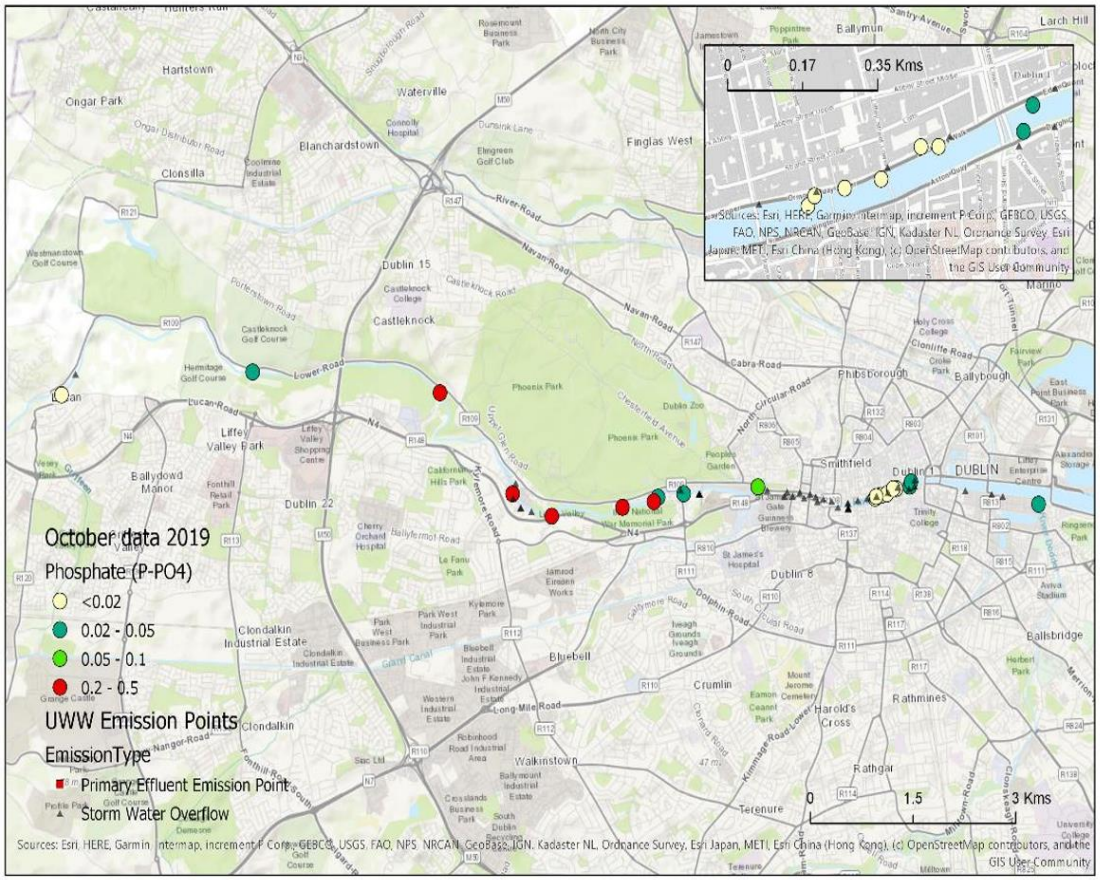

Figure 5.7 Map of the R. Liffey potential sampling points with layered phosphate level data from 2019.

Largest urban centre of the River Liffey catchment is located from Leixslip where it flows in an easterly direction to Islandbridge, it then turns from freshwater into brackish as it discharges at Dublin Bay. This section of the river has a controlled regulated flow, there are three

hydroelectric power stations, at Poulaphouca, Golden Falls and Leixlip, as well as some minor private installations and historical weirs controlling the flow of the river.

The Liffey catchment includes 17 sub catchments with 77 river water bodies, six lakes, six transitional and five coastal water bodies, and 16 groundwater bodies [289]. This subsection of the Liffey catchment is composed of the sedimentary rock limestone and shale bedrock and flows over limestone, this is important as it makes the river more alkaline which creates more conductive conditions for fish to survive. Along the River Liffey there are centres of industrial companies, which can pose pollution pressures to the catchment, it is also impacted by urbanised runoff and pollution loads. Recreational activities also take place on the Liffey such as swimming, kayaking, and rowing.

A report published in 2018 classified the Liffey as a nutrient sensitive water body which is at high risk from diffuse pollution resulting from urban and groundwater run-off and from point sources located within the catchment [289].

Figure 5.8 Map of chosen testing locations along the River Liffey, created using google earth and GIS to map out sampling site coordinates and phosphate levels.

Figure 5.9 displays the rainfall and temperature data for the days prior to the first field trial of the PhosphaLOAD sensor. The weather leading up to the field trial was dry but contained heavy precipitation the night before with relatively normal temperatures for May.

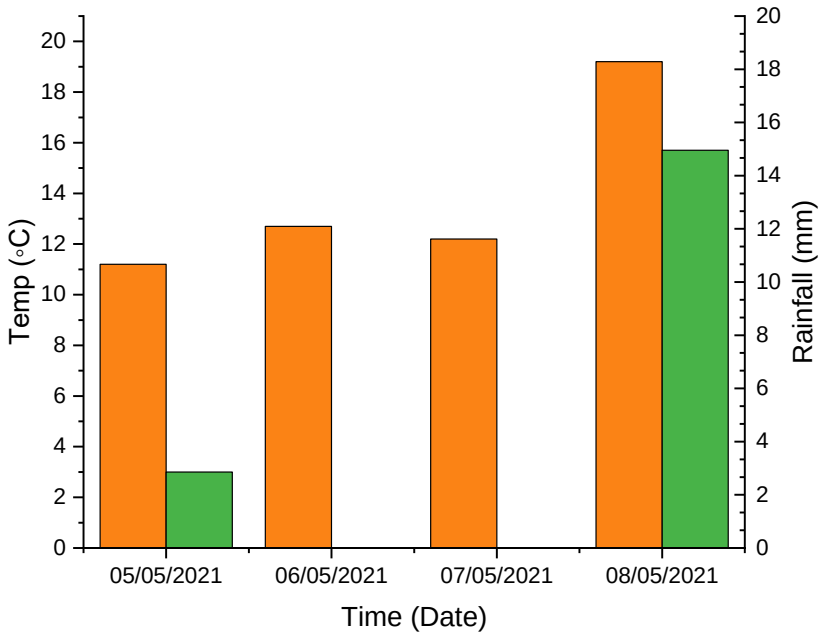

Figure 5.9 Rainfall (green) and temperature (orange) data for days prior to the R. Liffey field trail in May 2021. Rainfall and temperature data collected from the Phoenix Park weather station in Dublin, using Met Eireann data.

5.4.2 Site 1

The first site tested on the River Liffey was the furthest downstream near the opening to Dublin Bay at Samuel Beckett Bridge, closest in location to the docking point (Jeanie Johnson). Salinity levels vary in this section of the river due to tidal influence.

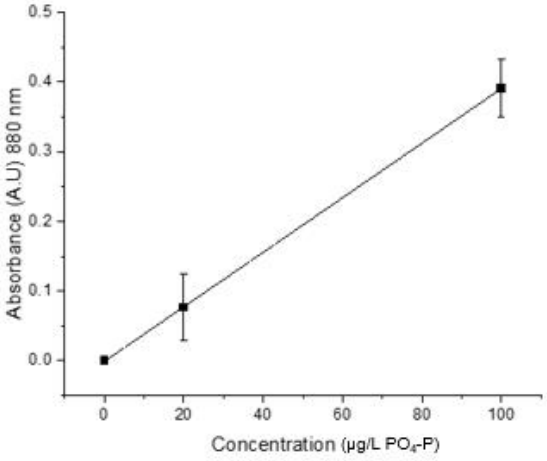

Sampling Site Number	PhosphaLOAD (ug/L)	Phosphate Kit (ug/L)
1	84	50 - 100

Figure 5.10 Left: Calibration curve of QC on disc method and concentration of phosphate measured on the PhosphaLOAD analyser compared to the phosphate kits. Right: River Liffey testing site 1, downstream from docking point near Dublin Bay, brackish water with high salinity depending on tidal levels.

The level of phosphate measured by the system for site 1 was 84 µg L^{-1}. The measurement obtained by the PhosphaLOAD analyser was then compared to the phosphate Kyoritsu PackTest kits (see Section 5.2.3) which measured the concentration of phosphate for that area ranging between 50 – 100 µg L^{-1}, confirming the result obtained by the analyser.

An EXO SONDE was used to collect supplementary data at each of the field testing sites. Table 5.1 highlights the measurements conductivity, turbidity, salinity, ORP, temperate and pH at site 1. This table also included the tidal data obtained from the Marine Institute website (http://www.marine.ie/Home/site-area/data-services/real-time-observations/tidal-observations) as this location had the potential of containing brackish water at the first sampling site as it was closest to Dublin Bay. The conductivity at site was significantly higher than the other sampling sites, it had measurement of 6630.0 µS/cm compared to the other three sites with ranged between 491.3 and 627.8 µS/cm. The tidal values at site 1 were higher than the other sites but not significantly. Turbidity measured for site 1 was also higher than the other sites tested.

Table 5.1 Summary of all supplementary data obtained from an EXO sonde and tidal values for the River Liffey, site 1.

Site	GPS Co-ordinates	Tidal Values	Conductivity (µS/cm)	Turbidity (FNU)	Salinity (psu)	ORP (mV)	Temperature (°C)	pH
1	53.34684, -6.23829	3.7	6630.8	6.8	5.1	162	10.9	8.2

5.4.3 Site 2

First upstream sampling point from the docking point and first freshwater water body site. The area consisted of a built-up urban area with brewing plant and industrial businesses either side of the river.

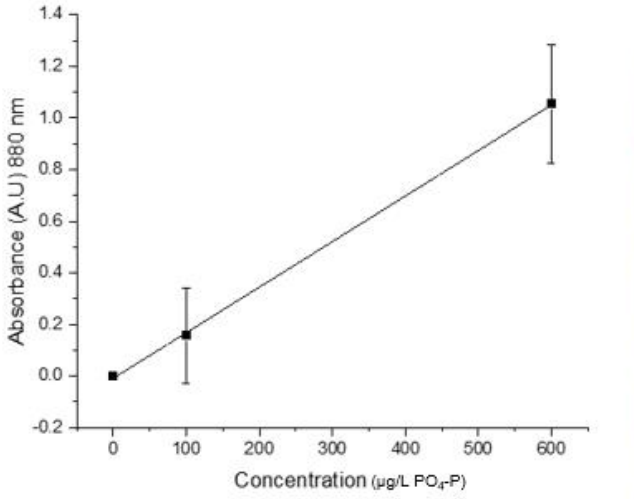

Sampling Site Number	PhosphaLOAD (ug/L)	Phosphate Kit (ug/L)
2	141	100 - 200

Figure 5.11 Left: Calibration curve of QC on disc method and concentration of phosphate measured on the PhosphaLOAD analyser compared to the phosphate kits. Right: River Liffey testing site 2, upstream from docking point, freshwater waterbody.

The level of phosphate measured by the system for site 2 was 141 µg L^{-1}. The measurement obtained by the PhosphaLOAD analyser was then compared to the phosphate Kyoritsu PackTest kits which measured the concentration of phosphate for that area ranging between 100 – 200 µg L^{-1}, confirming the result obtained by the analyser. This was the highest level of phosphate measured from all four sites tested. The industrial brewing business near this sampling point may be a factor in the higher levels of phosphate detected at this point.

The tidal value has decrease from site 1 but not significantly, this was to be expected as site 1 is downstream near the Dublin Bay opening, therefore slightly higher tidal values would be expected compared to site 2. However, the turbidity levels decreased considerably from 6.8 to 1.4 FNU. The conductivity at this site was also the lowest measured of the four sampling sites.

Table 5.2 Summary of all supplementary data obtained from an EXO sonde and tidal values for the River Liffey, site 2.

Site	GPS Co-ordinates	Tidal Values	Conductivity (µS/cm)	Turbidity (FNU)	Salinity (psu)	ORP (mV)	Temperature (°C)	pH
2	53.34759, -6.29984	3.0	491.3	1.4	0.3	142.3	11.7	8.5

5.4.4 Site 3

Further upstream, more suburban site, more greenery present.

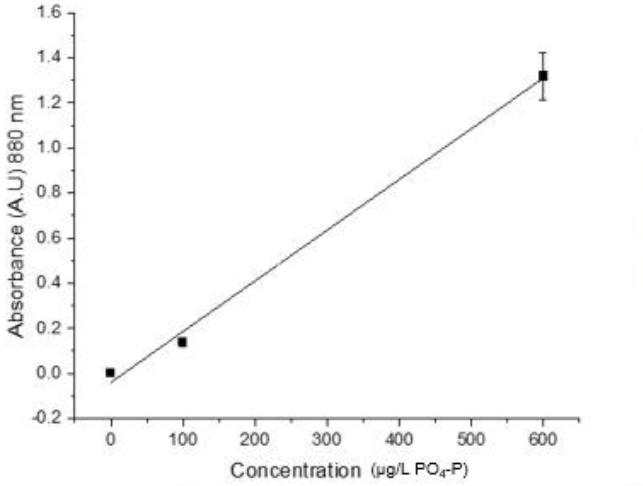

Sampling Site Number	PhosphaLOAD (ug/L)	Phosphate Kit (ug/L)
3	58	50 - 100

Figure 5.12 Left: Calibration curve of QC on disc method and concentration of phosphate measured on the PhosphaLOAD analyser compared to the phosphate kits. Right: River Liffey testing site 3, upstream freshwater waterbody.

The level of phosphate measured by the system for site 3 was 58 µg L^{-1}. The measurement obtained by the PhosphaLOAD analyser was then compared to the phosphate Kyoritsu PackTest kits which measured the concentration of phosphate for that area ranging between 50 – 100 µg L^{-1}, confirming the result obtained by the analyser. This was the lowest level of phosphate detected during the field trail of the analyser.

There is a noticeable increase in temperature from the measurements taken at the first sampling site due to the sampling times. The salinity measured at this point was one of the lowest measurements as expected as this site was upstream from Dublin Bay. The turbidity for sampling sites 3 and 4 is similar due to the closeness distance.

Table 5.3 Summary of all supplementary data obtained from an EXO sonde and tidal values for the River Liffey, site 3.

Site	GPS Co-ordinates	Tidal Values	Conductivity (µS/cm)	Turbidity (FNU)	Salinity (psu)	ORP (mV)	Temperature (°C)	pH
3	53.34748, -6.31256	2.5	627.8	5.1	0.4	163.2	14.3	8.3

5.4.5 Site 4

Last sampling site, furthest upstream sampling point, near Phoenix Park.

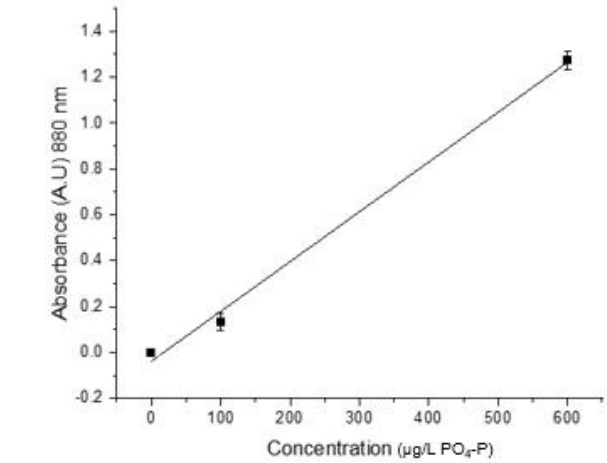

Sampling Site Number	PhosphaLOAD (ug/L)	Phosphate Kit (ug/L)
4	63	50 - 100

Figure 5.13 Left: Calibration curve of QC on disc method and concentration of phosphate measured on the PhosphaLOAD analyser compared to the phosphate kits. Right: River Liffey testing site 4, downstream (from docking point) freshwater waterbody, furthest upstream point tested.

The level of phosphate measured by the system for site 4 was 63 µg L^{-1}. The measurement obtained by the PhosphaLOAD analyser was then compared to the phosphate Kyoritsu PackTest kits which measured the concentration of phosphate for that area ranging 50 – 100 µg L^{-1}, confirming the result obtained by the analyser. The level detected at this site was similar in value to the level detected at site 3 which is to be expected due to the closeness in distance from the two sampling points, the landscape of the two sampling points was also very similar.

The temperature was highest at sampling site 4, each sampling point increased in temperature. The first sampling site was tested in the morning (11:00 h) and site 4 was tested in the afternoon (14:00 h), therefore the temperature was likely to have increased. The salinity measured (0.4 psu) at this point was one of the lowest measurements as expected as this site was furthest upstream. The pH measured at all four sampling sites was constant and ranged between 8.2 and 8.5.

Table 5.4 Summary of all supplementary data obtained from an EXO sonde and tidal values for the River Liffey, site 4.

Site	GPS Co-ordinates	Tidal Values	Conductivity (µS/cm)	Turbidity (FNU)	Salinity (psu)	ORP (mV)	Temperature (°C)	pH
4	53.34749, -6.29998	1.9	600.7	5.2	0.4	160	15.2	8.3

5.4.7 Conclusion

For the River Liffey case study four sampling sites were chosen starting from Samuel Becketts Bridge working upstream near Phoenix Park. For each of the sampling site three discs were used in triplicate with an on-board QC method of a low and high phosphate standard (100 and 600 µg/L respectively). Two samples were also measured per disc totalling six sample measurements per site. These samples were then measured against a phosphate kit for reference. A graph was generated for each site measurement (see Figure 5.10 - Figure 5.13). The graphs produced showed good linearity for each site measurement with n=3. The variation due to the error bars is mainly due to the disc-to-disc variation of the optical windows, as discussed in Chapter 2.

Figure 5.14 illustrates the combined calibration curve of the QC method which was used to determine the concentration of phosphate at each sampling site. This was also carried out to determine how reliable the on-board QC method is. The graph shows a good comparison for each of the QC standards measured on the discs for 100 and 600 ug/L P standards. With an average R^2 value of 0.9963 and a slope of 0.0021 showing excellent sensitivity for the QC method. The QC standards showed close agreement with the in lab calibrated standards, proving the reliability of the onboard QC method.

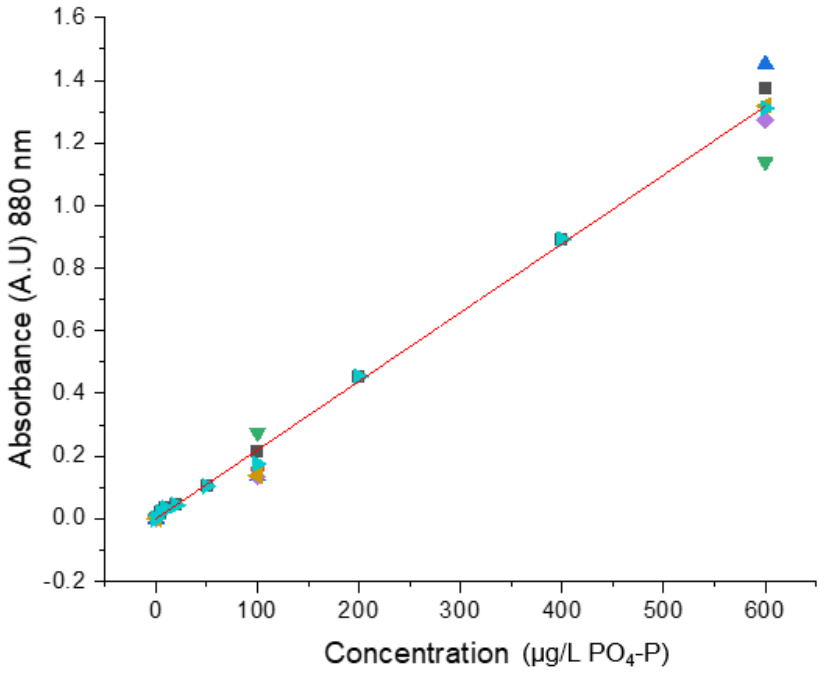

Figure 5.14 Phosphate standard calibration carried out on disc, with plotted QC standards on discs from the field trial, R^2 value 0.9996, with good sensitivity and slope of 0.0023

This field trial was the first onsite field test of the phosphate system and demonstrated excellent agreement in observed results for the PhosphaLOAD system and phosphate kits. This catchment was a suitable area for trialling the sensor due to its wide catchment area and high levels of phosphate, the impact of carrying out water quality monitoring on a boat and how this affects sample measurements was also investigated. A number of lessons learned from this field trial were implemented into the following two case studies (detailed in Section 5.7)

5.5 Case Study: Burrishoole Catchment

5.5.1 Site description

This catchment area is well known for its salmon (*Salmo salar*), trout (*Salmo trutta*) and eel (*Anguilla anguilla*) studies. The Burrishoole catchment provides a pool of knowledge about the surrounding area, the wildlife, and different ecosystems. A significant amount of data sets have been collected to date, such as; water quality parameters (turbidity, pH, conductivity, DO and DOC), fish species census and environmental data (nutrients). A considerable amount of funding that dates back to the 70's has been used to better understand, preserve and manage this catchment [290]. The Burrishoole catchment is connected to the Marine Institute, National Park and Wildlife Services, Coillte, Fisheries board and the Irish Environmental Protection Agency. This is a popular domain for carrying out research studies in the area of water quality, ecology, development of new technologies for environmental assessment and the monitoring of land use and water systems. The Burrishoole catchment is a highly instrumented and monitored catchment. Long-term data sets are widely available that date back to the 1950's [291]. These datasets contain information on water temperature, precipitation and water temperature. In later years, more detailed data has been collected on pH, dissolved oxygen and lake temperature as well as meteorological data. The Burrishoole catchment area is located in the northwest of County Mayo, Ireland (9º 34' 20" W, 53º 55' 22" N).

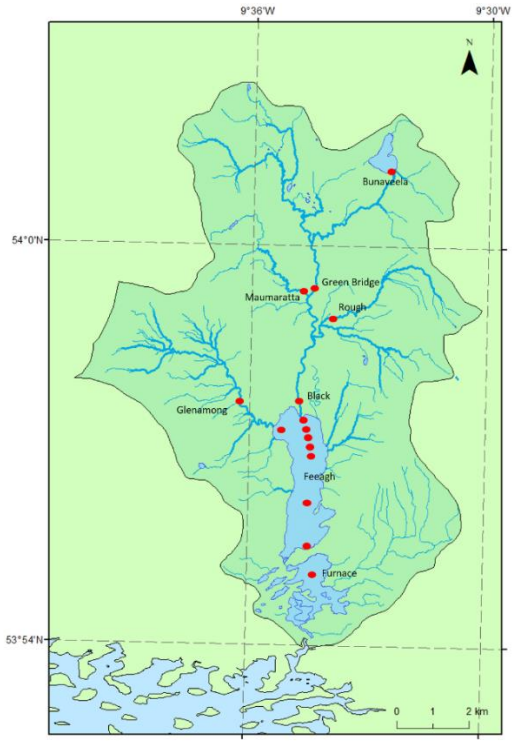

Figure 5.15 Burrishoole catchment with potential sampling points along the two main lakes (Feeagh and Furnace) and a number of rivers across the sub catchments.

The catchment area is surrounded centred in the heart of the Nephin Beg mountains. It has a north-southern directional drainage whereby it flows through a freshwater network, before reaching a brackish tidal lake (L. Furnace). The catchment then finally empties into the Atlantic Ocean at the northeast corner of Clew Bay. The surrounding area of the catchment comprises a series of steep and sloped mountain ranges, valleys and a network of lakes and streams, creating the most idyllic and picturesque scenery. The catchment consists of three main lakes, Furnace (brackish), Feeagh (freshwater) and Bunaveela (freshwater), with a number of rivers and sub catchments in the surrounding area.

The bedrock geology of the Burrishoole catchment is predominately characterised by metamorphic rocks of late Precambrian age, consisting of quartzites (44%), schists/gneiss (44%), Silurian quartzite (11%) and small areas of sandstone and limestone (1%) [290]. As a result of geological differences, the western and eastern sub-catchments of the Burrishoole catchment differ significantly. Rivers and streams on the western side (Glenamong, Altahoney and Maumaratta sub catchments) are generally more acidic and have low aquatic production [292]. The geology is more varied toward the east side of the catchment (Rough, Lodge and Goulaun sub-catchments), with quartzite/schist interspersed with veins of volcanic rock, dolomite, wacke and schist. The rivers draining the eastern sub catchments are relatively neutral in alkalinity with a higher aquatic live productivity. Towards the lower part of the catchment near the Clew Bay opening, metamorphic rocks dip below Devonian Old Red Sandstone and Carboniferous limestone [290]. An end moraine marks the border between metamorphic and sedimentary rock-types, separates the largest freshwater lake, Feeagh, from the tidal Furnace (see Figure 5.15). Peaty carbon-rich top horizons are common throughout the catchment. Blanket peat can also be found nearer the western side of the catchment.

The predominant land uses within the catchments focus on sheep grazing and forestry. The Black River also includes a small-scale section of intensively managed agricultural land. The Marine Institute Research station is located in the Burrishoole catchment, which focuses on research into freshwater and brackish ecosystems and their interactions with the environment and climate. Fishing (fly and shore) is also a major attraction within the catchment.

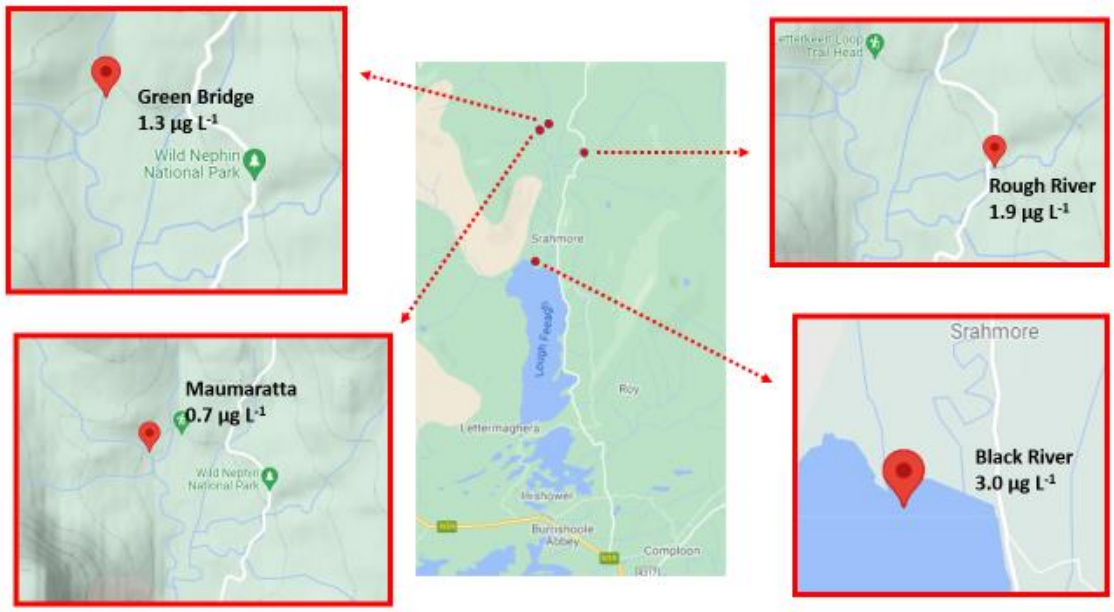

Figure 5.16 Selected sampling sites for potential successful on-site phosphate determination with the phosphate sensor and mapped phosphate results, with phosphate levels included.

5.5.2 Baseline Screening using sampling and remote sensing methods

To determine the most suitable sites for phosphate monitoring within the Burrishoole catchment, baseline screening was carried out for the 15 most common sampling sites (lakes and rivers combined) monitored in the catchment for various water quality parameters. Satellite and aerial images were obtained of the area to investigate if this would be a suitable approach to forecast areas with higher phosphate levels within the catchment.

5.5.2.1 Satellite and aerial imaging

Sentinel 2 images were processed using qGIS. The findings from this method of monitoring resulted in poor quality cloud covered images (see Figure 5.17). The level of cloud cover was characterised into low, moderate and high levels of cloud cover. It was determined that this would not be a suitable method of monitoring due to the geographical location of the catchment and the level of cloud cover experience in this part of the world.

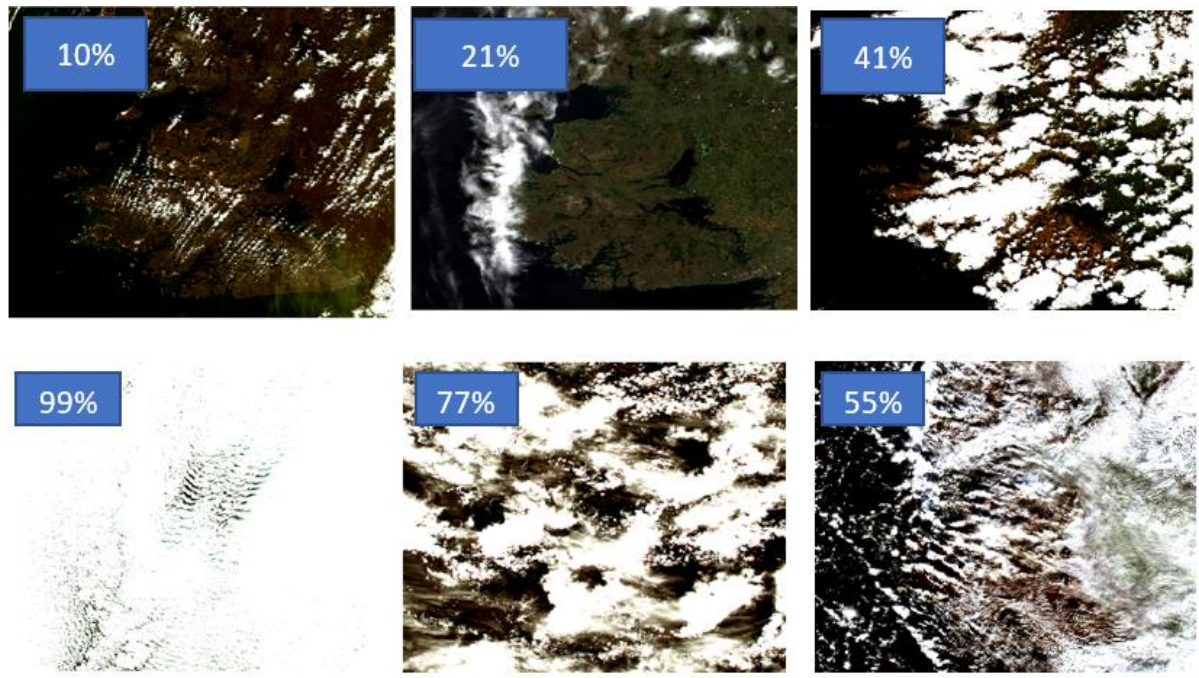

Figure 5.17 Downloaded and processed Sentinel 2 images of the Burrishoole catchment and the level of cloud cover experience as the satellite passed over the area of interest.

An aerial flyover of the catchment was carried out by Maynooth University on the 3rd of May 2017 but experience turbulence from the easterly winds on the lee side of the hills North of Newport (see Figure 5.18). This interfered with the stability of the aircraft and we had to abandon the mission as it became unsafe to continue. Therefore, providing more evidence for the need for more handheld *in-situ* technologies to effectively and frequently monitor the area.

Figure 5.18 Aerial flyover on the 3rd of May 2017, carried out by Maynooth university.

In-situ and traditional baseline sampling of the sites was carried determine the most suitable sites for testing the phosphate sensor in the Burrishoole catchment, due to the naturally low levels of phosphate generally present in the catchment. Water samples from eight different sampling sites were collected and measurements for turbidity, TP and TSS were determined. Supplementary data for those months was also collected. From this preliminary data collection, the testing sites for the PhosphaLOAD sensor field test were selected so that

measurement of phosphate levels could be determined. The baseline screening for the sampling sites was carried out at the end of summer/autumn of 2019 and the field trial of the phosphate sensor was carried out in the summer of 2021. Ireland experienced extremely high temperatures, with very limited precipitation in the days leading up to the sampling campaign (see Figure 5.19).

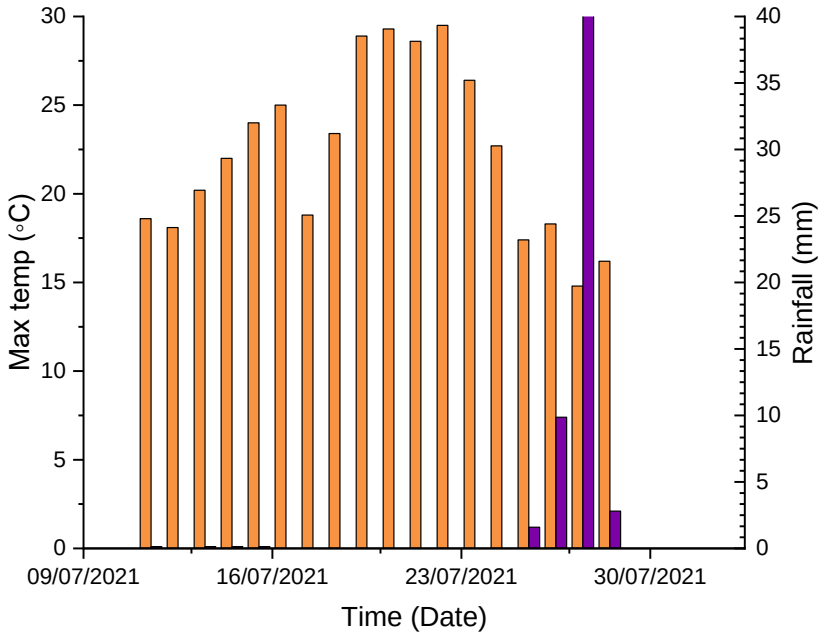

Figure 5.19 Rainfall (purple) and temperature (orange) data for the month of July obtained from Met Eireann data.

5.5.2.2 Turbidity

Turbidity is considered as an early warning indicator of phosphorus pollution. It is a simple and direct optical measurement that quantifies particulate matter suspended in water.

Over a four-month period water samples were collected once a month and analysed for turbidity using a nephelometer (see Figure 5.20). The results determined that the two rivers with the highest measurements of turbidity were the Rough River and the Black River, with Mill Race and Bunaveela having the lowest turbidity readings. This also provided a hypothesis as to what rivers would contain higher levels of TSS and TP.

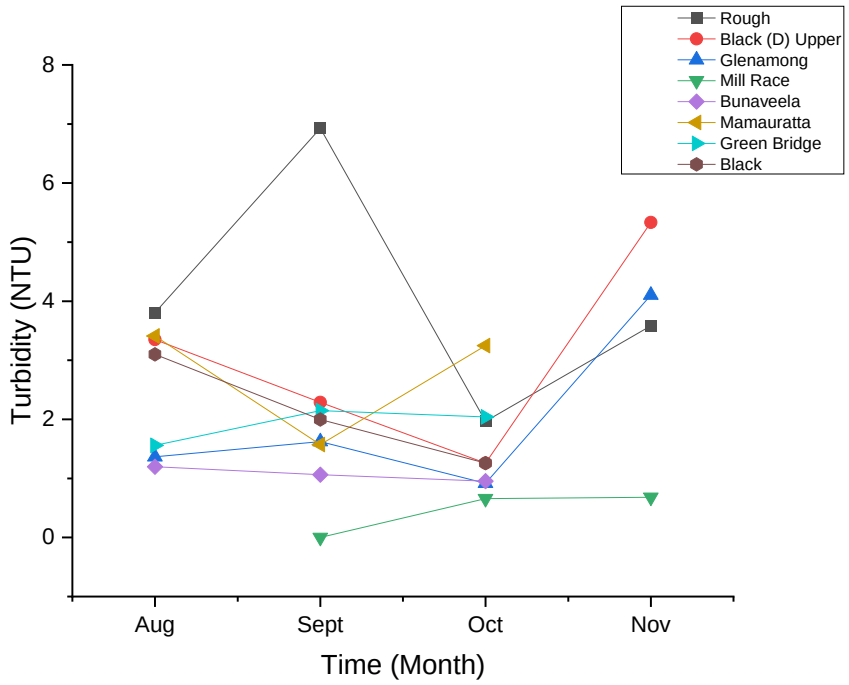

Figure 5.20 Variances in turbidity measurements over a four-month period for different sampling sites in the Burrishoole catchment to help determine possible testing sites for the PhosphaLOAD system.

5.5.2.3 Total suspended solids

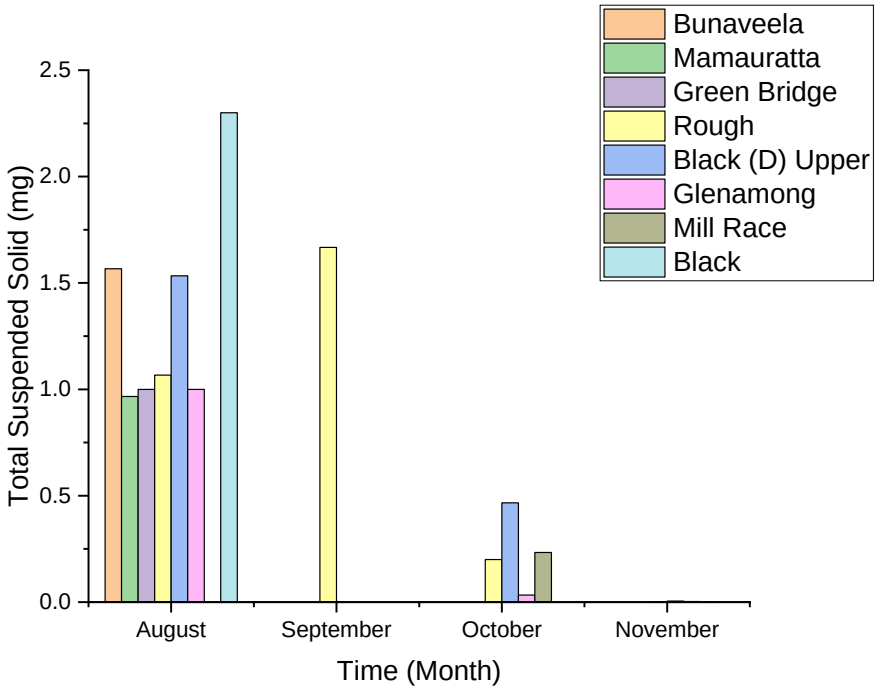

Figure 5.21 TSS measurements for eight different sampling sites over a four-month period in the Burrishoole catchment.

The levels of TSS measured over a four-month period determined that the Rough and the Black River had the highest levels, as suspected from the turbidity analysis carried out previously. This may be due to the fact that the Black River drains most of the Burrishoole catchment and the Rough River land cover is mainly forested and partly under the native woodland scheme.

5.5.2.4 Total Phosphorus

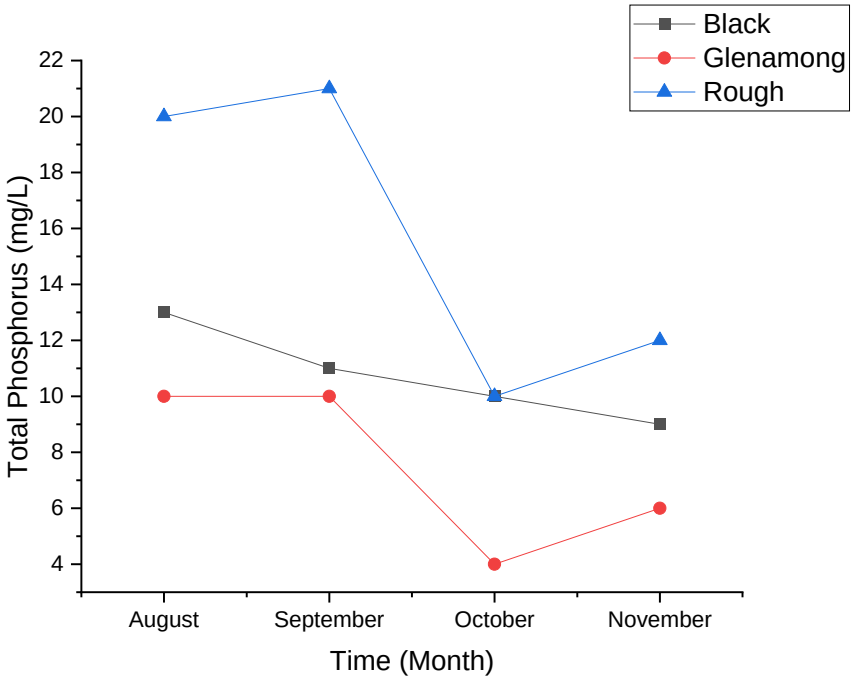

Figure 5.22 Levels of TP for each of the different sampling sites over a four-month period. Three rivers selected in the Burrishoole catchment to determine suitable testing sites for the phosphate system

As the previous analysis determined that the Rough and Black River would be the potential useful sites for phosphate determination during the sensor field trials the low measurement catchments for both turbidity and TSS were eliminated from the selection process. The Glenamong River remained as a low control comparison for the potentially higher phosphate sites. Similarly, the TP analysis indicated that both the Rough River and Black River showed the highest concentrations of TP.

From the preliminary screening of sample sites, the two rivers selected for the case study was the Black River and Rough River due to the levels of TP, TSS and turbidity measurements. These sites were selected as they were deemed most suitable for the field test as the likelihood of successful phosphate measurements determined by the preliminary analysis of each of the sampling sites. Two additional sites were also examined (Green Bridge and Maumaratta) as extremely low phosphate level sites to test out the capabilities of the sensor (see Figure 5.16).

5.5.3 Site 1: Black River

The Black River is one of two main inflows into Lough Feeagh, it drains most of the Burrishoole catchment. It is a man-made channel and the maintenance and access permission are facilitated by the landowners. The Black is surrounded by a small portion of intensively managed agricultural land. The soil type is peat and carbon rich top horizon which is common throughout the catchment.

The PhosphaLOAD sensor was tested in this area and as the levels were extremely low the sensor did not pick up any phosphate levels (see Figure 5.23), the concentration of phosphate detected by the sensor using the calibration curve was – 4.4 µg/L. The low QC standard (10 µg/L) was also unable to be detected by the sensor, this measurement was carried out in triplicate on three separate discs with a total of six site samples (two per disc). These measurements were compared to a UV/vis spectrometer where 2 µg/L P was measured in the site sample.

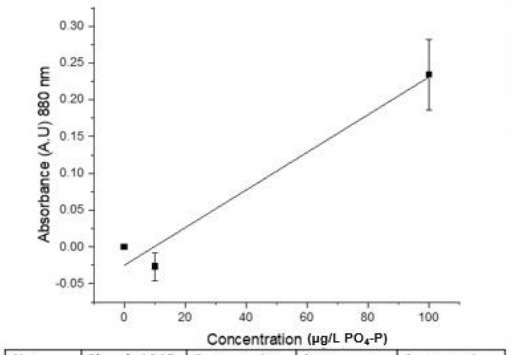

Site	PhosphaLOAD measurement (A.U)	Concentration (ug/L)	Spectrometer measurement (A.U)	Concentration (ug/L)
Black River	-0.035	-4.421	0.001	1.889

Figure 5.23 (A) Burrishoole: Black River testing site and (B) general landscape of the catchment. Individual calibration curve generated from the on-disc QC method for the two testing locations in Burrishoole, Black River. A set of standards blank, low and high phosphate standards (0, 10 and 100 ug/L). Black River (R^2 value 0.9598).

Supplementary data was gathered at the Black River sampling site using an EXO sonde, a total of 10 measurements were obtained at each site. The table also included lab phosphorus analysis (Table 5.5). The phosphorus analysis was carried out in the lab in triplicate and measured using a UV/vis spectrometer. The analysis included SRP, TP, TSP and TPP. The Black River sampling site measured the one highest levels of turbidity (7.3 FNU), this was to be expected as this site is located at one of the main inflows into Lough Feeagh. The SRP data was quite low measuring 1.9 µg/L and therefore proves that the levels present were too low to be measured by the PhosphaLOAD system due to its LOD of 16 µg/L. The TP as TSP levels were also considerably low, this could be due to the weather that was experience during the sampling period. The temperate had been warm for two weeks prior to sampling with little to no precipitation (see Figure 5.19).

Table 5.5 Supplementary data for the Black River testing site in the Burrishoole catchment, obtained from an EXO sonde in-situ measurements (n=10) and phosphorus lab analysis (n=3).

Sampling Site: Black River			
Parameter	**Measurement**	**St. Dev**	**Units**
Conductivity	905.1	0.0	µS/cm
Turbidity	7.3	1.2	FNU
Salinity	0.4	0.0	psu
ORP	109	2.6	mV
Temperature	23.2	0.4	°C
pH	7.8	0.1	
SRP	1.9	0.0	µg/L
TP	12.0	0.8	µg/L
TSP	8.1	1.4	µg/L
TSS	0.1	0.0	mg
TPP	3.8	0.1	µg/L

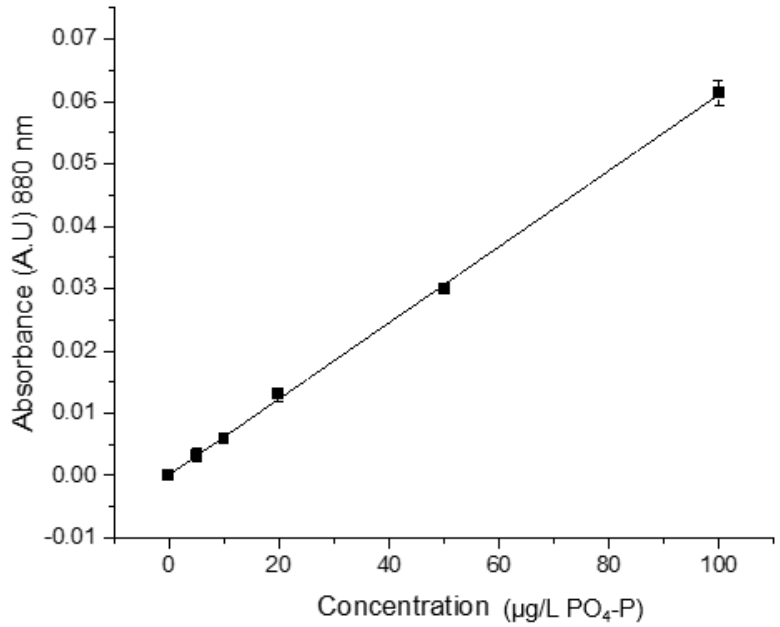

Figure 5.24 SRP generated calibration curve for standards, to measure SRP concentration in collected samples from the Burrishoole catchment. Calibration showing good linearity with an R^2 valie of 0.9996 and expected sensitvity from the spectrometer with a slope of 0.0006 (n=3).

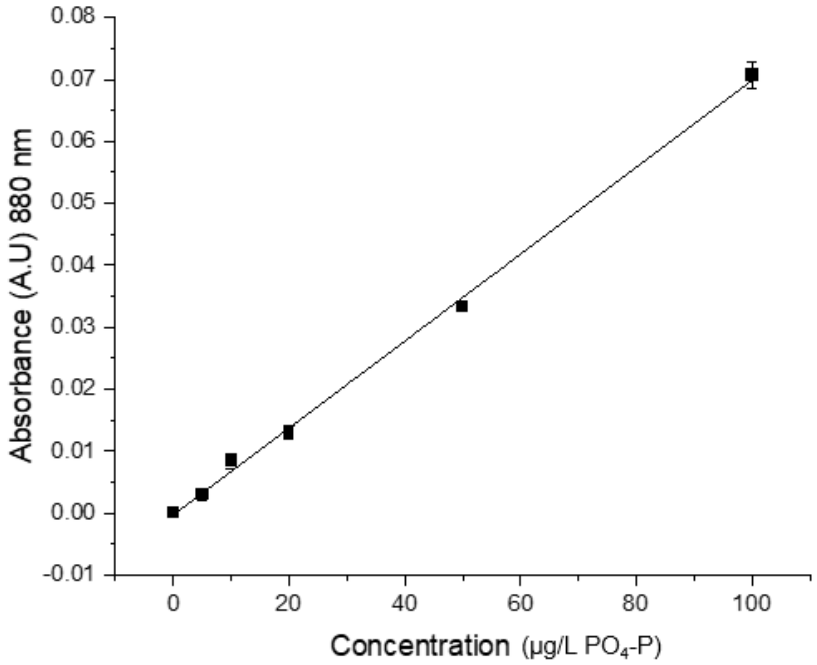

Figure 5.25 TP generated calibration curve for standards, to measure TP concentration in collected samples from the Burrishoole catchment. Calibration showing good linearity with an R^2 valie of 0.996 and expected sensitvity from the spectrometer with a slope of 0.0007 (n=3).

5.5.4 Site 2: Rough River

The Rough River is a tributary off the Black River. It is surrounded by forest and is partially under the native woodland scheme. The maintenance and access permission are again facilitated by landowners.

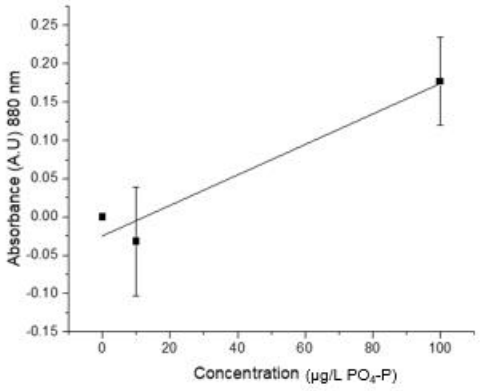

Site	PhosphaLOAD measurement (A.U)	Concentration (ug/L)	Spectrometer measurement (A.U)	Concentration (ug/L)
Rough River	-0.036	-3.309	0.002	3.000

Figure 5.26 Burrishoole: Rough River testing site. Individual calibration curve generated from the on-disc QC method for the two testing locations in Burrishoole, Rough River. A set of standards blank, low and high phosphate standards (0, 10 and 100 µg/L. Rough River (R^2 value 0.9553).

The levels in the Rough River were also too low to be detected by the sensor and a minus figure of – 3.3 µg/L was detected using the calibration curve generated. These results were compared against the spectrometer which determined the P concentration for that site to be 3 µg/L, which is over 5 times lower than the LOD of the sensor.

The lab analysis indicates that the Rough River contained the highest phosphate levels, obtaining an SRP measurement of 3.0 µg/L, compared to the 1.9 µg/L measured at the Black River. The measurements for TP were also higher at this site. The measurements for turbidity and conductivity were lower at this site.

Table 5.6 Supplementary data for the Rough River testing site in the Burrishoole catchment, obtained from an EXO sonde in-situ measurements (n=10) and phosphorus lab analysis (n=3).

Sampling Site: Rough River			
Parameter	**Measurement**	**St. Dev**	**Units**
Conductivity	270.9	0.6	µS/cm
Turbidity	5.6	0.2	FNU
Salinity	1.0	0.0	psu
ORP	100.4	3.9	mV
Temperature	22.3	0.1	°C
pH	8.1	0.2	
SRP	3.0	0.0	µg/L
TP	13.8	1.4	µg/L
TSP	4.3	1.8	µg/L
TSS	0.2	0.0	mg
TPP	9.5	0.0	µg/L

5.5.5 Site 3: Green Bridge

The Green Bridge sampling site is located northwest of the Black River, the landscape is green and forested, which is typical of this area. This sampling site was eliminated from the study to reduce waste of prepared discs as the levels of phosphate were unable to be detected at the higher phosphate sites. Water samples from the Green Bridge site were collected and analysed in the lab for SRP, TP, TSP, TPP and TSS.

Figure 5.27 Burrishoole: Green Bridge testing site.

Table 5.7 illustrates the water quality parameters measured for the Green Bridge site in the Burrishoole catchment. Salinity levels at Green Bridge are low as expected and obtained a value of 0.1 psu. The lab analysis for SRP were also extremely low measuring 1.3 µg/L, therefore the levels would be over 12 times too low to be detected by the PhosphaLOAD system. The levels of TP, TSP, and TPP were also considerably low as expected for this sampling site. With measurements for conductivity and turbidity showing a significant reduction compared to the Black River and Rough River sites.

Table 5.7 Supplementary data for the Green Bridge testing site in the Burrishoole catchment, obtained from an EXO sonde in-situ measurements (n=10) and phosphorus lab analysis (n=3).

Sampling Site: Green Bridge			
Parameter	**Measurement**	**St. Dev**	**Units**
Conductivity	185.5	8.6	µS/cm
Turbidity	2.0	1.9	FNU
Salinity	0.1	0.0	psu
ORP	86.8	3.2	mV
Temperature	25.9	0.5	°C
pH	8.2	0.0	
SRP	1.3	0.0	µg/L
TP	12.4	1.4	µg/L
TSP	3.3	0.8	µg/L
TSS	1.1	0.0	mg
TPP	9.0	0.0	µg/L

5.5.6 Site 4: Maumaratta

The Maumaratta sampling site is located northwest of the Black River and in close proximity to the Green Bridge sampling site, with similar landscape. Water samples were also collected from the Maumaratta sampling site and analysed for SRP, TP, TSP, TPP and TSS in the lab.

Figure 5.28 Burrishoole: Maumaratta testing site.

The water quality parameters and phosphorus analysis for the Maumaratta sampling site are summarised in Table 5.8. As expected, the SRP analysis measured for the site was extremely low obtaining a value of 0.8 µg/L. Highlighting the demand for low LOD sensor required to monitor this catchment. The turbidity measurement for this was unexpectedly high compared to the low phosphorus analysis measurements obtained. This may have been caused by larger particles in the water body being detected by the sonde but filtered out of the sample prior to analysis. The landscape of this sampling site is highly forested with an abundance of greenery, therefore larger particles and debris would be common in the water body.

Table 5.8 Supplementary data for the Maumaratta testing site in the Burrishoole catchment, obtained from an EXO sonde in-situ measurements (n=10) and phosphorus lab analysis (n=3).

Sampling Site: Maumaratta			
Parameter	**Measurement**	**St. Dev**	**Units**
Conductivity	891.1	5.8	µS/cm
Turbidity	7.7	3.1	FNU
Salinity	0.4	0.1	psu
ORP	134.3	5.8	mV
Temperature	26.0	0.8	°C
pH	7.8	0.1	
SRP	0.8	0.0	µg/L
TP	12.0	0.8	µg/L
TSP	4.3	1.6	µg/L
TSS	1.0	0.0	mg
TPP	7.6	0.0	µg/L

5.5.7 Conclusion

The Burrishoole catchment was chosen due to its well-established monitoring programme and historical data available. The novel PhophaLOAD analyser was tested in Burrishoole to demonstrate its performance in a low-level phosphate catchment and evaluate the potential of adding value to the existing monitoring platform.

The Burrishoole catchment also provided a testbed for the demonstration of using remotely sensed images for catchment scale monitoring of nutrients such as phosphate. However, due to the geographical location and cloud cover experienced this was deemed to be unsuccessful, providing the basis for more *in-situ* sensors for increase monitoring providing increased temporal and spatial data.

Due to the low levels of phosphate in the catchment, a low phosphate QC standard of 10 µg/L and a high of 100 µg/L was chosen. Due to the poor optical clarity of discs used per site (n=3) the low standard was not detected by the PhosphaLOAD platform (see Figure 5.23 and Figure 5.26). The low standard falls below the x axis and represents minus phosphate concentrations, generating poor calibration curves with an R^2 of 0.9553 (Black River) and 0.9598 (Rough River). The calibration curve in Figure 5.29 was used to determine the phosphate levels and to determine the reproducibility of the QC method across the six discs used in the combined sites. Figure 5.29 highlights the significant variation in the low 10 µg/L phosphate QC standard and the decrease variation in the higher 100 µg/L phosphate QC standard, as the variation in optical clarity is less noticeable the higher the presence of phosphate.

The phosphorus analysis measurements obtained for the four sites monitored the UV/vis spectrometer for SRP and TP are typical values for the catchment [293].

In total 12 samples were measured for phosphate on the PhosphaLOAD system, 60 samples were measured for phosphorus speciation and 240 measurements were obtained by the sonde for general water quality parameters during the field trial for the Burrishoole catchment case study.

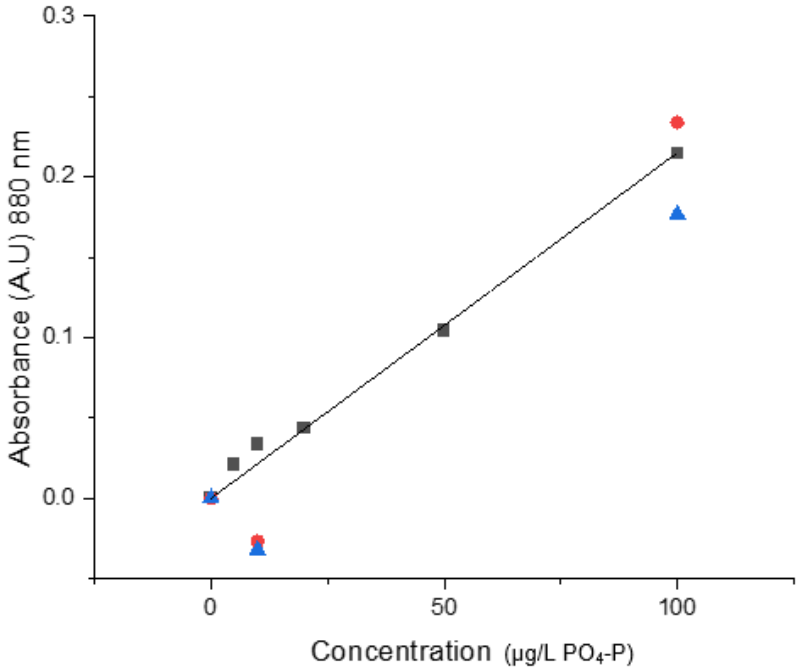

Figure 5.29 Phosphate standard calibration carried out on disc, with plotted QC standards on discs from the field trials, R^2 value 0.9953, with good sensitivity and slope of 0.0021. However variation in QC standards due to variation in clarity of optical windows from disc to discs (shown by use of error bars). Site 1 Black (red) and site 2 Rough (blue).

Due to the extremely low levels of phosphate present in the Burrishoole catchment the PhosphaLOAD sensor was not sensitive enough to detect these trace levels. The low QC standard was unable to be detected by the sensor also resulting in minus phosphate concentration measurements. The sensor has previously demonstrated an LOD of 16 µg/L (see Chapter 4) therefore this low QC standard was too low to obtain a true value.

Data availability and data processing involved in obtaining satellite data is one of the shortcomings of this monitoring technology. Due to the geographical location of the catchment cloud cover was a major issue. Figure 5.17 highlights the levels of cloud cover captured on a

number of Sentinel 2 pass overs, making it almost impossible to process the data to obtain the level of resolution need to determine different land use/change impacts on the surrounding land within the Burrishoole catchment. Therefore, this method of monitoring did not provide the spatial data needed for the case study. The temporal data was also hindered by the delay in data collection as the satellite pass over frequency of the observed area every 5 days [294]. There was also a number of issues with the use of aerial imagery as this method can be affected by weather conditions [295]. During the scheduled flyover of the Burrishoole catchment the mission was abandoned due to turbulence. The limitations of both methods support the evidence that the demand for handheld sensing technologies can help overcome the limitations of the more sophisticated monitoring techniques.

5.6 Case Study: Unshin Catchment

5.6.1 Site description

The Unshin catchment is drained by the River Drowns in Sligo Bay, located in between Lenadoon Point and Aughrus Point, Co. Donegal. The overall catchment including all sub catchments has a surface area of 1,800 km^2 [296]. The catchment is a eutrophic and generally flat slow-flowing river.

The Unshin is relatively unmanaged river habited by rare plant and fish life due to its unusual physico-chemical composition. The land type in the surrounding area is mainly semi natural grasslands and shrublands. The Unshin also has a substantial plant growth in the channel, the natural riverbanks can be seen in the Lisconny section of the river. Also observed from the field test was the recent drainage works being carried out in the nearby field (Figure 5.33). It is mostly a lowland inland area, however some areas contain steep topography with poor drainage

The geology of the catchment is made of a mix of peat, till and limestone till. The soils are comprised of gleys, peaty gleys and grey-brown podsolics predominately in the Unshin and Owenmore

Brown podsolics, brown earths and grey-brown podsolics are situated near Ballysadare and ballygrania. For the most part the soil type can be described as peaty or clayey-silt-laden.

Agriculture is one of the predominant land uses of this sub catchment, causing serious pressures on the surface water bodies, making it a high-risk catchment. The use of forestry is also significant within the catchment which has hydromorphological threats such as the release of sediment which is connected to tree felling. It is also an urbanised area with urban wastewater treatment plants, the Owenmore River is significantly affected by this [296].

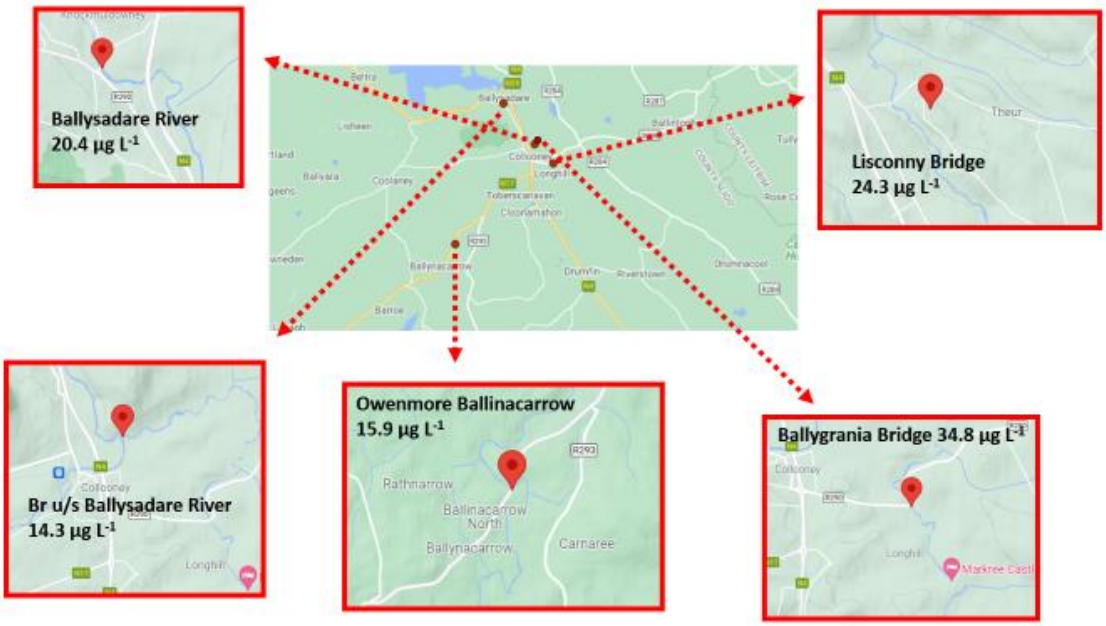

Figure 5.30 Map of different testing locations along the Unshin catchment in Sligo, created using google earth and GIS to map out sampling site coordinates and associated levels of phosphate at each site.

5.6.2 Baseline screening of Unshin Sligo catchment

In the 2 weeks before the planned field test Ireland experienced a period of extremely dry weather with high temperatures and little to no precipitation (see Figure 5.31) therefore a baseline screening of the testing sites was carried out to determine if the field test could be carried out. The baseline screening test of the five catchment sites involved the analysis of SRP.

5.6.2.1 Soluble reactive phosphorus analysis

The results from the baseline screening samples from the five catchment sampling sites contained relatively low levels of phosphate from a maximum of 10.3 µg/L to a minimum of 5.3 µg/L. As the sensor was previously tested in a catchment area with low levels of phosphate (max 3 µg/L), these results were deemed too low to carry out the field trial. Therefore, the field trial was postponed until a period of heavy rainfall followed the dry spell.

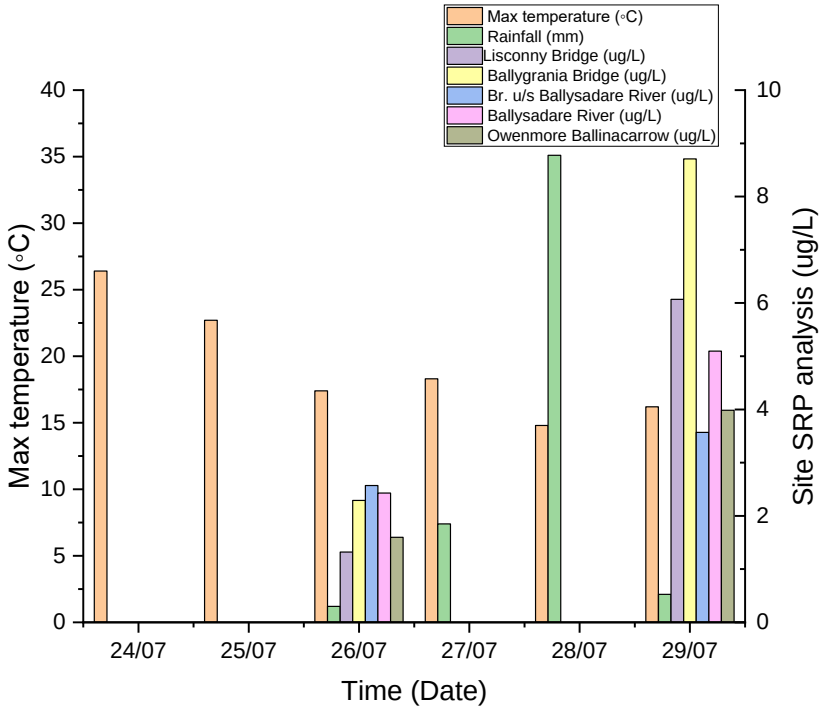

Figure 5.31 Rainfall data correlated to SRP analysis (comparing SRP measurements after a period of dry weather and a period of rainfall). Rainfall collected from Markree Castle weather station in Sligo using Met Eireann data.

The SRP data obtained during the dry period showed low levels of phosphate ranging from 10 – 5 ug/L (see Figure 5.31 and Figure 5.32) compared to the measurements carried out after a period of heavy rainfall ranging between 14 – 34 ug/L (see Figure 5.33, Figure 5.36, Figure 5.37, Figure 5.38 and Figure 5.39). This gave promising potential for demonstrating the PhosphaLOAD system.

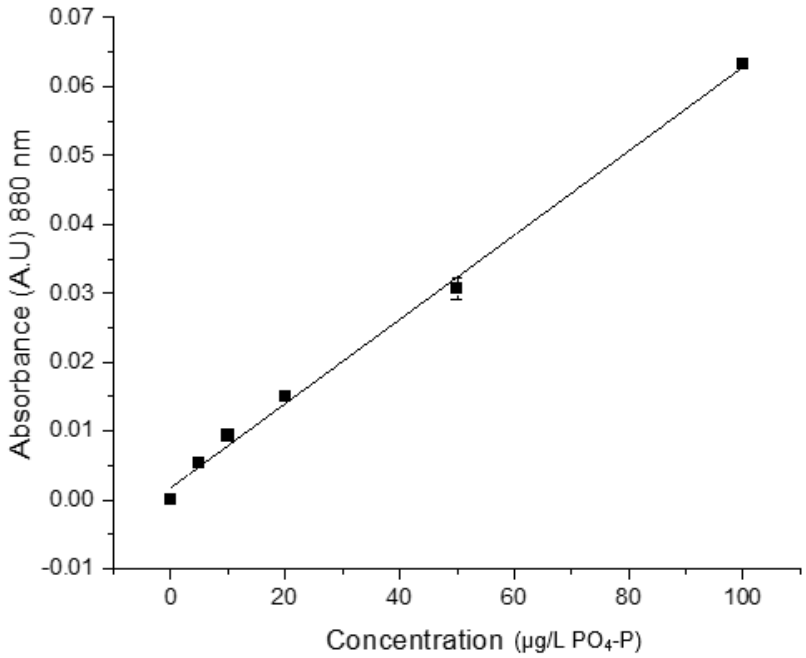

Figure 5.32 SRP analysis for the baseline study for the Unshin catchment Sligo, obtaining a slope of 0.0006 and an R^2 value of 0.9929 (n=3).

5.6.3 Site 1: Lisconny Bridge

The site at Lisconny Bridge was the first testing site, as shown in Figure 5.33 there had been recent drainage works carried out in the area. The PhosphaLOAD sensor measured 37 µg/L for the site compared to the spectrometer which measured 24 µg/L.

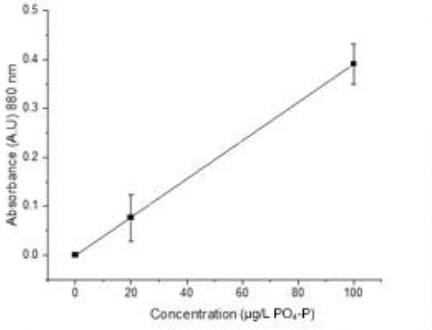

Site	PhosphaLOAD (ug/L)	St. Deviation	Spectrometer (ug/L)	St. Deviation
Lisconny Bridge	37.25	0.04	24.28	0.01

Figure 5.33 Individual calibration curve generated from the on-disc QC method. A set of standards blank, low and high phosphate standards (0, 20 and 100 ug/L) n=3. Lisconny Bridge sampling site generated a calibration curve with an R^2 value of 0.9999 and measured 37 ug/L phosphate compared to the spectrometer reference measurement of 24 ug/L.

Table 5.9 summarises the water quality parameters measurements and phosphorus analysis that was measured from the Lisconny Bridge sampling site. The turbidity value obtained was lower than expected due to the heavy rainfall that was experienced prior to sampling and the recent drainage works that can be observed in Figure 5.33. The SRP levels had significantly increased compared to the baseline screening experiments that were carried out during the dry weather, they increase from 5.3 to 24.3 µg/L. The increase in SRP levels facilitated the successful determination of phosphate using the PhosphaLOAD system.

Table 5.9 Supplementary data for the Lisconny Bridge testing site in the Unshin catchment, obtained from an EXO sonde in-situ measurements (n=10) and phosphorus lab analysis (n=3).

Sampling Site: Lisconny Bridge			
Parameter	**Measurement**	**St. Dev**	**Units**
Conductivity	373.1	0.4	µS/cm
Turbidity	3.5	1.9	FNU
Salinity	0.2	0.0	psu
ORP	188.5	1.0	mV
Temperature	15.4	0.1	°C
pH	7.7	0.0	
SRP	24.3	1.9	µg/L
TP	39.6	2.2	µg/L
TSP	30.3	0.7	µg/L
TSS	6.2	0.0	mg
TPP	9.2	0.0	µg/L

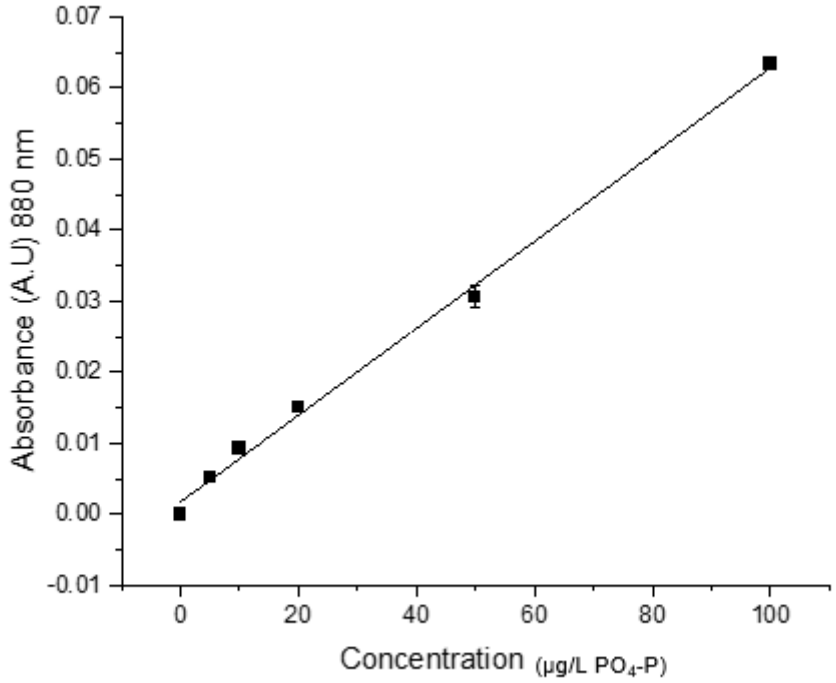

Figure 5.34 SRP generated calibration curve for standards, to measure SRP concentration in collected samples from the Unshin catchment. Calibration showing good linearity with an R^2 value of 0.9969 and expected sensitvity from the spectrometer with a slope of 0.0006 (n=3).

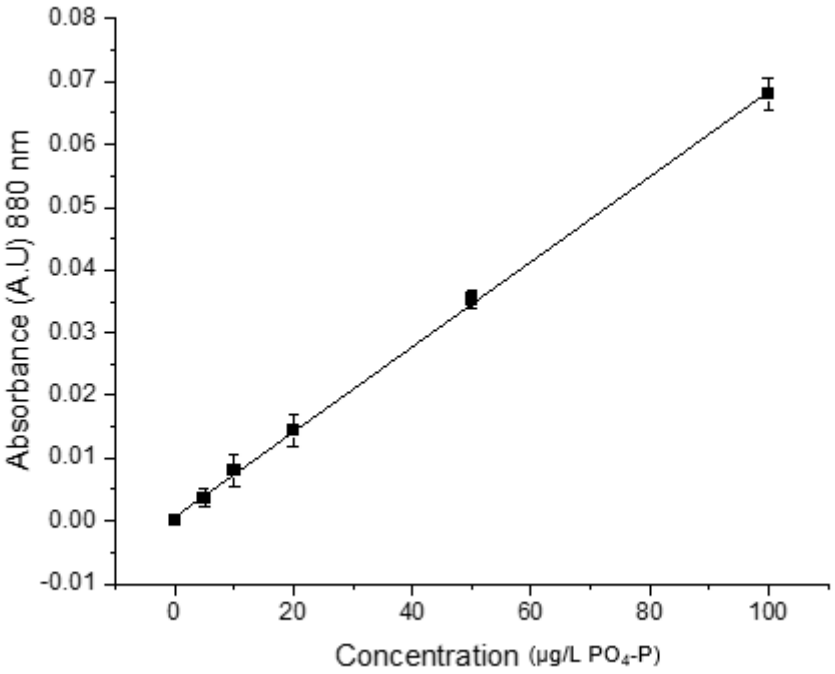

Figure 5.35 TP generated calibration curve for standards, to measure TP concentration in collected samples from the Unshin catchment. Calibration showing good linearity with an R^2 value of 0.9995 and expected sensitvity from the spectrometer with a slope of 0.0007 (n=3).

5.6.4 Site 2: Ballygrania Bridge

The testing site of Ballygrania Bridge is close to Lisconny Bridge with similar landscape. Therefore, the levels of phosphate were expected to be within a similar range to Lisconny Bridge. The PhosphaLOAD sensor measured 40 µg/L P for the site compared against the spectrometer which measured 34 µg/L. The levels of phosphate measured at this site were the second closest measurements in agreement with the analytical method.

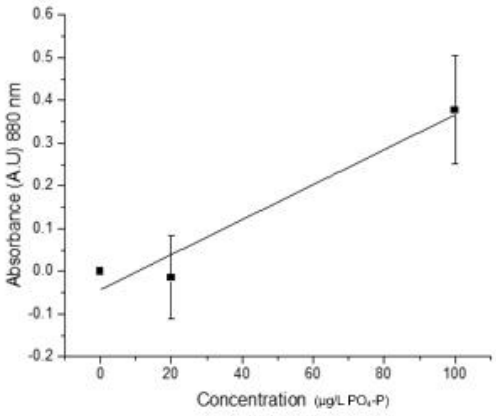

Site	PhosphaLOAD (ug/L)	St. Deviation	Spectrometer (ug/L)	St. Deviation
Ballygrania Bridge	39.53	0.16	34.83	0.00

Figure 5.36 Individual calibration curve generated from the on-disc QC method. A set of standards blank, low and high phosphate standards (0, 20 and 100 ug/L) n=3. Ballygrania Bridge sampling site generated a calibration curve with an R^2 value of 0.9511 and measured 40 ug/L phosphate compared to the spectrometer reference measurement of 35 ug/L.

The measurements obtained by the sonde (Table 5.10) detected significantly higher turbidity levels in the Ballygrania Bridge sampling site, measuring 10.7 FNU compared to the other sampling sites which ranged between 2.3 and 4.6 FNU. The samples collected at this site were more opaque compared to the other testing sites, therefore higher levels of turbidity would be expected.

Table 5.10 Supplementary data for the Ballygrania Bridge testing site in the Unshin catchment, obtained from an EXO sonde in-situ measurements (n=10) and phosphorus lab analysis (n=3).

Sampling Site: Ballygrania Bridge			
Parameter	**Measurement**	**St. Dev**	**Units**
Conductivity	253.3	0.8	µS/cm
Turbidity	10.7	2.3	FNU
Salinity	0.2	0.5	psu
ORP	153.5	2.9	mV
Temperature	15.4	0.4	°C
pH	7.9	0.3	
SRP	34.8	5.4	µg/L
TP	37.7	1.4	µg/L
TSP	21.8	0.7	µg/L
TSS	8.3	0.0	mg
TPP	15.9	0.0	µg/L

5.6.5 Site 3: Bridge upstream Ballysadare River

The Ballysodare river is approximately 6 km in length and flows from Collooney to Ballysodare. The other test sites – the Unshin River and the Owenmore River are tributaries of this river. The river flows through pastures, forest (Union Wood) and meanders underneath the dual carriage road and the railway from Sligo to Dublin.

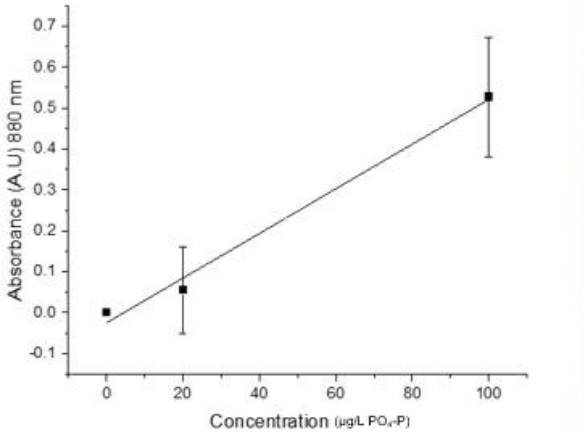

Site	PhosphaLOAD (ug/L)	St. Deviation	Spectrometer (ug/L)	St. Deviation
Br. u/s Ballysadare River	30.20	0.18	14.28	0.00

Figure 5.37 Individual calibration curve generated from the on-disc QC method. A set of standards blank, low and high phosphate standards (0, 20 and 100 ug/L) n=3. Br. u/s Ballysadare River sampling site generated a calibration curve with an R^2 value of 0.9909 and measured 30 ug/L phosphate compared to the spectrometer reference measurement of 14 ug/L.

The sensor measured 30 µg/L P for the site which was compared against the spectrometer which measured 14 µg/L P. This had the biggest significant difference in readings from the PhosphaLOAD sensor compared to the reference standard. The turbidity levels were analysed to determine if this could have been a factor, however the turbidity levels were typical for a freshwater river see Table 5.11 for reference. Another possible factor was the optical clarity of one of the discs not being as clear as the other two used in the analysis.

The TP analysis for this site was lower that the SRP measurement obtained, this did not occur in any of the other sites tested. This may be due to the removal of the colour during the digestion in the sample preparation.

Table 5.11 Supplementary data for the Br. u/s Ballysadare River testing site in the Unshin catchment, obtained from an EXO sonde in-situ measurements (n=10) and phosphorus lab analysis (n=3).

Sampling Site: Br. u/s Ballysadare River			
Parameter	**Measurement**	**St. Dev**	**Units**
Conductivity	414.3	1.2	µS/cm
Turbidity	2.3	1.3	FNU
Salinity	0.2	0.2	psu
ORP	188.3	3.6	mV
Temperature	15.6	0.2	°C
pH	7.9	0.1	
SRP	14.3	2.0	µg/L
TP	12.0	4.9	µg/L
TSP	22.8	1.0	µg/L
TSS	15.9	0.0	mg
TPP	-10.8	0.0	µg/L

5.6.6 Site 4: Ballysadare River

This sampling site was in the centre of Ballysadare village. After the bridge in Ballysodare village, the river drops over some fast rapids. This river is also commonly used for fishing and water sport activities. The sensor measured 31 µg/L P for the site which was compared against the spectrometer which measured 20 µg/L P. In the QC calibration curve presented in Figure 5.38, there is significant variation in the high QC standard and the R^2 value obtained was poor, this could have contributed to the variation in the measurements taken by the sensor compared to that of the spectrometer.

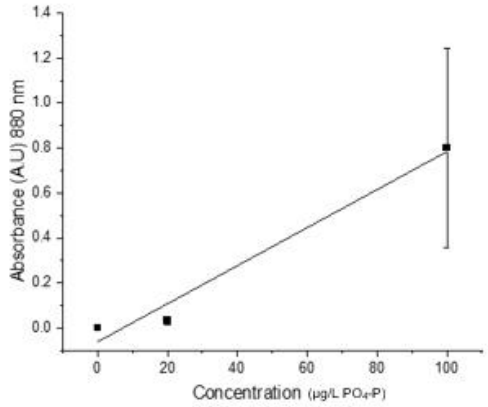

Site	PhosphaLOAD (ug/L)	St. Deviation	Spectrometer (ug/L)	St. Deviation
Ballysadare River	31.26	0.08	20.39	0.00

Figure 5.38 Individual calibration curve generated from the on-disc QC method. A set of standards blank, low and high phosphate standards (0, 20 and 100 ug/L) n=3. Ballysadare River sampling site generated a calibration curve with an R^2 value of 0.9764 and measured 31 ug/L phosphate compared to the spectrometer reference measurement of 20 ug/L.

The water quality parameters and phosphorus analysis measurement for the Ballysadare river are summarised in Table 5.12. This sampling site was the located in the village of Ballysadare therefore was the most urbanised area tested in the Unshin catchment case study. The river was faster flowing at this sampling site than the previous. The conductivity measurement for this site (248.0 µS/cm) is typical of most rivers which range between (200 – 1000 µS/cm) therefore making it suitable for most species of fish and invertebrates [297].

Table 5.12 Supplementary data for the Ballysadare River testing site in the Unshin catchment, obtained from an EXO sonde in-situ measurements (n=10) and phosphorus lab analysis (n=3).

Sampling Site: Ballysadare River			
Parameter	**Measurement**	**St. Dev**	**Units**
Conductivity	248.0	2.4	µS/cm
Turbidity	4.6	2.1	FNU
Salinity	0.2	0.1	psu
ORP	136.7	2.3	mV
Temperature	15.5	0.1	°C
pH	8.1	0.2	
SRP	20.4	7.3	µg/L
TP	35.3	0.0	µg/L
TSP	19.9	1.0	µg/L
TSS	11.9	0.0	mg
TPP	15.4	0.0	µg/L

5.6.7 Site 5: Owenmore River Ballinacarrow

The Owenmore River source is in the south of Sligo, from which it runs for 52.3 km to its where it connects to the Unshin River near Collooney to form the Ballysadare River. The sensor measured 12 µg/L for the site which was compared against the spectrometer which measured 16 µg/L. This site measurement was the closest in agreement to the reference measurements. However, the QC standard calibration curve is poor with significant variation in the higher QC standards (n=3).

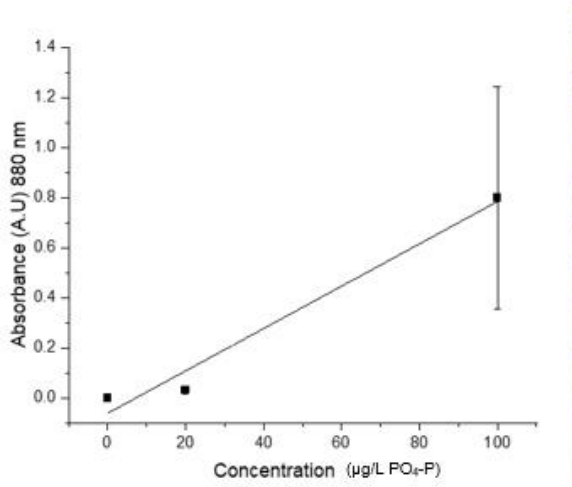

Site	PhosphaLOAD (ug/L)	St. Deviation	Spectrometer (ug/L)	St. Deviation
Owenmore Ballinacarrow	12.37	0.13	15.94	0.00

Figure 5.39 Individual calibration curve generated from the on-disc QC method. A set of standards blank, low and high phosphate standards (0, 20 and 100 ug/L) n=3. Owenmore Ballinacarrow sampling site generated a calibration curve with an R^2 value of 0.9987 and measured 12 ug/L phosphate compared to the spectrometer reference measurement of 16 ug/L.

Figure 5.40 Images of river samples being analysed in the field, showing how the filtered water sample is pipetted into the disc to facilitate sample and reagent mixing and analyte concentration detection.

The sampling site at the Owenmore River Ballinacarrow, was the lowest water level tested during the field trial, the turbidity measured at this site was also one of the lowest turbidity measurements throughout the Unshin catchment case study obtaining a value of 2.8 FNU. The water samples collected at this site were the clearest out of all samples collect which reflects the low turbidity measurements.

Table 5.13 Supplementary data for the Owenmore River Ballinacarrow testing site in the Unshin catchment, obtained from an EXO sonde in-situ measurements (n=10) and phosphorus lab analysis (n=3).

Sampling Site: Owenmore River Ballinacarrow			
Parameter	**Measurement**	**St. Dev**	**Units**
Conductivity	420.8	3.4	µS/cm
Turbidity	2.8	1.1	FNU
Salinity	0.2	0.2	psu
ORP	157.2	3.6	mV
Temperature	17.2	0.2	°C
pH	8.1	0.2	
SRP	15.9	5.5	µg/L
TP	32.5	3.3	µg/L
TSP	16.6	0.2	µg/L
TSS	0.0	0.2	mg
TPP	15.9	0.0	µg/L

5.6.8 Conclusion

The Unshin catchment was studied to demonstrate the performance of the sensor in a catchment where the levels of phosphate fluctuate, and the landscape varies from rural to urban. The levels of phosphate found in this catchment are generally much higher than the Burrishoole catchment therefore increasing the chances of successfully monitoring the levels throughout the catchment. A broad sampling campaign of five sites chosen were distributed out throughout the catchment where EPA data for the sites was available.

The phosphate measurements obtained by the PhosphaLOAD system and the UV/vis spectrometer are on the lower range of the levels of phosphate typically found in the Unshin catchment, levels of phosphate recorded in this area can reach 100 µg/L in certain areas according to a report published by Irish Water in 2021 [297]. The low levels measured during the case study might be due to the unusually long period of dry weather prior to the analysis.

In total 30 samples were measured for phosphate on the PhosphaLOAD system, 75 samples were measured for phosphorus speciation and 300 measurements were obtained by the sonde for general water quality parameters during the field trial for the Burrishoole catchment case study.

The individual QC calibration curves for the five testing sites was generated (see Figure 5.41) the method for generating these graphs is described above. The variation between the measurements for the QC standards is caused by the variation in optical clarity of the optical windows on each of the discs used per site measurement.

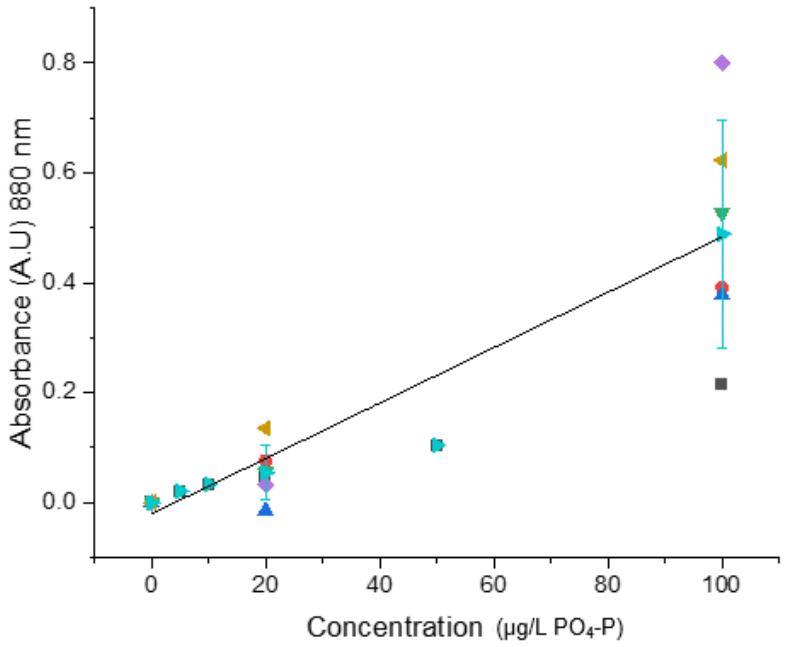

Figure 5.41 Phosphate standard calibration carried out on disc, with plotted QC standards on discs from the field trials, R^2 value 0.996, with good sensitivity and slope of 0.0039, however significant variation between QC standards measured on disc due to optical window variation (shown by large error bars).

The calibration curve for the discs used in the field test with the on-board QC contained phosphate standards with a low concentration of 20 ug/L and a high concentration of 100 ug/L. The graph in Figure 5.41 shows some significant variation between the different QC standards on the different discs used during the case study, again caused by the difference in optical clarity between the discs used for each site measurement. This is highlighted in the Ballysadare River and Owenmore Ballinacarrow sampling sites as the variation between the QC onboard standards is visible for the higher concentration of 100 ug/L, generally the optical clarity affects the lower concentrations more. However, if an optical window on the disc is particularly poor this can cause significant variation in all readings obtained from the system.

5.7 Overall conclusion

The complete datasets from the three case studies are presented in Sections 5.4, 5.5 and 5.6. The three case studies showed close to similar agreement between the data from the PhosphaLOAD sensor and a standard reference method. The catchments tested were selected to investigate the capabilities of the sensing platform. The River Liffey was selected as a high phosphate catchment in an urbanised and industrialised area. The Burrishoole catchment in Newport Co. Mayo, was selected as it is a rural and well-preserved area, where agriculture and cultivation are at a minimum. It is also a highly instrumented and monitored area. The Unshin catchment in Co. Sligo was chosen as a medium phosphate catchment which extends from rural and urban with an abundance of agricultural activity. The PhosphaLOAD sensor performed well in the R. Liffey and the Unshin catchment case studies demonstrating its suitability for water quality monitoring in catchments.

However, the trace levels of phosphate present in the Burrishoole catchment were too low and could not be detected by the phosphate sensor due to its minimum LOD of 16 ug/L in its current configuration. The variation in the readings were mainly due to the clarity of the optical windows on the microfluidic discs. The lower concentrations are heavily impacted by the variation in optical clarity. This limitation can be further investigated to improve the LOD of the device. Different techniques can be used to enhance the optical window clarity such as vapor polishing [298], index matching epoxy glue [299] or flame coating techniques [300] to mitigate the effects of surface roughness on optical window clarity. These techniques can be easily incorporated into the fabrication process. Each of the techniques can be utilized to minimise the effect laser cutting has on the PMMA surface of the optical windows by smoothing the surface preventing the incident light being scattered by surface roughness. Different detection methods could also be investigated such as fluorescence. Measurement of fluorescence can achieve up to 1000 times improvement on LOD [301]. A sequential injection analysis system (SIA) for the simultaneous determination of phosphate and ammonia in rivers and marine environments was reported by *Frank et al.,* phosphate was reacted with acid molybdate to form phosphomolybdate, which formed non-fluorescent ion pairs with rhodamine 6G. The remaining rhodamine was detected by excitation at 470 nm and fluorescence was measured at 550 nm. The detection limit for this method was reported as 0.3 µM phosphate [302], which has a significantly lower LOD than the system presented in this thesis.

The portability and the facilitation of multi-sample measurements per disc allows the device to be translated from lab to field for water quality monitoring, this was demonstrated through the successful field trials in three different catchments. Further optimisation of the device will

improve the limit of detection in order to maximise the potential of the sensor for lower phosphate concentration catchments.

From the demonstration of the PhosphaLOAD sensor and its application in the field there has been a number of successful outcomes and results. Whilst this chapter focuses primarily on the performance of the phosphate sensor in the field, this section is dedicated to the trouble shooting, and lessons learned through transporting this device from lab into the field.

Throughout the three field trials carried out a number of issues from the field application protocol and technical issues from the sensor were reported. The first field trial was carried out on the R. Liffey which a boat was used for sampling. This posed some technical issues for the motor in the sensor. During the field trial the sensor failed to stop spinning during the analysis of a sample, this may have been caused by the rocking of the boat or rainfall interfering with wiring. To counteract this problem, a test run was incorporated into the sample measurement protocol. A test run incorporating a blank disc was carried out before any sample was run on the system. The lid was closed to protect any wires exposed to the elements. Another troubleshooting issue involved the effect incident light on the sensor and potentially interfering with readings, again the lid of the sensor was closed during measurements to ensure ambient light did not interfere with light from the LED being captured by the PD. This problem was not encountered in the lab with fluorescent lighting. It was observed that the evaporation of disc sample in the discs due to disc handling while waiting from sample and reagent to mix can occur. Therefore, the discs needed to be covered from sunlight during the development period. Covering the discs with tissue seemed to draw out the fluid in the introduction chamber. The discs were covered with tinfoil to protect them from the light whilst developing.

Chapter 6: Conclusion and future works

The increase in demand for nutrient sensors that can provide real-time or near real-time measurements in the field for environmental water quality monitoring, will facilitate the move towards successful implementation of sensor networks, wireless communication, open access data banks, and the internet of things to form an integrated observation monitoring framework. This research was funded by the Marine Institute as part of the BEYOND 2020 project, (Burrishoole Ecosystem Observatory Network 2020) which is a multi-institute research cluster which aims to build on the pre-existing biological and sensor monitoring programmes within the Burrishoole catchment in Co. Mayo through next generation science and technology to highlight and monitor the ecosystems response to environmental changes. As outlined at the beginning of this thesis the aim of developing a platform that can monitor phosphate on-site in near real-time is the driving force behind this research. In particular the development of a fully integrated, low-cost, reliable and robust handheld sensor that has the ability to be used continuously in catchments. The development of such a device will facilitate the monitoring of changes in the many water ways that make up a catchment area, the fabrication and validation of the complete sensor is discussed in Chapters 2-5. The cost of developing these types of platforms must be as low as possible to successfully achieve the end goal of using a number of these nutrient sensors to gather as much data as possible from as many catchments as possible. The development of these low-cost handheld devices will aid in the successful implementation of observation monitoring frameworks in catchments as they present solutions to the expensive current *in-situ* sensors on the market and bridge the temporal gap in data collection that satellite sensing is unable to facilitate.

The development of a microfluidic disc for the successful detection of phosphate is discussed in Chapter 2. The use of microfluidics is a critical area of research in the field of low-cost sensing devices, this thesis has presented innovative and novel methods of developing a fully integrated sensor that is centred around centrifugal microfluidics. The disc was designed for automated multisampling field applications. The novel microfluidic approaches investigated and tested allowed for smaller sample and reagent volumes, sample automation therefore, lowering costs further. Using material chemistries such PMMA and PSA to fabricate the microfluidic discs lowered the cost of manufacturing hence, more discs could be fabricated. Different methods of manufacturing these devices were investigated and results showed that outsourcing the disc manufacturing process was the most reproducible method. The novel fluidic design of the discs facilitates six samples to be measured on a single disc, therefore, increasing number of catchment sites can be measured on a single disc and decreasing the number of discs and materials needed for catchment monitoring. Another advantage of developing a multi-sample disc is that a QC control method can also be incorporated into the disc to ensure accurate and reliable results. Issues surrounding the optical clarity of

microfluidic discs can have a serious impact on the sensitivity and LOD of the overall sensor. A number of investigations were carried out in Chapter 2 to minimise the effect the optical clarity can have when obtaining an accurate reading. This work involved comparing manufacturing methods and developing in lab pre-calibration methods to reduce this effect.

It has been established that phosphate can be difficult to monitor in water bodies due to the complex and unstable reaction of the molybdenum blue method for low phosphate detection [52]. Therefore, in Chapter 3, a novel adapted method of this assay was developed for integration into a microfluidic manifold. The study has demonstrated for the first time, the integration of the molybdenum blue method into a low-cost, microfluidic sensing device enabling near real-time detection of phosphate in freshwater environments. The results presented in Chapter 3 display excellent correlation with a UV/vis spectrometer when analysing real world environmental samples. The novel integration of this wet chemistry assay has improved the lifetime of the reagent from 4 h to 7 days, demonstrating the ability of this method to be used in the field. To improve this application of reagent integration further optimisation of this method could be carried out to prolong the lifetime of the reagents. This would improve the stability and shelf-life of the reagent on the discs which would be commercially advantageous. This could be done by use of dosing machines so that the extremely small compounds could be measured out accurately and reproducibly into each reservoir of the disc. This solid compound form would reduce the risk of moisture content interfering with the reaction and causing an undesirable effect recorded in the ascorbic acid. The value of the work presented in this thesis shows promising results for the optimisation of onboard storage of the molybdenum blue assay, enabling the development of fully integrated, self-contained device for onsite phosphate monitoring.

The characterisation and validation of the PhosphaLOAD sensing platform discussed in Chapter 4, demonstrates the performance of the complete analysis platform and microfluidic device with onboard chemical storage for the first time. The complete system was validated in the lab using environmental samples and compared to a UV/vis spectrometer. The PhosphaLOAD system showed excellent agreement with the laboratory standard method.

The PhosphaLOAD system has a component cost of ca. €1002.20 delivering an extremely competitive cost comparison to commercial nutrient sensors currently on the market [102] due to its simplistic design, low reagent consumption, low waste production and acceptable analytical performance. The cost of manufacturing the microfluidic discs is ca. €28.00, with the mass production of discs this cost can be further decreased.

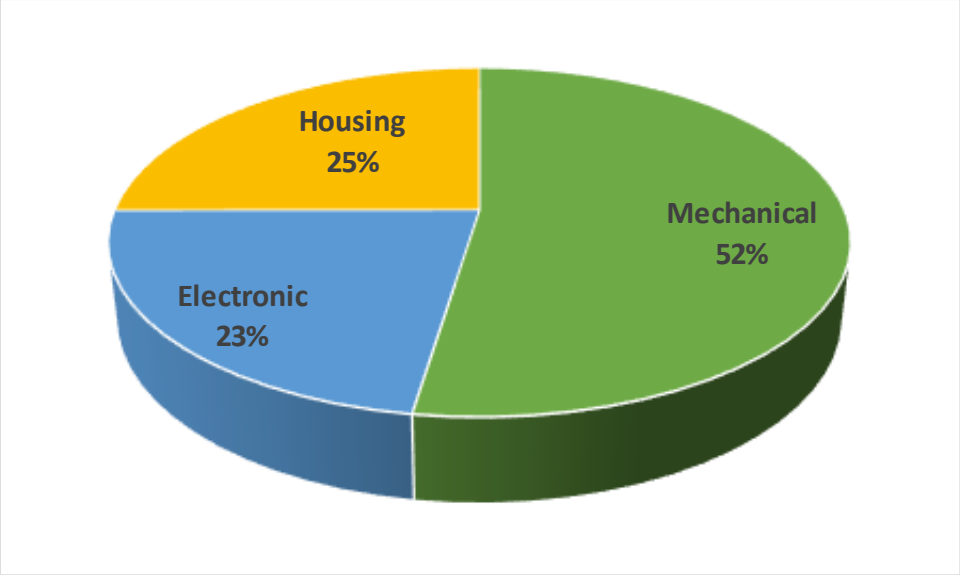

Figure 6.1 Cost breakdown for the phosphate sensing platform components. The component list was divided into three main sections, mechanical (€427.03), electronic (€183.77) and physical housing (€204.00) excluding 23% VAT.

The successful build of a low-cost sensor involved the investigation of different materials and component manufacturing techniques to ensure that the sensor was not only cost competitive but was also highly sensitive and selective. The system developed enabled the detection of phosphate with a concentration of 16 µg/L in freshwater bodies. The mechanical components of the system were the most expensive comprising 52% of the total cost. The motor and actuator were customised components and were outsourced to manufacturing companies therefore, increasing the fabrication costs. The electronics were the cheapest components which made up 23% of the overall development cost. The optical detection method using a LED and PD contributed to this low cost. The overall cost of the platform can be increased with the need to filter the samples which is necessary when measuring extremely low volumes of an analyte. The use of disposable filters and syringes can increase the cost of a sampling campaign. The molybdenum blue method has shown significant advances in inhibiting some interferences (see 2.4.1 Optical enhancements used in sensing devices). However, interferences such as debris needs to be removed before sample analysis.

While shortcomings and obstacles are mainstream in sensor development, it can often take more than a decade to finalise the development of a prototype system and convert it into a commercially available product, however through the work presented in this thesis and all parties involved this has been achieved within a four-year period.

Chapter 5 highlights the benefits of integrating the highly sensitive molybdenum blue method into a microfluidic centrifugal disc. The case studies presented in this thesis demonstrate the different ranges of phosphate that could be measured accurately in different environments. Its

portable, handheld, lightweight, low power consumption, and reagent less design makes this platform attractive to catchment managers, when compared to traditional methods such as ion chromatography [303], flow injection [304] and electrochemical [305] transduction methods. These traditional methods of detection utilize expensive instruments and for the samples to transported back to the lab for analysis increasing the cost and analysis time.

The case studies discussed in Chapter 5 illustrate the robustness and reliability of the PhosphaLOAD system for water quality monitoring in catchments that contain low to high levels of phosphate. The sensor was tested in three different catchments across Ireland. A number of different waterbodies across the catchments were analysed for phosphate during each case study. Translating the device from lab to field was a major milestone and success within this research. These field trials not only demonstrated that the system could be used in the field without any supporting power supply other than the battery within the system, it also highlighted the robustness of the system and stability of the on-board stored reagents. A number of lessons learned, and outcomes were gained from these different case studies which has improved the device and has offered more ideas on how the further optimise the PhosphaLOAD system regarding the issues with the clarity of the optical windows on the disc, which limit the LOD to 16 ug/L.Chapter 5 discusses this issue in the case study field trials carried out using the prototype and how this can heavily impact the collection of data for lower phosphate level catchments.

A key goal for the application of the PhosphaLOAD system is to monitor catchments with low phosphate level. To extend the limit of detection of the PhosphaLOAD system, investigating different techniques that could be used in the manufacturing of microfluidic discs to optimise the clarity of the optical window and make it more reproducible is essential. This could be done by using a vapor polishing technique. This technique is commonly used enhance component features or improve optical clarity on plastic materials such as Acrylic (PMMA), Polycarbonate or Ultem [306].

An investigation into other detection methods could also be explored to overcome the problems and limitations of optical window clarity and detection limit. This may involve the integration of a camera imaging device that would facilitate the capture of phosphate levels in the sample. This could be facilitated by a top-down approach rather than an end coupling of an LED and PD. Using the top-down approach with a camera mitigates the need for a pathlength. As the long pathlength would not be required using this method, it would also facilitate an increase in the number of tests per disc. The thin material used in the top and

bottom layers of PMMA (0.5 mm) would also be an added advantage to exploring this method, as the imaging camera would have a thin layer to image through.

Another aspect to improve on would be the waste generated from the use of microfluidic discs, although the cost and waste produced from reagent and samples is minimised. Only the required amount of reagent is used in each test, the waste from the number microfluidic discs used could be significantly reduced to support the circular economy.

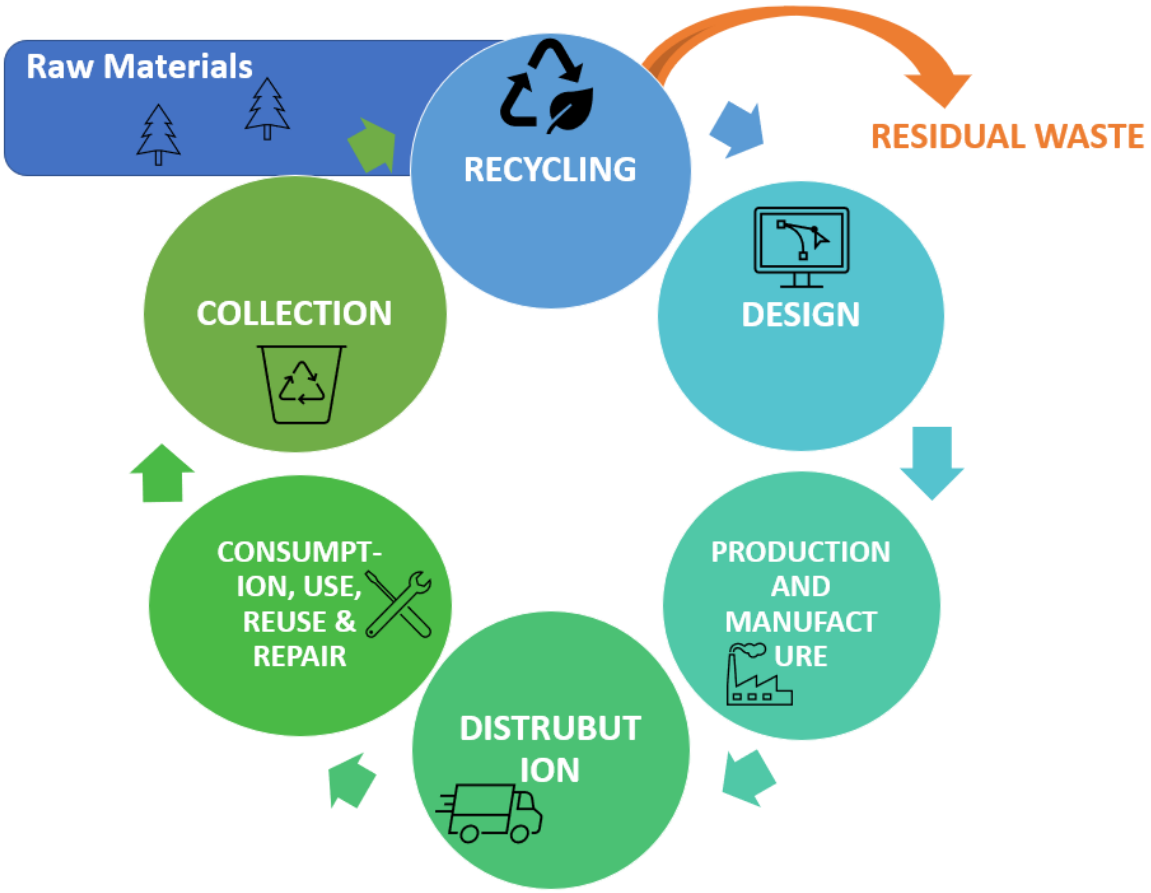

Figure 6.2 Infographic of the circular economy.

Now more than ever the need to reduce and recycle materials is at the forefront of society and this has been extended to research [307]. During this research, methods of reusing the discs during lab scale experiments were carried out where possible. Discs that were solely used to characterise the sensing system were reused to minimise the number of discs and reduce waste during the testing process. This was done by flushing out the fluid from the detection channel using a constant stream of nitrogen gas.

Investigating methods to reuse the discs would significantly reduce the plastic waste generated from the microfluidic discs. Replacing PSA which is used to create microchannels

by using milling or 3D printing combined with different sealing techniques so that the discs can be wiped down after a catchment study and reused a number of times.

This thesis demonstrates the novel and promising work for implementing handheld devices into observation frameworks to complement current monitoring devices employed in these frameworks. This was done by demonstrating the successful application of the PhosphaLOAD system during three individual case studies where the site description and land use varied significantly. This device facilitates the overall monitoring of an entire catchment. The robustness and portability of the device enables the successful monitoring of phosphate throughout the many water bodies that make up a catchment. It is hoped that the work carried out in this thesis and development the PhosphaLOAD prototype can be used to improve the performance and reliability of handheld sensors adding value to sensor research and observation frameworks in the future.

References

[1] K. Fabricius, G. De'ath, L. McCook, E. Turak, and D. M. B. Williams, "Changes in algal, coral and fish assemblages along water quality gradients on the inshore Great Barrier Reef," *Mar. Pollut. Bull.*, vol. 51, no. 1–4, pp. 384–398, 2005.

[2] "Guide to the Water Framework Directive - Catchments.ie - Catchments.ie." [Online]. Available: https://www.catchments.ie/guide-water-framework-directive/. [Accessed: 07-Feb-2019].

[3] D. Daly, M. Archbold, and J. Deakin, "Progress and challenges in managing our catchments effectively," *Biol. Environ.*, vol. 116B, no. 3, pp. 157–166, 2016.

[4] DHPLG, "River Basin Management Plan for Ireland 2018 - 2021 Executive Summary," 2017.

[5] D. V. Chapman *et al.*, "Developments in water quality monitoring and management in large river catchments using the Danube River as an example," *Environ. Sci. Policy*, vol. 64, pp. 141–154, 2016.

[6] J. Jiang, S. Tang, D. Han, G. Fu, D. Solomatine, and Y. Zheng, "A comprehensive review on the design and optimization of surface water quality monitoring networks," *Environ. Model. Softw.*, vol. 132, no. May, p. 104792, 2020.

[7] G. S. Bilotta and R. E. Brazier, "Understanding the influence of suspended solids on water quality and aquatic biota," *Water Res.*, vol. 42, no. 12, pp. 2849–2861, 2008.

[8] P. Amoatey and M. S. Baawain, "Effects of pollution on freshwater aquatic organisms," *Water Environ. Res.*, vol. 91, no. 10, pp. 1272–1287, 2019.

[9] OECD, "Agriculture ' s Impact on Aquaculture : Hypoxia and Eutrophication in," pp. 1–46, 2012.

[10] K. K. Vass, A. Wangeneo, S. Samanta, S. Adhikari, and M. Muralidhar, "Phosphorus dynamics, eutrophication and fisheries in the aquatic ecosystems in India," 2015.

[11] by Teagasc, J. Castle, W. Authors, K. Daly, and P. Mills, "Environmental RTDI Programme 2000-2006 EUTROPHICATION FROM AGRICULTURAL SOURCES-Relating Catchment Characteristics to Phosphorus Concentrations in Irish Rivers (2000-LS-2.2.2) Final Report Prepared for the Environmental Protection Agency," 2006.

[12] D. E. Walling, A. L. Collins, and R. W. Stroud, "Tracing suspended sediment and particulate phosphorus sources in catchments," *J. Hydrol.*, vol. 350, no. 3–4, pp. 274–289, Feb. 2008.

[13] EPA, "Water quality in 2020, an indicators report," 2021.

[14] C. Alewell, B. Ringeval, C. Ballabio, D. A. Robinson, P. Panagos, and P. Borrelli, "Global phosphorus shortage will be aggravated by soil erosion," *Nat. Commun.*, vol. 11, no. 1, 2020.

[15] I. Chaubey, K. W. Migliaccio, C. H. Green, J. G. Arnold, and R. Srinivasan, "Phosphorus modeling in soil and water assessment tool (SWAT) model," *Model. Phosphorus Environ.*, no. November 2014, pp. 163–187, 2006.

[16] K. R. Ready, R. H. Kadlec, E. Flaig, and P. M. Gale, "Phosphorus retention in streams and wetlands: A review," *Crit. Rev. Environ. Sci. Technol.*, vol. 29, no. 1, pp. 83–146, 1999.

[17] E. T. Alori, B. R. Glick, and O. O. Babalola, "Microbial phosphorus solubilization and its potential for use in sustainable agriculture," *Front. Microbiol.*, vol. 8, no. JUN, pp. 1–8, 2017.

[18] C. J. Penn and J. J. Camberato, "A critical review on soil chemical processes that control how soil ph affects phosphorus availability to plants," *Agric.*, vol. 9, no. 6, pp. 1–18, 2019.

[19] D. Menezes-Blackburn *et al.*, "Opportunities for mobilizing recalcitrant phosphorus from agricultural soils: a review," *Plant Soil*, vol. 427, no. 1–2, pp. 5–16, 2018.

[20] S. Sato and N. B. Comerford, "Influence of soil pH on inorganic phosphorus sorption and desorption in a humid Brazilian Ultisol," *Rev. Bras. Cienc. do Solo*, vol. 29, no. 5, pp. 685–694, 2005.

[21] T. YEAGER and J. BARRETT, "Phosphorus leaching from," *Hortscience*, vol. 19, no. 2, pp. 216–217, 1984.

[22] A. Sharpley, H. P. Jarvie, A. Buda, L. May, B. Spears, and P. Kleinman, "Phosphorus Legacy: Overcoming the Effects of Past Management Practices to Mitigate Future Water Quality Impairment," *J. Environ. Qual.*, vol. 42, no. 5, pp. 1308–1326, 2013.

[23] K. A. Macintosh *et al.*, "Transforming phosphorus use on the island of Ireland: A model for a sustainable system," *Sci. Total Environ.*, vol. 656, pp. 852–861, 2019.

[24] J. FROEBRICH, "New Challenges in Lake and River Monitoring," *Freshw. Forum*, vol. 23, no. 1999, pp. 155–165, 2005.

[25] E. M. Mockler, J. Deakin, M. Archbold, L. Gill, D. Daly, and M. Bruen, "Sources of nitrogen and phosphorus emissions to Irish rivers and coastal waters: Estimates from a nutrient load apportionment framework," *Sci. Total Environ.*, vol. 601–602, pp. 326–339, 2017.

[26] S. O'Boyle, R. Quinn, N. Dunne, E. M. Mockler, and S. Ní Longphuirt, "What have we learned from over two decades of monitoring riverine nutrient inputs to Ireland's marine environment?," *Biol. Environ.*, vol. 116B, no. 3, 2016.

[27] E. Murray, "Towards deployable analytical systems for nutrient monitoring in natural waters," no. January, 2020.

[28] B. Y. A. Spivakov, T. A. Maryutina, and H. Muntau, "Phosphorus speciation in water and sediments (Technical Report)," *Pure Appl. Chem.*, vol. 71, no. 11, pp. 2161–2176, 1999.

[29] J. V Paraskova, *Organic phosphorus speciation in environmental samples*. 2014.

[30] S. Plant, N. J. Ii, M. D. R. O. N. Vaz, A. C. Edwards, C. A. Shand, and M. S. Cresser, "Phosphorus fractions in soil solution : Influence of soil acidity and fertiliser additions Author (s): M . D . RON VAZ , A . C . EDWARDS , C . A . SHAND and M . S . CRESSER Published by : Springer Stable URL : http://www.jstor.org/stable/42938785 Phosph," vol. 148, no. 2, pp. 175–183, 2016.

[31] C. S. REYNOLDS and P. S. DAVIES, "Sources and bioavailability of phosphorus fractions in freshwaters: a British perspective," *Biol. Rev. Camb. Philos. Soc.*, vol. 76, no. 1, p. S1464793100005625, Feb. 2001.

[32] B. Y. Spivakov, T. A. Maryutina, and H. Muntau, "Phosphorus Speciation in Water and Sediments," *Pure Appl. Chem.*, vol. 71, no. 11, pp. 2161–2176, 1999.

[33] S. Daneshgar, A. Callegari, A. G. Capodaglio, and D. Vaccari, "The potential phosphorus crisis: Resource conservation and possible escape technologies: A review," *Resources*, vol. 7, no. 2, 2018.

[34] B. Dabkowski and M. White, "Understanding the Different Phosphorus Tests," *Hach*, pp. 1–4, 2015.

[35] A. D. Tappin, S. Comber, and P. J. Worsfold, "Orthophosphate-P in the nutrient impacted River Taw and its catchment (SW England) between 1990 and 2013," *Environ. Sci. Process.*

Impacts, vol. 18, no. 6, pp. 690–705, 2016.

[36] H. H. Huang, "The Eh-pH diagram and its advances," *Metals (Basel).*, vol. 6, no. 1, 2016.

[37] R. Kent, T. D. Johnson, and M. R. Rosen, "Status and trends of orthophosphate concentrations in groundwater used for public supply in California," *Environ. Monit. Assess.*, vol. 192, no. 8, 2020.

[38] J. Reijenga, A. van Hoof, A. van Loon, and B. Teunissen, "Development of methods for the determination of pKa values," *Anal. Chem. Insights*, vol. 8, no. 1, pp. 53–71, 2013.

[39] K. Y. Koh, S. Zhang, and J. P. Chen, "Improvement of Ultrafiltration for Treatment of Phosphorus-Containing Water by a Lanthanum-Modified Aminated Polyacrylonitrile Membrane," *ACS Omega*, vol. 5, no. 13, pp. 7170–7181, 2020.

[40] EPA, "United States Environmental Protection Agency. Quality Criteria for Water. Office of Water Planning and Standards," *U S Environ. Prot. Agency*, 1976.

[41] D. Tierney and S. O'Boyle, *Water Quality in 2016: An indicators report*. 2018.

[42] C. Warwick, A. Guerreiro, and A. Soares, "Sensing and analysis of soluble phosphates in environmental samples: A review," *Biosens. Bioelectron.*, vol. 41, no. 1, pp. 1–11, 2013.

[43] C. Li *et al.*, "An integrated optofluidic platform enabling total phosphorus on-chip digestion and online real-time detection," *Micromachines*, vol. 11, no. 1, pp. 1–12, 2020.

[44] S. Andreescu and O. A. Sadik, "Trends and challenges in biochemical sensors for clinical and environmental monitoring," *Pure Appl. Chem.*, vol. 76, no. 4, pp. 861–878, 2004.

[45] L. Liu, X. Zhou, J. S. Wilkinson, P. Hua, B. Song, and H. Shi, "Integrated optical waveguide-based fluorescent immunosensor for fast and sensitive detection of microcystin-LR in lakes: Optimization and Analysis," *Sci. Rep.*, vol. 7, no. 1, pp. 1–9, 2017.

[46] P. Yeh, N. Yeh, C. H. Lee, and T. J. Ding, "Applications of LEDs in optical sensors and chemical sensing device for detection of biochemicals, heavy metals, and environmental nutrients," *Renew. Sustain. Energy Rev.*, vol. 75, no. November 2016, pp. 461–468, 2017.

[47] M. M. Grand *et al.*, "A lab-on-chip phosphate analyzer for long-term In Situ monitoring at fixed observatories: Optimization and performance evaluation in estuarine and oligotrophic coastal waters," *Front. Mar. Sci.*, vol. 4, no. AUG, pp. 1–16, 2017.

[48] M. S. A. C. Neves, M. R. S. Souto, I. V. Tóth, S. M. A. Victal, M. C. Drumond, and A. O. S. S. Rangel, "Spectrophotometric flow system using vanadomolybdophosphate detection chemistry and a liquid waveguide capillary cell for the determination of phosphate with improved sensitivity in surface and ground water samples," *Talanta*, vol. 77, no. 2, pp. 527–532, 2008.

[49] R. Gaikwad, D. Kumbhar, and C. Ganeshkhind, "Development of Portable Optical Sensor Based System for Detection of Phosphate in Wastewater Development of Portable Optical Sensor Based System for Detection of Phosphate in Waste ... Development of Portable Optical Sensor Based System for Detection of P," no. March, 2018.

[50] S. R. Crouch and H. V. Malmstadt, "A Mechanistic Investigation of Molybdenum Blue Method for Determination of Phosphate," *Anal. Chem.*, vol. 39, no. 10, pp. 1084–1089, 1967.

[51] C. X. Galhardo and J. C. Masini, "Spectrophotometric determination of phosphate and silicate by sequential injection using molybdenum blue chemistry," *Anal. Chim. Acta*, vol. 417, no. 2,

pp. 191–200, 2000.

[52] E. A. Nagul, I. D. McKelvie, P. Worsfold, and S. D. Kolev, "The molybdenum blue reaction for the determination of orthophosphate revisited: Opening the black box," *Anal. Chim. Acta*, vol. 890, pp. 60–82, 2015.

[53] D. S. Baldwin, "Reactive 'organic' phosphorus revisited," *Water Res.*, vol. 32, no. 8, pp. 2265–2270, 1998.

[54] G. S. Clinton-Bailey *et al.*, "A Lab-on-Chip Analyzer for in Situ Measurement of Soluble Reactive Phosphate: Improved Phosphate Blue Assay and Application to Fluvial Monitoring," *Environ. Sci. Technol.*, vol. 51, no. 17, pp. 9989–9995, 2017.

[55] and W. E. F. American Public Health Association, American Water Works Association, "Standard Methods for the Examination of Water and Wastewater," *Am. Public Heal. Assoc.*, no. 20th ed, 1998.

[56] M. Eichhorn *et al.*, "Modular AUV system with integrated real-time water quality analysis," *Sensors (Switzerland)*, vol. 18, no. 6, pp. 1–17, 2018.

[57] K. S. Adu-Manu, C. Tapparello, W. Heinzelman, F. A. Katsriku, and J.-D. Abdulai, "Water Quality Monitoring Using Wireless Sensor Networks," *ACM Trans. Sens. Networks*, vol. 13, no. 1, pp. 1–41, 2017.

[58] M. O'Neill and H. Kerr, "Wastewater sampling procedures," pp. 1–17, 2013.

[59] J. Tuominen, T. Lipping, and P. Oy, "Detection of Environmental Change Using Hyperspectral Remote Sensing at Olkiluoto Repository Site," p. 56, 2011.

[60] W. Turner, S. Spector, N. Gardiner, M. Fladeland, E. Sterling, and M. Steininger, "Remote sensing for biodiversity science and conservation," vol. 18, no. 6, pp. 306–314, 2003.

[61] A. B. Bugnot *et al.*, "A novel framework for the use of remote sensing for monitoring catchments at continental scales," *J. Environ. Manage.*, vol. 217, pp. 939–950, 2018.

[62] J. O'Grady, D. Zhang, N. O'Connor, and F. Regan, "A comprehensive review of catchment water quality monitoring using a tiered framework of integrated sensing technologies," *Sci. Total Environ.*, vol. 765, p. 142766, 2021.

[63] L. Malic and A. G. Kirk, "Integrated miniaturized optical detection platform for fluorescence and absorption spectroscopy," *Sensors Actuators, A Phys.*, vol. 135, no. 2, pp. 515–524, 2007.

[64] G. Liu, J. Wei, B. A. Muthu, and R. D. Jackson Samuel, "Chlorophyll-a concentration in the hailing bay using remote sensing assisted sparse statistical modelling," *Eur. J. Remote Sens.*, vol. 54, no. sup2, pp. 284–295, 2021.

[65] Ş. M. Kaymaz and E. Ates, "Reviews and research estimating chlorophyll-a concentration using remote sensing techniques," *Ann. Rev. Res.*, vol. 4, no. 2, pp. 9–11, 2018.

[66] S. J. McGrane, M. G. Hutchins, J. D. Miller, G. Bussi, T. R. Kjeldsen, and M. Loewenthal, "During a winter of storms in a small UK catchment, hydrology and water quality responses follow a clear rural-urban gradient," *J. Hydrol.*, vol. 545, pp. 463–477, 2017.

[67] M. Stutter *et al.*, "Evaluating the use of in-situ turbidity measurements to quantify fluvial sediment and phosphorus concentrations and fluxes in agricultural streams," *Sci. Total Environ.*, vol. 607–608, pp. 391–402, 2017.

[68] C. E. M. Lloyd, J. E. Freer, P. J. Johnes, and A. L. Collins, "Using hysteresis analysis of high-

resolution water quality monitoring data, including uncertainty, to infer controls on nutrient and sediment transfer in catchments," *Sci. Total Environ.*, vol. 543, pp. 388–404, 2016.

[69] P. J. Blaen *et al.*, "High-frequency monitoring of catchment nutrient exports reveals highly variable storm event responses and dynamic source zone activation," *J. Geophys. Res. Biogeosciences*, vol. 122, no. 9, pp. 2265–2281, 2017.

[70] A. M. Meyer, C. Klein, E. Fünfrocken, R. Kautenburger, and H. P. Beck, "Real-time monitoring of water quality to identify pollution pathways in small and middle scale rivers," *Sci. Total Environ.*, vol. 651, pp. 2323–2333, 2019.

[71] Á. G. Mayor, S. Bautista, and J. Bellot, "Scale-dependent variation in runoff and sediment yield in a semiarid Mediterranean catchment," *J. Hydrol.*, vol. 397, no. 1–2, pp. 128–135, 2011.

[72] A. Villa, J. Fölster, and K. Kyllmar, "Determining suspended solids and total phosphorus from turbidity: comparison of high-frequency sampling with conventional monitoring methods," *Environ. Monit. Assess.*, vol. 191, no. 10, 2019.

[73] M. Shore, P. Jordan, A. R. Melland, P. E. Mellander, N. McDonald, and G. Shortle, "Incidental nutrient transfers: Assessing critical times in agricultural catchments using high-resolution data," *Sci. Total Environ.*, vol. 553, pp. 404–415, 2016.

[74] J. Linjama, M. Puustinen, J. Koskiaho, T. Sirkka, H. Kotilainen, and K. Granlund, "Implementation of automatic sensors for continuous monitoring of runoff quantity and quality in small catchments," *Agric. Food Sci.*, vol. 18, no. 3–4, pp. 417–427, 2009.

[75] R. W. Douglas, W. Menary, and P. Jordan, "Phosphorus and sediment transfers in a grassland river catchment," *Nutr. Cycl. Agroecosystems*, vol. 77, no. 3, pp. 199–212, 2007.

[76] R. M. Monaghan, R. J. Wilcock, L. C. Smith, B. Tikkisetty, B. S. Thorrold, and D. Costall, "Linkages between land management activities and water quality in an intensively farmed catchment in southern New Zealand," *Agric. Ecosyst. Environ.*, vol. 118, no. 1–4, pp. 211–222, 2007.

[77] M. Masocha, A. Murwira, C. H. D. Magadza, R. Hirji, and T. Dube, "Remote sensing of surface water quality in relation to catchment condition in Zimbabwe," *Phys. Chem. Earth*, vol. 100, pp. 13–18, 2017.

[78] D. Pullanikkatil, L. G. Palamuleni, and T. M. Ruhiiga, "Land use/land cover change and implications for ecosystems services in the Likangala River Catchment, Malawi," *Phys. Chem. Earth*, vol. 93, pp. 96–103, 2016.

[79] M. Waseem, F. Kachholz, W. Klehr, and J. Tränckner, "Suitability of a coupled hydrologic and hydraulic model to simulate surfacewater and groundwater hydrology in a typical north-eastern germany lowland catchment," *Appl. Sci.*, vol. 10, no. 4, 2020.

[80] G. Mouri, S. Takizawa, and T. Oki, "Spatial and temporal variation in nutrient parameters in stream water in a rural-urban catchment, Shikoku, Japan: Effects of land cover and human impact," *J. Environ. Manage.*, vol. 92, no. 7, pp. 1837–1848, 2011.

[81] Q. D. Lam, B. Schmalz, and N. Fohrer, "Assessing the spatial and temporal variations of water quality in lowland areas, Northern Germany," *J. Hydrol.*, vol. 438–439, pp. 137–147, 2012.

[82] S. Mollaee, "Estimation of phytoplankton chlorophyll-a concentration in the western basin of Lake Erie using Sentinel-2 and Sentinel-3 data," p. 80, 2018.

[83] J. Park, K. T. Kim, and W. H. Lee, "Recent advances in information and communications technology (ICT) and sensor technology for monitoring water quality," *Water (Switzerland)*, vol. 12, no. 2, 2020.

[84] P. S. Roy, • M D Behera, and • S K Srivastav, "Satellite Remote Sensing: Sensors, Applications and Techniques," *Proc. Natl. Acad. Sci. India Sect. A Phys. Sci.*, vol. 87, 2017.

[85] X. Liu *et al.*, "Remote sensing of secchi depth in highly turbid lake waters and its application with MERIS data," *Remote Sens.*, vol. 11, no. 19, 2019.

[86] M. A. Gagnon, P. Tremblay, S. Savary, V. Farley, P. Lagueux, and M. Chamberland, "Airborne thermal hyperspectral imaging of urban and rural areas," *Int. Geosci. Remote Sens. Symp.*, pp. 1369–1372, 2014.

[87] H. Guo *et al.*, "A generalized machine learning approach for dissolved oxygen estimation at multiple spatiotemporal scales using remote sensing," *Environ. Pollut.*, vol. 288, no. March, p. 117734, 2021.

[88] S. N. Kane, A. Mishra, and A. K. Dutta, "Preface: International Conference on Recent Trends in Physics (ICRTP 2016)," *J. Phys. Conf. Ser.*, vol. 755, no. 1, pp. 2–10, 2016.

[89] R. Katlane, C. Dupouy, B. El Kilani, and J. C. Berges, "Estimation of Chlorophyll and Turbidity Using Sentinel 2A and EO1 Data in Kneiss Archipelago Gulf of Gabes, Tunisia," *Int. J. Geosci.*, vol. 11, no. 10, pp. 708–728, 2020.

[90] K. Osinska-Skotak, M. Kruk, and M. Mroz, "Possibilities of lake water quality monitoring based on CHRIS/PROBA superspectral data," *Glob. Dev. Environ. Earth Obs. from Sp.*, no. January, pp. 259–266, 2006.

[91] E. T. Slonecker, D. K. Jones, and B. A. Pellerin, "The new Landsat 8 potential for remote sensing of colored dissolved organic matter (CDOM)," *Mar. Pollut. Bull.*, vol. 107, no. 2, pp. 518–527, 2016.

[92] K. Kallio, S. Koponen, and J. Pulliainen, "Feasibility of airborne imaging spectrometry for lake monitoring - A case study of spatial chlorophyll a distribution in two meso-eutrophic lakes," *Int. J. Remote Sens.*, vol. 24, no. 19, pp. 3771–3790, 2003.

[93] M. A. Goodberlet, C. T. Swift, K. P. Kiley, J. L. Miller, and J. B. Zaitzeff, "Microwave remote sensing of coastal zone salinity," *J. Coast. Res.*, vol. 13, no. 2, pp. 363–372, 1997.

[94] K. Ngwenya and T. Marambanyika, "Trends in use of remotely sensed data in wetlands assessment and monitoring in Zimbabwe," *Afr. J. Ecol.*, vol. 59, no. 3, pp. 676–686, 2021.

[95] R. Muchini, W. Gumindoga, S. Togarepi, T. P. Masarira, and T. Dube, "Near real time water quality monitoring of Chivero and Manyame lakes of Zimbabwe," *Proc. Int. Assoc. Hydrol. Sci.*, vol. 378, pp. 85–92, 2018.

[96] M. A. P. Mahmud *et al.*, "Recent progress in sensing nitrate, nitrite, phosphate, and ammonium in aquatic environment," *Chemosphere*, vol. 259, p. 127492, 2020.

[97] M. Sequeira, D. Diamond, A. Daridon, J. Lichtenberg, S. Verpoorte, and N. F. De Rooij, "Progress in the realisation of an autonomous environmental monitoring device for ammonia," *TrAC - Trends Anal. Chem.*, vol. 21, no. 12, pp. 816–827, 2002.

[98] P. Duffy, G. Woods, J. Walsh, and M. Kane, "Online real-time water quality monitoring and control system," vol. 2, pp. 318–323, 2010.

[99] D. Cogan *et al.*, "Development of a low cost microfluidic sensor for the direct determination of nitrate using chromotropic acid in natural waters," *Anal. Methods*, vol. 7, no. 13, pp. 5396–5405, 2015.

[100] S. A. Bagloee, M. Tavana, M. Asadi, and T. Oliver, "Autonomous vehicles: challenges, opportunities, and future implications for transportation policies," *J. Mod. Transp.*, vol. 24, no. 4, pp. 284–303, 2016.

[101] A. Daniel *et al.*, "Toward a Harmonization for Using in situ Nutrient Sensors in the Marine Environment," *Front. Mar. Sci.*, vol. 6, no. January, pp. 1–22, 2020.

[102] D. Cogan and D. Diamond, "The Development of Low Cost Autonomous Chemical Sensors for Environmental Monitoring," 2015.

[103] L. Snyder, J. D. Potter, and W. H. McDowell, "An Evaluation of Nitrate, fDOM, and Turbidity Sensors in New Hampshire Streams," *Water Resour. Res.*, vol. 54, no. 3, pp. 2466–2479, 2018.

[104] R. W. Douglas, W. Menary, and P. Jordan, "Phosphorus and sediment transfers in a grassland river catchment," *Nutr. Cycl. Agroecosystems*, vol. 77, no. 3, pp. 199–212, Feb. 2007.

[105] L. Delauney, C. Compare, and M. Lehaitre, "Biofouling protection for marine environmental sensors," *Ocean Sci.*, vol. 6, no. 2, pp. 503–511, 2010.

[106] M. H. Gholizadeh, A. M. Melesse, and L. Reddi, "A comprehensive review on water quality parameters estimation using remote sensing techniques," *Sensors (Switzerland)*, vol. 16, no. 8, 2016.

[107] M. A. Gomarasca *et al.*, "Sentinel for applications in agriculture," *Int. Arch. Photogramm. Remote Sens. Spat. Inf. Sci. - ISPRS Arch.*, vol. 42, no. 3/W6, pp. 91–98, 2019.

[108] A. Monteiro, S. Santos, and P. Gonçalves, "Precision agriculture for crop and livestock farming—Brief review," *Animals*, vol. 11, no. 8, pp. 1–18, 2021.

[109] D. Lu, M. Batistella, E. Moran, and E. E. De Miranda, "A comparative study of landsat TM and SPOT HRG images for vegetation classification in the Brazilian Amazon," *Photogramm. Eng. Remote Sensing*, vol. 74, no. 3, pp. 311–321, 2008.

[110] C. S. Arvind, A. Vanjare, S. N. Omkar, J. Senthilnath, V. Mani, and P. G. Diwakar, "Flood Assessment using Multi-temporal Modis Satellite Images," *Procedia Comput. Sci.*, vol. 89, pp. 575–586, 2016.

[111] F. Shen and W. Verhoef, "Suppression of local haze variations in MERIS images over turbid coastal waters for retrieval of suspended sediment concentration," *Opt. Express*, vol. 18, no. 12, p. 12653, 2010.

[112] C. R. Anderson *et al.*, "Scaling Up From Regional Case Studies to a Global Harmful Algal Bloom Observing System," *Front. Mar. Sci.*, vol. 6, no. May, 2019.

[113] L. Gómez-Chova, G. Camps-Valls, J. Calpe-Maravilla, L. Guanter, and J. Moreno, "Cloud-screening algorithm for ENVISAT/MERIS multispectral images," *IEEE Trans. Geosci. Remote Sens.*, vol. 45, no. 12, pp. 4105–4118, 2007.

[114] M. V. Japitana, A. T. Demetillo, M. E. C. Burce, and E. B. Taboada, "Catchment characterization to support water monitoring and management decisions using remote sensing," *Sustain. Environ. Res.*, vol. 29, no. 1, pp. 1–10, 2019.

[115] K. Wang, S. E. Franklin, X. Guo, Y. He, and G. J. McDermid, "Problems in remote sensing of

landscapes and habitats," *Prog. Phys. Geogr.*, vol. 33, no. 6, pp. 747–768, 2009.

[116] A. Vander Woude, S. Ruberg, T. Johengen, R. Miller, and D. Stuart, "Spatial and temporal scales of variability of cyanobacteria harmful algal blooms from NOAA GLERL airborne hyperspectral imagery," *J. Great Lakes Res.*, vol. 45, no. 3, pp. 536–546, 2019.

[117] H. Zheng *et al.*, "Evaluation of RGB, color-infrared and multispectral images acquired from unmanned aerial systems for the estimation of nitrogen accumulation in rice," *Remote Sens.*, vol. 10, no. 6, 2018.

[118] A. Concha and J. Civera, "RGBDTAM : A Cost-Effective and Accurate RGB-D Tracking and," no. March, 2017.

[119] V. Lawley, M. Lewis, K. Clarke, and B. Ostendorf, "Site-based and remote sensing methods for monitoring indicators of vegetation condition : An Australian review," vol. 60, pp. 1273–1283, 2016.

[120] P. D. Wass, S. D. Marks, J. W. Finch, G. J. L. Leeks, and J. K. Ingram, "Monitoring and preliminary interpretation of in-river turbidity and remote sensed imagery for suspended sediment transport studies in the Humber catchment," *Sci. Total Environ.*, vol. 194–195, no. 96, pp. 263–283, 1997.

[121] Y. He, D. B. Wang, and Z. A. Ali, "A review of different designs and control models of remotely operated underwater vehicle," vol. 53, pp. 1561–1570, 2020.

[122] Y. Li, R. Liu, and S. Liu, "The Design of an Autonomous Underwater Vehicle for Water Quality Monitoring," *IOP Conf. Ser. Mater. Sci. Eng.*, vol. 301, no. 1, 2018.

[123] D. H. Song Bao wei, "Design and Prototype Development of a 1-DOF Flapping-foil & Gliding UUV," *J. Mar. Sci. Res. Dev.*, vol. s10, pp. 1–6, 2015.

[124] SMRU, "LITERATURE REVIEW : UNDERSTANDING THE CURRENT STATE OF AUTONOMOUS TECHNOLOGIES TO IMPROVE / EXPAND OBSERVATION AND Title : Autonomous Technology," 2016.

[125] B. Anderson and J. Crowell, "Workhorse AUV – A cost-sensible new Autonomous Underwater Vehicle (IVER2).pdf," pp. 1–6.

[126] K. Alam, T. Ray, and S. G. Anavatti, "Design and construction of an autonomous underwater vehicle," *Neurocomputing*, vol. 142, pp. 16–29, 2014.

[127] E. O'Connor, A. F. Smeaton, N. E. O'Connor, and F. Regan, "A neural network approach to smarter sensor networks for water quality monitoring," *Sensors*, vol. 12, no. 4, pp. 4605–4632, 2012.

[128] R. C. Ward, J. C. Loftis, and G. B. McBride, "The 'data-rich but information-poor' syndrome in water quality monitoring," *Environ. Manage.*, vol. 10, no. 3, pp. 291–297, 1986.

[129] O. Naughton, P. M. Johnston, T. McCormack, and L. W. Gill, "Groundwater flood risk mapping and management: examples from a lowland karst catchment in Ireland," *J. Flood Risk Manag.*, vol. 10, no. 1, pp. 53–64, 2017.

[130] D. Zhang, B. Eng, S. Prof, N. E. O. Connor, and P. F. Regan, "MULTI-MODAL SMART SENSING NETWORK FOR School of Electronic Engineering," 2015.

[131] D. Zhang, B. Heery, M. O'Neil, S. Little, N. E. O'Connor, and F. Regan, "A low-cost smart sensor network for catchment monitoring," *Sensors (Switzerland)*, vol. 19, no. 10, pp. 1–22, 2019.

[132] H. Zia, N. R. Harris, G. V. Merrett, M. Rivers, and N. Coles, "The impact of agricultural activities on water quality: A case for collaborative catchment-scale management using integrated wireless sensor networks," *Comput. Electron. Agric.*, vol. 96, pp. 126–138, 2013.

[133] M. T. Lazarescu, "Design of a WSN platform for long-term environmental monitoring for IoT applications," *IEEE J. Emerg. Sel. Top. Circuits Syst.*, vol. 3, no. 1, pp. 45–54, 2013.

[134] F. Regan, A. Lawler, and A. McCarthy, *SmartCoast Project - Smart Water Quality Monitoring System*, no. 30. 2009.

[135] M. B. Stuart, A. J. S. McGonigle, and J. R. Willmott, "Hyperspectral imaging in environmental monitoring: A review of recent developments and technological advances in compact field deployable systems," *Sensors (Switzerland)*, vol. 19, no. 14, 2019.

[136] B. P. Wong and B. Kerkez, "Real-time environmental sensor data: An application to water quality using web services," *Environ. Model. Softw.*, vol. 84, pp. 505–517, 2016.

[137] P. J. Blaen, K. Khamis, C. E. M. Lloyd, C. Bradley, D. Hannah, and S. Krause, "Real-time monitoring of nutrients and dissolved organic matter in rivers: Capturing event dynamics, technological opportunities and future directions," *Sci. Total Environ.*, vol. 569–570, pp. 647–660, 2016.

[138] N. Convery and N. Gadegaard, "Micro and Nano Engineering 30 years of micro fl uidics," vol. 2, no. January, pp. 76–91, 2019.

[139] C. Delattre *et al.*, "Macro to microfluidics system for biological environmental monitoring," *Biosens. Bioelectron.*, vol. 36, no. 1, pp. 230–235, 2012.

[140] I. Maguire, R. O'Kennedy, J. Ducrée, and F. Regan, "A review of centrifugal microfluidics in environmental monitoring," *Anal. Methods*, vol. 10, no. 13, pp. 1497–1515, 2018.

[141] L. Marle and G. M. Greenway, "Microfluidic devices for environmental monitoring," *TrAC - Trends Anal. Chem.*, vol. 24, no. 9, pp. 795–802, 2005.

[142] J. C. Jokerst, J. M. Emory, and C. S. Henry, "Advances in microfluidics for environmental analysis," *Analyst*, vol. 137, no. 1, pp. 24–34, 2012.

[143] T. M. G. Cardoso, P. T. Garcia, and W. K. T. Coltro, "Colorimetric determination of nitrite in clinical, food and environmental samples using microfluidic devices stamped in paper platforms," *Anal. Methods*, vol. 7, no. 17, pp. 7311–7317, 2015.

[144] F. Geißler *et al.*, "Lab-on-chip analyser for the in situ determination of dissolved manganese in seawater," *Sci. Rep.*, vol. 11, no. 1, pp. 1–13, 2021.

[145] J. Zhang, S. Liu, P. Yang, and G. Sui, "Rapid detection of algal toxins by microfluidic immunoassay," *Lab Chip*, vol. 11, no. 20, pp. 3516–3522, 2011.

[146] S. Sharma, J. Zapatero-Rodríguez, P. Estrela, and R. O'Kennedy, "Point-of-Care diagnostics in low resource settings: Present status and future role of microfluidics," *Biosensors*, vol. 5, no. 3, pp. 577–601, 2015.

[147] A. Lab-restricted, "Microfluidics : Microfluidics :," 2016.

[148] M. Device, "Microfluidic Technology Lab-on-a-chip techniques for high-throughput proteomics and drug discovery," 2019.

[149] H. E. Beck, A. I. J. M. Van Dijk, A. De Roo, E. Dutra, G. Fink, and R. Orth, "Letter TT Maybank (1).pdf," pp. 2881–2903, 2017.

[150] A. E. Kamholz and P. Yager, "Theoretical analysis of molecular diffusion in pressure-driven laminar flow in microfluidic channels," *Biophys. J.*, vol. 80, no. 1, pp. 155–160, 2001.

[151] K. Tedd *et al.*, *Assessing and Developing Natural Background Levels for Chemical Parameters in Irish Groundwater Identifying Pressures Developing Solutions*, no. 183. 2017.

[152] M. Nagasaka, H. Yuzawa, N. Takada, M. Aoyama, E. Rühl, and N. Kosugi, "Laminar flow in microfluidics investigated by spatially-resolved soft X-ray absorption and infrared spectroscopy," *J. Chem. Phys.*, vol. 151, no. 11, 2019.

[153] J. Novotný and F. Foret, "Fluid manipulation on the micro-scale: Basics of fluid behavior in microfluidics," *J. Sep. Sci.*, vol. 40, no. 1, pp. 383–394, 2017.

[154] D. A. McQuarrie, "Howard University General Chemistry: Atoms First Approach," vol. 53, no. 9, pp. 1689–1699, 2013.

[155] S. Vowell, "Microfluidics: the effects of surface tension," *2009-03-19)[2010-09-21], Http//Www, Phys. …*, pp. 1–10, 2009.

[156] O. Strohmeier *et al.*, "Centrifugal microfluidic platforms: advanced unit operations and applications," *Chem. Soc. Rev.*, vol. 44, no. 17, pp. 6187–6229, 2015.

[157] Y. Deng *et al.*, "Euler force actuation mechanism for siphon valving in compact disk-like microfluidic chips," *Biomicrofluidics*, vol. 8, no. 2, pp. 1–18, 2014.

[158] J. Park, G. H. Lee, J. Y. Park, J. C. Lee, and H. C. Kim, "A numerical study of the Coriolis effect in centrifugal microfluidics with different channel arrangements," *Microfluid. Nanofluidics*, vol. 20, no. 4, pp. 1–14, 2016.

[159] M. Tang, G. Wang, S. K. Kong, and H. P. Ho, "A review of biomedical centrifugal microfluidic platforms," *Micromachines*, vol. 7, no. 2, 2016.

[160] A. Olanrewaju, M. Beaugrand, M. Yafia, and D. Juncker, "Capillary microfluidics in microchannels: From microfluidic networks to capillaric circuits," *Lab Chip*, vol. 18, no. 16, pp. 2323–2347, 2018.

[161] J. Siegrist *et al.*, "Serial siphon valving for centrifugal microfluidic platforms," *Microfluid. Nanofluidics*, vol. 9, no. 1, pp. 55–63, 2010.

[162] E. Pishbin, M. Eghbal, S. Fakhari, A. Kazemzadeh, and M. Navidbakhsh, "The effect of moment of inertia on the liquids in centrifugal microfluidics," *Micromachines*, vol. 7, no. 12, pp. 1–12, 2016.

[163] S. U. Hassan and X. Zhang, "Design and fabrication of capillary-driven flow device for point-of-care diagnostics," *Biosensors*, vol. 10, no. 4, pp. 1–7, 2020.

[164] Y. Li *et al.*, "In-plane silicon microneedles with open capillary microfluidic networks by deep reactive ion etching and sacrificial layer based sharpening," *Sensors Actuators, A Phys.*, vol. 292, pp. 149–157, 2019.

[165] T. Wang, J. Chen, T. Zhou, and L. Song, "Fabricating microstructures on glass for microfluidic chips by glass molding process," *Micromachines*, vol. 9, no. 6, pp. 1–15, 2018.

[166] S. M. Scott and Z. Ali, "Fabrication methods for microfluidic devices: An overview," *Micromachines*, vol. 12, no. 3, 2021.

[167] B. Gale *et al.*, "A Review of Current Methods in Microfluidic Device Fabrication and Future Commercialization Prospects," *Inventions*, vol. 3, no. 3, p. 60, 2018.

[168] Y. C. Tsai, H. P. Jen, K. W. Lin, and Y. Z. Hsieh, “Fabrication of microfluidic devices using dry film photoresist for microchip capillary electrophoresis,” *J. Chromatogr. A*, vol. 1111, no. 2, pp. 267–271, 2006.

[169] V. N. Goral, Y. C. Hsieh, O. N. Petzold, R. A. Faris, and P. K. Yuen, “Hot embossing of plastic microfluidic devices using poly(dimethylsiloxane) molds,” *J. Micromechanics Microengineering*, vol. 21, no. 1, 2011.

[170] S. A. M. Shaegh *et al.*, “Rapid prototyping of whole-thermoplastic microfluidics with built-in microvalves using laser ablation and thermal fusion bonding,” *Sensors Actuators, B Chem.*, vol. 255, pp. 100–109, 2018.

[171] U. M. Attia, S. Marson, and J. R. Alcock, “Micro-injection moulding of polymer microfluidic devices,” *Microfluid. Nanofluidics*, vol. 7, no. 1, pp. 1–28, 2009.

[172] G. S. Fiorini and D. T. Chiu, “Disposable microfluidic devices: Fabrication, function, and application,” *Biotechniques*, vol. 38, no. 3, pp. 429–446, 2005.

[173] S. Properties and T. Delivery, *Encyclopedia of nanotechnology*, vol. 50, no. 06. 2013.

[174] J. W. and C. L. Anderson, Deborah K., Liang, “乳鼠心肌提取 HHS Public Access,” *Physiol. Behav.*, vol. 176, no. 5, pp. 139–148, 2017.

[175] Y. Xia, J. Tien, D. Qin, and G. M. Whitesides, “Non-Photolithographic Methods for Fabrication of Elastomeric Stamps for Use in Microcontact Printing,” *Langmuir*, vol. 12, no. 16, pp. 4033–4038, 2002.

[176] X. Han, X. Liu, L. Tian, H. Zhang, and Z.-G. Mao, “A Non-Photolithography Fabrication for a Microfluidic Chip Based on PMMA Polymer,” *Machines*, vol. 3, no. 2, pp. 107–122, 2015.

[177] A. Donohoe, G. Lacour, P. McCluskey, D. Diamond, and M. McCaul, “Development of a cost-effective sensing platform for monitoring phosphate in natural waters,” *Chemosensors*, vol. 6, no. 4, 2018.

[178] A. Abrishamkar *et al.*, “Microfluidic pneumatic cages: A novel approach for in-chip crystal trapping, manipulation and controlled chemical treatment,” *J. Vis. Exp.*, vol. 2016, no. 113, 2016.

[179] S. H. Lee, D. Van Noort, J. Y. Lee, B. T. Zhang, and T. H. Park, “Effective mixing in a microfluidic chip using magnetic particles,” *Lab Chip*, vol. 9, no. 3, pp. 479–482, 2009.

[180] J. W. Hong, Y. Chen, W. F. Anderson, and S. R. Quake, “Molecular biology on a microfluidic chip,” *J. Phys. Condens. Matter*, vol. 18, no. 18, 2006.

[181] D. Ogończyk, J. Wgrzyn, P. Jankowski, B. Dąbrowski, and P. Garstecki, “Bonding of microfluidic devices fabricated in polycarbonate,” *Lab Chip*, vol. 10, no. 10, pp. 1324–1327, 2010.

[182] M. Czugala *et al.*, “CMAS: Fully integrated portable centrifugal microfluidic analysis system for on-site colorimetric analysis,” *RSC Adv.*, vol. 3, no. 36, pp. 15928–15938, 2013.

[183] R. Lundberg, “Travelling light,” *J. Mod. Opt.*, vol. 68, no. 14, pp. 717–741, 2021.

[184] A. C. Sparavigna, “Reflection , Refraction and Transmission of Light in Grosseteste ’ s Physics Reflection , Refraction and Transmission of Light in Grosseteste ’ s Physics,” no. December, 2019.

[185] R. J. Ram and K. Lee, “Optical waveguides for microfluidic integration,” *Conf. Proc. - Lasers Electro-Optics Soc. Annu. Meet.*, pp. 371–372, 2009.

[186] R. Blue and D. Uttamchandani, "Recent advances in optical fiber devices for microfluidics integration," *J. Biophotonics*, vol. 9, no. 1–2, pp. 13–25, 2016.

[187] J. S. Bajić, D. Z. Stupar, A. Joža, M. P. Slankamenac, M. Jelić, and M. B. Živanov, "A simple fibre optic inclination sensor based on the refraction of light," *Phys. Scr.*, no. T149, 2012.

[188] A. Dmitriev *et al.*, "Enhanced nanoplasmonic optical sensors with reduced substrate effect," *Nano Lett.*, vol. 8, no. 11, pp. 3893–3898, 2008.

[189] R. J. Ram and K. Lee, "Optical waveguides for microfluidic integration," *Conf. Proc. - Lasers Electro-Optics Soc. Annu. Meet.*, vol. 1, pp. 371–372, 2009.

[190] J. T. Kim, H. Choi, E. J. Shin, S. Park, and I. G. Kim, "Graphene-based optical waveguide tactile sensor for dynamic response," *Sci. Rep.*, vol. 8, no. 1, pp. 1–6, 2018.

[191] H. Jamali, "Investigation and review of mirrors reflectance in parabolic trough solar collectors (PTSCs)," *Energy Reports*, vol. 5, pp. 145–158, 2019.

[192] A. Morales and A. Durán, "Sol-Gel Protection of Front Surface Silver and Aluminum Mirrors," *J. Sol-Gel Sci. Technol.*, vol. 8, no. 1–3, pp. 451–457, 1997.

[193] S. Reid and I. Martin, "Development of Mirror Coatings for Gravitational Wave Detectors," *Coatings*, vol. 6, no. 4, p. 61, 2016.

[194] J. R. Krogmeier, I. Schaefer, G. Seward, G. R. Yantz, and J. W. Larson, "An integrated optics microfluidic device for detecting single DNA molecules," *Lab Chip*, vol. 7, no. 12, pp. 1767–1774, 2007.

[195] D. Khan, A. Rehman, M. Z. Rafiq, A. M. Khan, and M. Ali, "Improving the optical properties of SnO2 nanoparticles through Ni doping by sol-gel technique," *Curr. Res. Green Sustain. Chem.*, vol. 4, no. April, 2021.

[196] M. H. Nateq and R. Ceccato, "Enhanced sol-gel route to obtain a highly transparent and conductive aluminum-doped zinc oxide thin film," *Materials (Basel).*, vol. 12, no. 11, 2019.

[197] A. L. Pénard, T. Gacoin, and J. P. Boilot, "Functionalized sol-gel coatings for optical applications," *Acc. Chem. Res.*, vol. 40, no. 9, pp. 895–902, 2007.

[198] A. Theuwissen, "CMOS Image Sensors," *Smart Sens. Syst. Emerg. Technol. Appl.*, vol. 9780470686, no. June, pp. 173–189, 2014.

[199] D. Bueno Hernández, R. K. Mishra, R. Muñoz, and J. L. Marty, "Low cost optical device for detection of fluorescence from Ochratoxin A using a CMOS sensor," *Sensors Actuators, B Chem.*, vol. 246, pp. 606–614, 2017.

[200] Q. Chen *et al.*, "A CMOS Image Sensor Integrated with Plasmonic Colour Filters," *Plasmonics*, vol. 7, no. 4, pp. 695–699, 2012.

[201] D. J. Duke, T. Knast, B. Thethy, L. Gisler, and D. Edgington-Mitchell, "A low-cost high-speed CMOS camera for scientific imaging," *Meas. Sci. Technol.*, vol. 30, no. 7, 2019.

[202] M. Yan *et al.*, "High-speed CMOS image sensor for high-throughput lensless microfluidic imaging system," *Sensors, Cameras, Syst. Ind. Sci. Appl. XIII*, vol. 8298, no. May 2014, p. 829804, 2012.

[203] R. Stojanovic and D. Karadaglic, "An optical sensing approach based on light emitting diodes," *J. Phys. Conf. Ser.*, vol. 76, no. 1, 2007.

[204] B. Kuswandi, Nuriman, J. Huskens, and W. Verboom, "Optical sensing systems for microfluidic devices: A review," *Anal. Chim. Acta*, vol. 601, no. 2, pp. 141–155, 2007.

[205] F. Kehl, V. F. Cretu, and P. A. Willis, "Open-source lab hardware: A versatile microfluidic control and sensor platform," *HardwareX*, vol. 10, p. e00229, 2021.

[206] Y. Koo, J. Sankar, and Y. Yun, "High performance magnesium anode in paper-based microfluidic battery, powering on-chip fluorescence assay," *Biomicrofluidics*, vol. 8, no. 5, p. 054104, 2014.

[207] A. S. Marsh, "Identifying Market Specifications for Affordable Nutrient Sensor Technologies: User Needs Study," vol. 20816, no. 301, 2014.

[208] I. Situ and D. Phosphate, "HydroCycle-PO 4," pp. 5–6.

[209] J. C. Yan *et al.*, "A miniaturized colorimeter with a novel design and high precision for photometric detection," *Sensors (Switzerland)*, vol. 18, no. 3, 2018.

[210] T. B. Outram, "Black Coatings to Reduce Stray Light," 2009.

[211] E. Ponz, J. L. Ladaga, and R. D. Bonetto, "Measuring Surface Topography with Scanning Electron Microscopy. I. EZEImage: A Program to Obtain 3D Surface Data," *Microsc. Microanal.*, vol. 12, no. 02, pp. 170–177, Apr. 2006.

[212] I. Q. Sensor *et al.*, "Data sheets," 2020.

[213] M. Bowden, M. Sequeira, J. P. Krog, P. Gravesen, and D. Diamond, "A prototype industrial sensing system for phosphorus based on micro system technology," *Analyst*, vol. 127, no. 1, pp. 1–4, 2002.

[214] J. Deng and X. Jiang, "Advances in Reagents Storage and Release in Self-Contained Point-of-Care Devices," *Adv. Mater. Technol.*, vol. 4, no. 6, pp. 1–16, 2019.

[215] O. Strohmeier *et al.*, "Centrifugal microfluidic platforms: advanced unit operations and applications," *Chem. Soc. Rev.*, vol. 44, no. 17, pp. 6187–6229, 2015.

[216] A. Kazemzadeh, P. Ganesan, F. Ibrahim, S. He, and M. J. Madou, "The Effect of Contact Angles and Capillary Dimensions on the Burst Frequency of Super Hydrophilic and Hydrophilic Centrifugal Microfluidic Platforms, a CFD Study," *PLoS One*, vol. 8, no. 9, pp. 1–12, 2013.

[217] J. M. Park, Y. K. Cho, B. S. Lee, J. G. Lee, and C. Ko, "Multifunctional microvalves control by optical illumination on nanoheaters and its application in centrifugal microfluidic devices," *2007 NSTI Nanotechnol. Conf. Trade Show - NSTI Nanotech 2007, Tech. Proc.*, vol. 3, no. C, pp. 308–311, 2007.

[218] K. Iwai, R. D. Sochol, and L. Lin, "Finger-powered, pressure-driven microfluidic pump," *Proc. IEEE Int. Conf. Micro Electro Mech. Syst.*, pp. 1131–1134, 2011.

[219] A. Kazemzadeh, A. Eriksson, M. Madou, and A. Russom, "A micro-dispenser for long-term storage and controlled release of liquids," *Nat. Commun.*, vol. 10, no. 1, pp. 1–11, 2019.

[220] A. Tupik, G. Rudnitskaya, A. Bulyanitsa, T. Lukashenko, D. Varlamov, and A. Evstrapov, "Microchip device with dry-stored reagents for Loop mediated isothermal amplification," *J. Phys. Conf. Ser.*, vol. 1124, no. 3, 2018.

[221] L. Wentland, R. Polaski, and E. Fu, "Dry storage of multiple reagent types within a paper microfluidic device for phenylalanine monitoring," *Anal. Methods*, vol. 13, no. 5, pp. 660–671, 2021.

[222] D. Das, A. Dsouza, N. Kaur, S. Soni, and B. J. Toley, "Paper Stacks for Uniform Rehydration of Dried Reagents in Paper Microfluidic Devices," *Sci. Rep.*, vol. 9, no. 1, pp. 1–12, 2019.

[223] S. Smith, R. Sewart, H. Becker, P. Roux, and K. Land, "Blister pouches for effective reagent storage on microfluidic chips for blood cell counting," *Microfluid. Nanofluidics*, vol. 20, no. 12, pp. 1–14, 2016.

[224] S. Smith, R. Sewart, K. Land, P. Roux, C. Gärtner, and H. Becker, "Blister pouches for effective reagent storage and release for low cost point-of-care diagnostic applications," *Microfluid. BioMEMS, Med. Microsystems XIV*, vol. 9705, no. May 2018, p. 97050F, 2016.

[225] B. M. Jayawardane, I. D. McKelvie, and S. D. Kolev, "A paper-based device for measurement of reactive phosphate in water," *Talanta*, vol. 100, pp. 454–460, 2012.

[226] B. M. Jayawardane, S. Wei, I. D. McKelvie, and S. D. Kolev, "Microfluidic paper-based analytical device for the determination of nitrite and nitrate," *Anal. Chem.*, vol. 86, no. 15, pp. 7274–7279, 2014.

[227] J. Hoffmann, D. Mark, R. Zengerle, and F. Von Stetten, "Liquid reagent storage and release for centrifugally operated LAB-on-a-chip systems based on a burstable seal," *TRANSDUCERS 2009 - 15th Int. Conf. Solid-State Sensors, Actuators Microsystems*, no. May 2014, pp. 1991–1994, 2009.

[228] K. W. Oh and C. H. Ahn, "A review of microvalves," *J. Micromechanics Microengineering*, vol. 16, no. 5, 2006.

[229] S. C. Terry, J. H. Herman, and J. B. Angell, "A Gas Chromatographic Air Analyzer Fabricated on a Silicon Wafer," *IEEE Trans. Electron Devices*, vol. 26, no. 12, pp. 1880–1886, 1979.

[230] C. Goll, W. Bacher, B. Büstgens, D. Maas, R. Ruprecht, and W. K. Schomburg, "An electrostatically actuated polymer microvalve equipped with a movable membrane electrode," *J. Micromechanics Microengineering*, vol. 7, no. 3, pp. 224–226, 1997.

[231] C. A. Rich and K. D. Wise, "A high-flow thermopneumatic microvalve with improved efficiency and integrated state sensing," *J. Microelectromechanical Syst.*, vol. 12, no. 2, pp. 201–208, 2003.

[232] D. C. S. Bien, S. J. N. Mitchell, and H. S. Gamble, "Fabrication and characterization of a micromachined passive valve," *J. Micromechanics Microengineering*, vol. 13, no. 5, pp. 557–562, 2003.

[233] "Development of Biofunctional and Biocompatible Surfaces for Biodiagnostic Applications Utilising Plasma Enhanced Chemical Vapour Deposition."

[234] A. V. Desai, J. D. Tice, C. A. Apblett, and P. J. A. Kenis, "Design considerations for electrostatic microvalves with applications in poly(dimethylsiloxane)-based microfluidics," *Lab Chip*, vol. 12, no. 6, pp. 1078–1088, 2012.

[235] E. Yildirim, M. A. S. Arikan, and H. Külah, "A normally closed electrostatic parylene microvalve for micro total analysis systems," *Sensors Actuators, A Phys.*, vol. 181, pp. 81–86, 2012.

[236] B. Yang and Q. Lin, "A latchable microvalve using phase change of paraffin wax," *Sensors Actuators, A Phys.*, vol. 134, no. 1, pp. 194–200, 2007.

[237] A. Bhatia, "Control Valve Basics: Sizing and Selection Credit: 4 PDH CONTROL VALVE BASICS – SIZING & SELECTION," no. 877, 2005.

[238] C. B. Goy, R. E. Chaile, and R. E. Madrid, "Microfluidics and hydrogel: A powerful combination," *React. Funct. Polym.*, vol. 145, no. July, 2019.

[239] M. Tijero, R. Díez-Ahedo, F. Benito-Lopez, L. Basabe-Desmonts, V. Castro-López, and A. Valero, "Biomolecule storage on non-modified thermoplastic microfluidic chip by ink-jet printing of ionogels," *Biomicrofluidics*, vol. 9, no. 4, pp. 6–8, 2015.

[240] E. M. Ahmed, "Hydrogel: Preparation, characterization, and applications: A review," *J. Adv. Res.*, vol. 6, no. 2, pp. 105–121, 2015.

[241] D. Williams and I. Sebastine, "Dielectrophoretic manipulation of DNA," *IEEE Proc. nanobiotechnology*, vol. 152, no. 6, pp. 207–211, 2005.

[242] E. A. Nagul, I. D. McKelvie, P. Worsfold, and S. D. Kolev, "The molybdenum blue reaction for the determination of orthophosphate revisited: Opening the black box," *Anal. Chim. Acta*, vol. 890, pp. 60–82, 2015.

[243] G. N. Doku, W. K. Agbozo, S. J. Haswell, and T. McCreedy, "Phosphomolybdenum Blue Detection – A Review of Characteristics, Achievements, Challenges and Future Prospects," *Ghana J. Sci.*, vol. 61, no. 1, pp. 43–49, 2020.

[244] J. Cleary, D. Maher, and D. Diamond, "Development and Deployment of a Microfluidic," pp. 125–148, 2013.

[245] C. Metcalfe, M. E. Hoque, T. Sultana, C. Murray, P. Helm, and S. Kleywegt, "Monitoring for contaminants of emerging concern in drinking water using POCIS passive samplers," *Environ. Sci. Process. Impacts*, vol. 16, no. 3, pp. 473–481, 2014.

[246] S. Khalid *et al.*, "A review of environmental contamination and health risk assessment of wastewater use for crop irrigation with a focus on low and high-income countries," *Int. J. Environ. Res. Public Health*, vol. 15, no. 5, pp. 1–36, 2018.

[247] A. Jang, Z. Zou, K. K. Lee, C. H. Ahn, and P. L. Bishop, "State-of-the-art lab chip sensors for environmental water monitoring," *Meas. Sci. Technol.*, vol. 22, no. 3, 2011.

[248] K. S. Adu-Manu, C. Tapparello, W. Heinzelman, F. A. Katsriku, and J. D. Abdulai, "Water quality monitoring using wireless sensor networks: Current trends and future research directions," *ACM Trans. Sens. Networks*, vol. 13, no. 1, 2017.

[249] M. Sarwar, J. Leichner, G. M. Naja, and C. Z. Li, "Smart-phone, paper-based fluorescent sensor for ultra-low inorganic phosphate detection in environmental samples," *Microsystems Nanoeng.*, vol. 5, no. 1, 2019.

[250] S. V. Mapare, P. L. Yu, A. Sarkar, and S. C. Mukhopadhyay, "A Review of sensor technology for in-field phosphate monitoring," *Proc. Int. Conf. Sens. Technol. ICST*, no. February 2015, pp. 411–418, 2013.

[251] E. Gencturk, S. Mutlu, and K. O. Ulgen, "Advances in microfluidic devices made from thermoplastics used in cell biology and analyses," *Biomicrofluidics*, vol. 11, no. 5, 2017.

[252] K. Liu and Z. H. Fan, "Thermoplastic microfluidic devices and their applications in protein and DNA analysis," *Analyst*, vol. 136, no. 7, pp. 1288–1297, 2011.

[253] S. Prakash and S. Kumar, "Fabrication of microchannels: A review," *Proc. Inst. Mech. Eng. Part B J. Eng. Manuf.*, vol. 229, no. 8, pp. 1273–1288, 2015.

[254] Z. Wang, J. Lv, J. Li, Y. Wang, and J. Sun, "Fabrication and evaluation of micro-channel array

for flexible on-chip PEMFC by new evaluation method and self-made hot embossing system," *Int. J. Adv. Manuf. Technol.*, vol. 108, no. 5–6, pp. 1381–1387, 2020.

[255] P. R. Konari, Y. D. Clayton, M. B. Vaughan, M. Khandaker, and M. R. Hossan, "Article experimental analysis of laser micromachining of microchannels in common microfluidic substrates," *Micromachines*, vol. 12, no. 2, pp. 1–13, 2021.

[256] B. Jiang, L. Zhu, L. Min, X. Li, Z. Zhai, and D. Drummer, "Characterization of microchannel replicability of injection molded electrophoresis microfluidic chips," *Polymers (Basel).*, vol. 11, no. 4, pp. 1–11, 2019.

[257] A. Alrifaiy, O. A. Lindahl, and K. Ramser, "Polymer-based microfluidic devices for pharmacy, biology and tissue engineering," *Polymers (Basel).*, vol. 4, no. 3, pp. 1349–1398, 2012.

[258] G. F. Tjandraatmadja, L. S. Burn, and M. J. Jollands, "The effects of ultraviolet radiation on polycarbonate glazing," *Proc. 8th Int. Conf. Durab. Build. Constr. Mater. Vancouver, Canada*, vol. 30, pp. 884–898, 1999.

[259] A. Ghosh, Ramagopal, Bonanno, Brenowitz, "乳鼠心肌提取 HHS Public Access," *Physiol. Behav.*, vol. 176, no. 10, pp. 139–148, 2018.

[260] Z. Yang, C. Li, Z. Zhang, G. Lu, Z. Cai, and W. Cao, "Development of an in situ analyzer based on sequential injection analysis and liquid waveguide capillary flow cell for the determination of dissolved reactive phosphorus in natural waters," *Sensors (Switzerland)*, vol. 20, no. 10, 2020.

[261] A. M. Nightingale, A. D. Beaton, and M. C. Mowlem, "Trends in microfluidic systems for in situ chemical analysis of natural waters," *Sensors Actuators, B Chem.*, vol. 221, pp. 1398–1405, 2015.

[262] J. Cleary, D. Maher, C. Slater, and D. Diamond, "In situ monitoring of environmental water quality using an autonomous microfluidic sensor," *2010 IEEE Sensors Appl. Symp. SAS 2010 - Proc.*, no. June 2014, pp. 36–40, 2010.

[263] N. J. K. Howden, T. P. Burt, F. Worrall, M. J. Whelan, and M. Bieroza, "Nitrate concentrations and fluxes in the River Thames over 140 years (1868-2008): Are increases irreversible?," *Hydrol. Process.*, vol. 24, no. 18, pp. 2657–2662, 2010.

[264] D. Kavetski, F. Fenicia, and M. P. Clark, "Impact of temporal data resolution on parameter inference and model identification in conceptual hydrological modeling: Insights from an experimental catchment," *Water Resour. Res.*, vol. 47, no. 5, pp. 1–25, 2011.

[265] F. Wang *et al.*, "Rapid nitrate determination with a portable lab-on-chip device based on double microstructured assisted reactors," *Lab Chip*, vol. 21, no. 6, pp. 1109–1117, 2021.

[266] L. Felgentreu, G. Nausch, F. Bitschofsky, M. Nausch, and D. Schulz-Bull, "Colorimetric chemical differentiation and detection of phosphorus in eutrophic and high particulate waters: Advantages of a new monitoring approach," *Front. Mar. Sci.*, vol. 5, no. JUN, 2018.

[267] G. Tsakiris, "The Status of the European Waters in 2015: A Review," *Environ. Process.*, vol. 2, no. 3, pp. 543–557, 2015.

[268] P. E. Mellander *et al.*, "Identifying contrasting influences and surface water signals for specific groundwater phosphorus vulnerability," *Sci. Total Environ.*, vol. 541, pp. 292–302, 2016.

[269] J. M. Stuart, R. Anderson, P. Lazzarino, K. A. Kuehn, and O. R. Harvey, "Physical processes dictate early biogeochemical dynamics of soil pyrogenic organic matter in a subtropical forest

ecosystem," *Front. Earth Sci.*, vol. 6, no. May, pp. 1–18, 2018.

[270] N. N. Rabalais, R. J. Díaz, L. A. Levin, R. E. Turner, D. Gilbert, and J. Zhang, "Dynamics and distribution of natural and human-caused hypoxia," *Biogeosciences*, vol. 7, no. 2, pp. 585–619, 2010.

[271] A. Lintern *et al.*, "Key factors influencing differences in stream water quality across space," *WIREs Water*, vol. 5, no. 1, pp. 1–31, 2018.

[272] R. Lucas, "Organizational Diagnostics: Translating the Political into the Technical," *J. Manage.*, vol. 13, no. 1, pp. 135–148, 1987.

[273] M. S. House, W.A.; Warwick, "3. House & Warwick. intense measurement of nutrient dynamics in R Swale.pdf," *The Science of the Total Environment*, vol. 210/211, no. 1–6. pp. 111–137, 1998.

[274] J. Schmedtmann and M. L. Campagnolo, "Reliable crop identification with satellite imagery in the context of Common Agriculture Policy subsidy control," *Remote Sens.*, vol. 7, no. 7, pp. 9325–9346, 2015.

[275] C. Tundu, M. J. Tumbare, and J. M. K. Onema, "Sedimentation and its impacts/effects on river system and reservoir water quality: Case study of Mazowe catchment, Zimbabwe," *Proc. Int. Assoc. Hydrol. Sci.*, vol. 377, pp. 57–66, 2018.

[276] Y. YI, Z. WANG, K. ZHANG, G. YU, and X. DUAN, "Sediment pollution and its effect on fish through food chain in the Yangtze River," *Int. J. Sediment Res.*, vol. 23, no. 4, pp. 338–347, 2008.

[277] W. Calmano, U. Förstner, and M. Series, "Solid Waste : Assessment , Monitoring and Remediation Comparative study of sediment and mussel aromatic compound content in European coastal environments . Rela- tionship with specific biomarkers," 2004.

[278] H. Sun, P. S. Cornish, and T. M. Daniell, "Turbidity-based erosion estimation in a catchment in South Australia," *J. Hydrol.*, vol. 253, no. 1–4, pp. 227–238, 2001.

[279] G. Boggs, C. Devonport, K. Evans, and P. Puig, "GIS-based rapid assessment of erosion risk in a small catchment in the wet/dry tropics of Australia," *L. Degrad. Dev.*, vol. 12, no. 5, pp. 417–434, 2001.

[280] P. Panagos, C. Karydas, P. Borrelli, C. Ballabio, and K. Meusburger, "Advances in soil erosion modelling through remote sensing data availability at European scale," *Second Int. Conf. Remote Sens. Geoinf. Environ.*, vol. 9229, no. August 2014, p. 92290I, 2014.

[281] S. R. Carpenter, N. F. Caraco, D. L. Correll, R. W. Howarth, A. N. Sharpley, and V. H. Smith, "Nonpoint pollution of surface waters with phosphorus and nitrogen," *Ecol. Appl.*, vol. 8, no. 3, pp. 559–568, 1998.

[282] D. G. Doody, M. Archbold, R. H. Foy, and R. Flynn, "Approaches to the implementation of the Water Framework Directive: Targeting mitigation measures at critical source areas of diffuse phosphorus in Irish catchments," *J. Environ. Manage.*, vol. 93, no. 1, pp. 225–234, 2012.

[283] P. A. Vanrolleghem, L. Benedetti, and J. Meirlaen, "Modelling and real-time control of the integrated urban wastewater system," *Environ. Model. Softw.*, vol. 20, no. 4 SPEC. ISS., pp. 427–442, 2005.

[284] P. Jordan, A. Arnscheidt, H. McGrogan, and S. McCormick, "Characterising phosphorus transfers in rural catchments using a continuous bank-side analyser," *Hydrol. Earth Syst. Sci.*,

vol. 11, no. 1, pp. 372–381, 2007.

[285] D. L. Danielopol *et al.*, "Incorporating ecological perspectives in European groundwater management policy," *Environ. Conserv.*, vol. 31, no. 3, pp. 185–189, 2004.

[286] E. Packtest, "Clean Water for Wildlife Technical Manual," no. December, 2016.

[287] J. Ma, Y. Yuan, T. Zhou, and D. Yuan, "Determination of total phosphorus in natural waters with a simple neutral digestion method using sodium persulfate," *Limnol. Oceanogr. Methods*, vol. 15, no. 4, pp. 372–380, 2017.

[288] T. G. O'Higgins and J. G. Wilson, "Impact of the river Liffey discharge on nutrient and chlorophyll concentrations in the Liffey estuary and Dublin Bay (Irish Sea)," *Estuar. Coast. Shelf Sci.*, vol. 64, no. 2–3, pp. 323–334, 2005.

[289] Environmental Protection Agency, "Liffey Catchment Assessment 2010-2015," *Catchment Sci. Manag. Unit*, vol. 3, no. 3, p. 44, 2018.

[290] R. Fealy *et al.*, "RESCALE: Review and Simulate Climate and Catchment Responses at Burrishoole Climate and Catchment Environment," 2007.

[291] R. Fealy *et al.*, "RESCALE : Review and Simulate Climate and Catchment Responses at Burrishoole," *Rev. Lit. Arts Am.*, 2013.

[292] E. Jennings, D. Taylor, S. Murnaghan, K. Bosch, E. De Eyto, and K. Sparber, "Past , current and future I nteractions between pressures , chemica L status and bio L ogical q U ality ele M ents for lakes IN contr A sting catchmen T s in Ir E land . EPA / ERTDI PROJECT # 2005-W-MS-40," 2005.

[293] E. De Eyto *et al.*, "The response of North Atlantic diadromous fish to multiple stressors, including land use change: A multidecadal study," *Can. J. Fish. Aquat. Sci.*, vol. 73, no. 12, pp. 1759–1769, 2016.

[294] M. Sudmanns, D. Tiede, H. Augustin, and S. Lang, "Assessing global Sentinel-2 coverage dynamics and data availability for operational Earth observation (EO) applications using the EO-Compass," *Int. J. Digit. Earth*, vol. 13, no. 7, pp. 768–784, 2020.

[295] M. Gao, C. H. Hugenholtz, T. A. Fox, M. Kucharczyk, T. E. Barchyn, and P. R. Nesbit, "Weather constraints on global drone flyability," *Sci. Rep.*, vol. 11, no. 1, pp. 1–13, 2021.

[296] C. Science, M. Unit, and E. P. Agency, "Sligo Bay Catchment Assessment," vol. 2015, no. 3, 2018.

[297] N. Rahmanian and S. H. . Ali, "Analysis of Physico-chemical Parameters to Evaluate the Drinking Water Quality," *J. Chem.*, pp. 0–1, 2015.

[298] D. Ogończyk, P. Jankowski, and P. Garstecki, "A method for simultaneous polishing and hydrophobization of polycarbonate for microfluidic applications," *Polymers (Basel).*, vol. 12, no. 11, pp. 1–11, 2020.

[299] T. Winther, J. Bannerman, H. Skogstad, M. K. G. Johansson, K. Jacobson, and J. Samuelsson, "Adhesives for adhering polystyrene plastic and their long-term effect," *Stud. Conserv.*, vol. 60, no. 2, pp. 107–120, 2015.

[300] Z. Bergant and J. Grum, "Quality improvement of flame sprayed, heat treated, and Remelted NiCrBSi coatings," *J. Therm. Spray Technol.*, vol. 18, no. 3, pp. 380–391, 2009.

[301] S. Götz and U. Karst, "Recent developments in optical detection methods for microchip

separations," *Anal. Bioanal. Chem.*, vol. 387, no. 1, pp. 183–192, 2007.

[302] C. Frank and F. Schroeder, "Using sequential injection analysis to improve system and data reliability of online methods: Determination of ammonium and phosphate in coastal waters," *J. Autom. Methods Manag. Chem.*, vol. 2007, 2007.

[303] I. Dahllöf, O. Svensson, and C. Torstensson, "Optimising the determination of nitrate and phosphate in sea water with ion chromatography using experimental design," *J. Chromatogr. A*, vol. 771, no. 1–2, pp. 163–168, 1997.

[304] K. S. Johnson and R. L. Petty, "Determination of nitrate and nitrite in seawater by flow injection analysis," *Limnol. Oceanogr.*, vol. 28, no. 6, pp. 1260–1266, 1983.

[305] J. Jońca, V. León Fernández, D. Thouron, A. Paulmier, M. Graco, and V. Garçon, "Phosphate determination in seawater: Toward an autonomous electrochemical method," *Talanta*, vol. 87, no. 1, pp. 161–167, 2011.

[306] C. W. Tsao and Z. K. Wu, "Polymer microchannel and micromold surface polishing for rapid, low-quantity polydimethylsiloxane and thermoplastic microfluidic device fabrication," *Polymers (Basel).*, vol. 12, no. 11, pp. 1–15, 2020.

[307] M. Geissdoerfer, P. Savaget, N. M. P. Bocken, and E. J. Hultink, "The Circular Economy – A new sustainability paradigm?," *J. Clean. Prod.*, vol. 143, pp. 757–768, 2017.